Solid-State Microwave Generators for the Batch and Flow Synthesis of Mesoporous Silica and Other Nanoparticulated Oxides

VNIVERSITAT DE VALÈNCIA

****

Memoria presentada por Cristina Rodríguez Carrillo
para aspirar al grado de Doctora en Química

****

Supervisada por:

Dr. José Vicente Ros Lis
Dr. Jamal El Haskouri Bennagi

Mayo, 2025

D. JOSE VICENTE ROS LIS, doctor por la Universitat Politècnica de València y actualmente Catedrático y profesor del Departamento de Química Inorgánica de la Universitat de València e investigador del Instituto Interuniversitario de Investigación de Reconocimiento Molecular y Desarrollo Tecnológico (IDM). Y D. JAMAL EL HASKOURI BENNAGI, doctor por la Universitat de València y actualmente investigador del Instituto de Ciencia de los Materiales (ICMUV).

CERTIFICAN:

Que la memoria presentada por Dña. Cristina Rodríguez Carrillo con título "Solid-state microwave generators for the batch and flow synthesis of mesoporous silica and other nanoparticulated oxides" corresponde a su Tesis Doctoral y ha sido realizada bajo su dirección en la Facultad de Química de la Universitat de València, autorizando mediante este escrito la presentación de la misma para optar al grado de Doctora.

En Burjassot, a 15 de Mayo de 2025.

JOSE VICENTE\| ROS\|LIS
Firmado digitalmente por JOSE VICENTE\| ROS\|LIS
Fecha: 2025.05.15 13:17:43 +02'00'

Dr. José Vicente Ros Lis

EL HASKOURI BENNAGI JAMAL - 49352407L
Firmado digitalmente por EL HASKOURI BENNAGI JAMAL - 49352407L
Fecha: 2025.05.15 13:29:46 +02'00'

Dr. Jamal El Haskouri Bennagi

A todos los que confiaron en mí,

pero sobre todo a los que no lo hicieron.

AGRADECIMIENTOS

Cuesta creer que esto, lo primero que se lee en una tesis, sea justamente lo último que escribo. Pero ha llegado el momento de agradecer, con todo el corazón, a todas las personas que, de una forma u otra, hicieron posible que este trabajo llegara a su fin. Cada una dejó su huella en este camino, y por eso les estaré siempre agradecida.

En primer lugar, quisiera agradecer a mi director de tesis, José Vicente, por haberme dado la oportunidad de empezar a trabajar con vosotros sin conocerme de nada. Yo solo era una niña sin nota en la carrera que pensaba que no iba a conseguir hacer una tesis porque nunca conseguiría una beca, y ahí estabas tú, para ofrecerme un contrato y poder realizar este sueño. Gracias. También a mi otro director, Jamal, y a Pedro, que no ha sido mi director pero como si lo fuera. Gracias por resolverme cada duda que tenía, por dedicarme el tiempo que me habéis dedicado, o incluso por las charletas en el pasillo que hacían más ameno el ir a trabajar.

Otra persona a quien quiero agradecer es a Ruth, siempre estando a un whatsapp de distancia dispuesta a ayudarme cuando tenía problemas con los equipos. Gracias a tu visión y apoyo he logrado apreciar el verdadero valor de mi trabajo, más allá de mis propias percepciones.

Particularmente, quiero agradecer a Luis Roca. Fue mi director de TFM y la primera persona que me dijo que yo valía para hacer una tesis, y que confió en mí cuando le dije que quería hacerla. Gracias por ese impulso tan necesario en ese momento.

Durante estos años también he compartido laboratorio con mucha gente. Gracias a Lola por haberme acogido desde el principio y por estar siempre ahí para cualquier consulta. Y a Miriam por enseñarme todo lo que sé sobre la UVM-7, fuiste mi guía hasta que ya pude volar sola. Gracias a Sara por traer el mundo esotérico a mi vida. Aunque luego se te olvidara cerrar las puertas a los malos espíritus, me has dado la confianza para saber que mi vida va a ir bien. Gracias a Álex por haber conseguido que mi última etapa experimental fuera tan llevadera con tus dotes informáticas. A Inés, hemos coincidido poco tiempo, pero me ha gustado que alguien compartiera la misma neurona que yo con todas las referencias malas. Y a Youssef, por haberme recordado no vivir por inercia y esforzarme cada día por ser la mejor versión de mí misma.

Y más que a mis compañeros de trabajo, quiero agradecer a mis amigos. A la Angelita, que te mudaste con tu flamenquito, tus plantas y todo tu desorden, pero que ojalá lo hubieras hecho antes. A Sheila, por estar ahí desde el principio y ser un +1 siempre. A veces me conoces tan bien, que hasta me asusto. Hiciste que dejara de decir "compañeros de trabajo" a decir "amigos". A Ainhoa, por su energía, por estar siempre para todo, y por ser tan echada para adelante; eres la compañera perfecta de locuras. Nos vemos por Bilbo. A Alberto, el gym bro de confianza, gracias por incluirme tanto y tan bien en tu vida siempre. Aunque no te lo creas eres de las personas más buenas que he conocido nunca. Sé que siempre vas a estar a un mensaje de distancia para mandarme tu ubicación en tiempo real para todo el día y que me una cuando quiera, y menos mal.

A Adolfito, que empezó siendo el pesado que madrugaba y no se le veía el pelo, y acabó siendo el pesado al que le contaba toda mi vida cada mañana al llegar al laboratorio. Eres de los pocos falleros que me caen bien, aprécialo. A Jose Huertas, lo primero es pedir perdón, por haber conseguido que todo el mundo le añada una S a tu apellido, sin yo ser consciente de ello. Y también gracias, porque aunque no nos viéramos todos los días, has sabido estar presente siempre. Prometo que veré "La La Land" pronto. A Luisfer, fuente inagotable de marujeos. Gracias por tu alegría y tu salero latino. Voy a echar de menos el ir por los pasillos del ICMUV y recibir un abrazo tuyo. Y a Albertillo, porque aunque siempre he ido de dura, y de que no me afecta nada, me has calado desde el principio. Y gracias por existir, porque cuando todos pensamos que vamos mal o estamos estresados, solo hay que pensar en ti y se nos pasa.

También estaban ahí para alegrarme los días la gente del ICMol, que empezaron siendo los compañeros de trabajo de mi compañero de piso, y acabaron siendo también mis amigos. En especial quiero darle las gracias a Carmen, por haberme arropado tan bien desde que llegué a Valencia. Por ser mami, taxi, gymsis, fotógrafa, y amiga. Si consigo hacer todo el papeleo de la tesis, es gracias a ti. A Ramón, gracias por resolver todas y cada una de las dudas que he tenido. Incluso salir a tomar algo y acabar ensayando mi presentación para un congreso, y tú haciéndome preguntas para prepararme las respuestas. Eres uno de mis referentes científicos, que lo sepas.

Y a Galle, que antes de conocernos ya éramos tan iguales que estaba destinado que acabáramos siendo amigos. Si tuviera que llevar a alguien a mi pueblo, eres tú sin ninguna duda, y cuidado, que eso no se le ofrece a cualquiera. Eres el imprescindible, ya lo sabes.

Pero sobre todo, quiero darle las gracias a Luis. Esta tesis es casi tan tuya como mía, a saber si la habría acabado de no haber sido por ti. Eres la primera persona a la que he recurrido cuando tenía algún problema, y a la primera a la que le contaba cuando todo iba bien, tanto en ciencia como en la vida en general. Eres mi director de tesis y de vida en la sombra. Gracias por estar, y por dejarme ser, siempre.

Y no se me olvida Jesús. Nunca olvidaré el día que decidí ser amiga vuestra en primero de carrera porque fui a preguntaros una duda de clase, y tú me ofreciste una napolitana de jamón y queso porque en el pack venían 3 y os sobraba 1. Ahí ya estaba destinado que hiciéramos equipo. Ojalá hubieras vivido aquí en Valencia y no solo los findes de visita.

También se lo dedico a mis amigos del pueblo, a mis atunes. Nada recargaba tanto las pilas y desconectaba de la tesis como bajar al pueblo con vosotros. Cada mes ya estaba esperando con ansias ese finde en el que bajábamos todos, y cada domingo al volver casi siempre iba aguantando las lágrimas porque no quería irme. Que suerte la mía la de tener un pueblo así.

Tampoco me olvido de mis pilares desde pequeña, Bujes y Lorena. Habéis estado ahí, aunque hayamos tomado caminos tan distintos, sin cuestionar las decisiones que he tomado y apoyándome siempre.

Por último, y en este caso sí es lo más importante, se lo dedico a mi familia, a mis padres, que me han apoyado siempre en todos los aspectos de mi vida, incluso cuando sabían que lo estaba haciendo mal pero no quería reconocer que me estaba equivocando. Porque un sábado por la noche llegué y les dije "mañana me voy a Valencia, con vuestra ayuda o sin ella". Claro, que yo no había pensado que al día siguiente era domingo y no iba a encontrar piso, ni transporte, ni nada, pero ahí estaban ellos, para ayudarme sin quejarse. Os debo todo. A mi hermana, que casi sin ninguna duda es la persona que más pendiente está de mí. Me conoces a niveles que ni yo entiendo, gracias por estar siempre ahí. Y a mis abuelos, por presumir siempre tanto de mí, cuando ni siquiera yo pensaba que estuviera haciendo algo importante con mi vida.

Y bueno, ya que estamos, gracias a mí también, ¿no? No conozco a persona que le eche más huevos a la vida. Disfrútalo, que lo has conseguido reina.

Gracias.

Abstract

This doctoral thesis follows the format of a compilation of articles. It consists of an initial section, which presents the overall framework of the research and provides an introduction to each of the topics discussed in this work. Subsequently, a series of chapters related to the articles derived from this research will be presented. Each chapter begins with an introduction to the respective article, explaining the motivation behind it. The articles themselves are then included. Specifically, this thesis comprises four articles of empirical studies that address the objectives of this doctoral research. The results of these studies have been disseminated to the academic community through publications in prestigious scientific journals.

This doctoral research focuses on the synthesis and upscaling of different advanced materials using solid-state microwave generators. The study primarily examines the preparation and characterization of mesoporous silica UVM-7, its functionalization with titanium (Ti-UVM-7) and cerium (Ce-UVM-7), as well as the synthesis of cerium oxide (CeO_2) nanoparticles. Through a systematic investigation, the thesis explores novel methodologies for achieving efficient material synthesis while leveraging the advantages of solid-state microwave technology.

Chapter 1: Introduction and Context

The first Chapter establishes the theoretical basis and the scientific relevance of the research. It begins by introducing nanomaterials and the different synthetic procedures, where we can find the microwave-assisted synthesis, which constitutes the core focus of this work. It introduces the importance of

microwave-assisted synthesis in material science, highlighting the benefits of solid-state microwave generators over conventional methods and the significant advancements made in this field over time.

Chapter 2: Objectives

Chapter 2 presents the main objectives, centered on developing scalable, energy-efficient synthesis methods for mesoporous silica and CeO_2 nanoparticles using solid-state microwave technology.

Chapter 3: Synthesis and Upscaling of UVM-7

Chapter 3 provides an in-depth discussion of mesoporous silicas, with a specific focus on UVM-7. Furthermore, the Chapter explores the synthesis and large-scale production of UVM-7. The primary objective is to optimize synthetic conditions to achieve larger yields while maintaining the structural integrity and desired physicochemical properties of UVM-7. Two key strategies are employed for upscaling: the use of larger reactors and the implementation of continuous flow synthesis. The effectiveness of these approaches is critically evaluated through various characterization techniques. Furthermore, post-functionalization methods for UVM-7 are adapted to both systems, ensuring the material retains its mesoporosity and tailored surface properties.

Chapter 4: Functionalization of UVM-7 with Titanium and Cerium

In this Chapter, the advantages of the atrane method for incorporating heteroelements into mesoporous matrices are discussed, particularly in the functionalization of UVM-7 with titanium and cerium using a one-pot

synthesis approach. The formation of Ti-UVM-7 and Ce-UVM-7 is carefully investigated, with Ce-UVM-7 representing a novel contribution to the field. The synthesis and upscaling of these functionalized materials are examined in both batch and continuous flow processes, ensuring the feasibility of large-scale production. Additionally, the potential applications of Ti-UVM-7 and Ce-UVM-7 in ultraviolet (UV) light absorption are evaluated, particularly in their suitability for use as active components in sunscreen formulations. A comparative study is conducted to assess their performance against commercial UV-blocking materials.

Chapter 5: Synthesis of CeO_2 Nanoparticles

Chapter 5 expands the research beyond mesoporous silica materials, focusing on the synthesis of inorganic metal oxides using solid-state microwave generators. CeO_2 is selected as a model material due to its extensive applications in catalysis, energy storage, and environmental remediation. The synthesis of CeO_2 nanoparticles is conducted in both batch and continuous flow systems, and various parameters such as precursor concentration, reaction time, and microwave power are optimized to achieve controlled particle size and morphology. Advanced characterization techniques are employed to assess the physicochemical properties of the synthesized CeO_2 nanoparticles. Furthermore, the catalytic performance of CeO_2 is investigated to determine its suitability for specific applications. The study evaluates its ROS scavenging properties, ensuring that the synthesized material retains not only its morphological attributes but also its functional effectiveness.

Resumen

Esta tesis doctoral sigue el formato de una compilación de artículos. Consta de una sección inicial, que presenta el marco general de la investigación y proporciona una introducción a cada uno de los temas abordados en este trabajo. Posteriormente, se presentan una serie de capítulos relacionados con los artículos derivados de esta investigación. Cada capítulo comienza con una introducción al artículo correspondiente, explicando la motivación detrás del mismo. Luego, se incluyen los artículos en sí. En concreto, esta tesis comprende cuatro artículos de estudios empíricos que abordan los objetivos de esta investigación doctoral. Los resultados de estos estudios han sido difundidos en la comunidad académica mediante publicaciones en revistas científicas de prestigio.

Esta investigación doctoral se centra en la síntesis y escalado de diferentes materiales avanzados utilizando generadores de microondas de estado sólido. El estudio estudia principalmente la preparación y caracterización de la sílice mesoporosa UVM-7, su funcionalización con titanio (Ti-UVM-7) y cerio (Ce-UVM-7), así como la síntesis de nanopartículas de óxido de cerio (CeO_2). A través de una investigación sistemática, la tesis explora nuevas metodologías para lograr una síntesis eficiente de materiales aprovechando las ventajas de la tecnología de microondas de estado sólido.

Capítulo 1: Introducción y Contexto

El primer Capítulo establece la base teórica y la relevancia científica de la investigación. Comienza introduciendo los nanomateriales y los diferentes procedimientos sintéticos, donde se encuentra la síntesis asistida por

microondas, que constituye el núcleo central de este trabajo. Se introduce la importancia de la síntesis asistida por microondas en la ciencia de materiales, destacando las ventajas de los generadores de microondas de estado sólido frente a los métodos convencionales y los importantes avances que se han producido en este campo a lo largo del tiempo.

Capítulo 2: Objetivos

El Capítulo 2 presenta los objetivos principales, centrados en desarrollar métodos escalables y energéticamente eficientes para la síntesis de sílice mesoporosa y nanopartículas de CeO_2 utilizando tecnología de microondas en estado sólido.

Capítulo 3: Síntesis y Escalado de UVM-7

En el Capítulo 3 se analizan en profundidad las sílices mesoporosas, con especial atención a la UVM-7. El capítulo explora la síntesis y la producción a gran escala de UVM-7. El objetivo principal de este capítulo es optimizar las condiciones de síntesis para conseguir mayores rendimientos, manteniendo al mismo tiempo la integridad estructural y las propiedades fisicoquímicas deseadas de UVM-7. Para ello se emplean dos estrategias clave: el uso de reactores más grandes y la aplicación de la síntesis en flujo continuo. La eficacia de estos enfoques se evalúa críticamente mediante diversas técnicas de caracterización. Además, los métodos de postfuncionalización de UVM-7 se adaptan a ambos sistemas, garantizando que el material conserve su mesoporosidad y sus propiedades superficiales a medida.

Capítulo 4: Funcionalización de UVM-7 con Titanio y Cerio

En el Capítulo 4 se discuten las ventajas del método de los atranos para la incorporación de heteroelementos en matrices mesoporosas, particularmente en la funcionalización de UVM-7 con titanio y cerio utilizando un método de síntesis one-pot. Se investiga cuidadosamente la formación de Ti-UVM-7 y Ce-UVM-7, representando el Ce-UVM-7 una novedosa contribución a este campo. La síntesis y el escalado de estos materiales funcionalizados se examinan tanto en procesos en lotes como de flujo continuo, garantizando la viabilidad de la producción a gran escala. Además, se evalúan las aplicaciones potenciales de Ti-UVM-7 y Ce-UVM-7 en la absorción de luz ultravioleta (UV), particularmente en su idoneidad para el uso como componentes activos en formulaciones de protección solar. Se realiza un estudio comparativo para evaluar su rendimiento frente a los materiales comerciales que bloquean los rayos UV.

Capítulo 5: Síntesis de Nanopartículas de CeO_2

El Capítulo 5 amplía la investigación más allá de los materiales de sílice mesoporosa, centrándose en la síntesis de óxidos metálicos inorgánicos utilizando generadores de microondas de estado sólido. Se selecciona el CeO_2 como material modelo debido a sus amplias aplicaciones en catálisis, almacenamiento de energía y remediación ambiental. La síntesis de nanopartículas de CeO_2 se lleva a cabo tanto en sistemas en lotes como en flujo, optimizando diversos parámetros como la concentración de precursores, el tiempo de reacción y la potencia de microondas para lograr un control preciso del tamaño y la morfología de las partículas. Se emplean

técnicas avanzadas de caracterización para evaluar las propiedades fisicoquímicas de las nanopartículas de CeO_2 sintetizadas. Además, se investiga el desempeño catalítico del CeO_2 para determinar su idoneidad en aplicaciones específicas. Se evalúan sus propiedades como eliminador de especies reactivas de oxígeno (ROS), garantizando que el material sintetizado conserve no solo sus atributos morfológicos, sino también su eficacia funcional.

Resum

Aquesta tesi doctoral seguix el format d'una compilació d'articles. Consta d'una secció inicial, que presenta el marc general de la investigació i proporciona una introducció a cada un dels temes abordats en este treball. Posteriorment, es presenten una sèrie de capítols relacionats amb els articles derivats d'aquesta investigació. Cada capítol comença amb una introducció a l'article corresponent, explicant la motivació darrere d'aqueste. Després, s'inclouen els articles en si. En concret, esta tesi es composa de quatre articles d'estudis empírics que aborden els objectius d'aquesta investigació doctoral. Els resultats d'aquestos estudis han sigut difosos en la comunitat acadèmica mitjançant publicacions en revistes científiques de prestigi.

Aquesta investigació doctoral es centra en la síntesi i escalat de diferents materials avançats utilitzant generadors de microones d'estat sòlid. L'estudi aborda principalment la preparació i caracterització de la sílice mesoporosa UVM-7, la seua funcionalització amb titani (Ti-UVM-7) i ceri (Ce-UVM-7), així com la síntesi de nanopartícules d'òxid de ceri (CeO_2). A través d'una investigació sistemàtica, la tesi explora noves metodologies per a aconseguir una síntesi eficient de materials aprofitant els avantatges de la tecnologia de microones d'estat sòlid.

Capítol 1: Introducció i Context

El primer Capítol establix la base teòrica i la rellevància científica de la investigació. Comença introduint els nanomaterials i els diferents procediments sintètics, on es troba la síntesi assistida per microones, que constitueïx el nucli central d'aqueste treball. S'introduïx la importància de la

síntesi assistida per microones en la ciència de materials, destacant els avantatges dels generadors de microones d'estat sòlid enfront dels mètodes convencionals i els importants avanços que s'han produït en aqueste camp al llarg del temps.

Capítol 2: Objectius

El Capítol 2 presenta els objectius principals, centrats en desenvolupar mètodes escalables i energèticament eficients per a la síntesi de sílice mesoporosa i nanopartícules de CeO_2 utilitzant tecnología de microones en estat sòlid.

Capítol 3: Síntesi i Escalat de UVM-7

En el Capítol 3 s'analitzen en profunditat les sílices mesoporoses, amb especial atenció a la UVM-7. El Capítol explora la síntesi i la producció a gran escala de UVM-7. L'objectiu principal d'aqueste capítol és optimitzar les condicions de síntesis per a aconseguir majors rendiments, mantenint al mateix temps la integritat estructural i les propietats fisicoquímiques desitjades de UVM-7. Per a això s'empren dos estratègies clau: l'ús de reactors més grans i l'aplicació de la síntesi en flux continu. L'eficàcia d'aquestos enfocaments s'avalua críticament mitjançant diverses tècniques de caracterització. A més, els mètodes de postfuncionalització de UVM-7 s'adapten tant als sistemes en lot com als de flux continu, garantint que el material conserve la seua mesoporositat i les seues propietats superficials a mesura.

Capítol 4: Funcionalització de UVM-7 amb Titani i Ceri

En el Capítol 4 es discuteixen els avantatges del mètode dels atrans per a la incorporació de heteroelements en matrius mesoporoses, particularment en la funcionalització de UVM-7 amb titani i ceri utilitzant un mètode de síntesi d'un sol recipient. S'investiga acuradament la formació de Ti-UVM-7 i Ce-UVM-7, representant el Ce-UVM-7 una nova contribució a aquest camp. La síntesi i l'escalat d'aquestos materials funcionalitzats s'examinen tant en processos en lot com de flux continu, garantint la viabilitat de la producció a gran escala. A més, s'avaluen les aplicacions potencials de Ti-UVM-7 i Ce-UVM-7 en l'absorció de llum ultraviolada (UV), particularment en la seua idoneïtat per a l'ús com a components actius en formulacions de protecció solar. Es realitza un estudi comparatiu per a avaluar el seu rendiment enfront dels materials comercials que bloquegen els raigs UV.

Capítol 5: Síntesi de Nanopartícules de CeO_2

El Capítol final amplia la investigació més enllà dels materials de sílice mesoporosa, centrant-se en la síntesi d'òxids metàl·lics inorgànics utilitzant generadors de microones d'estat sòlid. Es selecciona el CeO_2 com a material model degut a les seues àmplies aplicacions en catàlisi, emmagatzematge d'energia i remediació ambiental. La síntesi de nanopartícules de CeO_2 es porta a terme tant en sistemes en lot com en flux, optimitzant diversos paràmetres com la concentració de precursors, el temps de reacció i la potència de microones per a aconseguir un control precís de la grandària i la morfologia de les partícules. S'empren tècniques avançades de caracterització per a avaluar les propietats fisicoquímiques de les nanopartícules de CeO_2

sintetitzades. A més, s'investiga el desenvolupament catalític del CeO_2 per a determinar la seua idoneïtat en aplicacions específiques. S'avaluen les seues propietats com a eliminador d'espècies reactives d'oxigen (ROS), garantint així que el material sintetitzat conserve tant els seus atributs morfològics, com la seua eficàcia funcional.

Publications

The following scientific Works were published during the course of this PhD:

(1) Rodríguez-Carrillo, C., Torres García, J., Benítez, M., El Haskouri, J., Amorós, P., & Ros-Lis, J. V. (2022). Batch and flow synthesis of CeO_2 nanomaterials using solid-state microwave generators. *Molecules*, *27*(9), 2712.

(2) Rodríguez-Carríllo, C., Benítez, M., El Haskouri, J., Amorós, P., & Ros-Lis, J. V. (2023). Novel Microwave-Assisted Synthesis of COFs: 2020–2022. *Molecules*, *28*(7), 3112.

(3) Benítez, M., Rodríguez-Carrillo, C., Sánchez-Artero, S., El Haskouri, J., Amorós, P., & Ros-Lis, J. V. (2023). Scaled-up microwave-assisted batch and flow synthesis and life cycle assessment of a silica mesoporous material: UVM-7. *Green Chemistry*, *26*(2), 785-793.

(4) Rodríguez-Carrillo, C., Benítez, M., González-Fernández, M., De los Reyes, R., Murcia, S., El Haskouri, J., Amorós, P., Ros-Lis, J.V. (2024). Flow and batch minute-made synthesis of Ce-UVM-7 using microwave-assisted reaction: scaling-up, optical and catalytic applications, and impact assessment. *ACS Sustainable Chemistry & Engineering*, 12(35), 13208-13219.

(5) Rodríguez-Carrillo, C., Benítez, M., De los Reyes, R., El Haskouri, J., Amorós, P., Ros-Lis, J.V. (2024). Solid-state microwave assisted batch and flow synthesis, and life cycle assessment, of titanium containing UMV-7 mesoporous silica. *Microporous and Mesoporous Materials*, 380, 113314.

Table of contents

List of Abbreviations

ANOVA	Analysis Of Variance
APTES	(3-Aminopropyl)triethoxysilane
AVERT	Avoided Emissions and Generation Tool
BE	Binding Energies
BET	Brunauer–Emmett–Teller (surface area measurement)
BJH	Barrett-Joyner-Halenda model (for adsorption)
COLIPA	European Cosmetic and Perfumery Association
CTABr	Cetyltrimethylammonium bromide
DIW	Deionized Water
DLS	Dynamic Light Scattering
DMSO	Dimethyl sulfoxide
EDX	Energy-Dispersive X-Ray
EISA	Evaporation-Induced Self-Assembly mechanism
EPA	Environmental Protection Agency
ESI	Electronic Supplementary Information
FDA	Food and Drug Administration
FESEM	Field Emission Scanning Electron Microscopy
FWHM	Full Width at Half Maximum
HMS	Hexagonal Mesporous Silica
HRTEM	High Resolution Transmission Electron Microscopy
IUPAC	International Union of Pure and Applied Chemistry
JRC	Joint Reseach Centre

LCA	Life Cycle Assessment
LCIA	Life Cycle Impact Assessment
LCT	Liquid-Crystal Templating Mechanism
MAS	Microwave Assisted Synthesis
MCM-X	Mobil Composition of Matter material
MOF	Metal Organic Framework
MSU-X	Michigan State University material
NC	Non-Calcined samples
NPs	Nanoparticles
OOPS	Oxide One-Pot Synthesis
PEG	Polyethylene Glycol
PEO	Polyethylene Oxide
PMMA	Polymethylmethacrylate
PPO	Polyphenol Oxidase
ROS	Reactive Oxygen Species
SBA-X	Santa Barbara Amorphous material
SD	Standard Deviation
SPF	Sunburn Protection Factor
SS	Solid-State
TEAH3	Triethanolamine
TEM	Transmission Electronic Microscopy
TEOS	Tetraethylortosilicate
TGA	Thermogravimetric Analysis

TMB	3,3',5,5'-Tetramethylbenzidine
UV	Ultraviolet
UVA	Ultraviolet A
UVM-X	University of Valencia Material
XPS	X-Ray Photoelectron Spectroscopy
XRD	X-Ray Powder Diffraction

Summary of the doctoral thesis

This doctoral thesis follows the format of a compilation of articles. It consists of an initial section that presents the general framework of the research and provides an introduction to the methodology to be used. Subsequently, a series of chapters related to the articles derived from this research are presented. Each chapter begins with an introduction to the corresponding article, explaining the motivation behind it. The articles themselves are then included. Specifically, this thesis comprises four empirical research articles that address the objectives of this doctoral study. The results of these studies have been disseminated within the academic community through publications in prestigious scientific journals.

OBJECTIVES

The main objective of this research is to develop and optimize energy-efficient synthesis methods for the production of mesoporous silica UVM-7, either pure or functionalized with cerium and titanium (UVM-7-Ce and UVM-7-Ti), using solid-state microwave technology, with a focus on scalability in both batch and flow systems. Additionally, the aim is to extend these methodologies to the synthesis of CeO_2 nanoparticles. Through systematic research, the thesis explores new methodologies to achieve efficient material synthesis by leveraging the advantages of solid-state microwave technology.

METHODOLOGY

Synthesis: Before starting the experiments, it is essential to calibrate the microwave in order to select the most suitable frequencies that maximize radiation absorption by the load, thereby avoiding losses due to reflection on the reactor walls or the return of energy to the antenna. For the scale-up of microwave-assisted synthesis, the process begins with the selection of optimal conditions for synthesis at the conventional scale using microwaves.

Once the system has been calibrated, various experimental tests are carried out by varying both the irradiation times and the applied power levels. After a thorough characterization of the materials obtained, the most suitable conditions are determined. Based on these, the scaling-up process begins, verifying that these conditions remain effective as the reaction volume increases. It is important to consider that the greater the load volume, the higher the energy required, which necessitates an increase in time and/or power.

For flow synthesis, the amount of energy applied is kept constant, but the volume of reactants is significantly increased. The mixture is introduced through tubes connected to a peristaltic pump, which continuously feeds the reactor in a downward-flow configuration designed to prevent accumulation within the system. Tests are carried out at different pumping speeds, as this determines the effective irradiation time for each fraction. Finally, various aliquots are collected and characterized to verify the homogeneity of the process or, if necessary, to discard the initial fractions until a steady-state regime is reached.

The characterization techniques used are:

- Powder X-ray diffraction (XRD): to determine the crystalline structure of the materials.
- Transmission electron microscopy (TEM): provides high-resolution images of the particles.
- Energy-dispersive X-ray spectroscopy (EDX): to determine the elemental composition of the material.
- Nitrogen adsorption (N_2 adsorption): to determine the porosity and surface area of the materials.
- Dynamic light scattering (DLS): to determine the hydrodynamic size of the materials.
- Zeta potential: to assess stability by studying the electrostatic repulsion or attraction between particles.
- Thermogravimetric analysis (TGA): determines the mass loss of a material by heating the sample.

Chapter 1

The first chapter of the thesis provides a detailed introduction, with special emphasis on microwave generators, which are the equipment used to carry out the experimental part of the work.

We focus on nanoparticles and nanomaterials. Their interest lies in their unique properties at the nanometric scale (1–100 nm), although this range may vary depending on the type of material. They are classified according to their dimensionality (from 0D to 3D) and can be synthesized using two approaches: top-down (reducing larger materials) and bottom-up (building from smaller units). Among the bottom-up methods, microwave-assisted synthesis stands out for accelerating key processes and will be the main approach of this thesis.

Electromagnetic radiation transmits energy in the form of waves through space and spans a wide spectrum of frequencies, from radio waves to gamma rays. Microwaves, which are part of this spectrum, lie between 300 MHz and 300 GHz. Microwaves are widely used in domestic, industrial, and scientific applications, especially at specific frequencies such as 2.45 GHz, due to their ability to effectively interact with polar molecules like water, generating heat through molecular friction.

The efficiency of microwave heating depends on how microwaves interact with materials, which is determined by their electrical properties. Materials such as metals reflect microwaves, others like glass transmit them, and absorbers, such as water, convert them into heat.

Unlike conventional heating, microwaves heat the interior of the material directly, accelerating processes and improving energy efficiency. They speed up the heating of materials whose conventional synthesis can take days, enabling them to be obtained in minutes or hours using microwaves.

Microwave generators are divided into two types:

- Electron-vacuum devices: Use vacuum tubes to generate or amplify microwaves, such as magnetrons (domestic) and gyrotrons (industrial).
- Solid-state devices: Use semiconductor materials.

Domestic microwave ovens use magnetron generators, which produce high-power microwaves at a fixed frequency but have limitations such as unpredictable heating patterns. Solid-state generators allow precise control of power and frequency, offering more uniform and efficient heating.

Regarding process scalability, the transition from laboratory to industrial scale faces challenges such as temperature gradients and mixing. Approaches to overcome these issues include the use of larger reactors and continuous procedures, which allow for more precise and efficient control. The use of microwaves in industrial synthesis improves energy efficiency and offers environmental and sustainability advantages.

Chapter 2

Chapter 2 sets out the main objectives of this research, focusing on the development and optimization of scalable and energy-efficient synthesis methods for the production of mesoporous silica, either pure or functionalized, using solid-state microwave technology. Additionally, it aims to extend these methods to the synthesis of CeO_2 nanoparticles.

Chapter 3

Chapter 3 explores the large-scale synthesis and production of UVM-7, based on previously successful methodologies for its preparation and functionalization.

The results obtained are published in the following article: “Scaled-up microwave-assisted batch and flow synthesis and life cycle assessment of a silica mesoporous material: UVM-7”, with reference: Benítez, M.; Rodríguez-Carrillo, C.; Sánchez-Artero, S.; El Haskouri, J.; Amorós, P.; Ros-Lis, J.V. *Green Chemistry* **2024**, *26*, 785-793.

UVM-7 (University of Valencia Material) is a porous silica-based material distinguished by its bimodal pore system, with smaller pores generated by the surfactant and larger pores formed by the aggregation of pseudo-spherical primary mesoporous nanoparticles. Our research group has been working with this material since its discovery, dedicating years to deepening its understanding and optimizing its properties. The latest advancement achieved was the synthesis of this material using solid-state microwave heating to reduce synthesis time, so we will continue developing this process

on a large scale. To the best of our knowledge, this is the first example of microwave-assisted flow synthesis for mesoporous silica materials.

The functionalization of mesoporous materials with different chemical groups is a key aspect after calcination, as it imparts the desired functionality to the solid for its application in various fields. Considering all the chemical groups that can be incorporated onto the surface using commercial trialkoxysilanes, the amine group is probably the most widely used to functionalize silica solids due to its ability to interact with proteins, metals, and certain gases. For this reason, APTES was selected as the target molecule to optimize microwave-assisted surface functionalization and to compare it with the modification obtained using the conventional methodology.

In the present work, we set the objective of achieving a scale factor of 100. The first approach to obtaining large quantities of material consists of continuing to work in batch mode by increasing the reactor size.

In batch mode, the material will be obtained after irradiation at 800 W for 12.5 minutes. The material obtained under these experimental conditions exhibits the typical characteristics of UVM-7. Low-angle X-ray diffraction shows a peak around 2° (2θ), corresponding to the (100) reflection of the hexagonal mesoporous structure. Additionally, a broad, lower-intensity signal is observed in the range of 3.5–4.0° (2θ), attributed to the overlapping (110) and (200) reflections of a hexagonal lattice.

TEM images reveal the characteristic structure of this type of material, composed of small mesoporous particles that cluster together, resulting in the formation of large textural pores between them. This morphology is

confirmed by the N_2 adsorption/desorption analysis, which shows a high specific surface area of approximately 956 $m^2 g^{-1}$ and a bimodal pore system with two well-defined adsorption steps.

To carry out the flow synthesis, two solutions were prepared: one containing the atrane complex and another with the water necessary for hydrolysis and condensation. Both solutions are mixed just before entering the microwave, where they are irradiated using the solid-state source. A power of 100 W and a residence time of 1 minute inside the oven were established. Samples of the prepared material were collected over 20 minutes in 4 fractions to compare homogeneity throughout the reaction time. There is a significant difference between the material generated in the first 5 minutes (FS-1) and the subsequent fractions. Compared to the material obtained through conventional UVM-7 synthesis, the FS-1 fraction shows a slight shift toward a higher angle (2.3°) in the X-ray diffraction, indicating a slightly smaller cell size.

Additionally, the TEM images show that FS-1 is composed of large mesoporous particles surrounded by smaller particles. This structure differs from the typical morphology of UVM-7, which is usually formed by aggregated small particles. It is likely that the reactor had not reached steady state during the first minutes, so this fraction should be discarded. The remaining fractions exhibit the typical characteristics of UVM-7. The textural properties of fractions FS-2 to FS-4 are consistent with those of UVM-7, and the variability throughout the synthesis is relatively low, reinforcing the idea that microwave-assisted flow synthesis is a suitable strategy for obtaining materials with homogeneous properties.

The scaled-up procedures, both in batch and flow, allow the synthesis of materials in less than 15 minutes, obtaining products with a topology similar to that achieved by conventional methodologies. The batch synthesis method would enable the preparation of more than 150 g of calcined material in just one hour, paving the way for its industrial application. Flow synthesis would allow the preparation of 82 g of material after calcination in one hour. Although this amount is lower than that of the scaled-up batch synthesis, it nonetheless opens the door to automated production of UVM-7 in large quantities.

For the functionalization with APTES, our goal in this case was to achieve a scale 50 times larger without increasing the reaction times. To obtain a more sustainable process and reduce the reaction volume, the concentrations of the reagents were tripled, maintaining a constant APTES:UVM-7 ratio. A power of 200 W was selected, and different irradiation times were used (up to 16 minutes). In just 4 minutes, TGA analysis revealed a high degree of functionalization, achieving the addition of 3.2 mmol of APTES per gram of silica on the surface of UVM-7, a value similar to the 3.6 mmol of APTES per gram of silica obtained through conventional synthesis. Extending the reaction time increased the organic content per gram of silica. However, we consider that, for most applications, the slight increase in loading does not justify the higher energy consumption and longer time in this synthesis process.

Functionalization is more complex than synthesis. Hydrolysis and condensation are fundamental processes in a homogeneous medium, whereas for functionalization we start with a solid, resulting in a heterogeneous phase reaction. For this reason, the equipment setup was

slightly different from that used in the synthesis stage. APTES and the material were added directly to the acetonitrile solution, so only a peristaltic pump was needed. Additionally, some adaptations were made to facilitate the flow of the material through the tubing. Although acetonitrile is a commonly used solvent for functionalization, attempts were made to increase the solution's viscosity to improve material transport by changing the solvent or mixing solvents, but the best results were obtained with acetonitrile, so we focused on modifying the system. Among these adaptations, the use of tubing with an appropriate internal diameter stands out—small enough to conduct the solution homogeneously, but large enough to prevent the material from clogging the tubing. The organic loading is 3.1 mmol of APTES per gram of silica, similar to that obtained in batch.

Considering a reaction time of 4 minutes, approximately 40 grams of UVM-7 could be functionalized in batch mode within one hour, while continuous functionalization produces 59 grams of functionalized material in one hour.

In summary, in less than one hour, it is possible to synthesize precursor material for over 150 g of calcined UVM-7 and functionalize up to 60 g.

Life Cycle Assessment (LCA) is a methodology that allows identifying the processes with the greatest environmental impact. Although at first glance one process may seem more sustainable than another, this methodology enables us to quantify and pinpoint the reagents or processes with the highest impact in order to attempt reducing it. In our case, the LCA has been applied to both scaled-up and non-scaled syntheses and functionalizations, as well as to conventional synthesis. The objective is to determine whether the

application of microwaves and scalability, in addition to reducing time, results in a variation in the environmental impact of UVM-7 synthesis and functionalization.

Large-scale synthesis offers a substantial reduction in environmental impact, with a fivefold decrease in equivalent CO_2 emissions compared to non-scaled synthesis, and up to half the emissions compared to conventional synthesis.

Chapter 4

This chapter explores the functionalization of UVM-7 with titanium and cerium using a one-step (one-pot) synthesis approach.

The results obtained are published in two different articles, one concerning Ti-UVM-7: "Solid-state microwave-assisted batch and flow synthesis, and life cycle assessment, of titanium containing UVM-7 mesoporous silica", with reference: Rodríguez-Carrillo, C.; Benítez, M.; González-Fernández, M.; De los Reyes, R.; Murcia, S.; El Haskouri, J.; Amorós, P.; Ros-Lis, J.V. *Microporous and Mesoporous Materials* **2024**, *380*, 113314. The other article that makes up this chapter concerns Ce-UVM-7: "Flow and Batch Minute-Made Synthesis of Ce-UVM-7 Using Microwave-Assisted Reaction: Scaling-Up, Optical and Catalytic Applications, and Impact Assessment" with reference: Rodríguez-Carrillo, C.; Benítez, M.; De los Reyes, R.; El Haskouri, J.; Amorós, P.; Ros-Lis, J.V. *ACS Sustainable Chem. Eng.* **2024**, *12*, 13208-13219.

In the previous chapter, we achieved the synthesis and post-functionalization of UVM-7 with APTES, all using solid-state microwave generators. In this chapter, we continue working with this mesoporous silica material, but this

time we aim to obtain in situ functionalization with titanium and cerium independently. To this end, a systematic study of the synthesis conditions at a small scale was first carried out. Different combinations of heating times and microwave powers were evaluated, as well as various molar ratios between the heteroelements (Si/Ti and Si/Ce). Subsequently, the obtained materials were characterized to identify those with the most favorable properties and, consequently, determine the optimal synthesis conditions.

The atrane method enables the incorporation of titanium and cerium into the mesoporous silica network. EDX analysis confirms the presence of both elements, showing a clear correlation between nominal and actual values: the greater the amount of heteroelement added, the higher the quantity detected by EDX. Additionally, an enrichment of both heteroelements is observed. This phenomenon is explained by the difference in solubility between the oxides, as SiO_2 is significantly more soluble than TiO_2 or CeO_2. After the hydrolysis of the atrane complexes, condensation reactions occur, during which oligomers interact with surfactant molecules, facilitating nucleation and growth of the Ti-UVM-7 particles. As the content of heteroelements in the pore walls increases, the regions enriched in titanium or cerium exhibit lower solubility than silica. Consequently, the enrichment in titanium and cerium can be attributed to a partial dissolution process of the silica.

X-ray diffraction (XRD) was also used at both low and high angles. At low angles, the characteristic silica peak around 2° (2θ), corresponding to the (100) plane, was identified, as well as a shoulder associated with the overlapping of the (110) and (200) planes, indicative of the typical hexagonal structure of mesoporous materials. At high angles, the analysis allowed the

determination of the presence or absence of crystalline domains of TiO_2 or CeO_2 in the synthesized materials. In the case of Ce-UVM-7 materials, when a molar ratio of Si/Ce = 8 was used, characteristic peaks of CeO_2 were observed, suggesting that cerium was not incorporated into the silica network. However, with a Si/Ce ratio of 25, these peaks were absent, indicating possible incorporation of cerium into the silica structure. For the Ti-UVM-7 materials, molar ratios of Si/Ti of 10, 25, and 50 were used, and in none of the cases were peaks corresponding to TiO_2 detected, suggesting that titanium can be incorporated into the silica network in significant amounts using this synthesis method.

UV-Visible absorption spectra of the materials were also measured, showing an increased content of Ti or Ce, evidenced by an increase in UV absorption at a wavelength of 200 nm for Ti-UVM-7 and around 300 nm for Ce-UVM-7, whereas undoped UVM-7 does not exhibit any absorption peaks. For Ti-UVM-7, Raman spectroscopy measurements were also conducted to confirm the absence of both rutile and anatase phases of titanium, indicating that titanium is predominantly dispersed within the matrix.

In all cases, the obtained isotherms exhibited two adsorption stages, one associated with mesopores and the other with macropores. The only exception was observed in the Ce-UVM-7 sample with a Si/Ce ratio of 8, where both adsorption stages were not detected. Additionally, this sample showed surface areas of approximately 300 m^2g^{-1}, significantly lower compared to the 700–800 m^2g^{-1} recorded in the other materials. This behavior can be attributed to pore saturation due to the presence of a high concentration of CeO_2 nanodomains. Furthermore, it was observed that longer irradiation

times lead to an increase in surface area, suggesting that the silica had more time to organize its structure, promoting greater porosity.

The images obtained by transmission electron microscopy (TEM) confirmed the presence of the UVM-7 type structure in all samples (both Ti-UVM-7 and Ce-UVM-7), showing a homogeneous distribution of mesopores throughout the material and the formation of larger macropores due to particle aggregation.

To evaluate the stability of the materials, zeta potential (ζ) measurements were carried out, obtaining values similar to those of the non-functionalized UVM-7, around -30 mV, in all cases. In the case of cerium, although the data were not included in the article, measurements showed even more positive values than those obtained for titanium. This behavior is attributed to the incorporation of titanium and cerium into the silica network, since, being elements with higher Lewis acidity compared to silicon, they promote the deprotonation of surface –OH groups. As a consequence, the negative surface charge is reduced, which decreases the electrostatic repulsion between particles and, therefore, the colloidal stability of the suspension.

With all this information, we can select the best synthesis conditions. In the case of cerium, performing a linear regression with the different variables shows that none of the variables are significant except for the Si/Ce ratio. As mentioned, the samples with Si/Ce = 8 were not properly Ce-UVM-7, while the rest were. In the case of Ti-UVM-7, the conditions hold true for all the Si/Ti ratios. Therefore, the different power and time settings we tested can be

considered valid, allowing us to say that we have obtained Ce-UVM-7 and Ti-UVM-7 in just 30 seconds.

It is observed that obtaining Ti-UVM-7 with different Si/Ti ratios is easier compared to the incorporation of cerium. This is because Ti^{4+} has a tetrahedral geometry, similar to that of Si^{4+}, whereas Ce^{4+} adopts an octahedral geometry. Consequently, the incorporation of titanium causes less distortion in the mesostructure compared to cerium, which facilitates its integration into the mesoporous silica network.

It is observed that obtaining Ti-UVM-7 with different Si/Ti ratios is easier compared to the incorporation of cerium. This is because Ti^{4+} has a tetrahedral geometry, similar to that of Si^{4+}, whereas Ce^{4+} adopts an octahedral geometry. Consequently, the incorporation of titanium causes less distortion in the mesostructure compared to cerium, which facilitates its integration into the mesoporous silica network.

Sunscreens commonly contain TiO_2 and ZnO nanoparticles, but their high refractive index leaves a whitish tone on the skin and, when exposed to UV radiation, they can generate radicals that damage cellular DNA. In contrast, CeO_2 offers strong UV absorption with greater transparency in visible light, although its high catalytic activity limits its use in cosmetics. For this reason, the UV absorption activity of the prepared materials was studied. A representative sample of Ti-UVM-7 and Ce-UVM-7 was evaluated and compared with commercial TiO_2 and CeO_2, as well as pure UVM-7. In the case of CeO_2, its incorporation into UVM-7 allowed achieving a Sun Protection Factor (SPF) of up to 69 with 20% material loading, outperforming pure CeO_2

and optimizing UV absorption without compromising transparency. On the other hand, TiO_2 in UVM-7 showed an SPF of up to 2.4 with 10% loading, being more efficient when considering only its titanium content. Additionally, the mesoporous matrix improved the stability and reduced the photocatalytic activity of TiO_2. These results highlight the potential of mesoporous silica for developing more effective and safer sunscreens.

Another study will be carried out with Ce-UVM-7. Cerium oxide possesses reactive oxygen species (ROS) scavenging properties, so it was investigated whether the Ce-UVM-7 materials exhibit similar activity. Compared to the peroxidase activity of CeO_2 synthesized by a microwave-assisted method in a study that will be presented in the next chapter, which showed a reaction rate of 8×10^{-3} min^{-1}, an analogous result was obtained for materials prepared in batch with a Si/Ce molar ratio of 8. However, samples with lower cerium content demonstrated higher activity, with reaction rates of 23×10^{-3} and 27×10^{-3} min^{-1} under batch and flow conditions, respectively. The formation of CeO_2 aggregates in materials with Si/Ce = 8 could reduce the exposure of cerium atoms to reactants. The mesoporous network facilitates access to active sites and prevents undesired growth of metallic nanoparticles. The similarity in the activity of materials produced under both batch and flow conditions aligns with their structural characteristics, confirming that the flow synthesis approach allows obtaining Ce-UVM-7 materials with properties comparable to those obtained by batch synthesis.

As done in the previous chapter, a Life Cycle Assessment (LCA) was carried out to evaluate the environmental impact of the material. In this study, in addition to confirming that the reaction can be effectively scaled in batch and adapted

to flow synthesis without altering the typical UVM-7 topology, the production of hundreds of grams of material was achieved. Moreover, the Life Cycle Assessment showed a reduced impact, with values of 8 and 10 points in the LCA per kg of Ce-UVM-7 and Ti-UVM-7, respectively, a result that could be further optimized at the industrial level or through modifications in the reactants. These findings are consistent with those obtained in previous studies, reaffirming the viability of the process from both a synthetic and environmental perspective.

Chapter 5

The final chapter expands the research beyond mesoporous silica materials, focusing on the synthesis of inorganic metal oxides using solid-state microwave generators. CeO_2 is selected as a model material due to its wide-ranging applications in catalysis, energy storage, and environmental remediation.

The results obtained are published in the article “Batch and Flow Synthesis of CeO_2 Nanomaterials Using Solid-State Microwave Generators” with reference: Rodríguez-Carrillo, C.; Torres-García, J.; Benítez, M.; El Haskouri, J.; Amorós, P.; Ros-Lis, J. V. *Molecules* **2022**, *27*, 2712. In this work, we present the optimization of synthetic conditions for the preparation of CeO_2 using solid-state microwave generators.

Despite its excellent catalytic activity, cerium oxide had not previously been prepared using solid-state generators nor by microwave-assisted flow synthesis.

For the batch synthesis, cerium acetate and sodium hydroxide were dissolved in a molar ratio of 1:4 in deionized water. The solution was then transferred to a microwave-compatible glass vial, which was placed inside the microwave oven for processing. Different power and time settings were tested: 50 W for 2 minutes and 30 seconds, 100 W for 1 minute, and 200 W for 30 seconds, with experiments conducted at pH 11 and pH 12. As expected, increasing the power reduced the time required to obtain the product. Afterwards, the samples were washed with water and ethanol until neutral pH was reached, then dried and calcined at 800°C.

The materials were characterized by X-ray diffraction (XRD), and all samples exhibited the peaks of CeO_2 with a fluorite-type cubic structure. The most intense peaks, located at 2θ angles of 28.7°, 47.6°, and 56.5°, correspond to the crystallographic planes (111), (220), and (311), respectively, with no peaks associated with Ce_2O_3 detected. The XRD analysis of the other samples showed peaks at the same positions and similar full width at half maximum (FWHM), indicating that under the experimental conditions used, the crystalline phase formed and the degree of crystallinity of the materials were comparable. The non-calcined material was also characterized, revealing characteristic peaks of CeO_2. This result suggests that rapid microwave treatment is sufficient to obtain cerium oxide (IV) with a crystalline structure. However, the FWHM was significantly larger compared to the calcined materials, indicating lower crystallinity or smaller particle size.

The materials consisted of individual particles along with aggregates of irregularly shaped CeO_2 nanoparticles, with an average size of 40 nm and a

distribution ranging from 20 to 60 nm. At the lower pH of 11, the particles were statistically larger than those at pH 12, indicating greater growth, while the power had minimal effect on particle size.

Regarding the effect of calcination on the material's morphology, unlike the calcined materials (which exhibited dense and well-defined particles) the material obtained directly from the microwave reactor was primarily composed of much smaller nanoparticles (~4 nm). These primary nanoparticles consolidated during the high-temperature treatment to form the final particles. As expected, in a homogeneous environment with rapid microwave heating, the material began forming from small primary nanoparticles (~4 nm or even smaller). These nanoparticles gradually joined and fused, resulting in larger crystalline particles after the calcination process.

For the flow synthesis, the fastest condition (200W for 30 seconds) at pH 12 was selected due to the similarity of the materials obtained in batch. The results from the characterization of the materials were similar, confirming that flow synthesis is a viable methodology for the production of CeO_2 nanoparticles.

To evaluate the catalytic properties, peroxidase-like activity was measured. This enzyme decomposes hydrogen peroxide, using it to oxidize other substrates; in this case, 3,3',5,5'-tetramethylbenzidine (TMB), which is colorless but turns blue when oxidized. The appearance of this blue color indicates that the reaction is taking place, reflecting significant peroxidase activity. In our study, all materials produced the blue color, corresponding to high peroxidase-like activity.

CONCLUSIONS

In conclusion, the scaling up of the synthesis of mesoporous silica UVM-7 has been successfully achieved under both batch and flow conditions, as well as its one-pot functionalization with titanium and cerium, and post-functionalization with amine groups. This demonstrates that microwave technology is not only effective for synthesis but also for advanced functionalization processes. Additionally, the synthesis and scaling of cerium oxide using microwave generators has been achieved for the first time, representing a significant advance in the development of faster, more efficient, and sustainable methodologies. These results position microwave heating as a key tool for the design and large-scale production of high-value functional materials.

Chapter 1:

Introduction

1.1. Nanomaterials: A brief overview

Long before microscopes or modern science, nanoparticles and nanomaterials were already shaping the universe. Emerging from the earliest moments after the Big Bang, they have been formed through cosmic events such as stellar explosions and planetary evolution. Although they have only recently been studied in detail, these nanoscale structures have always been essential building blocks of matter throughout the cosmos.[1]

Nanomaterials (NMs) have long held significant importance due to their unique properties compared to their larger-scale materials,[2] which is evident in the wide variety of definitions provided by different organizations, institutions, governments, and industries.[3] The International Organization for Standardization defines nanomaterial as "material with any external dimension in the nanoscale or having an internal structure or surface in the nanoscale" defining nanoscale from 1 nm to 100 nm.[4] However, in some cases, this range has been extended below 1 nm (such as in the case of fullerenes and graphene) or beyond 100 nm, as seen with certain aggregates and agglomerates, which are held together by weak, easily breakable bonds.[5] Beyond their nanoscale size, nanoparticles can also be classified according to their dimensionality (Figure 1.1.a), encompassing structures that range from zero-dimensional (0D) to three-dimensional (3D) forms.[6]

There are two synthetic approaches (Figure 1.1.b): the top-down procedure, where small shapes are formed from larger materials using techniques like lithography, ablation, and electrochemical methods. In contrast, bottom-up

procedures build nanostructures from tiny units through processes like self-assembly, microwave treatment, and hydrothermal methods.[2]

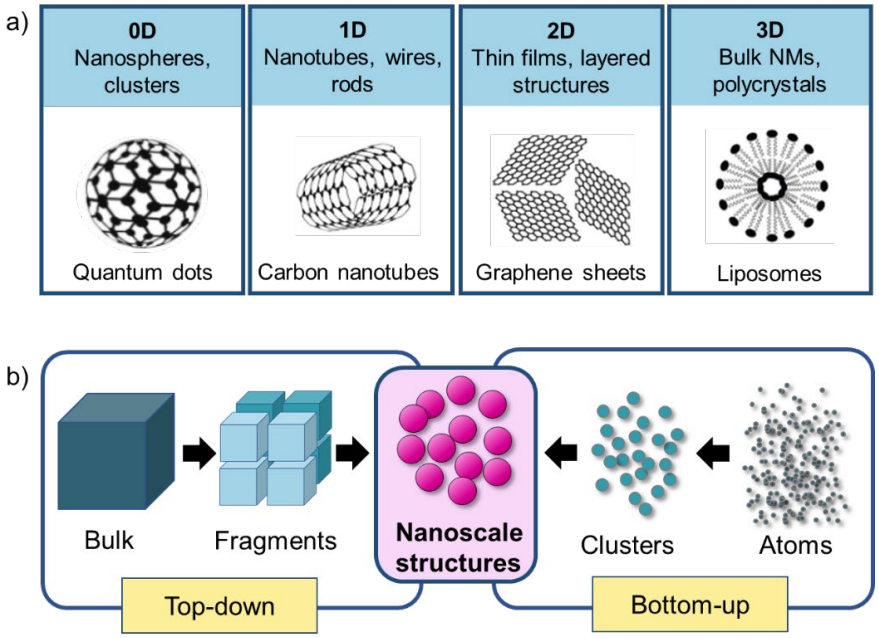

***Figure 1.1**. a) Nanomaterial's classification based on dimensionality. Adapted from reference.[7] b) Top-down and bottom-up procedures for the synthesis of nanoparticles.[8]*

The most commonly employed methods are bottom-up approaches, as they offer greater control over the size and morphology of the particles. In contrast, top-down methods typically result in particles with more irregular shapes and less uniform size distributions.[9]

As previously mentioned, one of the bottom-up approaches is the microwave-assisted method. This type of radiation accelerates key processes such as gel formation and promotes the creation of supersaturated solutions due to the rapid decomposition of precursors, leading to fast nucleation.[10,11] This

doctoral dissertation will center on this technique; consequently, the subsequent sections will present a comprehensive overview of microwave radiation, aiming to establish a solid conceptual foundation for the subject under investigation.

1.2. Electromagnetic radiation: Microwaves

Electromagnetic radiation transmits energy and propagates through space in form of waves. The entire range of frequencies that constitute this radiation is collectively known as the electromagnetic spectrum (Figure 1.2). This spectrum is categorized based on the wavelengths and corresponding frequencies, ranging from radio waves at the low-frequency end to gamma rays at the high-frequency end.[12]

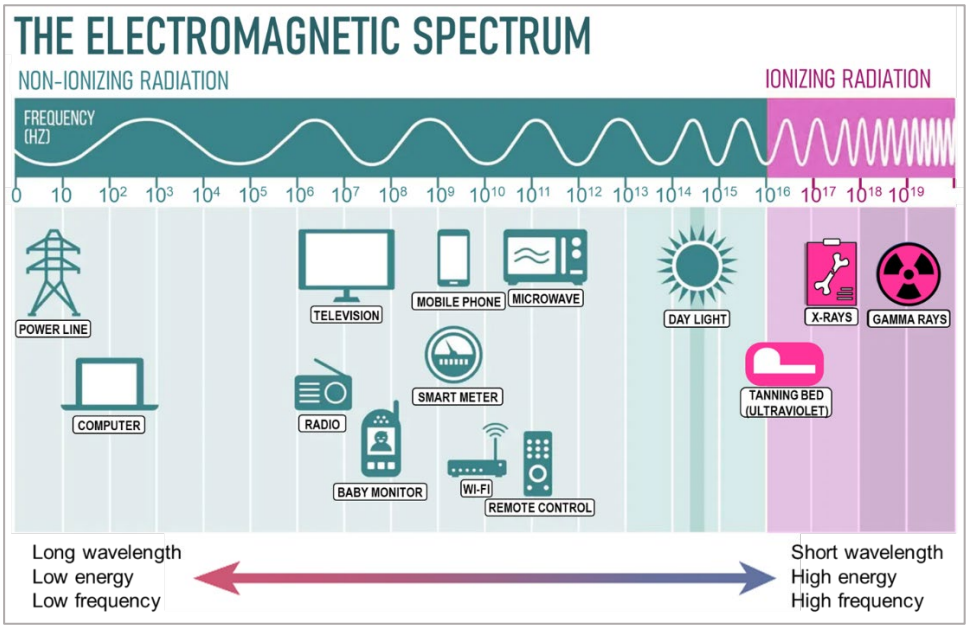

***Figure 1.2**. The electromagnetic spectrum.*[13]

The rapid advancement of radio technology in the early 1900s was primarily limited to the High Frequency (HF) and Very High Frequency (VHF) ranges due to the lack of reliable microwave sources and associated components. It was not until the 1940s, spurred by radar development during World War II, that significant focus was directed toward microwave theory and technology. Following the arrival of radar, microwave-based communication systems emerged, using the research originally done for radar.[14] The discovery of microwave heating is attributed to the american engineer Percy Spencer.[15] At that time, he was engaged in radar technology development during World War II, working with a magnetron, a device that converts electrical energy into high-frequency electromagnetic waves. During a routine day at the laboratory, Spencer noticed that a chocolate bar he had in his pocket had melted, an effect caused by exposure to microwave radiation emitted by the radar equipment. This serendipitous observation prompted him to systematically investigate the thermal effects of microwave radiation on different materials, ultimately leading to the development of the first microwave oven. His scientific curiosity and keen observational skills catalyzed the emergence of a transformative technology in the field of thermal processing.[16]

Microwaves are a type of electromagnetic radiation in the range of 300 MHz to 300 GHz, corresponding to a wavelength from 10 cm to 1mm.[14] This energy is characterized by its ability to transmit data, heat objects, and interact with materials in ways that are useful for various applications.[17] However, microwave heating systems are generally confined to specific frequencies within the industrial, scientific, and medical (ISM) band.[18,19]

The frequency of a microwave refers to the rate at which the electromagnetic waves oscillate. The most commonly used frequency is 2450 MHz for commercial, domestic, and industrial applications across most countries because it offers adequate penetration depth,[20] while for industrial purposes, the frequencies are 896 MHz (in the UK) and 915 MHz (in the Americas and China) (Figure 1.3.).[19] In most household microwave ovens, this frequency is 2.45 GHz, meaning the electromagnetic field alternates direction 2.45 billion times per second.

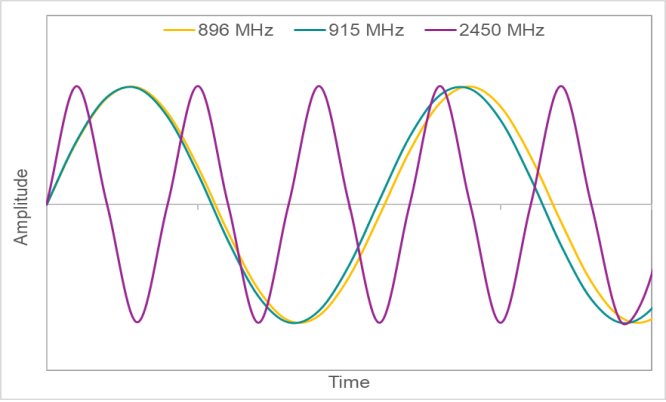

***Figure 1.3**. Sinusoidal waves representing different microwave frequencies.*

This specific frequency is chosen because it interacts efficiently with polar molecules, such as water, which are present in most foods. The oscillating electric field causes these polar molecules to continuously reorient themselves to align with the field, creating molecular friction. This friction results in the generation of thermal energy, which is responsible for heating the food.[21,22]

Another important consideration is related to the wavelength and the size of the resonant cavity and antenna that will be used. The relationship between frequency (f) and wavelength (λ) is given by the equation $\lambda = c/f$, where c is the speed of light in a vacuum.[23] As a result, at lower frequencies, the wavelength becomes longer, and therefore the resonant cavity must have larger dimensions to effectively resonate with the electromagnetic waves. Similarly, antenna dimensions are also related to the wavelength, and at lower frequencies, where the wavelength is longer, larger antennas are required. Conversely, at higher frequencies, the wavelength becomes shorter, allowing for smaller cavities and antennas while still achieving high gain, which is advantageous in compact system designs.[14] This concept was demonstrated by S. P. Yeong, who conducted experiments to test water heating using 2.45 GHz and 915 MHz microwaves. The study showed that the 2.45 GHz microwave effectively heats the water, while the 915 MHz microwave fails to heat the water due to the weak electric field distribution in the microwave cavity (Figure 1.4.).[24]

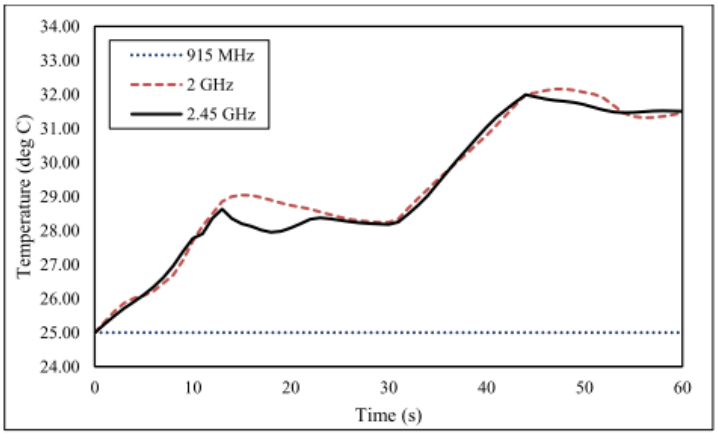

Figure 1.4. *Temperature variation of water heated at different frequencies.*[24]

1.3. Interaction of microwaves with materials

The interaction of microwaves with different materials is a crucial aspect in material synthesis using this technology. When a wave travels from the generator to a load, if the load impedance is not “matched” there is also reflected wave from the load back to the generator.[25] A high load impedance within a microwave oven indicates that the material or object placed inside offers significant opposition to the absorption of microwave energy.[26] The target is to have it as low as possible to avoid failures, but also, to maximize efficiency in energy transfer.

This condition typically arises when the load consists of materials with low dielectric loss, such as dry ceramics, plastics, glasses or an empty cavity, resulting in minimal interaction with the electromagnetic field. Consequently, a substantial portion of the microwave energy is reflected back toward the magnetron rather than being absorbed by the load, which not only reduces heating efficiency but may also pose a risk of damage to the microwave generator due to sustained power reflections.[27]

Microwaves interact differently with different types of materials based on their electrical and magnetic properties, which influences the heating and efficiency of the synthesis process,[28] for example polar molecules tend to absorb microwave radiation more effectively than non-polar molecules,[29] because they get polarize more easily in the presence of an external applied field.[25,30]

When microwaves interact with a material, the incident energy can undergo three primary processes: reflection, absorption and transmission.[30] Based on these interactions, materials can be classified as (Figure 1.5.):

- Transparent: they have low dielectric loss,[31] and allow microwaves to pass through them with minimal absorption, like glass, plastics or ceramics.
- Opaque or reflective: most notably metals, they do not allow microwaves to penetrate and instead reflect the energy back, often leading to interference patterns or even damage to the microwave source if improperly used.
- Absorbent: they have high dielectric loss,[31] and interact strongly with microwave fields, efficiently absorbing the energy and converting it into thermal energy. Polar liquids, such as water and alcohols, along with solutions containing dissolved ions, display varying degrees of microwave absorption.[22]

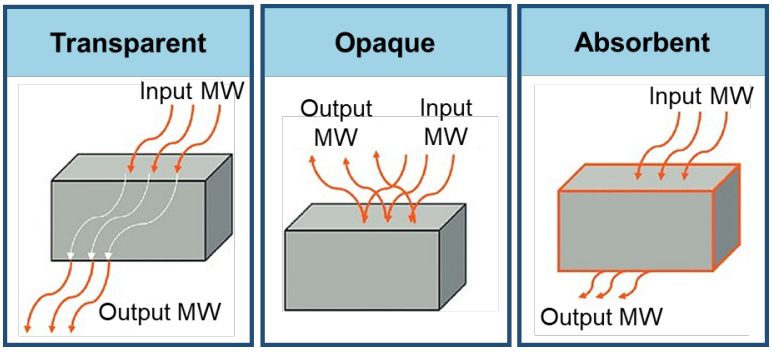

Figure 1.5. *Different interactions of materials with microwaves.*[32]

For optimal energy transfer and thermal performance, it is essential that the load impedance is appropriately matched to the system's output impedance, thereby minimizing reflection and maximizing absorption.

In light of this, microwave ovens are constructed using materials selected for their specific interactions with radiation. The internal cavity is typically made of a reflective metal, such as stainless steel or coated steel, which ensures that microwaves are contained and uniformly distributed within the oven. The door includes a transparent glass or plastic window combined with a metal mesh; while the glass or plastic is generally transparent to microwaves, the fine metal mesh reflects them, preventing leakage and ensuring user safety. Components inside the oven are carefully shielded, with reflective materials enclosing areas where microwave containment is essential, while non-metallic, microwave-transparent materials are used in areas that require wave transmission, such as turntable supports or sensor housings.[21]

1.4. Evolution of synthesis using microwave generators

In contrast to conventional heating techniques (conduction and convection techniques) microwaves heat substances by delivering energy directly into the bulk of the material, making the heating process much faster (Figure 1.6.).[24,33] Due to this faster and more direct transfer of energy into the material, reaction times are reduced and energy efficiency is improved, which has led to the increasingly widespread use of such equipment for material synthesis.

The first documented paper on microwave-assisted synthesis was published in 1985 by Komarneni and Roy, titled "Titania gel spheres by a new sol-gel process" in *Materials Letters*.[35]

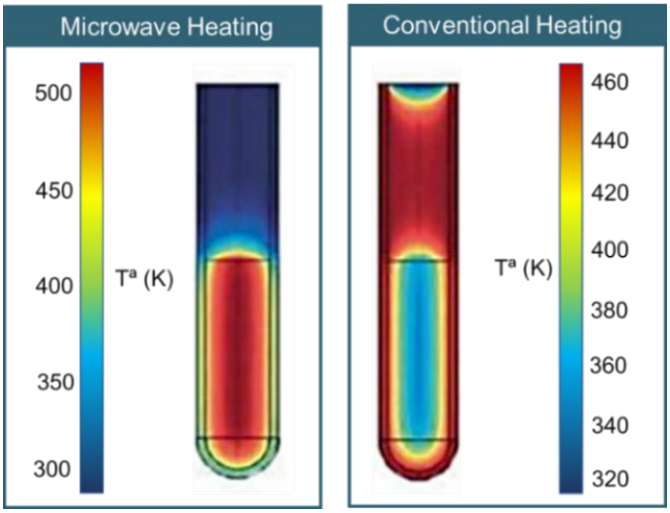

Figure 1.6. *Differences between conventional heating and microwave heating.*[34]

However, it was in 1986 when Gedye and Giguère published “The Use Of Microwave Ovens For Rapid Organic Synthesis”[36] and "Application of Commercial Microwave Ovens to Organic Synthesis"[37] respectively in *Tetrahedron Letters*, which are often credited for introducing microwave-assisted synthesis due to its explicit focus on the use of household microwave ovens to accelerate organic reactions.[38] These publications played an essential role in initiating widespread interest in microwave-assisted synthesis and laid the foundation for the development of microwave chemistry as a recognized subfield.

Initial experiments involved carrying out reactions in Teflon or glass containers using standard household microwave ovens, without any means of monitoring temperature or pressure. As a result, the uncontrolled rapid heating of organic solvents occasionally led to hazardous explosions.[39]

Numerous improvements have been implemented to enhance the usability and safety of microwave synthesis equipment, including the adoption of sealed reactor systems capable of operating at elevated pressures, which made it possible to overcome the boiling point of the solvent under irradiation.[40] Another improvement is that modern laboratory microwave equipment incorporates precise control of temperature, pressure and agitation, and even programming of sequential thermal steps. By combining the advantages of rapid microwave heating with the controlled conditions provided by sealed vessels, this technique has become increasingly preferred and is expected to become the standard for laboratory-scale microwave-assisted synthesis.

Since its initial application, microwave-assisted synthesis has evolved into a highly effective approach for producing a wide variety of materials. Among the most prominent are inorganic materials, including metallic nanoparticles like Au, Ag or Pt;[41] metal oxides such as TiO_2,[42] ZnO[43] and Fe_2O_3,[44] as well as complex oxides like $BaTiO_3$[45] or ferrites ($NiFe_2O_4$,[46] $CoFe_2O_4$)[47]. Furthermore, it has been successfully applied to synthesize metal sulphide nanostructures, including PbS,[48] CuS, Fe_2S and ZnS.[49] In addition to inorganic compounds, the approach has been extended to the synthesis of carbon-based nanomaterial, such as graphene and its composites.[50]

Among the materials of greatest interest within the framework of this thesis are mesoporous materials, due to their unique structural properties and broad applicability. Included in this group are metal organic frameworks (MOFs),[51] covalent organic frameworks (COFs)[52] and mesoporous silicas, which will be the main focus of this study. The main challenge with these

materials lies in the fact that, under conventional hydrothermal heating, synthesis typically requires several hours or even days, whereas microwave-assisted methods can achieve comparable results in just minutes or a few hours.

The first patent for the application of microwave heating in the synthesis of zeolites was filed in 1988, as shown in the timeline in Figure 1.7.[53] Curtis Conner and colleagues conducted a comprehensive survey of the advances achieved through the use of this type of generators in zeolites.[54] A notable improvement was observed in the synthesis time of Na-A zeolite, which could be obtained at 250 W within just 10 minutes,[55] being the crystallization time 10 times lower than in conventional hydrothermal synthesis.[53] Similarly, Y-zeolite was synthesized in as little as 30 seconds at 120 °C. In contrast, more structurally complex zeolites such as ZSM-5 required more specific conditions and additional processing steps, including a staged treatment at 160°C for 1 minute followed by 30 minutes at 140°C.[56]

This breakthrough catalyzed the synthesis of other types of mesoporous materials. The first reported synthesis of mesoporous silica using microwave heating occurred in 1996, during the preparation of MCM-41. This represented a significant advancement, reducing the traditional heating process at 100°C over several days to a much shorter treatment involving an initial heating at 160°C for one minute, followed by 80 minutes at 150°C.[57] This was followed by the synthesis of other mesoporous materials, including MCM-48 (reduced from 4 days under conventional hydrothermal treatment to 2h),[58] SBA-15 (reduced from 48h to 2h)[59], and FDU-1 (from 24h to 30 min).[60]

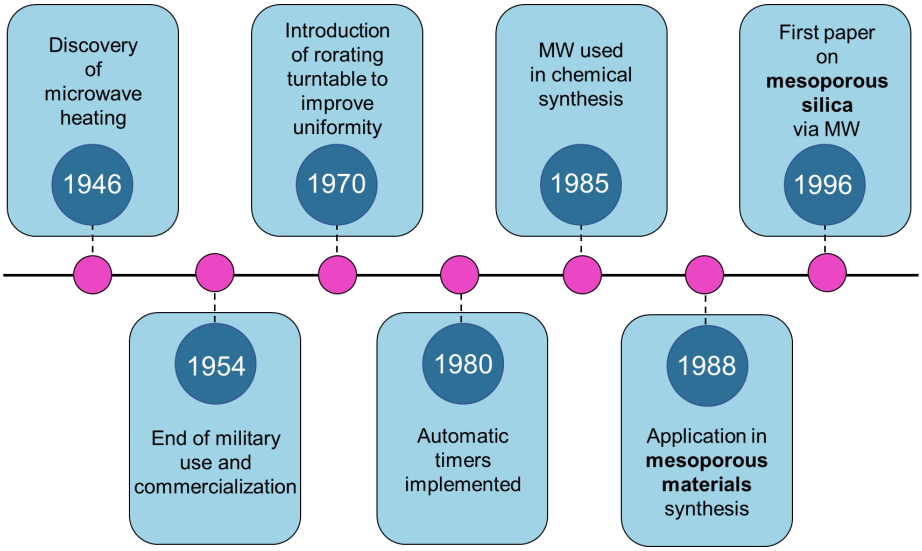

***Figure 1.7**. Timeline of microwave technology in chemical synthesis.*

1.5. Different types of microwave generators

They are divided in two categories: electro-vacuum microwave devices and semiconductor or solid-state microwave devices. The type of generator employed depends on the specific application for which it is intended. Below, we present the main types of microwave generators.

1.5.1. Electro-vacuum microwave devices

Vacuum tube is an electronic device that controls the flow of electrons in vacuum, and it is used to generate (oscillators) or amplify (amplifiers) microwave power at microwave frequency range.[61]

Examples of oscillators include:

- **Magnetrons:** they are used for domestic applications.[62a] They generate microwaves through the interaction of electron streams with magnetic fields. In a magnetron, electrons are emitted from a heated cathode and are influenced by a perpendicular magnetic field, causing them to spiral outward rather than travel directly to the anode. Surrounding the cathode are a series of resonant cavities (Figure 1.8.). As electrons spiral past these cavities, they induce oscillations in the electromagnetic fields, building up microwave energy within the structure.[25]

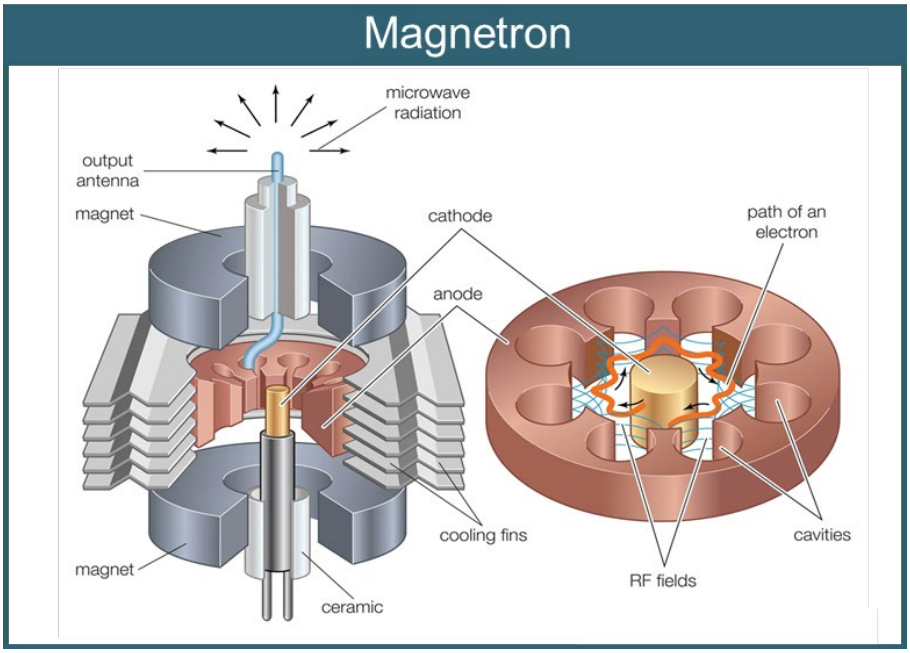

Figure 1.8. *Magnetron diagram. Image data: Encyclopædia Britannica.*[62b]

- **Gyrotrons:** they are employed in advanced industrial applications, including plasma heating in nuclear fusion reactors. In a gyrotron, a beam of electrons is emitted from a cathode and accelerated into a region with a strong axial magnetic field (Figure 1.9.). Instead of moving linearly, the electrons spiral around the magnetic field lines at their natural cyclotron frequency. As they travel, they interact with a resonant cavity or waveguide mode, transferring energy from their rotational motion to electromagnetic waves.[63,64]

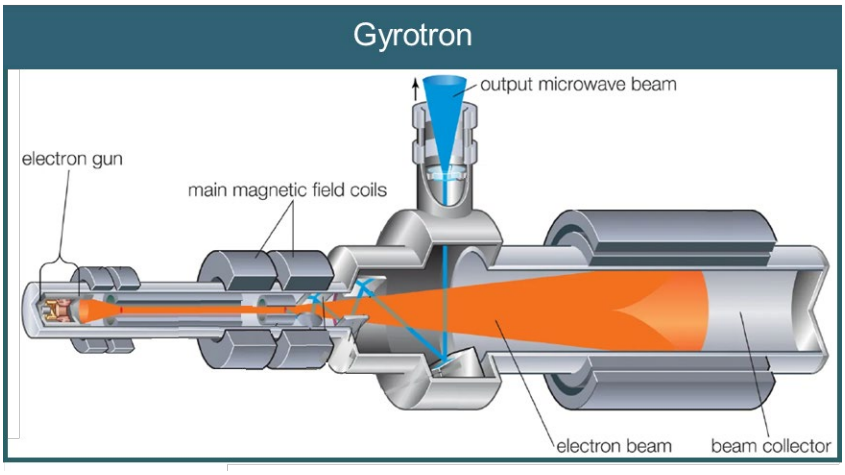

Figure 1.9. *Gyrotron diagram. Image data: Encyclopædia Britannica.* [62b]

Conversely, amplifiers are employed to enhance the microwave signal. The most commonly utilized types are as follows:

- **Traveling Wave Tubes (TWTs):** they are used for radar systems and satellites. They amplify microwave signals by continuously transferring energy from an electron beam to a traveling radio-frequency wave.[65] As the electrons move along the tube, they interact with the oscillating

electric field of the traveling wave, gradually bunching together and transferring part of their kinetic energy to the wave (Figure 1.10.).

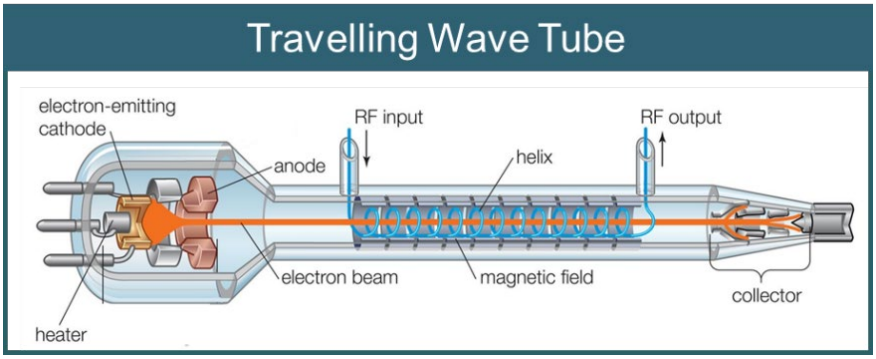

Figure 1.10. *Travelling wave tube diagram. Image credit: Encyclopædia Britannica.* [62b]

- **Klystrons:** they are used for high-power scientific and industrial applications, such as particle accelerators.[62a] They amplify microwave signals by manipulating the velocity of an electron beam. Initially, electrons are emitted and accelerated along a vacuum tube toward a series of resonant cavities (Figure 1.11.). As the electron beam passes through cavities, the incoming microwave signal creates an oscillating electric field that causes some electrons to speed up and others to slow down, resulting in the formation of dense clusters, or "bunches", of electrons.[66] As the tightly grouped electrons pass through this field, they transfer their kinetic energy to the microwave signal, thereby amplifying it.[67]

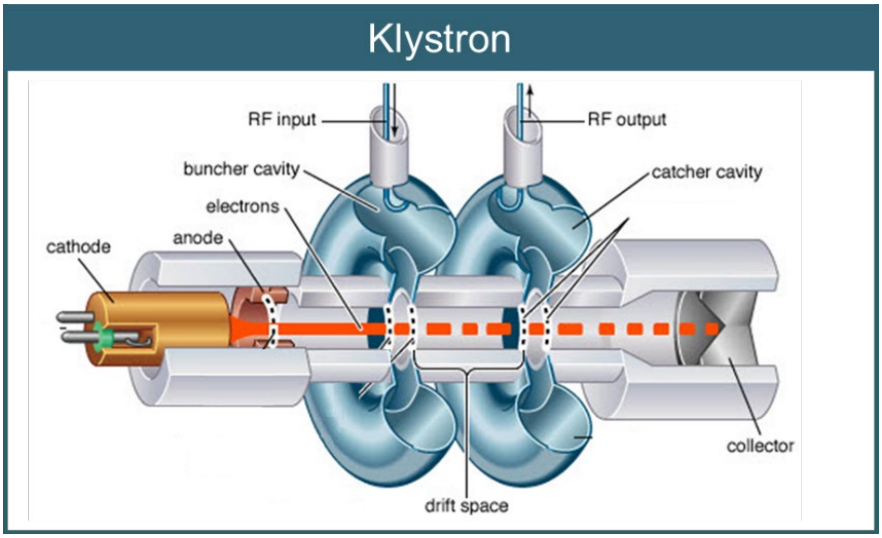

Figure 1.11. *Klystron diagram. Image credit: Encyclopædia Britannica.* [62b]

1.5.2. Solid-state or semiconductor microwave devices

In the other hand, solid-state microwave devices operate by controlling the movement of charge carriers, primarily electrons, within semiconductor materials such as silicon, gallium arsenide, or gallium nitride. Unlike vacuum tubes, where electrons travel freely through a vacuum, in solid-state devices electrons move through a crystalline lattice, interacting with the material's electric fields to generate, amplify, or modulate microwave signals.

Generally, these devices fall into two main categories: diodes and transistors.

- Diodes (such as Gunn, IMPATT, TRAPATT, and BARITT) take advantage of physical phenomena like negative differential resistance, avalanche breakdown, or carrier transit-time effects to produce microwave oscillations. For example the Gunn effect, which consists of applying a constant voltage to a gallium arsenide crystal to produce microwave

radiation.[68] Some are primarily used as signal generators, while others serve as amplifiers.

- Transistors (such as MESFETs and HEMTs) are widely used for amplifying microwave signals by controlling the current flow between terminals in response to an input signal.[69]

In addition, Monolithic Microwave Integrated Circuits (MMICs) combine multiple active and passive microwave components onto a single chip, offering compact and high-performance solutions for advanced communication and radar systems.[70]

Together, these solid-state technologies enable efficient, compact, and robust generation and amplification of microwave signals across a wide range of applications.[71] Table 1.1 outlines the differences among the different types of microwave generators.

Table 1.1. *Differences Among Microwave Generators*

Generator	Power Level	Typical Frequency	Common Applications
Solid-State Generator	Low to medium	0.9–6 GHz	Medical devices, laboratory use, precision industrial heating
Magnetron	Medium	~2.45 GHz	Domestic microwaves, food processing, basic industrial heating
Gyrotron	Very high	>30 GHz	Plasma heating in nuclear fusion, advanced materials processing
TWT	Medium	Broad range	Satellite communications, radar, research
Klystron	High	Variable	Particle accelerators, scientific research

Vacuum electronic devices are capable of generating significantly higher power levels at elevated frequencies compared to semiconductor-based devices due to the significantly greater electron mobility in vacuum. In contrast, limited electron mobility in semiconductor devices causes severe transit time effects at high frequencies. To reduce these problems, the devices must be made smaller, but that also lowers how much power they can handle. Vacuum tubes, unaffected by such mobility constraints, can operate efficiently at high power levels even as frequency increases.[61,63]

1.6. Why solid-state generators?

Microwave ovens commonly used in domestic settings are typically equipped with magnetron-type generators. These devices have been widely adopted due to their ability to efficiently produce high-power microwave radiation at a fixed frequency suitable for heating applications.[25] In the following section, we will examine the reasons behind the selection of this particular technology for household microwave generation.

The main difference between conventional and solid-state microwave systems for the user is the complexity of operation. Conventional systems are simpler to use; users only need to set the desired power and time. In contrast, solid-state systems are more complex, offering not only the ability to adjust power and time but also frequencies and phases. This ability to control more parameters makes solid-state systems more precise in their operation. Focusing on the ability to adjust power, one of the key advantages of solid-state generators is their capacity for precise and continuous control over the power output. One of their main limitations of conventional generators is the

tendency to produce unpredictable heating patterns in food due to their broad and randomly distributed frequency spectrum.[72] They offer a limited range of pre-set power levels (typically between 400W and 1000W depending on the model) solid-state systems allow users to select specific power values. In domestic microwave ovens, they operate through on-off cycles, where microwaves are either fully generated or completely paused to simulate lower power, resulting in intermittent periods without microwave emission leading to fluctuations in energy delivery.[53] This pulsed operation can lead to uneven energy delivery and slower heating rates. In contrast, solid-state microwave generators provide continuous and stable irradiation throughout the entire operating time. They provide direct and stable control across the full power range, from 0W up to the maximum output of the device. This consistent energy input leads to more efficient coupling with the material and enables a faster and more uniform temperature increase.[73] These variations make it hard to control heating patterns in food, limiting its heating homogeneity (Figure 1.12.). In contrast, solid-state g enerators c an produce microwaves within a much narrower and more stable frequency range, enabling more precise and predictable heating.[74a]

Magnetron-based microwave systems typically use rigid metallic waveguides to direct energy, which limits flexibility in system design (Figure 1.12.). In contrast, solid-state microwave systems utilize coaxial cables transmitting the microwave signal to the antennas, offering greater flexibility in positioning the microwave entry points within the cavity.

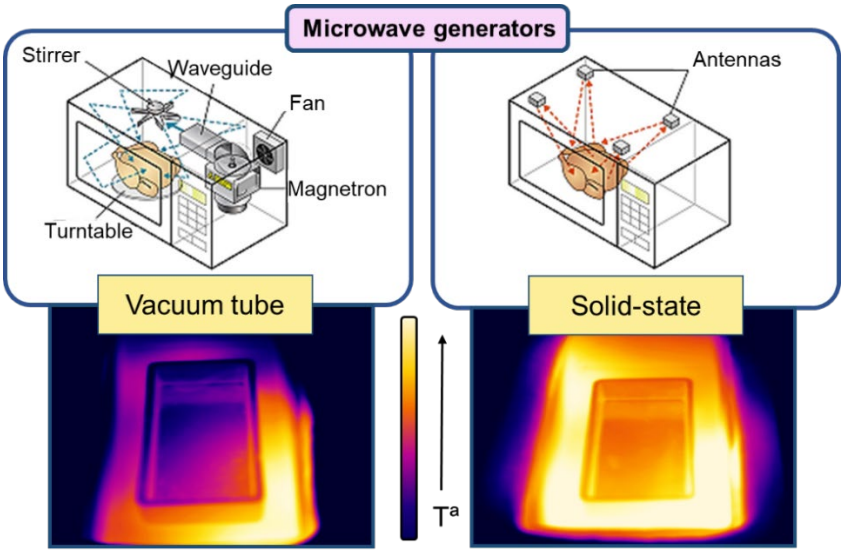

Figure 1.12. *Comparison between conventional and solid-state microwave systems. Adapted from reference [74b]. Thermal mapping using thermographic imaging of a cresol heated by magnetron and solid-state microwave generators.*

This enables more precise control over heating patterns and system configuration. Additionally, coaxial cables transmit signals in the gigahertz range with minimal signal loss, making them an efficient and adaptable alternative for applications requiring frequency agility and spatial versatility.[75]

Furthermore, conventional systems exhibit dispersion of energy, while solid-state systems allow focused delivery, with all the radiation being directed precisely into the load. This focused irradiation not only increases efficiency but also enhances durability, as it prevents the microwaves from reflecting back toward the antennas, something that is more likely to happen in conventional systems.[21]

In conclusion, solid-state microwave systems are more promising than magnetron-based ones due to their greater precision, adaptability, and simpler, more efficient design. Their ability to focus energy directly into the load, with minimal loss, makes them better suited for advanced applications where control and reliability are essential.

1.7. Importance of microwave generators

The microwave generator market is on a solid growth trajectory, with a consistent annual increase, indicating a healthy and expanding industry. As of 2024, the global market for microwave devices is experiencing notable growth driven by several key factors. The market was valued at approximately $11.26 billion in 2024 and is projected to continue expanding at a compound annual growth rate (CAGR) of 5.3% through 2035, potentially reaching around $17.91 billion by the end of this period.[76] This significant growth indicates a rising demand for microwave generators, likely driven by technological advancements, increased industrial applications, and broader adoption of microwave technologies across various sectors. This aligns with the number of scientific works publicated per year about microwave generators, and more specifically, on the use of these generators for chemical synthesis, which is the subject of our present study (Figure 1.13.).

Microwave energy has been demonstrated to be both effective and efficient for thermal applications across a range of environments, including industrial and domestic settings.[17] Furthermore, microwaves are recognized as a significant energy source for facilitating chemical reactions and synthesis

processes,[59] given that numerous molecular, atomic, and nuclear resonances occur at microwave frequencies.[14]

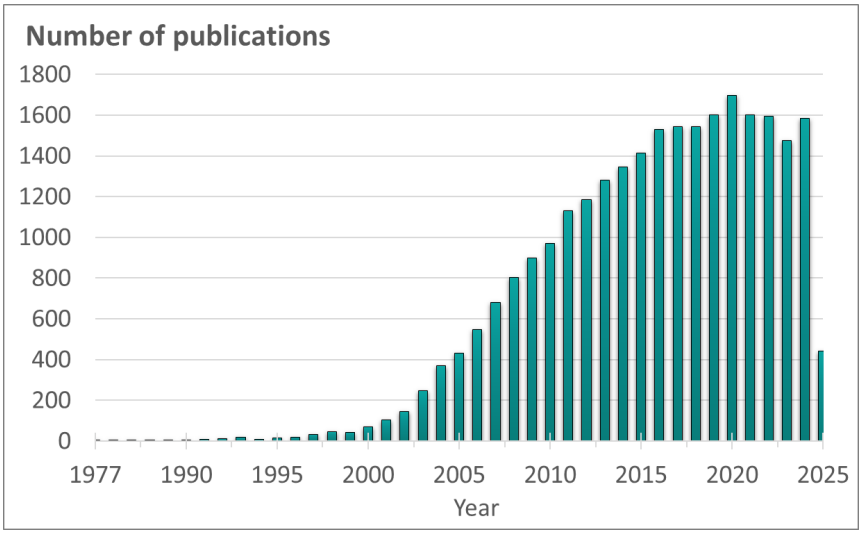

***Figure 1.13**. Number of publications on microwave assisted synthesis; data from Web of Science.*

1.8. Scaled-up synthesis procedures

The scaling of synthesis procedures from laboratory to industrial scale involves a careful consideration of different technical, economic, and environmental factors to ensure that the process remains efficient, reproducible, and cost-effective. Principally, the translation of reaction conditions (such as temperature, pressure, and reaction time) requires optimization to accommodate larger volumes and different heat and mass transfer dynamics. In a laboratory setting, reactions are often conducted in small batches with relatively straightforward mixing and thermal control. However, as the scale increases, heat and mass transfer limitations can become more pronounced

due to issues like the penetration depth, leading to challenges such as temperature gradients (Figure 1.14.), poor mixing, and incomplete reactions, which can significantly affect yield and product quality.[73]

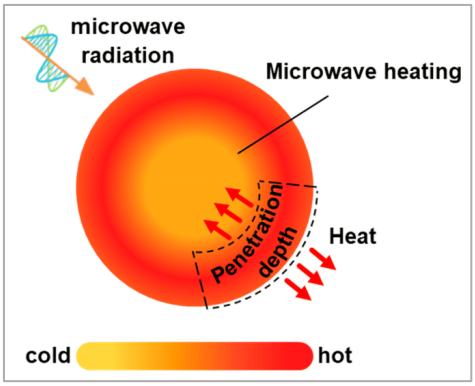

Figure 1.14. *Penetration depth of microwave absorption in materials.*[33]

Additionally, the rheological properties of materials, such as viscosity, can change with scale, requiring modifications in reactor design, such as the use of larger or more powerful mixers and heat exchangers to maintain efficient mixing and energy distribution.

Two primary approaches to scaling are commonly used: scaling with larger reactors and flow-based procedures. While laboratory reactors may rely on simple batch processes, industrial reactors are often designed for continuous operation to maximize throughput and minimize production costs.

- **Scaling with larger reactors:** it involves increasing the size of batch reactors to handle greater volumes of reactants while maintaining similar conditions to those in the laboratory. This approach often requires modifications in the reactor's design. In order to increase the microwave

power delivered to the system, we will employ four microwave generator sources instead of a single one. This configuration will allow us to scale up from 200 W to a total of 800 W, with each source contributing 200 W (Figure 1.15). The larger reactor must also account for longer residence times. To ensure load homogeneity, a magnetic stirring plate is coupled beneath the cavity, allowing the use of a magnetic stir bar inside the load. This promotes continuous agitation and uniform distribution of the material,[33] thereby enhancing the homogeneity of the heating process.

- **Flow-based procedures**: they offer a continuous method of synthesis where reactants flow through a reactor in a constant stream, rather than being processed in batches. This procedure is particularly advantageous for reactions requiring precise control over residence time, temperature, and mixing. By using this method, issues related to penetration depth are minimized, as the reactor cell is smaller. However, since it operates as a continuous process, it is still possible to obtain large quantities of product over time. To prevent the accumulation of reactants inside the reactor, the system has been arranged in a downward orientation as can be seen in Figure 1.15, allowing gravity to facilitate continuous flow and minimize the risk of material build-up.

The choice between batch and continuous systems must be made based on the nature of the reaction and the desired product consistency. In both cases, the control of temperature and pressure becomes more complex at larger scales, requiring advanced control systems to ensure stable reaction conditions.

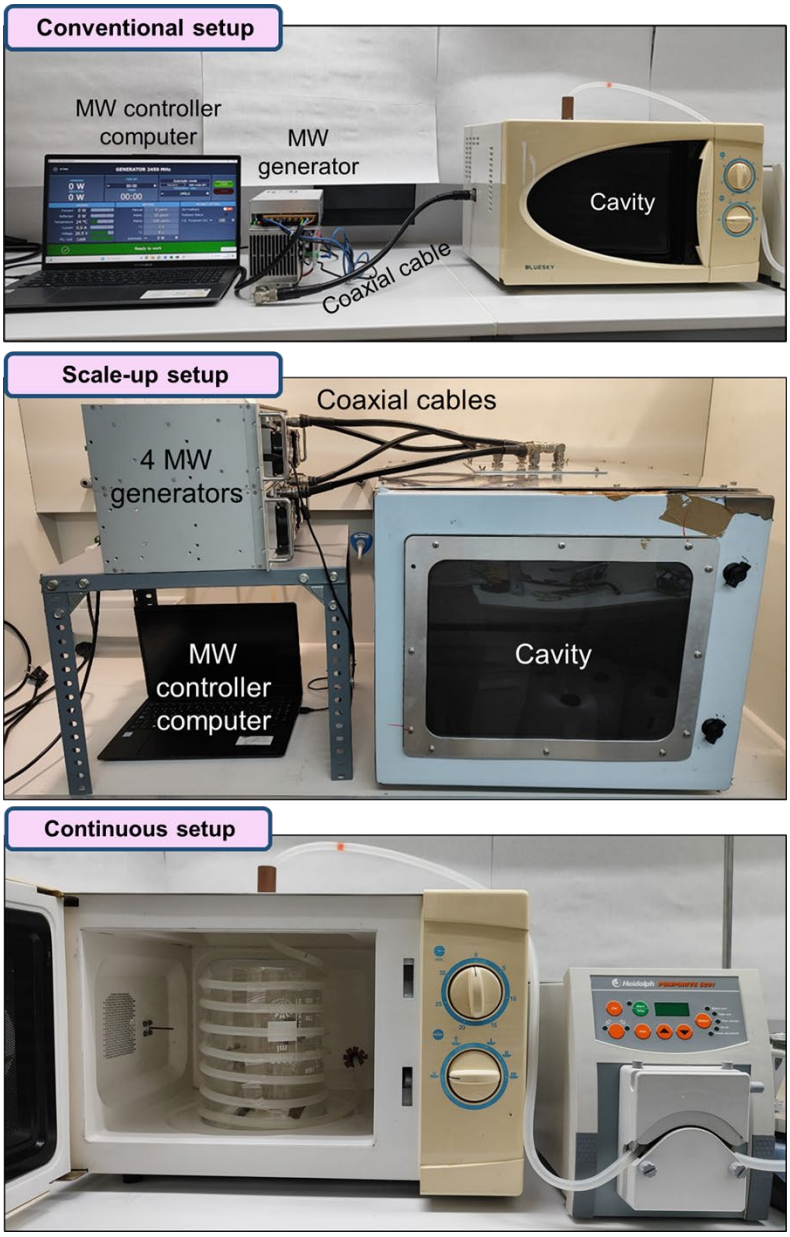

Figure 1.15. *Comparison between conventional, scale-up and continuous setup.*

The use of microwave heating as an alternative to conventional thermal methods presents notable environmental benefits, especially when applied to large-scale processes. Unlike traditional heating, which relies on external conduction and often leads to significant energy losses, microwave technology enables direct and volumetric energy transfer, resulting in faster heating and greater energy efficiency.[33] This becomes particularly advantageous at industrial scales, where even modest improvements in efficiency can lead to substantial reductions in total energy consumption. These factors contribute to a more sustainable and environmentally responsible approach to large-scale chemical manufacturing.

In conclusion, scaling up a synthesis process involves many interconnected factors and requires a well-rounded approach. It is important to consider not only technical improvements, but also economic and environmental impacts. To move from small-scale to industrial-scale production successfully, one must understand how heat and materials move through the system, how the reactor is designed, how materials behave, and how to control the process. This ensures that the final production remains efficient, high-quality, and sustainable.

1.9. References

(1) Hochella, M.F.; Mogk, D.W.; Ranville, J.; Allen, I.C.; Luther, G.W.; Marr, L.C.; McGrail, B.P.; Murayama, M.; Qafoku, N.P.; Rosso, K.M.; Sahai, N.; Schroeder, P.A.; Vikesland, P.; Westerhoff, P.; Yang, Y. Natural, incidental, and engineered nanomaterials and their impacts on the Earth system. *Science* **2019**, *363*, 6434.

(2) Ji, Z.; Guo, W.; Sakkiah, S.; Liu, J.; Patterson, T.A.; Hong, H. Nanomaterial databases: data sources for promoting design and risk assessment of nanomaterials. *Nanomaterials* **2021**, *11*, 1599.

(3) Boverhof, D.R.; Bramante, C.M.; Butala, J.H.; Clancy, S.F.; Lafranconi, M.; West, J.; Gordon, S.C. Comparative assessment of nanomaterial definitions and safety evaluation considerations. *Regul. Toxicol. Pharmacol*. **2015**, *73*, 137–150.

(4) International Organization for Standardization. *Nanotechnologies — Plain language explanation of selected terms from the ISO/IEC 80004 series. ISO/TR 18401*, **2017**.

(5) International Organization for Standardization. *Nanotechnologies — Vocabulary — Part 1: Core terms. ISO 80004-1*, **2023**.

(6) Asmatulu, E.; Andalib, M.N.; Subeshan, B.; Abedin, F. Impact of nanomaterials on human health: a review. *Environ. Chem. Lett.*, **2022**, *20*, 2509–2529.

(7) Poh, T.Y.; Mohamed Ali, N.A.B.; Mac Aogáin, M.; Kathawala, M.H.; Setyawati, M.I.; Ng, K.W.; Chotirmall, S.H. Inhaled nanomaterials and the respiratory microbiome: Clinical, immunological and toxicological perspectives. *Part. Fibre Toxicol.*, **2018**, *15*, 46.

(8) Rawat, R.S. Dense plasma focus – from alternative fusion source to versatile high energy density plasma source for plasma nanotechnology. *J. Phys. Conf. Ser.* **2015***, 591,* 012003*.*

(9) Abid, N.; Khan, A.M.; Shujait, S.; Chaudhary, K.; Idram, M.; Imran, M; Haider, J.; Khan, M.; Khan, Q.; Maqbool, M. Synthesis of nanomaterials using various top-down and bottom-up approaches, influencing factors, advantages, and disadvantages: A review. *Adv. Colloid Interface Sci.*, **2022**, *300*, 102597.

(10) Tompsett, G.A.; Curtis Conner, W.; Yngvesson, K.S. Microwave synthesis of nanoporous materials. *ChemPhysChem*, **2006**, *7,* 296–319.

(11) Predoană, L.; Attila Karajz, D.; Otieno Odhiambo, V.; Stanciu, I.; Szilágyi, I.M.; Pokol, G.; Zaharescu, M. Influence of the Microwaves on the sol-gel syntheses and on the properties of the resulting oxide nanostructures. In *Microwave Heating - Electromagnetic Fields Causing Thermal and Non-Thermal Effects,* IntechOpen*,* **2021**.

(12) Gupta, M.; Leong, W.W. Microwaves and metals. *John Wiley & Sons*, **2007**.

(13) **iStock.** *El espectro electromagnético*; https://www.istockphoto.com/es/vector/el-espectro-electromagn%C3%A9tico-gm951632822-259758551(accessed April 28, 2025).

(14) Pozar, D.M. Microwave Engineering, *4th ed. Wiley*: Hoboken, NJ, **2012**.

(15) Spencer, P.L. High efficiency magnetron. *U.S. Patent 2.408.235*, **1941**, Serial No. 425.071.

(16) Carlisle, R. Scientific american inventions and discoveries : all the milestones in ingenuity--from the discovery of fire to the invention of the microwave oven. *Turner Publishing Company*, **2008**.

(17) Mehta, A.; Vasudev, H.; Jeyaprakash, N. Role of sustainable manufacturing approach: microwave processing of materials. *Int*. *J. Interact. Des. Manuf*. **2023**, *18*, 5283–5299.

(18) Ohring, M.; Kasprzak, L. Electronic devices: how they operate and are fabricated. In *Reliability and Failure of Electronic Materials and Devices*, Elsevier, **1998**, 39–109.

(19) Atuonwu, J.C.; Tassou, S.A. Quality assurance in microwave food processing and the enabling potentials of solid-state power generators: A review. *J. Food Eng*. **2018**, *234*, 1–15 (2018).

(20) Mehdizadeh, M. The impact of fields on materials at RF/microwave frequencies. In *Microwave/RF applicators and probes for material heating, sensing, and plasma generation,* Elsevier*,* **2010,** 1–34.

(21) Priecel, P.; Lopez-Sanchez, J.A. Advantages and limitations of microwave reactors: from chemical synthesis to the catalytic valorization of biobased chemicals. *ACS Sustain. Chem. Eng.* **2019***, 7*, 3–21.

(22) Risman, P.O. Microwave dielectric properties of foods and some other substances. In *Development of Packaging and Products for Use in Microwave Ovens, Woodhead Publishing,* **2020***,* 225–246.

(23) Huray, P.G. Maxwell's equations. *John Wiley & Sons*, **2009**.

(24) Yeong, S.P.; Law, M.C.; Vincent Lee, C.C.; Chan, Y.S. Modelling batch microwave heating of water. *IOP Conf. Series: Mater. Sci. Eng*. **2007**, *217*, 012035.

(25) National Research Council, Division on Engineering and Physical Sciences, National Materials Advisory Board, Commission on Engineering and Technical Systems. Microwave processing of materials. *National Academies Press*, Washington DC, **1994**, *473*.

(26) Ma, S.J.; Zhou, X.W.; Su, X.J.; Mo, W.; Yang, J.L.; Liu, P. A new practical method to determine the microwave energy absorption ability of materials. *Miner. Eng*. **2009**, *22*, 1154–1159.

(27) Chen, Q.; Chen, X.; Chen, Z.Z.; Zhang, B.; Zheng, Y.Q. High-efficiency microwave heating method based on impedance matching technology. *AIP Adv.* **2019**, *9*, 15113 (2019).

(28) Jacob, J.; Chia, L.H.L.; Boey, F.Y.C. Thermal and non-thermal interaction of microwave radiation with materials. *J. Mater. Sci.* **1995**, *21*, 5321–5327.

(29) Gedye, R.; Smith, F.; Westaway, K. Microwaves in Organic and organometallic synthesis. *J. Microw. Power Electromagn. Energy* **1991**, 1, 3–17.

(30) Sharma, S.; Parne, S.R.; Panda, S.S.S.; Gandi, S. Progress in microwave absorbing materials: A critical review. *Adv. Colloid Interface Sci*. **2024**, *327*, 103143.

(31) Rao, K.J.; Ramesh, P.D. Use of microwaves for the synthesis and processing of materials. *Bull. Mater. Sci* **1995**, *18*, 447–465.

(32) Borrell, A.; Salvador, M.D. advanced ceramic materials sintered by microwave technology. In *Sintering Technology - Method and Application*, **2018**, *10*, 3–24.

(33) Li, Z.; Peng, K.; Ji, N.; Zhang, W.; Tian, W.; Gao, Z. Advanced mechanisms and applications of microwave-assisted synthesis of carbon-based materials: a brief review. *Nanoscale Adv.* **2025**, *7*, 419–432.

(34) Boppella, R.K.; Manjula, P.; Arunkumar, S.; Manorama, S.V. Advances in synthesis of nanostructured metal oxides for chemical sensors. *Chem. Sens*. **2014**, *4*, 19.

(35) Komarneni, S.; Roy, R. Titania gel spheres by a new sol-gel process. *Mater. Lett*. **1985**, *3*, 165–167.

(36) Gedye, R.; Smith, F.; Westaway, K.; Ali, H.; Baldisera, L.; Laberge, L.; Rousell, J. The use of microwave ovens for rapid organic synthesis. *Tetrahedron Lett*. **1986**, *27*, 279–282.

(37) Giguere, R.J.; Bray, T.L.; Duncan, S.M.; Majetich, G. Application of commercial microwave ovens to organic synthesis. *Tetrahedron Lett*. **1986**, *27*, 4945–4948.

(38) Nüchter, M.; Ondruschka, B.; Bonrath, W.; Gum, A. Microwave assisted synthesis – a critical technology overview. *Green Chem.* **2004**, *6*, 128–141 (2004).

(39) Bassyouni, F.A.; Abu-Bakr, S.M.; Rehim, M.A. Evolution of microwave irradiation and its application in green chemistry and biosciences. *Res. Chem. Interm*. **2012**, *38*, 283–322.

(40) Strauss, C.R.; Trainor, R.W. Developments in microwave-assisted organic chemistry. *Aust. J. Chem*. **1995**, *48*, 1665–1692.

(41) Tsuji, M. Microwave-assisted synthesis of metallic nanomaterials in liquid phase. *ChemistrySelect* **2017**, *2*, 805–819.

(42) Cui, L.; Hui, K.N.; Hui, K.S.; Lee, S.K.; Zhou, W.; Wan, Z.P.; Thuc, C.N.H. Facile microwave-assisted hydrothermal synthesis of TiO_2 nanotubes. *Mater. Lett*. **2012**, *75*, 175–178.

(43) Ma, M.G.; Zhu, Y.J.; Cheng, G.F.; Huang, Y.H. Microwave synthesis and characterization of ZnO with various morphologies. *Mater. Lett*. **2008**, *62*, 507–510.

(44) Liao, X.; Zhu, J.; Zhong, W.; Chen, H.Y. Synthesis of amorphous Fe_2O_3 nanoparticles by microwave irradiation. *Mater. Lett.* **2001**, *50*, 341–346.

(45) Katsuki, H.; Furuta, S.; Komarneni, S. Semi-continuous and fast synthesis of nanophase cubic $BaTiO_3$ using a single-mode home-built microwave reactor. Mater. Lett. **2012**, *83*, 8–10.

(46) Carpenter, G.; Sen, R.; Malviya, N.; Gupta, N. Microwave-assisted synthesis and characterization of nickel ferrite nanoparticles. *AIP Conf. Proc.* **2015**, *1675*.

(47) Fariñas, J.C.; Moreno, R.; Pérez, A.; García, M.A.; García-Hernández, M.; Salvador, M.D.; Borrell, A. Microwave-assisted solution synthesis, microwave sintering and magnetic properties of cobalt ferrite. *J. Eur. Ceram. Soc*. **2018**, *38*, 2360–2368.

(48) Hu, H.; Deng, C.; Zhang, K.; Yin, P. Facile microwave-assisted synthesis of PbS nanotubes. *Micro Nano Lett*. **2012**, *7*, 464–466.

(49) Becerra-Paniagua, D.K.; Díaz-Cruz, E.B.; Baray-Calderón, A.; Garcia-Angelmo, A.R.; Regalado-Pérez, E.; Del Pilar Rodriguez-Torres, M.; Martínez-Alonso, C. Nanostructured metal sulphides synthesized by microwave-assisted heating: a review. *J. Mater. Sci.: Mater. Electron*. **2022**, *33*, 22631–22667.

(50) Li, J.S.; Huang, H.; Zhou, Y.J.; Zhang, C.Y.; Li, Z.T. Research progress of graphene-based microwave absorbing materials in the last decade. *J. Mater. Res*. **2017**, *32*, 1213–1230.

(51) Blăniţă, G.; Ardelean, O.; Lupu, D.; Borodi, G.; Mihet, M.; Coros, M.; Vlassa, M.; Misan, I.; coldea, I.; Popeneciu, G. Microwave assisted synthesis of MOF-5 at atmospheric pressure. Rev. Roum. Chim. 2011, 56, 583–588.

(52) Rodríguez-Carríllo, C.; Benítez, M.; El Haskouri, J.; Amorós, P.; Ros-Lis, J.V. Novel microwave-assisted synthesis of COFs: 2020–2022. *Molecules* **2023**, *28*, 3112.

(53) Zhao, J.; Yan, W. Microwave-assisted Inorganic Syntheses. In *Modern Inorganic Synthetic Chemistry,* Elsevier*,* **2011**, 173–195.

(54) Conner, W.C.; Tompsett, G.; Lee, K.H.; Yngvesson, K.S. Microwave synthesis of zeolites: 1. Reactor engineering. *J. Phys. Chem. B* **2004**, *108*, 13913–13920.

(55) Han, Y.; Ma, H.; Qiu, S.; Xiao, F.S. Preparation of zeolite A membranes by microwave heating. *Microporous Mesoporous Mat*. **1999**, *30*, 321–326.

(56) Arafat, A.; Jansen, J.C.; Ebaid, A.R.; Van Bekkum, H. Microwave preparation of zeolite Y and ZSM-5. *Zeolites* **1993**, *13*, 162–165.

(57) Wu, C.G.; Bein, T. Microwave synthesis of molecular sieve MCM-41. *ChemComm* **1996**, *8*, 925–926.

(58) Bandyopadhyay, M.; Gies, H. Synthesis of MCM-48 by microwave-hydrothermal process. *C. R. Chim*. **2005**, *8*, 621–626.

(59) Díaz de Greñu, B.; De Los Reyes, R.; Costero, A.M.; Amorós, P.; Ros-Lis, J.V. Recent progress of microwave-assisted synthesis of silica materials. *Nanomaterials* **2020**, *10*, 1092.

(60) Fantini, M.C.D.A.; Matos, J.D.R.; Da Silva, L.C.; Mercuri, L,P.; Chiereci, G.O.; Celer, E.B.; Jaroniec, M. Ordered mesoporous silica: microwave synthesis. *MSEB* **2004**, *112*, 106–110.

(61) Singh, U.; Kumar, N.; Sinha, A.K. Gyrotron and its electron beam source: A review. *J. Fusion Energy* **2012**, *31*, 489–505.

(62) a) Luo, J.; Feng, J.; Gong, Y. A review of microwave vacuum devices in China: theory and device development including high-power klystrons, spaceborne TWTs, and Gyro-TWTs. *IEEE Microw. Mag*. **2021**, *22*, 18–33. b) Encyclopædia Britannica. *Encyclopædia Britannica*; https://www.britannica.com/ (accessed April 23, 2025).

(63) Kumar, N.; Singh, U.; Singh, T.P.; Sinha, A.K. A review on the applications of high power, high frequency microwave source: Gyrotron. *J. Fusion Energy* **2011**, *30*, 257–276.

(64) Garven, M.; Spark, S.N.; Cross, A.W.; Cooke, S.J.; Phelps, A.D.R. Gyrotron experiments employing a field emission array cathode. *Phys. Rev. Lett*. **1996**, *77*, 2320.

(65) Mendel, J.T. Helix and coupled-cavity traveling-wave tubes. *Proc. IEEE* **1973**, *61*, 280–298.

(66) Whitaker, J.C. Power Vacuum Tubes Handbook, *Second Edition - Jerry Whitaker* - CRC Press, **1999**.

(67) Gilmour, A.S. Principles of traveling wave tubes. *Artech House*, Boston, **1994**.

(68) Bowers, R. A Solid-state source of microwaves. *Sci. Am.* **1966**, *215*, 22–31.

(69) Allen, S.T.; Pribble, W.L.; Sadler, R.A.; Alcorn, T.S.; Ring, Z.; Palmour, J.W. Invited-progress in high power SiC microwave MESFETs. *IEEE MTT-S Int. Microw. Symp. Dig.* **1999**, *1*, 321–324.

(70) Niehenke, E.C.; Pucel, R.A.; Bahl, I.J. Microwave and millimeter-wave integrated circuits. *IEEE Trans. Microw. Theory Tech*. **2002**, *50*, 846–857.

(71) Trew, R.J. Wide bandgap semiconductor transistors for microwave power amplifiers. *IEEE Microw. Mag.* **2000**, *1*, 46–54.

(72) Zhou, X.; Tang, Z.; Pedrow, P.D.; Sablani, S.S.; Tang, J. Microwave heating based on solid-state generators: New insights into heating pattern, uniformity, and energy absorption in foods. *J. Food Eng*. **2023**, *357*, 111650.

(73) De la Hoz, A.; Alcázar, J.; Carrillo, J.; Herrero, M.A.; Muñoz, J.D.M.; Prieto, P.; De Cózar, A.; Díaz-Ortiz, A. Reproducibility and scalability of microwave-assisted reactions. In *Microwave Heating,* IntechOpen*,* **2011**.

(74) a) Zhou, X.; Pedrow, P.D.; Tang, Z.; Bohnet, S.; Sablani, S.S.; Tang, J. Heating performance of microwave ovens powered by magnetron and solid-state generators. *IFSET* **2023**, *83*, 103240. b) Rutronik. High-Q Capacitor for Solid-State Microwave Oven; *Rutronik Tech News*, https://rutronik-tec.com/high-q-capacitor-for-solid-state-microwave-oven/ (accessed March 10, 2025).

(75) Taghian Dinani, S.; Kubbutat, P.; Kulozik, U. Assessment of heating profiles in model food systems heated by different microwave generators: Solid-state (semiconductor) versus traditional magnetron technology. *IFSET* **2020**, *63*, 102376.

(76) Expert Market Research. Microwave Devices Market Report 2024–2032; https://www.expertmarketresearch.com/reports/microwave-devices-market (accessed Feb 20, 2025).

Chapter 2:

Objectives

General Objectives

To develop and optimize energy-efficient synthesis methods to synthesize pure or functionalized ordered mesoporous silica using solid-state microwave technology, with a focus on scalable production in both batch and continuous-flow systems, and extend these methods to the synthesis of another nanoparticles, in this case CeO_2 nanoparticles.

Specific Objectives

- To design and implement microwave-assisted synthesis based on solid-state microwave generators for pure ordered mesoporous silica, reducing energy consumption while preserving structural order and performance.
- To compare the efficiency, structural properties, and functional performance of materials synthesized by conventional methods versus solid-state microwave-assisted techniques.
- To develop post-synthesis functionalization of mesoporous silica using microwave-assisted methods to enhance efficiency and reduce reaction times.
- To explore one-pot microwave-assisted synthesis strategies for the simultaneous formation and functionalization of ordered mesoporous silica.
- To evaluate and scale up the microwave synthesis processes for mesoporous silica using both batch and continuous-flow systems, ensuring reproducibility and industrial applicability.

– To adapt scalable microwave-assisted synthesis techniques for the preparation of CeO_2 nanoparticles with controlled size, morphology, and functional properties.

Chapter 3:

Inorganic Mesoporous Materials

3.1. Mesoporous materials background

According to the IUPAC, porous materials are commonly classified based on their pore size into three categories: microporous, mesoporous, and macroporous. Microporous materials have pore sizes smaller than 2 nm, mesoporous materials range between 2 and 50 nm, and macroporous materials exhibit pore sizes larger than 50 nm.[1]

The discovery of porous materials dates back to ancient times with substances like pumice and charcoal. In the 18th century, scientists like Carl Wilhelm Scheele studied activated carbon's ability as adsorbent,[2] paving the way for modern materials like zeolites, mesoporous silicas and MOFs, now used in gas storage and filtration. Zeolites were discovered in 1756 by Swedish mineralogist Axel Fredrik Cronstedt, who observed that certain minerals released water when heated, leading him to coin the term "zeolites" from the Greek words "zeo" (to boil) and "lithos" (stone).[3] Zeolites are crystalline materials composed of a three-dimensional framework of silicon and aluminum tetrahedra, interconnected by oxygen atoms (Figure 3.1). Their structure features uni-, bi-, and tridimensional channels that come together to form solids with large internal surface areas. These channels are typically occupied by water molecules and hydrated cations, which contribute to material's ion-exchange and adsorption properties.[4]

During the 1940s and 1950s, there was a surge of interest in the study of these materials, particularly due to their potential use in catalytic applications within the petrochemical industry. This big increase in research was driven by

the unique properties of zeolites, including their high surface area, thermal stability, and ability to act as catalysts in processes like cracking.[3]

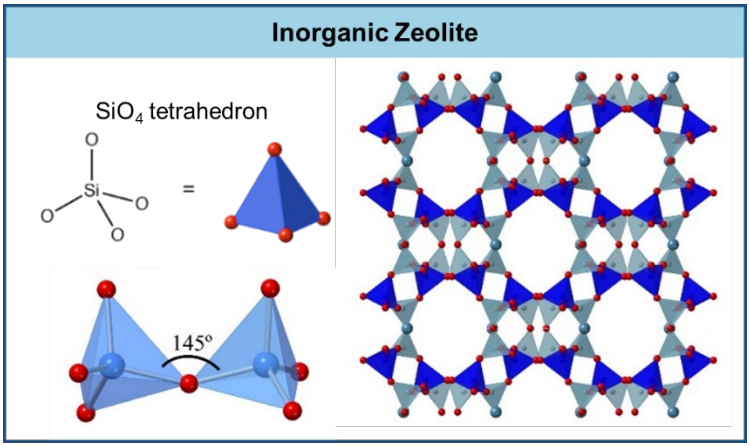

Figure 3.1. *Structure of tetrahedral silicon units which conform the zeolite framework.*[5]

The discovery of the first method for the synthesis of mesoporous materials represented a significant breakthrough in the field of materials science. The first reported mesoporous silica was documented in 1990 by Yanagisawa. They created a compound by mixing a single-layered silica material called kanemite with alkyltrimethylammonium chloride solutions. During this process, the silica layers joined together to form three-dimensional silica structures.[6] In 1992, researchers at Mobil Oil Corporation, while attempting to develop new zeolites with larger pores, made a significant breakthrough with the discovery of the M41S (Mobil Composition of Matter No. 41) family of mesoporous materials, including the well-known MCM-41.[6] This family of materials is distinguished by its high pore volumes and extensive surface areas, along with their remarkable thermal stability, making them suitable for a wide range of applications, particularly in catalysis and adsorption processes. Unlike zeolites, these materials have mesopores ranging from 2 to

10 nanometers, making them suitable for a broader range of catalytic processes involving large molecular species. This discovery marked a new era in the design of porous materials, extending their applications in catalysis, adsorption, and separation technologies, as evidenced by the substantial increase in the number of scientific publications on the subject (Figure 3.2).

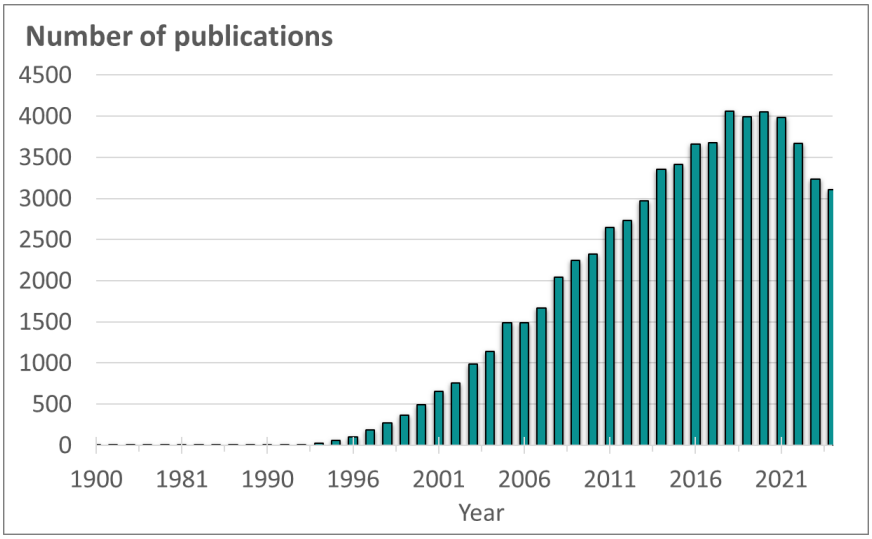

***Figure 3.2**. Number of publications containing the words "mesoporous material" over the years. Data from Web of Science.*

3.2. Different mesoporous silica materials

The synthesis of mesoporous materials typically involves sol-gel and hydrothermal methods.[7] Among these, MCM-41 is the most extensively studied member from de M41S family, characterized by its hexagonal arrangement of uniform mesopores.[8] Other notable variants within this family include MCM-48, with a cubic mesostructure, and MCM-50, exhibiting a lamellar configuration—both offering unique structural properties suitable for diverse applications.[9] Since the initial discovery of these materials, additional

mesoporous structures have been developed (Figure 3.3), distinguished by variations in different factors such as synthesis conditions or templating agents. Hexagonal Mesoporous Silica (HMS) materials, for example, are synthesized at neutral pH using uncharged primary amines as structure-directing agents in a precipitation process.[10] In contrast, MSU-X materials (Michigan State University materials) are prepared under acidic conditions near the isoelectric point (pH_{iep}) of silica, employing non-ionic PEO-based polymers to facilitate hydrolysis and condensation.[11] Santa Barbara Amorphous (SBA) material[12] shares similarities with MSU-X in terms of templating with non-ionic surfactants, but is synthesized under much more strongly acidic conditions, where counter-ion-mediated hydrogen bonding leads to highly ordered mesostructures.[10] Similarly, KIT-type materials,[13] are closely related to SBA-15 but incorporate a co-surfactant, typically 1-butanol, to promote the formation of a more intricate cubic mesostructure.[14]

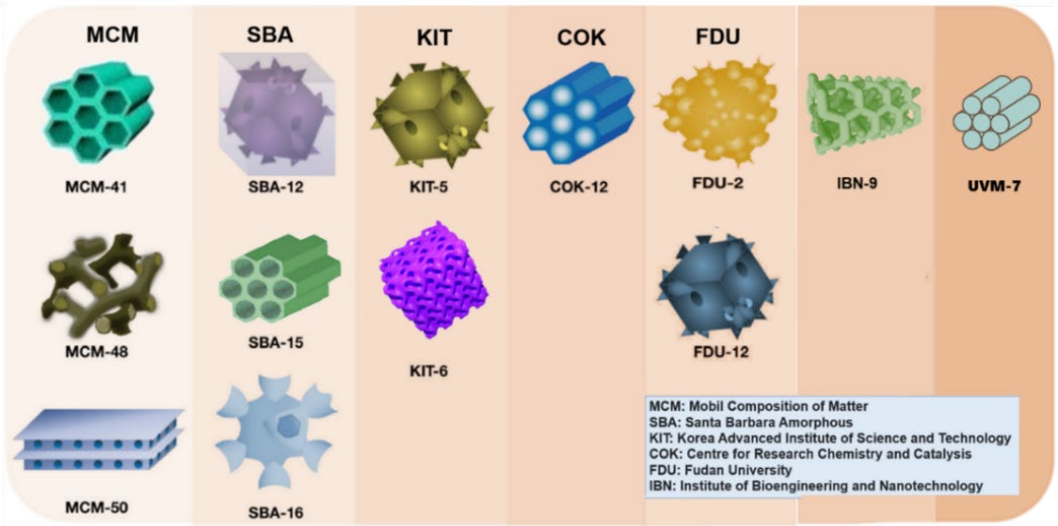

***Figure 3.3**. Structure of different ordered mesoporous materials.[15]*

In general, most available mesoporous materials are unimodal mesoporous silicas, which can lead to poor accessibility to active sites due to pore blockage issues.[16] To address this limitation, hierarchical porous materials, such as UVM-7, have been synthesized. These materials feature more than one type of pore, providing a structured hierarchy that mitigates the risk of pore occlusion and enhances their functional performance.[17]

3.3. Synthesis Procedure

A wide range of hierarchical porous materials has been reported, featuring two or even three interconnected pore systems with diverse porosity combinations, such as micro/macroporosity, meso/macroporosity, or micro/meso/microporosity.[18] These materials are typically synthesized through procedures that require a variety of templating agents to define the different pore types, since using single non-ionic surfactants for the synthesis of HMS materials,[19] to cationic surfactants for synthesizing MCM-41.[20] A critical objective is reducing the particle size of mesoporous materials, as this inherently shortens the mesopore length and generates additional inter-particle porosity due to particle packing. Key procedural variables influencing inter-particle (textural) porosity have been identified in different systems: for example, the polarity of the medium is crucial in HMS synthesis, while the pH of the precursor solution determines porosity in MCM-41-like silicas. Highly polar solvents or moderately basic conditions (pH~10) are required to synthesize bimodal HMS or MCM-41-like materials, respectively.

As evidenced, there are numerous strategies to fabricate hierarchical porous materials, yet these often involve complex and labor-intensive processes. To streamline the synthesis, we will use the classical atrane method, a technique in which our group has significant expertise, offering a reliable and efficient pathway to produce high-quality mesoporous materials.

The atrane route for the synthesis of ordered mesoporous materials was first proposed by the research group of Pedro Amorós in 1999.[21] This method is based on the Oxide One-Pot Synthesis (OOPS) technique coined by Laine, in which atranes are utilized as reagents for the preparation of mixed oxides. The OOPS technique involves the dissolution of oxides, hydroxides, or salts in triethanolamine (TEA), leading to the formation of atrane complexes.[22]

An atrane is a type of tricyclic compound in which a central metal or non-metal atom is coordinated to three donor atoms, typically from a chelating ligand like TEA. This creates a stable, cage-like structure with strong intramolecular interactions (Figure 3.4).[23]

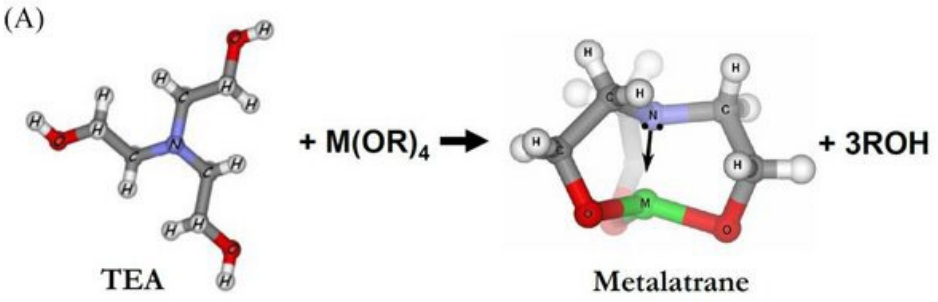

Figure 3.4. *Reaction followed for the formation of atrane complexes.*[24]

This method is represented in Figure 3.5. It employs a surfactant, which self-assembles into micelles that direct the formation of a mesostructured

framework. Simultaneously, an atrane complex is prepared by reacting a metal alkoxide with TEA. The atrane species then interact with the micellar structure through hydrolysis and condensation reactions, leading to the formation of an organized silica network. Finally, the template is removed by calcination, leaving behind a well-defined mesoporous silica structure.[25]

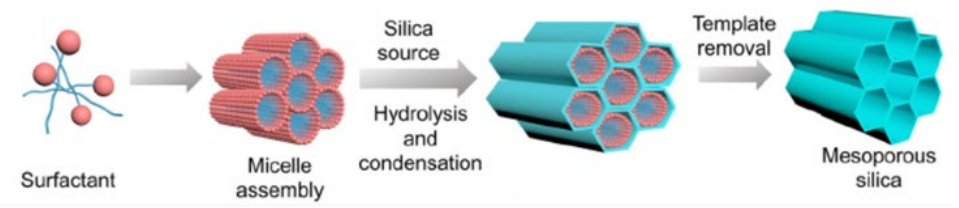

Figure 3.5. *Scheme procedure for the synthesis of mesoporous silica using and template agent.*[26]

The selection of the atrane method is based on its key advantages, particularly the formation of stable atrane complexes, which enhance the reproducibility of the synthesis and provide greater control over porosity and structural organization. Furthermore, this method allows for the use of milder reaction conditions, reducing the reliance on harsh acidic or basic environments, thereby offering a more controlled and versatile approach for the synthesis of advanced materials.

3.4. UVM-7

In 2002, Jamal El Haskouri, from Pedro Amorós' research group at the Universitat de València, developed a novel mesoporous material known as UVM-7 (University of Valencia Material). UVM-7 is a silica-based porous material distinguished by its bimodal pore system, featuring smaller pores

generated by the surfactant and larger pores formed by the aggregation of pseudo-spherical mesoporous primary nanoparticles (Figure 3.6).[20]

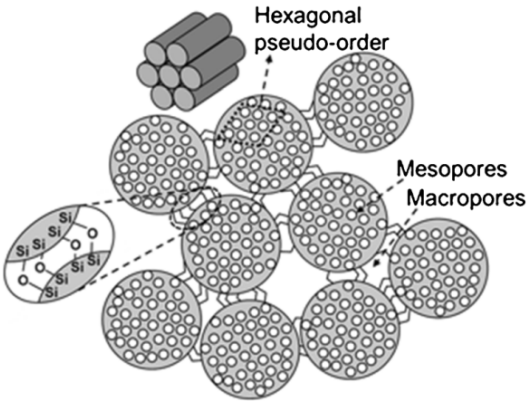

***Figure 3.6**. Chemical structure of the UVM-7.*[27]

UVM-7 is a nanometric version of MCM-41, where the particles aggregate into clusters. The synthesis process for both materials uses similar proportions of reactants; however, there is a key difference in pH control. In MCM-41 synthesis, NaOH is added to raise the pH to 10.5, creating a strongly basic environment. In contrast, UVM-7 synthesis omits sodium hydroxide, resulting in a lower pH of around 9. This reduced pH limits the redissolution of nuclei or small particles, promoting the formation of smaller particles in UVM-7 compared to MCM-41.[24]

Our research group has been working with this material since its discovery, dedicating years to refining its understanding and optimizing its properties (Table 3.1). Over time, significant progress has been made in elucidating the mechanisms governing its synthesis and behavior. Furthermore, this knowledge has enabled the identification and development of its potential

applications. Recent developments focus on the synthesis of UVM-7 using microwave generators.

***Table 3.1**. Significant advancements in UVM-7 published by our research group. Functionalizations advancements are included in Chapter 4.*

Year	Objective	Ref
2002	First discover. Preparation of bimodal silicas (powders and monoliths)	20
2003	Preparation of silica-based monoliths with a trimodal pore system	29
2005	Used for immobilization of lysozyme and a-L-arabinofuranosidase	30
2006	A more detailed study on the synthesis of this material	18
2008	Control of the pore size by changing surfactant chain and control of aggregation	31
2012	Used for ibuprofen storage and delivery	32
2016	Used to encapsulate folic acid	33
2016	Increasement of the intra-particle mesopore size by using alkanes as swelling agents	34
2018	Evaluation of materials as solid-phase extraction sorbents for the isolation of phospholipids	35
2020	A sorbent based on UVM-7 for the determination of aflatoxin M-1 in milk and dairy products	36
2023	Synthesis using solid-state microwave generators	28
2023	Scale-up using microwave-assisted synthesis	37

Diaz de Greñu, focuses on the optimization of the UVM-7 synthesis process by significantly reducing reaction times. Microwave irradiation was applied to synthesize UVM-7 in as-made form in only 2 minutes at 50 W compared with conventional synthesis, which normally takes up to 12 h. Moreover, the calcination step was also optimized, reducing the time needed from 6 hours to 13 mins. Finally, it took only 4 min to achieve functionalization with APTES

compared to the ~5.5 h required for the conventional method.[28] These advancements demonstrate the significant potential of microwave-assisted synthesis for improving the efficiency and scalability of UVM-7 production.

The market is predominantly dominated by materials from the MCM and SBA families, whose chemical and physical properties make them highly versatile and in demand for both scientific and industrial applications (Figure 3.7). Hence, their market extends to research laboratories in both the public and private sectors.

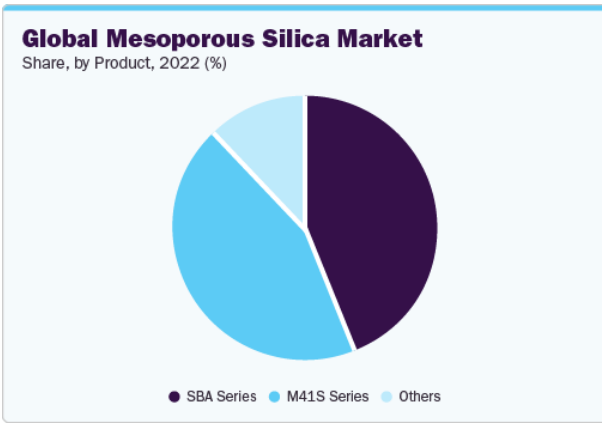

Figure 3.7. Global mesoporous market. Data from GrandViewResearch.[38]

We have conducted characterization studies that demonstrate that the textural properties of these commercial materials are not ideal, making them unsuitable for certain research purposes. Despite their potential applications, another concern is their high cost: 5g for 496 Euros.[39] An alternative way to make the product cheaper lies in lower energy consumption. If we are able to replace conventional thermal treatments (both in synthesis and in calcination

and subsequent functionalization) with other strategies that reduce treatment times, we can reduce the energy consumption of the product.

UVM-7, discovered by our research group, is a material with which we possess extensive expertise in its synthesis, characterization, functionalization, and application. Furthermore, we have pioneered its synthesis using solid-state microwave generators, a technique that enhances precision, efficiency, and scalability. Our experience ensures a high level of control and reliability when working with this material.

3.5. Objectives and scope of this study

The focus of this line is the optimization of syntheses using microwave ovens, with the potential to significantly reduce procedures times. Additionally, an alternative to scaling up the size of the furnaces is the preparation of the materials in flow, with the consideration of scaling up in mind. This would enable the production of materials to be done on demand in a short period of time.

Following the conventional procedure, the synthesis of UVM-7 typically requires extended reaction times, as the formation of the atrane complex requires heating for 12 hours.[20] This is followed by overnight drying, and the subsequent calcination step, which also requires an entire night for ending. In total, the synthesis process spans several days, yielding relatively small quantities, generally in the gram scale. The conventional method has been tested, resulting in approximately 1 g of material.[28] Furthermore, if functionalization of these materials is desired, an additional step is required, extending the overall process by another couple of days. To enhance the

efficiency of this process, the integration of microwave-assisted synthesis is proposed. The use of microwave irradiation significantly reduces the synthesis time, decreasing the typical 24-hour stirring requirement to just 2 minutes. Additionally, improvements in material production scalability will be addressed by implementing continuous-flow synthesis, which allows for the constant generation of material, alongside batch scaling, which enables the production of up to 100 times the quantity obtained using the conventional method.

3.6. References

(1) Ania, C.; Calero, S.; Silvestre-Albero, J.; Valdés-Solís, T. Materiales en Adsorción y Catálisis. *Revista del Grupo Especializado de Adsorción de la RSEQ* **2016**, *8*.

(2) Chen, J.Y. Activated Carbon Fiber and Textiles. (2017). doi:https://doi.org/10.1016/B978-0-08-100660-3.00001-8.

(3) Yan, W.; Yu, J. Our journey in zeolite science. *Microporous Mesoporous Mater.* **2023**, *358*, 112368.

(4) Schwanke, A. J.; Balzer, R.; Pergher, S. Microporous and mesoporous materials from natural and inexpensive sources. *Handb. Ecomater.* **2019**, *5*, 3379–3399.

(5) León Alcaide, L. Beyond Crystallinity in Zeolitic Imidazolate Frameworks. Doctoral Thesis, Universitat de València, España, **2024**.

(6) Li, Q.; Zhou, Y. Brief history, preparation method, and biological application of mesoporous silica molecular sieves: a narrative review. *Molecules* **2023**, 28, 2013.

(7) Corma, A.; Kan, Q.; Navarro, M.T.; Pérez-Pariente, J.; Rey, F. Synthesis of MCM-41 with different pore diameters without addition of auxiliary organics. *Chem. Mater.* **1997**, *9*, 2123–2126.

(8) Beck, J.S.; Vartuli, J.C.; Roth, W.J.; Leonowicz, M.E:, Kresge, C.T.; Schmitt, K.D.; Chu, C.T.-W.; Olson, D.H.; Sheppard, E.W.; McCullen, S.B.; Higgins, J.B.; Schlenker, J.L. A new family of mesoporous molecular sieves prepared with liquid crystal templates. *J. Am. Chem. Soc*. **1992**, *114*, 10834–10843.

(9) Kresge, C.T.; Vartuli, J.C.; Roth, W.J.; Leonowicz, M.E. The discovery of ExxonMobil's M41S family of mesoporous molecular sieves. *Stud. Surf. Sci. Catal*. **2004**, *148*, 53–72.

(10) Fotoohi, B.; Mercier, L. Some considerations regarding the mesopore structure and order in MSU-3 and MSU-F (organo)silicas. *Microporous Mesoporous Mater.* **2015**, *211*, 38–48.

(11) Prouzet, É.; Boissiére, C. A review on the synthesis, structure and applications in separation processes of mesoporous MSU-X silica obtained with the two-step process. *Comptes. Rendus. Chimie*. **2005**, *8*, 579–596.

(12) Huirache-Acuña, R.; Nava, R.; Peza-Ledesma, C.L.; Lara-Romero, J.; Alonso-Núez, G.; Pawelec, B.; Rivera-Muñoz, E.M. SBA-15 mesoporous silica as catalytic support for hydrodesulfurization catalysts—review. *Mater.* **2013**, 6, 4139-4167.

(13) Kerstens, D.; Smeyers, B.; Van Waeyenberg, J.; Zhang, Q.; Yu, J.; Sels, B.F. State of the art and perspectives of hierarchical zeolites: practical overview of synthesis methods and use in catalysis. *Adv. Mater.* **2020**, *32*, 2004690.

(14) Jo, C.; Kim, K.; Ryoo, R. Syntheses of high quality KIT-6 and SBA-15 mesoporous silicas using low-cost water glass, through rapid quenching of silicate structure in acidic solution. *Microporous Mesoporous Mater.* **2009**, *124*, 45–51.

(15) Asasian-Kolur, N.; Sharifian, S.; Haddadi, B.; Jordan, C.; Harasek, M. Ordered porous carbon preparation by hard templating approach for hydrogen adsorption application. *Biomass Convers. Biorefin.* **2023**, *14*, 18381–18416.

(16) Rolison, D.R. Catalytic nanoarchitectures-the importance of nothing and the unimportance of periodicity. *Science*, **2000**, *299*, 1698–1701.

(17) Pérez-Cabero, M.; Hungría, A.B.; Morales, J.M.; Tortajada, M.; Ramón, D.; Moragues, A.; El Haskouri, J.; Beltrán, A.; Beltrán, D.; Amorós, P. Interconnected mesopores and high accessibility in UVM-7-like silicas. *J. Nanopart. Res*. **2012**, *14*, 1045.

(18) Huerta, L.; Guillem, C.; Latorre, J.; Beltrán, A.; Martínez-Máñez, R.; Marcos, M.D.; Beltrán, D.; Amorós, P. Bases for the synthesis of nanoparticulated silicas with bimodal hierarchical porosity. *Solid State Sci.* **2006**, *8*, 940–951.

(19) Zhang, W.; Pauly, T.R.; Pinnavaia, T.J. Tailoring the framework and textural mesopores of HMS molecular sieves through an electrically neutral (S°I°) assembly pathway. *Chem. Mater.* **1997**, *9*, 2491–2498.

(20) El Haskouri, J.; Ortiz de Zárate, D.; Guillem, C.; Latorre, J.; Caldés, M.; Beltrán, A.; Beltrán, D.; Descalzo, A.B.; Rodríguez-López, G.; Martínez-Máñez, R.; Marcos, M.D.; Amorós, P. Silica-based powders and monoliths with bimodal pore systems. *ChemComm* **2002**, *4*, 330–331.

(21) Cabrera, S.; El Haskouri, J.; Alamo, J.; Beltrán, A.; Beltrán, D.; Mendioroz, S.; Marcos, M.D.; Amorós, P. Surfactant-assisted synthesis of mesoporous alumina showing continuously adjustable pore sizes. *Adv. Mater.* **1999**, *11*, 379–381.

(22) Laine, R.M.; Treadwell, D.R.; Mueller, B.L.; Bickmore, C.R.; Waldner, K.F.; Hinklin, T.R. Processable aluminosilicate alkoxide precursors from metal oxides and hydroxides. The oxide one-pot synthesis process. *J. Mater. Chem.* **1996**, *6*, 1441–1443.

(23) Verkade, J. G. Main group atranes: chemical and structural features. *Coord. Chem. Rev*. **1994**, *137*, 233–295.

(24) Garrido, M.D.; Benítez, M.; Ros-Lis, J.V.; Amorós, P. A travel though the atrane route, a versatile tool for the materials soft-synthesis: A twenty-five years perspective. *Nano Select* **2024**, *5*, 2300169.

(25) Cabrera, S.; El Haskouri, J.; Guillem, C.; Latorre, J.; Beltrán-Porter, A.; Beltrán-Porter, D.; Marcos, M.D.; Amorós, P. Generalised syntheses of ordered mesoporous oxides: the atrane route. *Solid State Sci.* **2000**, *2*, 405–420.

(26) Sutrisno, L.; Ariga, K. Pore-engineered nanoarchitectonics for cancer therapy. *NPG Asia Mater.* **2023**, *15*.

(27) Pellicer-Castell, E.; Belenguer-Sapiña, C.; Borràs, V.J.; Amorós, P.; El Haskouri, J.; Herrero-Martínez, J.M.; Mauri-Aucejo, A.R. Extraction of aflatoxins by using mesoporous silica (type UVM-7), and their quantitation by HPLC-MS. *Microchimica Acta* **2019**, *186*, 792.

(28) Díaz de Greñu, B.; Muñoz-Pina, S.; De los Reyes, R.; Benítez, M.; El Haskouri, J.; Amorós, P.; Ros-Lis, J.V. Fast microwave-assisted synthesis, calcination and functionalization of a silica mesoporous nanomaterial: UVM-7. *ChemSusChem* **2023**, *16*, e202300123.

(29) Huerta, L.; Guillem, C.; Latorre, J.; Beltrán, A.; Beltrán, D.; Amorós, P. Large monolithic silica-based macrocellular foams with trimodal pore system. *Chem. Commun*. **2003**, *2003*, 1448–1449.

(30) Tortajada, M.; Ramón, D.; Beltrán, D.; Amorós, P. Hierarchical bimodal porous silicas and organosilicas for enzyme immobilization. *J. Mater. Chem*. **2005**, *15*, 3859–3868.

(31) El Haskouri, J.; Morales, J.M.; Ortiz de Zárate, D.; Fernández, L.; Latorre, J.; Guillem, C.; Beltrán, A.; Beltrán, D.; Amorós, P. Nanoparticulated silicas with bimodal porosity: Chemical control of the pore sizes. *Inorg. Chem*. **2008**, *47*, 8267–8277.

(32) Burguete, P.; Beltrán, A.; Guillem, C.; Latorre, J.; Pérez-Pla, F.; Beltrán, D.; Amorós, P. Pore length effect on drug uptake and delivery by mesoporous silicas. *ChemPlusChem* **2012**, *77*, 817–831.

(33) Pérez-Esteve, É.; Ruiz-Rico, M.; De la Torre, C.; Villaescusa, L.A.; Sancenón, F.; Marcos, M.D.; Amorós, P.; Martínez-Máñez, R.; Barat, J.M. Encapsulation of folic acid in different silica porous supports: A comparative study. *Food Chem*. **2016**, *196*, 66–75.

(34) Moragues, A.; Guillem, C.; Mauri-Aucejo, A.; Totajada, M.; Beltrán, A.; Beltrán, D.; Amorós, P. Enlarged pore size in nanoparticulated bimodal porous silicas: Improving accessibility. *Microporous and Mesoporous Materials* **2015**, *221*, 150–158.

(35) Martínez Pérez-Cejuela, H.; Ten-Doménech, I.; El Haskouri, J.; Amorós, P.; Simó-Alfonso, E.F.; Herrero-Martínez, J.M. Solid-phase extraction of phospholipids using mesoporous silica nanoparticles: application to human milk samples. *Anal. Bioanal. Chem*. **2018**, *410*, 4847–4854.

(36) Pellicer-Castell, E.; Belenguer-Sapiña, C.; Amorós, P.; Herrero-Martínez, J.M.; Mauri-Aucejo, A.R. Bimodal porous silica nanomaterials as sorbents for an efficient and inexpensive determination of aflatoxin M1 in milk and dairy products. *Food Chem*. **2020**, *333*, 127421.

(37) Benítez, M.; Rodríguez-Carrillo, C.; Sánchez-Artero, S.; El Haskouri, J.; Amorós, P.; Ros-Lis, J.V. Scaled-up microwave-assisted batch and flow synthesis and life cycle assessment of a silica mesoporous material: UVM-7. *Green Chem*. **2023**, *26*, 785–793.

(38) Grand View Research. Mesoporous silica market size, share & trends analysis report by product, by application, by region, and segment forecasts, 2024 - 2030. Grand View Research. (Accessed May 7, 2025). https://www.grandviewresearch.com/industry-analysis/mesoporous-silica-market

(39) Sigma-Aldrich. Silica. (Accessed May 7, 2025). https://www.sigmaaldrich.com/ES/es/substance/silica1234598765

Scaled-up microwave-assisted batch and flow synthesis and life cycle assessment of a silica mesoporous material: UVM-7

Miriam Benítez[1], Cristina Rodríguez-Carrillo[1], Sheila Sánchez-Artero[1], Jamal El Haskouri[2], Pedro Amorós[2] and Jose V. Ros-Lis[1,*]

[1]Departamento de Química Inorgánica, Universitat de València, Doctor Moliner 50, P.O. Box 73, 46100 Butjassot, Spain

[2]Institut de Ciència dels Materials, Universitat de València, P.O. Box 22085, 46071 Valencia, Spain

*Correspondence: j.vicente.ros@uv.es; Tel.: +34-963544856

Green Chemistry **2024**, *26*, 785-793

DOI: 10.1039/D3GC02875E

Received: 2nd August 2023, Accepted: 24th October 2023

Published: 31th October 2023

Abstract

The development of scaled-up processes for the synthesis and functionalization of silica materials is a key issue for its adoption in various applications. This report introduces innovative batch and flow methodologies for the synthesis and functionalization of substantial quantities of UVM-7, a silica mesoporous material exhibiting a bimodal pore system. The synthesis benefits from the combination of the atrane route with a reduction in reaction time induced by microwaves generated with a solid-state source. To our knowledge, this is the first example of a flow microwave-assisted synthesis of silica mesoporous materials. The materials were characterized by thermogravimetric analysis, X-ray diffraction, transmission electron microscopy and N_2 absorption/desorption isotherms. The scaled-up procedures, encompassing both batch and flow, are capable of synthesizing as-made materials in less than 15 minutes, yielding materials with a topology characteristic of UVM-7 akin to those synthesized via conventional methodologies. The functionalization process can be executed in less than five minutes with loadings of organic moieties of 3.2 mmol of APTES (g of silica)$^{-1}$. Within an hour, the as-made material for more than 150 g of calcined UVM-7 could be synthesized, and up to 60 g could be functionalized. Life Cycle Assessment (LCA) using the ReCiPe method indicates that the most significant impacts are in the categories of freshwater ecotoxicity, marine ecotoxicity, and human carcinogenic toxicity. The scaled-up synthesis offers a substantial reduction in environmental impacts in these categories, a 5-fold reduction in CO_2 equivalent emissions compared to the non-scaled synthesis and up to half

compared to conventional synthesis. The main contributors are solvents in the functionalization and energy consumption during the calcination.

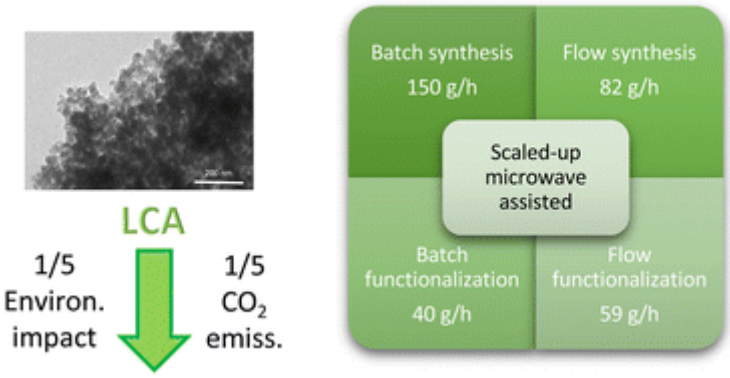

1. INTRODUCTION

Silica mesoporous materials have been widely explored at the research level in recent decades. We can cite as the first example the MCM-41 published in 1992.[1] These materials are characterized by an ordered mesopore system with a pore diameter of around 2 nm. The presence of a pore system with a uniform size distribution and the ease of functionalization with both organic molecules and inorganic oxides or nanoparticles have allowed the development of a wide range of materials with the most diverse applications.[2] The pore size of MCM-41 limited its application, so other materials with larger pore sizes quickly appeared, such as SBA-15 or SBA-16.[3] Among the fields in which silica mesoporous materials have been used, we can mention catalysis, biomedicine, sensors, controlled release, etc.[4] In contrast to MCM-41, which shows a unimodal mesopore system, nanoparticulated silicas can also offer hierarchical bimodal porosity, and this feature can improve accessibility and mass transfer (in both directions, between the pores and the outside). For example, UVM-7, prepared through a one-pot procedure by using a simple template agent and starting from silicon atrane complexes as inorganic precursors, presents a very open architecture based on a continuous network constructed from covalently bonded pseudospherical mesoporous primary nanoparticles whose aggregation defines a nonordered secondary system of large textural pores.[5] This organization favours the mass-transfer processes inside UVM-7 silicas, which improve their applicability.[6]

The preparation of mesoporous silica materials is mainly based on the sol–gel method in a hydroalcoholic medium in the presence of a surfactant or

polymer. These act as structure directing agents and generate the final material, the mesoporous structure. The typical synthesis process for this class of materials comprises synthesis (at room temperature or heating, generally including an aging process), emptying of the pores by calcination or extraction, and a subsequent functionalization process. This method, which we could describe as "conventional", has been complemented with other strategies aimed at obtaining materials more quickly, with higher yields or novel morphologies. Some examples of alternative methodologies use ultrasounds, microwaves, or mechanochemistry.[7] Among them, microwaves are especially suitable for this purpose since they considerably increase the reaction rate, which means less processing time. In this sense, the authors of the present work reported a microwave-assisted UVM-7 synthesis method that allows the use of solid-state microwave generation technology to prepare, calcinate, and functionalize a mesoporous silica material in only 4 hours.[8] In part, the success of the result is due to the use of solid-state (SS) microwave generators that allow the generation of radiation with a controlled and stable power, even for small powers, and with a narrow range of frequencies.[9] Compared to other silica materials such as zeolites or fumed silica that are usually prepared in large quantities, mesoporous materials are generally prepared only in batches and at the gram level, limiting their practical application. Thus, the development of synthesis procedures that allow one to obtain larger quantities of materials is a topic of interest. The reported scaled-up synthesis methods tend to depart from organosilanes or a low-cost source of silica such as sodium silicate or rice husk following the common sol–gel procedures.[10] In other cases, more scalable alternative

techniques such as spray drying are applied.[11] However, they are limited in general to a few grams, even only 1 gram. Conversely, the gradual injection of reactants has been revealed as an interesting technique for the preparation of dozens of grams of monodisperse microporous silica particles in 3 hours, but unfortunately, the resulting material had a pore diameter narrower than 1 nm.[12] An attempt to use the same technique in the presence of a surfactant to obtain an ordered large-sized pore structure produced only disordered materials with an area of approximately 500 m^2g^{-1}.[13] Remarkably, Zhang et al. were able to obtain up to 1 kg of spherical silica nanoparticles with a stellate, worm-like or raspberry-like morphology departing from TEOS upon heating the react i on mixture for 2 hours.[14] Going a step further, 1 kilogram of mesoporous silica nanospheres with a surface area of 500 m^2g^{-1} were prepared in the absence of organic solvents in 3 hours using a combination of cationic and anionic surfactants.[15] However, none of these examples take advantage of the possibilities that microwaves offer to speed up synthesis.

Another possibility for obtaining large amounts of materials is the development of flow synthesis strategies. This allows the continuous production of materials with homogeneous properties and facilitates automation. However, until now, it has generally been limited to microfluidic systems and the use of this approach to obtain silica materials in large quantities has not been reported. A particular case is the use of a roll-to-roll fabrication technique coupled with evaporation induced self-organization for the preparation of ordered mesoporous materials.[16]

In the present work, we hypothesize that the use of solid-state microwaves in batch or flow systems may be a good strategy to obtain mesoporous silica,

specifically UVM-7, in large quantities while reducing the environmental impact.

2. RESULTS AND DISCUSSION

The preparation process of mesoporous silica materials can be divided into two independent stages: (i) the formation of the silica structure, “synthesis” from now on, and (ii) the surface modification with organic silanes, “functionalization” from now on. In the present work we set ourselves the objective of achieving a scaling factor of 100 in both stages. The first approach to obtain large amounts of materials is to continue working in batch while increasing the size of the reactor. This is not immediate since aspects such as the mixture of the reagents, the homogeneity of the reaction, and the transmission of energy can be dependent on the batch size. An alternative approach is the use of flow synthesis, which offers the main advantages of maintaining a smaller reactor size and the possibility of automation.

2.1. Scaling-up of the microwave-assisted batch synthesis and functionalization

2.1.1. Batch synthesis.

Fig. 1a shows a scheme of the synthesis setup. The power source consists of four 2450 MHz SS microwave generators. The power generated by each of the sources is transferred to the cavity through a coaxial cable connected to an antenna. Thus, the cavity is fed by four antennas. The reaction mixture is placed in a glass container and elevated above the cavity to avoid a field decrease in the vicinity of the surface. Following our previous results, as an initial approximation, we proposed a scaled synthesis process in which the use

of energy was proportional to the amount of water.[8] Considering that we sought to multiply by 100 the amount of material, a microwave power of 5 kW was implied. This value is much higher than the combined potency of 800 W of the four solid state sources. Thus, we increased the irradiation time to 12.5 minutes. This could also be advantageous, since in our previous results a longer irradiation time led to an increase in the volume of inter-particle pores and therefore the expected diffusion capacity.[8]

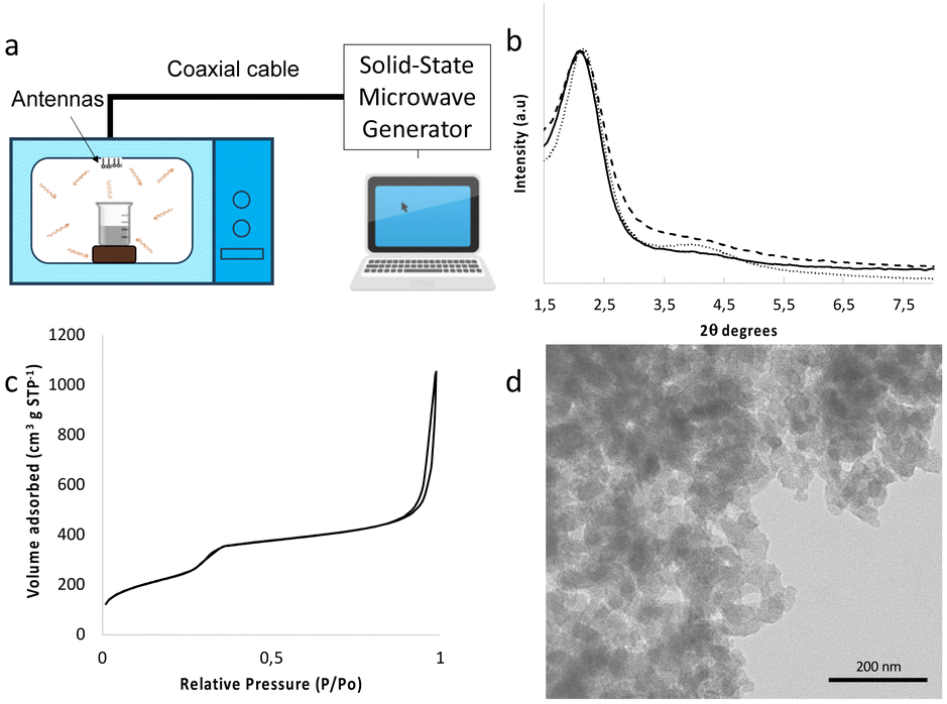

Fig. 1 *(a) Scheme of the batch reactor; (b) normalized XRD of the materials BS800 (solid line), BS400 (dashed line) and a conventional synthesis (dotted line); (c) nitrogen adsorption–desorption isotherms of BS800; (d) representative TEM images of BS800.*

As expected, the formation of a white solid in the reactor due to condensation and the growth of silica is observed experimentally. The process occurs quickly

in about 10 minutes and is accompanied by a decrease in reflected power. This suggests that the gel formed couples better with the incident radiation than the solution or sol before gelation and may be a tool to detect the end point of the reaction. After calcination, 35 g of material is obtained, equivalent to a yield of 95%. Nearly all the silicon from TEOS is incorporated into the final material.

The material obtained under these experimental conditions (BS800) presents the typical characteristics of UVM-7. Low angle XRD shows a peak at around 2° (2θ) corresponding to the (100) reflection of the hexagonal mesoporous structure. In addition, a wide signal of lower intensity is observed at 3.5–4.0° (2θ) due to the overlapped (110) and (200) reflections of a hexagonal lattice (Fig. 1b). TEM shows the structure of this class of materials consisting of small mesoporous particles that aggregate giving rise to the presence of large textural pores between them (Fig. 1d). This type of morphology is confirmed by the N_2 absorption/desorption analysis, which includes a high surface area of about 956 m^2g^{-1} and a bimodal pore system with two well-differentiated adsorption steps (Fig. 1c and Table 1). The first one, occurring at relatively low relative pressures ($0.2 < P/P_0 < 0.4$) is related to capillary condensation in the 2.8 nm mesopores of the particles. Its shape, sharp and without a hysteresis loop, suggests that these mesopores are uniform and cylindrical. The second step, occurring at high relative pressures ($P/P_0 > 0.8$), corresponds to the filling of 37.2 nm interparticle pores formed between primary nanoparticles. If we compare our material with that obtained by conventional synthesis, it is observed that in general, it has the same properties. The UVM-7 prepared following conventional procedures has larger inter-particle pores, but typically

this parameter is one of those that presents greater variation.[8] This fact opens the possibility of modulating larger pores in a finer way through a modification of the MW preparative conditions.

Table 1. *Textural properties of UVM-7 mesoporous materials synthesized or functionalized in this work.*

Material	*2θ[a] (°)*	*Area[b] (m^2g^{-1})*	*Meso vol.[c] (cm^3g^{-1})*	*Mesopore diameter[c] (nm)*	*Textural diameter[c] (nm)*	*Textural vol.[c] (cm^3g^{-1})*
BS800	2.11	956	0.82	2.8	37.5	2.05
BS800c	2.23	801	0.85	2.6	69.9	1.62
BS800s	2.01	1024	0.67	2.6	29.9	0.58
BS400	2.17	937	0.51	2.5	30.7	1.37
BF-4	2.15	372	0.15	2.3	33.6	0.46
FS-1	2.29	928	0.78	2.8	47.8	2.30
FS[d]	2.04	980 ± 50	0.84 ± 0.04	2.82 ± 0.04	34.0 ± 1.8	0.77 ± 0.13
FF[e]	2.01	220 ± 160	0.08 ± 0.04	2.7 ± 0.2	54 ± 4	1.02 ± 0.10
Conv. Synth.	2.13	969	0.78	2.7	49.9	1.44
Conv. Funct.	2.14	251	0.15	2.6	39.6	0.96

[a]Angle of incidence for the reflection plane. [b]BET specific surface calculated from N_2 adsorption–desorption isotherms. [c]Pore volumes and pore sizes (diameter) calculated from N_2 adsorption–desorption isotherms. [d]Average and SD of the fractions FS-2 to FS-4. [e]Average and SD of the fractions collected during the flow functionalization.

Since the reactor has a diameter of 14 cm, one of the aspects that worried us was that inhomogeneities could be generated in the reaction medium. The combination of a short reaction time with the limited penetration capacity of

the microwaves could lead to hot and cold spots, with a consequent decrease in the homogeneity of the final product. Thus, a new batch irradiated at 800 W for 12.5 minutes was prepared, and samples were taken from the center (BS800c) and the side (BS800s) of the reaction flask. Although in all cases the material can be qualified as UVM-7 (see Table 1 and Fig. S1 in the ESI†), there is indeed a certain difference between the properties of both samples. The mesopore size in both cases is equal and the BET area, despite its variation, falls into the range of a mesoporous UVM-7 (typically between 800 and 1100 cm^3g^{-1}) (Table 1). Again, the main difference lies in the process of aggregation of the particles to form the large-pore architecture. In any case, it is appropriate to limit the width of the reactor to ensure the homogeneity of UVM-7. Additionally, a longer reaction time was applied (400 W and 25 minutes) maintaining the energy input (BS400). Although BS400 is a bimodal mesoporous material, it presents a lower volume of mesopores and a slight reduction in the pore diameter (see Table 1 and Fig. S1 in the ESI†). Furthermore, only 25 g of material before calcination was obtained, which corresponds to a yield of 68%. It seems that microwave power is not an innocent element and that it has a considerable influence on the kinetics of the hydrolysis and condensation reactions.

The microwave-assisted UVM-7 synthesis process is a widely scalable process. Extrapolating our results and considering our equipment, the proposed synthesis method would allow one to prepare the “as-made” material to obtain more than 150 g of calcined material in just one hour, which opens the way to its industrial application.

2.1.2. Batch functionalization.

Functionalization is a common process in the preparation of silica nanomaterials. The surface modification allows the materials to act as sensors, controlled release materials, etc. In our case, the synthesis equipment and configuration are the same as those used in the Batch synthesis section. Our goal in this case was to achieve a 50-fold scale without increasing reaction times. To obtain a more sustainable process and reduce the reaction volume, the concentrations of the reactants were tripled. The APTES:UVM-7 ratio remained constant. The power selected was 200 W and different times of irradiation (4, 8, 12 and 16 minutes) were employed. In only 4 minutes, TGA revealed that a high degree of functionalization was achieved. 3.2 mmol of APTES (g of silica)$^{-1}$ were added to the surface of UVM-7, similar to the 3.6 mmol of APTES (g of silica)$^{-1}$ that can be obtained by conventional synthesis. An extension of the reaction time to 8, 12 and 16 minutes increases the organic content to 3.3, 3.7 and 4.0 mmol APTES (g of silica)$^{-1}$ respectively. However, we believe that for most applications, the slight increase in load does not justify the need for higher energy and time consumption in this synthesis process. This degree of functionalization is significantly higher than that previously found for microwave functionalization (1.8 mmol) for the same time.[8] Although we cannot rule out other reasons, we believe that this result could be due to the increase in concentration derived from the reduction in solvent volume. As expected from the functionalization process, chemically mild to silica, the silica structure is not affected (see Table 1 and Fig. S1 in the ESI†). However, the coating of organic matter reduces the size and accessibility of the pores. This effect is more pronounced in the mesopores due to their

smaller size, leading to a reduction in the total surface area of the material to 372 m^2g^{-1} (Table 1). In view of the results, we can conclude that microwave-assisted batch functionalization is also a very scalable process and that it can help considerably reduce reaction times. If we consider that the reaction time is 4 minutes, in 1 hour, about 40 grams of the mesoporous material UVM-7 could be functionalized.

2.2. Flow microwave-assisted synthesis

Flow synthesis offers an interesting option for the preparation of materials in large quantities due to its versatility and the homogeneity that is conferred on the products. In addition, in the case of microwaves, it allows the avoidance of the formation of hot and cold spots because the liquid is in motion, and the diameter of the conduction can be adjusted to avoid significant power losses. Unlike batch synthesis, as the dissolution mass is lower, the power requirements are lower. Thus, we work with a source of only 200 W and one antenna.

2.2.1. Flow synthesis.

To carry out the flow synthesis, we departed from two solutions, one containing the atrane complex and the other containing the water necessary for hydrolysis and condensation. Both are mixed just before the microwave inlet, within which they are irradiated with the solid-state source. A schematic of the synthesis setup can be seen in Fig. 2a. A power of 100 W and a residence time of the solution inside the furnace of 1 minute were established. Samples of the prepared material were collected for 20 minutes in 4 batches to compare the homogeneity throughout the reaction time. As can be seen in

Fig. 2 and from the data in Table 1, there is a significant difference between the material generated in the first 5 minutes (FS-1) and the following fractions. In comparison with the material obtained in the conventional synthesis of UVM-7, the FS-1 fraction presents a certain displacement at a larger angle (2.3°) in XRD, indicative of a slightly smaller cell size (Fig. 2d). In addition, TEM shows that FS-1 presents a structure composed of large mesoporous particles surrounded by smaller ones (Fig. 2b). This structure diverges from the common UVM-7 composed of aggregated small particles. Probably the reactor has not reached the steady state during the first few minutes, and this fraction should be discarded. The rest of the fractions have the characteristics of UVM-7. Table 1 shows that the textural properties of fractions FS-2 to FS-4 are common for UVM-7 and that the variability throughout the synthesis is relatively small, reinforcing the idea that microwave-assisted flow synthesis may be an appropriate strategy to obtain materials with homogeneous properties. XRD shows that the peak has a slight displacement at a smaller angle (from 2.13° for conventional synthesis to 2.06° for flow synthesis) which corresponds to a slightly larger cell size. Regarding the structure of the particles, TEM shows that in microwave-assisted flow synthesis, the UVM-7 structure is maintained (Fig. 2c, e and f). The flow synthesis would allow the preparation of 82 g of material after calcination in one hour. This value is lower than the scaled-up synthesis in batch but, in any case, opens the door to an automatic preparation of UVM-7 in large quantities.

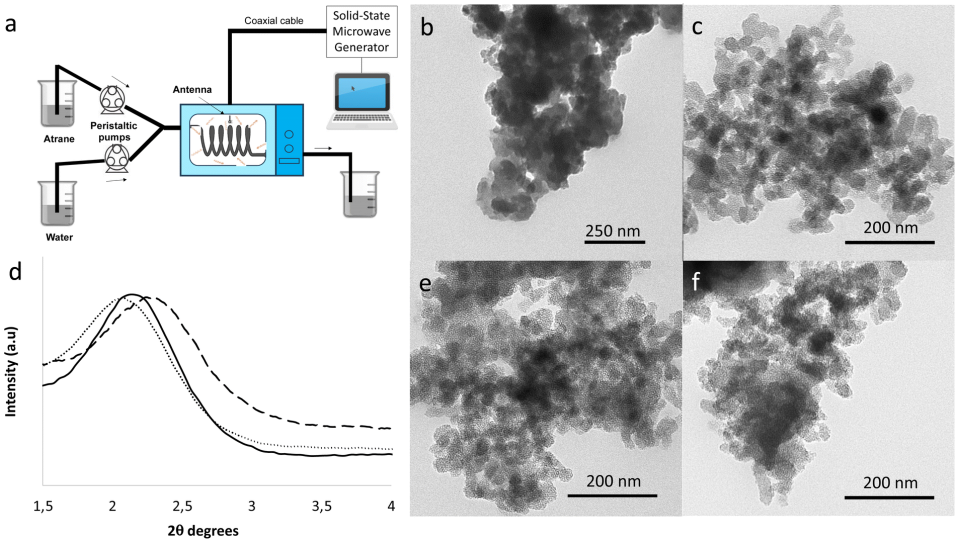

Fig. 2 *(a) Scheme of the batch reactor; representative TEM images of FS-1 (b), FS-2 (c), FS-3 (e) and FS-4 (f); (d) normalized XRD of the materials FS-1 (dashed line), FS-2 to 4 (dotted line), and conventional synthesis (solid line).*

2.2.2. **Flow functionalization**.

Finally, we studied the possibility of developing a continuous process for the functionalization step. Functionalization is more complex than synthesis. Hydrolysis and condensation are fundamental processes in a homogeneous medium. The synthesis parameters were adjusted so that the formation of the material occurred in the final part of the reactor. However, for functionalization, we started with a solid and it was a heterogeneous phase reaction. The configuration of the equipment for functionalization was slightly different from that of the synthesis step. APTES and the material were added directly to the acetonitrile solution, so that only the use of a peristaltic pump was necessary. In addition, it was necessary to make some adaptations to facilitate the transit of the material through conduction. Although acetonitrile

is a solvent commonly used for functionalization, we tried to increase the viscosity of the solution to increase the drag. We tested ACN:glycerol 2:1 v/v mixtures without obvious improvements. We also tested water, which gave an adequate drag for the material, but we discarded it due to the risk of hydrolysis and condensation reactions between the APTES molecules in parallel to the reaction on the surface of UVM-7. Finally, we evaluated the possibility of using DMSO, which, although offered good transport of materials and functionalization of around 18.0 ± 0.5% by mass, was discarded due to the difficulty of working with this type of solvent in large-scale productions. Therefore, we decided to use acetonitrile as the solvent and focus on modifying the system. Among these adaptations we can highlight the achievement of a tube of adequate inner diameter, small enough to drive the solution homogeneously but large enough to avoid blocking the conduction by the material, and a configuration in which the tube was always advancing in favor of gravity. We opted for a rubber with an internal diameter of 6 mm. The organic load stands at 13.2 ± 1.4% (equivalent to 3.1 mmol APTES (g of silica)$^{-1}$). The measurements of nitrogen adsorption/desorption show the expected reduction in the total area due to the blockage of the pores by APTES. The variation in the total area between the fractions is higher in the flow functionalization in comparison with the flow synthesis, which could be assigned to the heterogeneous character of the reaction and possible variations in the residence time of the material. Continuous microwave-assisted functionalization allows the production of 59 g of functionalized material in one hour.

2.3. Life cycle assessment and reduction of the environmental impact

Life Cycle Analysis (LCA) is a methodology that allows the identification of those processes that have the greatest environmental impact. It covers not only global warming, but also many other parameters of great importance for the sustainability of human actions. Although at first glance it may seem that one process is more sustainable than another, this methodology allows us to quantify it and identify those reagents or processes with the greatest impact to try to reduce it.

In our case, the LCA has been applied to the four scaled-up processes, the non-scaled synthesis and functionalization, and the conventional synthesis. The objective is to determine if, through the application of microwaves and scaling, in addition to a reduction in time, there is a variation in the environmental impact of the synthesis and functionalization of UVM-7. The system boundaries have been defined as a cradleto-gate system. The use and disposal of the material have been left out of the study, as well as the emissions. The functional unit has been defined as the preparation of 1 kg of calcined UVM-7 or the functionalization of 1 kg of UVM-7. Life cycle inventories can be found in Table 2. For a better data analysis, energy and solvents have been broken down into the different stages of the process and/or functions.

Table 2. *Life cycle inventory for the production or functionalization of 1 kg of UVM-7.*

Inventory	Reagents (kg) or energy (kWh)			
	MW escalated batch	*MW escalated flow*	*MW non-escalated*	*Conventional*
TEOS	3.7	3.7	3.7	3.7
TEAH	8.4	8.4	8.4	9.2
CTABr	1.3	1.3	1.3	1.6
DIW synthesis	28.6	28.6	28.6	28.5
DIW washing	71.4	71.4	428.6	177.9
Ethanol washing	2.9	2.9	57.1	8.9
APTES	1.3	1.3	1.3	2.2
Acetonitrile functionalization	47.2	47.2	235.8	23.6
Acetonitrile washing	15.7	7.9	157.2	23.6
Energy synthesis	3.5	3.5	22.9	201.4
Energy calcination	360.5	360.5	970.0	1924.0
Energy functionalization	24.0	18.0	200.0	55.0

The main results of the life cycle impact assessment (LCIA) have been collected in Fig. 3–5. First, we considered the sum of the normalized impact values to identify which categories generated the greatest impact (see Fig. 3a). Unlike other studies where the contribution to global warming is highlighted, in our case the greatest impacts are in the categories of freshwater ecotoxicity, marine ecotoxicity, and human carcinogenic toxicity and these are largely dependent on the type of synthesis process. Also, the global warming potential has been calculated and displayed in Fig. 3b. The scaled synthesis developed in this work offers a 5-fold reduction in the kg of CO_2 eq. generated

per kg of material with respect to the non-scaled synthesis and up to half compared to conventional synthesis.

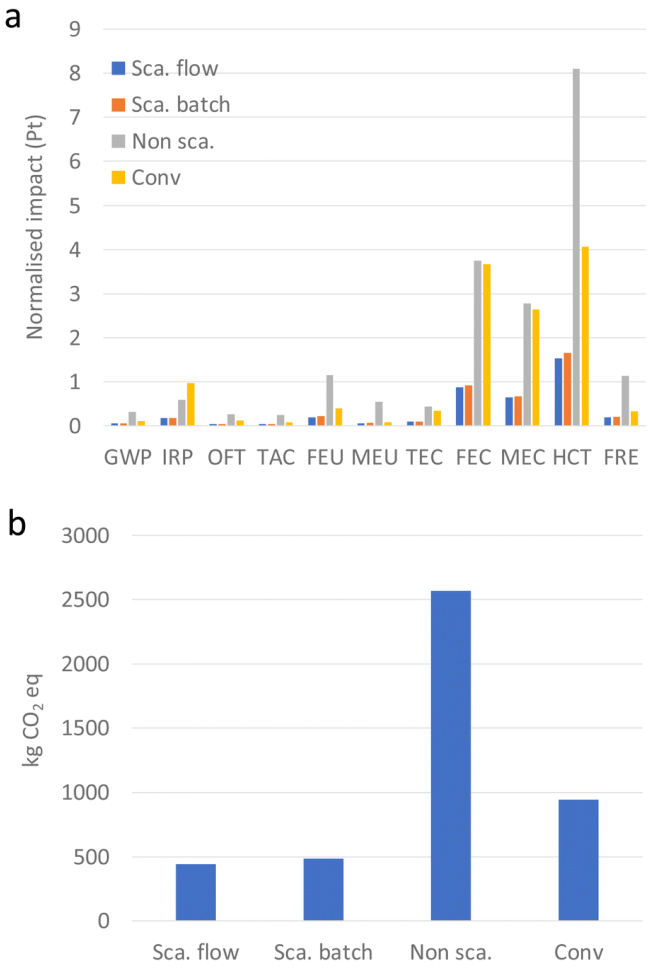

Fig. 3 *(a) Normalised impact of different synthesis methods and impact categories: global warming (GWP), ionizing radiation (IRP), ozone formation (terrestrial ecosystems) (OFT), terrestrial acidification (TAC), freshwater eutrophication (FEU), marine eutrophication (MEU), terrestrial ecotoxicity (TEC), freshwater ecotoxicity (FEC), marine ecotoxicity (MEC), human carcinogenic toxicity (HCT), and fossil resource scarcity (FRE). (b) Emission of CO_2 eq.*

We can use the single score calculated from the endpoint analysis to gain a deeper understanding of the factors that influence the overall impact. To facilitate the analysis, we have divided the synthesis into the preparation of the "as-made" material, which has the surfactant inside the pores, and the calcination. If we review the influence of the different stages of preparation of the functionalized UVM-7 (see Fig. 4a), we can observe that the different steps have a diverse level of impact and that this largely depends on the process type.

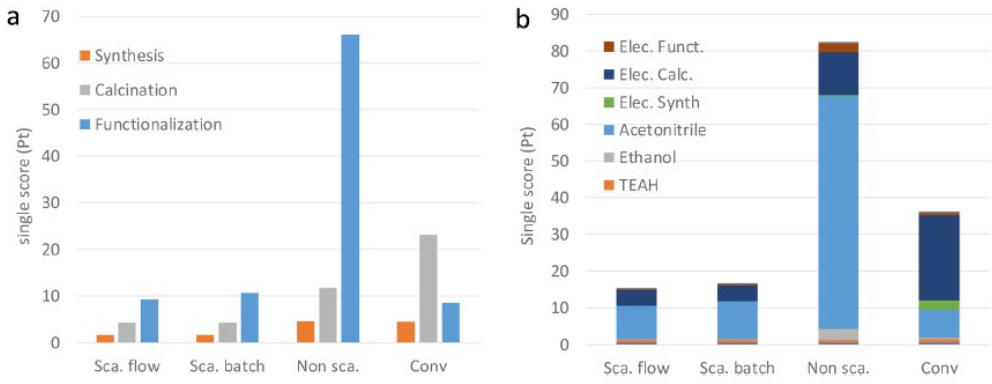

Fig. 4 *(a) Single score obtained from the synthesis methods [conventional (Conv), non-scaled-up MW assisted synthesis (Non sca.), scaled-up MW assisted batch synthesis (Sca. batch), and scaled-up MW assisted flow synthesis (Sca. flow)] and the steps of reaction; (b) single score obtained from the synthesis methods and the items of the inventory.*

Once again, it can be seen how the escalated processes have a much lower impact than the conventional or non-escalated processes and are similar beween them. Regarding the steps, the preparation of the "as

made" material has in all cases a lower impact than the calcination and functionalization phases. Functionalization is especially important in the case of a non-scaled process. A better understanding of these results can be deduced from the impact of the different elements of the inventory (see Fig. 4b). The two main elements contributing to the impact are the use of acetonitrile in the functionalization and the electricity used in the calcination, which account for between 85 and 91% of the impact depending on the type of process.

The cost of synthesis was estimated based on the LCIA data and our unitary costs (see ESI Tables S1 and S2†). Although the cost can be overestimated due to the use of laboratory cost data, it can be useful to compare the four synthesis methods and identify opportunities for saving. The scaled-up processes offer a reduction of cost from almost 36€ g^{-1} to approximately 7.5€ g^{-1}, a 5-fold reduction. The most expensive step is functionalization, due to the use of acetonitrile. Next, the second source of cost is the acquisition of reagents. By contrast, the energy cost is relatively low. If we compare the scaled processes with the conventional ones, the main reduction is due to the reduction in the consumption of electricity.

From the LCA results and cost analysis we can conclude that the next steps to improve the scaled synthesis should be focused on reducing acetonitrile consumption and the impact of energy use. To reduce the consumption of acetonitrile, we can vary the solvent, but a more sustainable option may be to recover the solvent by distillation, using it in successive syntheses. Accordingly, we have proposed a scenario in which the energy cost increases due to distillation and 95% of acetonitrile can be recovered in each cycle. To

reduce the impact of energy consumption in calcination, one option is to use electricity from renewable sources such as photovoltaics. Finally, we have proposed a scenario in which the previous two options are combined. The results of the scenarios applied to scaled-up flow synthesis, the one with the lower impact, can be seen in Fig. 5.

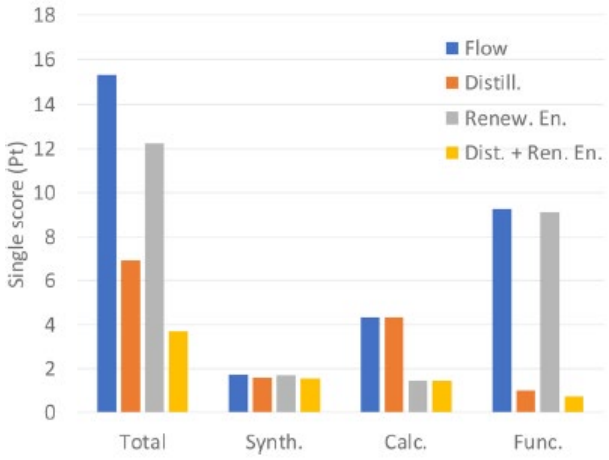

Fig. 5. *Single score for each scenario and synthesis step.*

The use of renewable energy in calcination almost avoids any impact in this phase, while distillation reduces the impact of functionalization by 9 times. When we combine both strategies, the sum of the single score drops from 15.3 to just 3.7. Regarding the cost, savings higher than 60% could be obtained.

3. EXPERIMENTAL

3.1. Chemicals

All the synthesis reagents were analytically pure and were used without further purification. Tetraethyl orthosilicate (TEOS), triethanolamine ($TEAH_3$),

cetyl-trimethylammonium bromide (CTABr), and (3-aminopropyl)triethoxysilane (APTES) were purchased from Sigma Aldrich (Madrid, Spain). Acetonitrile and ethanol were purchased from Scharlab S.L

3.2. Microwave devices

Two different solid-state (SS) devices, one for batch processes and the other for flow processes, were used. Both devices were provided by Microbiotech S.L. The batch device consists of four microwave sources connected through a coaxial cable to the irradiation cavity. Each source operates at a maximum power of 200 W with selectable potency in 1 W increments rising to a maximum power of 800 W in total. The frequency of each source can be adjusted independently to tune the system and optimise the absorbed power within the 2420 MHz – 2480 MHz range in 1 Hz increments. The flow device consists of a SS microwave source with characteristics similar to the batch device (maximum power of 200 W) but with selectable potency in 5 W increments.

3.3. Microwave-assisted synthesis of UVM-7

3.3.1. Escalated batch synthesis.

The synthesis of UVM-7 was performed based on a previously reported method for UVM-7 preparation following the atrane route in combination with microwave irradiation.[8] 1 L of deionized water was added to 412 mL of the atrane mixture containing Si:$TEAH_3$:CTABr in a 1:3.4:0.25 mole ratio (263 mL of $TEAH_3$, 137 mL of TEOS, and 45 g of CTABr). The mixture was smoothly shaken until homogeneity, then placed into the microwave oven cavity and then irradiated for 12 minutes at 800 W until the gel was formed. As a result,

a white solid was obtained. This solid was isolated by filtration, washed with water and ethanol, dried in an oven at 80 °C overnight and calcined at 550 °C under a static air atmosphere, as an oxidant atmosphere, for 5 h to remove the CTABr surfactant. The resulting material was denoted as BS800 (batch synthesis at 800 W). Samples collected at the centre and the side of the reactor were denoted as BS800c and BS800s respectively. Also, a batch of material irradiated at 400 W for 25 minutes (BS400) and UVM-7 prepared with the conventional method in the absence of MW were synthesized for comparative purposes.[5]

3.3.2. Escalated batch functionalization.

For microwave-assisted functionalization, 2.5 g of calcined UVM-7 were dispersed in 150 mL of an APTES (15 mmol) solution in acetonitrile. The mixture was shaken for 10 seconds and then placed into the microwave oven cavity. The suspension was irradiated for 4 to 16 minutes at 200 W. After irradiation, the white solid was collected by filtration, washed with acetonitrile, and dried in an oven at 40 °C overnight. The resulting material was denoted as BF-minutes (batch functionalization). The conventional procedure was also carried out as a reference.[6] The mixture of UVM-7, APTES and acetonitrile was stirred for 5.5 hours at room temperature. The solid was isolated, washed and dried as described above.

3.3.3. Flow synthesis of UVM-7.

The flow synthesis of UVM-7 was also performed based on a reported method for UVM-7 preparation following the atrane route.[5] The atrane mixture was prepared as described above in the batch synthesis. The reagents, atrane and

water were pushed through the microwave system using two peristaltic pumps, one for each reagent. The pumping rates were fixed at 10 rpm for the water and 5 rpm for the atrane to ensure an appropriate atrane:water ratio (0.41:1 v/v) and an irradiation time (remaining time inside the cavity) of 1 min. The microwave potency was set at 100 W. The product generated during the first minute was rejected and fractions were collected each 5 minutes. All the fractions were filtered, washed with water and ethanol, dried at 80 °C in an oven overnight, and calcined at 550 °C under a static air atmosphere, as an oxidant atmosphere, for 5 h to remove the CTABr surfactant. The fractions were denoted as FS-1 to FS-4 (flow synthesis).

3.3.4. Flow functionalization.

A 300 mL acetonitrile suspension containing 5 g of UVM-7 and 30 mmol of APTES under stirring was pumped through the microwave using a peristaltic pump. The pump speed was adjusted to 10 or 20 rpm (depending on the diameter of the conduction) to ensure a remaining time of 1 minute inside the cavity. The amount of material released was weighed at different times to ensure a continuous flux. The white solid was collected by filtration, washed with acetonitrile, and dried in an oven at 40 °C overnight. The resulting material was denoted as FF (flow functionalization). During the optimization, the effects of the solvent and the diameter of the conduction were evaluated to ensure that the material moved uniformly through the system.

3.4. Characterization of the materials

All solids were characterized by X-ray powder diffraction (XRD) at low angles (Bruker D8 Advance diffractometer) using a monochromatic Cu Kα source

operated at 40 kV and 40 mA. Patterns were collected in steps of 0.04° (2θ) over the angular range 1.3–8.3° (2θ) for 1 s per step. Transmission electron microscopy (TEM) images were taken with a JEOL-JEM-1010 instrument operated at 100 kV (equipped with the digital camera MegaView III and "ANALYSIS" software). Samples were gently ground in ethanol, and grains were deposited on a holey carbon film supported on a Cu grid. Nitrogen adsorption–desorption isotherms (−196 °C) were recorded on a Micromeritics ASAP 2020 automated analyser. The samples were degassed in situ at 120 °C and 10^{-6} Torr for 15 h prior to analysis. Specific surface areas were calculated from the adsorption data within the low-pressure range using the Brunauer–Emmett–Teller (BET) model. Pore sizes and pore volumes were determined following the Barrett–Joyner–Halenda (BJH) model on the adsorption branch. Thermogravimetric analysis (TGA) was performed with a SETARAM SETSYS 16–18 instrument (Caluire-et-Cuire, France) under a dry air flow at a heating rate of 10 °C min^{-1} up to 1000 °C.

3.5. Life cycle analysis

Life cycle analysis (ISO 14040:2006) on a cradle-to-gate basis was applied to the scaled processes. This technique allows the identification of the environmental impacts of the processes and determines opportunities to improve their sustainability. The inventory was defined using the synthesis procedures and the energy consumption measured in the laboratory. The impact was calculated using the Ecoinvent 3 database and the ReCiPe 2016 Endpoint (H) V1.08/World (2010) H/A model available in the SimaPro software. Data from Spain or Europe have been used if they were available in the database, otherwise worldwide data were used. The method includes as

impact categories global warming, stratospheric ozone depletion, ionizing radiation, ozone formation (human health), fine particulate matter formation, ozone formation (terrestrial ecosystems), terrestrial acidification, freshwater eutrophication, marine eutrophication, terrestrial ecotoxicity, freshwater ecotoxicity, marine ecotoxicity, human carcinogenic toxicity, human non-carcinogenic toxicity, land use, mineral resource scarcity, fossil resource scarcity and water consumption. CTABr and APTES are not available in the database, thus, estequat (a cationic surfactant) and TEOS (a silane) were used for the analysis.

4. CONCLUSIONS

We have reported for the first time a scaled-up batch microwave-assisted synthesis of UVM-7, a silica mesoporous material. Also, we have described the first, to our knowledge, flow microwave-assisted synthesis of a silica mesoporous material. The materials obtained following batch and flow scaled procedures have structures and properties similar to those prepared under conventional conditions. The as-made material for the preparation of 168 and 59 g of calcined material per hour can be obtained with the batch and flow methods respectively. The functionalization of UVM-7 can be performed in less than 5 minutes with loadings of organic groups of 3.2 mmol of APTES (g of silica)$^{-1}$. Up to 59 g of UVM-7 per hour can be functionalized. LCA shows that the scaled-up synthesis offers a strong reduction in the environmental impact, but it could be further reduced by the reutilization of solvents and the use of renewable energy.

Conflicts of interest

There are no conflicts to declare.

Acknowledgements

This research was carried out under the grant PID2021-126304OB-C43 funded by MCIN/AEI/10.13039/501100011033 and “ERDF A way of making Europe”, the grant INNVA1/2020/44 funded by the Agencia Valenciana de Innovación, Genertalitat Valenciana, and the AGROALNEXT programme supported by MCIN with funding from European Union Next Generation EU (PRTR-C17.I1) and by Generalitat Valenciana grant number EUAGROALNEXT/2022/065.

References

(1) Kresge, C.T.; Leonowicz, M.E.; Roth, W.J.; Vartuli J.; Beck, J.S. Ordered mesoporous molecular sieves synthesized by a liquid-crystal template mechanism. *Nat.* **1992**, *359*, 710.

(2) Costa, J.A.S.; De Jesus, R.A.; Santos, D.O.; Mano, J.F.; Romao, L.P.C.; Paranhos C.M. Recent progresses in the adsorption of organic, inorganic, and gas compounds by MCM-41-based mesoporous materials. *Microporous Mesoporous Mater.* **2020**, *291*, 109698; Liu, C.; Li, Q.X.; Zhang, D.; Li, Y.J.; Liu, J.Q.; Xiao, X.L. Prog. Chem., 2021, 33, 2085; Pasricha, S.; Gahlot, P.; Mittal, K.; Rai, D.; Avasthi, N.; Kaur, H.; Rai, S. Functionalized MCM-41: Versatile catalysts for organic transformations. *ChemistrySelect*, **2022**, *7*, 202103674.

(3) Zhao, D.Y.; Huo, Q.S.; Feng, J.L.; Chmelka, B.F.; Stucky, G.D. Nonionic triblock and star diblock copolymer and oligomeric surfactant syntheses of highly ordered, hydrothermally stable, mesoporous silica structures. *J. Am. Chem. Soc*. **1998**, *120*, 6024.

(4) Niculescu, V.C. Mesoporous silica nanoparticles for bio-applications. *Front. Mater.*, **2020***, 7*, 36; Singh, B.; Na, J.; Konarova, M.; Wakihara, T.; Yamauchi, Y.; Salomon, C.; Gawande, M.B. Functional mesoporous silica nanomaterials for catalysis and environmental applications. *Bull. Chem. Soc. Jpn*. **2020**, *93*, 1459.

(5) El Haskouri, J.; Ortiz de Zárate, D.; Guillem, C.; Latorre, J.; Caldés, M.; Beltrán, A.; Beltrán, D.; Descalzo, A.B.; Rodríguez-López, G.; Martínez-Máñez, R.; Marcos, M.D.; Amorós, P. Silica-based powders and monoliths with bimodal pore systems. *ChemComm* **2002**, *4*, 330–331.

(6) Muñoz-Pina, S.; Ros-Lis, J.V.; Argüelles, Á.; Coll, C.; Martínez-Máñez, R.; Andrés, A. Full inhibition of enzymatic browning in the presence of thiol-functionalised silica nanomaterial. *Food Chem*. **2018**, *241*, 199–205.

(7) Marquez-Medina, M.D.; Mhadmhan, S.; Balu, A.M.; Romero, A.A.; Luque, R. Post-synthetic mechanochemical incorporation of Al-species into the framework of porous materials: Toward more sustainable redox chemistries. *ACS Sustainable Chem. Eng.* **2019**, *7*, 9537; Díaz de Greñu, B.; De Los Reyes, R.; Costero, A.M.; Amorós, P.; Ros-Lis, J.V. Recent progress of microwave-assisted synthesis of silica

materials. *Nanomaterials* **2020**, *10*, 1092; Głowniak, S.; Szczęśniak, B.; Choma, J.; Jaroniec, M. Recent developments in sonochemical synthesis of nanoporous materials. *Molecules* **2023**, *28*, 2639.

(8) Díaz de Greñu, B.; Muñoz-Pina, S.; De los Reyes, R.; Benítez, M.; El Haskouri, J.; Amorós, P.; Ros-Lis, J.V. Fast microwave-assisted synthesis, calcination and functionalization of a silica mesoporous nanomaterial: UVM-7. *ChemSusChem* **2023**, *16*, e202300123.

(9) Zhou, X.; Pedrow, P.D.; Tang, Z.; Bohnet, S.; Sablani, S.S.; Tang, J. Heating performance of microwave ovens powered by magnetron and solid-state generators. *IFSET* **2023**, *83*, 103240

(10) Morales, J.M.; Latorre, J.; Guillem, C.; Beltrán-Porter, A.; Beltrán-Porter, D.; Amorós, P. Scale-up low-cost synthesis of bimodal mesoporous silicas., *Solid State Sci.* **2005**, *7*, 415; Castillo, R.R.; De la Torre, L.; García-Ochoa, F.; Ladero, M.; Vallet-Regí, M. Production of MCM-41 nanoparticles with control of particle size and structural properties: optimizing operational conditions during scale-up. *Int. J. Mol. Sci.* **2020**, *21*, 7899.

(11) Wang, H.C.; Lu, C.S.; Bai, H.L.; Hwang, J.F.; Lee, H.H.; Chen, W.; Kang, Y.H.; Chen, S.T.; Su, F.S.; Kuo, S.C.; Hu, F.C. Pilot-scale production of mesoporous silica-based adsorbent for CO_2 capture. *Appl. Surf. Sci*. **2012**, *258*, 6943; Emmanuelawati, I.; Yang, J.; Zhang, J.; Zhang, H.; Zhou, L.; Yu, C. Low-cost and large-scale synthesis of functional porous materials for phosphate removal with high performance. *Nanoscale*, **2013***, 5*, 6173.

(12) Shimogaki, T.; Tokoro, H.; Tabuchi, M.; Koike, N.; Yamashina, Y.; Takahashi, M. Large-scale synthesis of monodisperse microporous silica nanoparticles by gradual injection of reactants. *J. Sol-Gel Sci. Technol*. **2015**, *74*, 109–113.

(13) Shimogaki, T.; Tokoro, H.; Tabuchi, M.; Koike, N.; Yamashina, Y.; Takahashi, M. Large-scale preparation of morphology-controlled microporous silica particles via gradual injection of reactants with different surfactants. *J. Sol-Gel Sci. Technol*., **2016**, *79*, 440; Kim, C.; Yoon, S.; Lee, J.H. Facile large-scale synthesis of mesoporous silica nanoparticles at room temperature in a monophasic system with fine size control. *Microporous Mesoporous Mater*. **2019**, *288*, 109595.

(14) Zhang, K.; Xu, L.L.; Jiang, J.G.; Calin, N.; Lam, D.F.; Zhang, S.J.; Wu, H.H.; Wu, G.D.; Albela, B.; Bonneviot, L.; Wu, P. Facile large-scale synthesis of monodisperse mesoporous silica nanospheres with tunable pore structure. *J. Am. Chem. Soc*. **2013**, *135*, 2427–2430.

(15) Liu, P.C.; Yu, Y.J.; Peng, B.; Ma, S.Y.; Ning, T.Y.; Shan, B.Q.; Yang, T.Q.; Xue, Q.S.; Zhang, K.; Wu, P. A dual-templating strategy for the scale-up synthesis of dendritic mesoporous silica nanospheres. *Green Chem*. **2017**, *19*, 5575.

(16) Qiang, Z.; Guo, Y.; Liu, H.; Cheng, S.Z.; Cakmak, M.; Cavicchi, K.A.; Vogt, B.D. Large-scale roll-to-roll fabrication of ordered mesoporous materials using resol-assisted cooperative assembly. *ACS Appl. Mater. Interfaces* **2015**, *7*, 4306–4310.

Scaled-up microwave-assisted batch and flow synthesis and life cycle assessment of a silica mesoporous material: UVM-7

SUPPLEMENTARY INFORMATION

Miriam Benítez[1], Cristina Rodríguez-Carrillo[1], Sheila Sánchez-Artero[1], Jamal El Haskouri[2], Pedro Amorós[2] and Jose V. Ros-Lis[1,*]

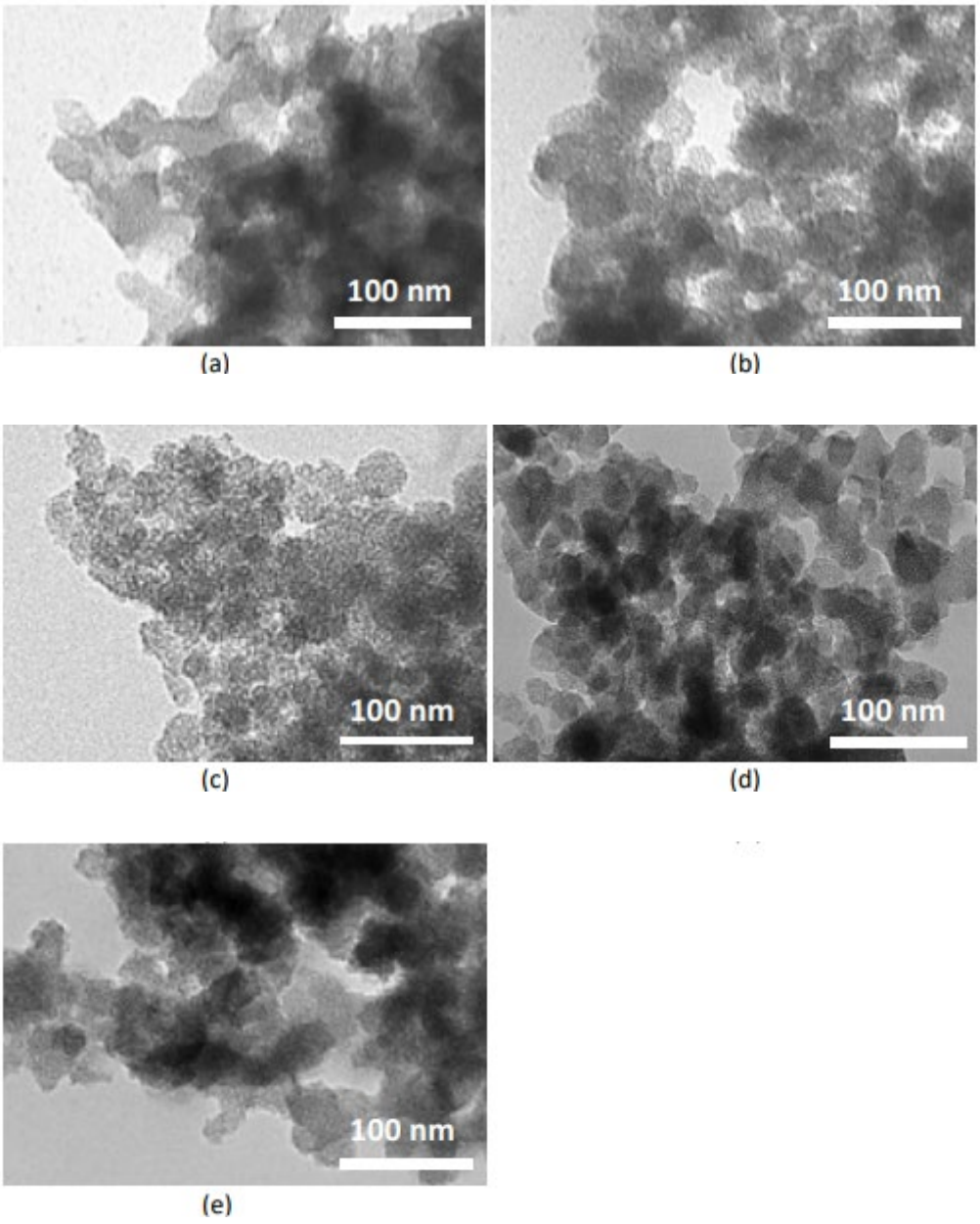

***Figure S1**: Representative TEM images of a) BS800c, b) BS800s, c) BS400, d) BF-4, and e) FF.*

Table S1: *Cost of reagents, solvents and energy used in the cost analysis.*

Inventory element	*€ per kg or kWh*
TEOS	125.4
TEA	90.8
CTABr	336.0
DIW	3.0
Ethanol	9.8
APTES	505.3
Acetonitrile	78.8
Energy	0.25

Table S2: *Summary of the cost analysis for the diverse procedures.*

	Euros per g of calcined and/or functionalized UVM-7			
	MW scalated batch	*MW scalated flow*	*MW non-scalated*	*Conventional*
Per step				
▪ **Synthesis**	2.0	2.0	3.6	2.6
▪ **Calcination**	0.1	0.1	0.2	0.5
▪ **Functionalization**	5.6	5.0	31.7	4.8
Per component				
▪ **Reagents**	2.3	2.3	2.3	2.9
▪ **Solvents**	5.3	4.7	32.9	4.4
▪ **Energy**	0.1	0.1	0.3	0.5
Total	7.7	7.1	35.5	7.9

Chapter 4:

Synthesis of Doped UVM-7

4.1. Functionalization of mesoporous silica

The functionalization of materials involves the introduction of new functional groups that impart enhanced properties to the material. In mesoporous silica materials, functionalization can occur within the pore, on the exterior surface, on both surfaces, or even within the silica framework itself. The degree of silica functionalization depends on the presence of silanol groups and their reactivity with other functional groups.[1] The two main methods employed to achieve functionalization are:

- Post-grafting: post-grafting functionalization is a widely used method in which mesoporous silica is first synthesized through conventional techniques, followed by surface modification in a separate step (Figure 4.1). This approach ensures that the structural integrity and mesoporous structure of the material remain intact.[2] Calcined mesoporous silicas contain surface silanol groups, which serve as anchoring sites for functionalization through silylation reactions.[3]

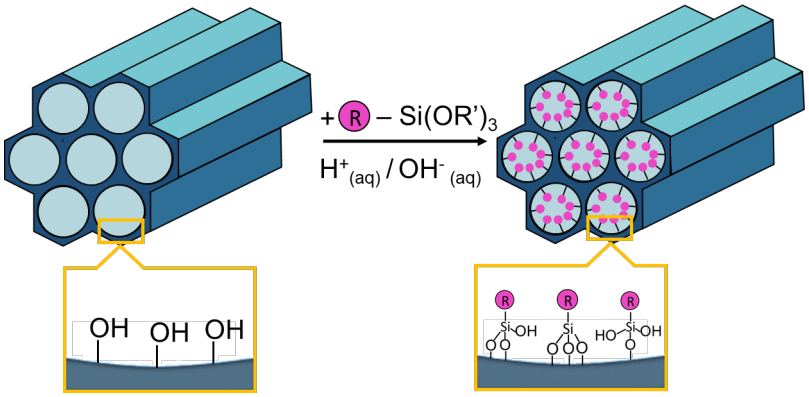

***Figure 4.1**. Post-synthetic functionalization of mesoporous silica. Adapted from reference [4].*

- Co-condensation: it is a one-pot method in which the functional groups are directly incorporated into the mesoporous material during the synthesis procedure (Figure 4.2).[2] This simultaneous incorporation allows for better control over the distribution, it enables the organic/inorganic groups to be integrated within the material framework from the very beginning, leading to enhanced material properties such as improved stability, selectivity, and reactivity.[1] being more homogeneous, but it can affect the pore structure and morphology of the material.

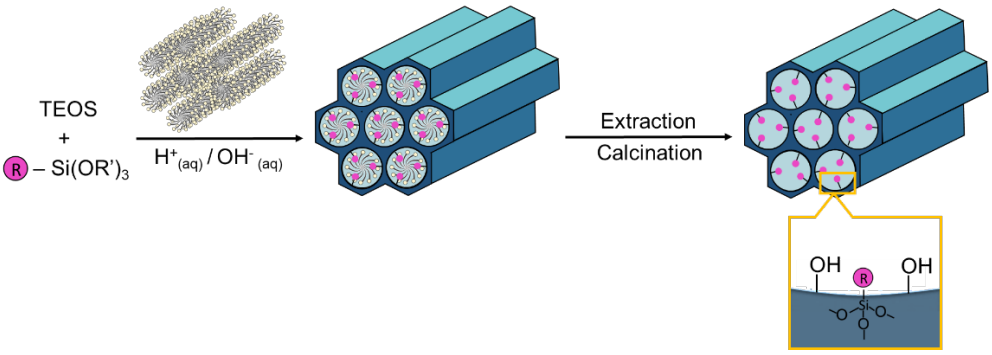

Figure 4.2. *Co-condensation functionalization of mesoporous silica. Adapted fron reference [4].*

In this Chapter, we will focus on the functionalization of UVM-7. Our research group has made significant advancements in the functionalization of this type of material, as summarized in Table 4.1.

Table 4.1. *Significant advancements in the functionalization of UVM-7.*

Year	Material	Objective	Ref
2002	M-UVM-7 (M=Al, Ti, V, Zr)	Preparation of bimodal silicas and doping with different elements	5
2002	Ti-UVM-7	Used as catalyst in olefin epoxidation	6
2003	Mn_{12}-UVM-7	Incorporation of Mn_{12} clusters within the pores	7
2006	Zr-UVM-7	Synthesis of mesoporous silica doped with Zr	8
2006	V-UVM-7	Used for selective oxidative activation of isobutane	9
2006	Ni_8-UVM-7	Support of small octanuclear Ni(II) with a relatively large ground spin state and magnetic anisotropy.	10
2007	UVM-7 covered ceramic foam	Preparation of trimodal silicas with UVM-7 nanoparticles and ceramic foams	11
2007	SnTf-UVM-7	New heterogeneous catalysts with unimodal and bimodal pores systems	12
2008	UVM-7-SH	Used in detection and adsorption of Hg^{2+}	13
2008	Fe-UVM-7	Synthesis of mesoporous silica doped with Fe	14
2009	Zn-UVM-7	Synthesis of ZnO nanoparticles embedded in UVM-7	15
2009	SnTf-UVM-7	Catalysts for the acylation of aromatics and heteroaromatics, and for the etherification of primary alcohols to symmetrical long chain ethers	16,17
2009	UVM-7-APTES	Prepared to be suitable anion hosts and used in selective colorimetric displacement assay	18
2010	Au/Co-UVM-7	Deposition of gold nanoparticles on metal nanodomains embedded in UVM-7 silica	19
2010	Al-UVM-7 AlTf-UVM-7	Used as green catalysts for the etherification of fatty alcohols and the conversion of ethylene glycol with n-octanol	20,21
2010	SnTf-UVM-7	Catalysts tested for transesterification of sunflower oil under both microwave and ultrasound activation.	22
2012	Au/Co-UVM-7	Catalysts for use in propane and toluene oxidation	23
2012	Au-UVM-7	Get a better understanding of the enhanced site accessibility	24
2012	UVM-7-APTES	Functionalized with APTES to anchor glucose groups onto the silica, to adsorb boron aqueous species.	25
2014	Au/M-UVM-7 (M=Ni + Ce, Sn)	Used for aerobic oxidative condensation of benzylamine to N-benzylidenebenzylamine	26

2014	ScTf-UVM-7	Catalyst in the hydroamination of aniline and substituted anilines with styrene	27
2015	Au/TiO_2-UVM-7	Heterogeneous gold catalyst to 1,4-addition of boronic acids to enones	28
2018	Mn-UMV-7	Addition of controlled microporosity by the addition of manganese nanodomains	29
2018	Pd-UVM-7	New catalyst tested for the Suzuki-Miyaura reaction	30
2018	Ti-UVM-7	For solid phase extraction of organophosphorus pesticides in environmental water samples	31
2018	UVM-7-SH	Study their ability to modulate PPO enzyme activity	32
2020	Au/TiO_2/UVM-7	As catalyst selective for the hydrogenation of 7-nitro-1-tetralone to 7-amino-a-tetralone	33
2020	Ti-UVM-7 Fe-UVM-7	Design of a novel air sampler	34
2020	UVM-7	Functionalized with different radicals to study their effect in the lipase catalyzed fat hydrolysis, and their ability to modulate PPO enzyme activity	35,36
2020	Pd-UVM-7/PDA	New catalysts based on Pd(0) nanoparticles	37
2021	Ti-UVM-7	Prepared as sorbent for the extraction of organophosphorus flame retardants	38
2022	Fe_3O_4NPs-UVM-7 -SH,-NH	Magnetized mesoporous silica functionalized to evaluate their effect on the enzymatic browning in fruits	39
2022	Fe-UVM-7	Applied to solid-phase extraction of perfluoroalkyl substances from environmental water samples.	40
2022	Gd-UVM-7	New synthetic route from hydroalcoholic solution starting from atrane complexes, optimizing the Gd dispersion	41
2022	UVM-7 with γ-cyclodextrin	For the isolation of veterinary antibiotics, and used as sorbent for extracting endocrine-disrupting chemicals from bottles apple juice	42,43
2022	Au-UVM-7	Used for organochloride pesticides extraction	44
2023	UVM-7-APTES	Synthesis and scale-up using microwave generators	45,46
2024	Ce-UVM-7	Scaled-up using microwave-assisted synthesis	47
2024	Ti-UVM-7	Scaled-up using microwave-assisted synthesis	48

4.2. The Atrane Route

A key advantage of this method is its ability to balance the hydrolysis and condensation processes of elements with widely varying reactivities, as the amine-trialkoxo complexes exhibit relative resistance to hydrolysis, depending on the pH and temperature conditions.[49] This capacity facilitates the controlled synthesis of mesoporous materials with tailored structures and properties, enhancing their potential applications in catalysis, adsorption, and other fields requiring high surface area and porosity.[50]

With this in mind, the synthesis procedure of mesoporous materials via the atrane method can be generalized into the following sequence of steps:

- **Step I:** Preparation of organometallic precursors (atrane).

The synthesis of atrane complexes is conventionally performed through transesterification reactions, utilizing alkoxy derivatives in the presence of anhydrous, nonaqueous solvents.[51] Among the various silicon source reagents, tetraethyl orthosilicate (TEOS) has been the most widely used due to its ease of handling and moderate cost. Typically, these reactions are conducted using organic solvents like ethylene glycol. To eliminate the presence of an external organic solvent, we use an excess of triethanolamine (TEA), allowing it to serve both as a reagent and as the reaction medium.[49] These conditions are critical to ensure the effective formation of the desired complexes.

This TEA-rich solution can incorporate all the desired elements intended for inclusion in the final material. The reaction is understood through a mechanism consisting of three successive nucleophilic substitution reactions,

leading to the complete coordination of TEA to the metal cation via its three alkoxide groups (Scheme 4.1).

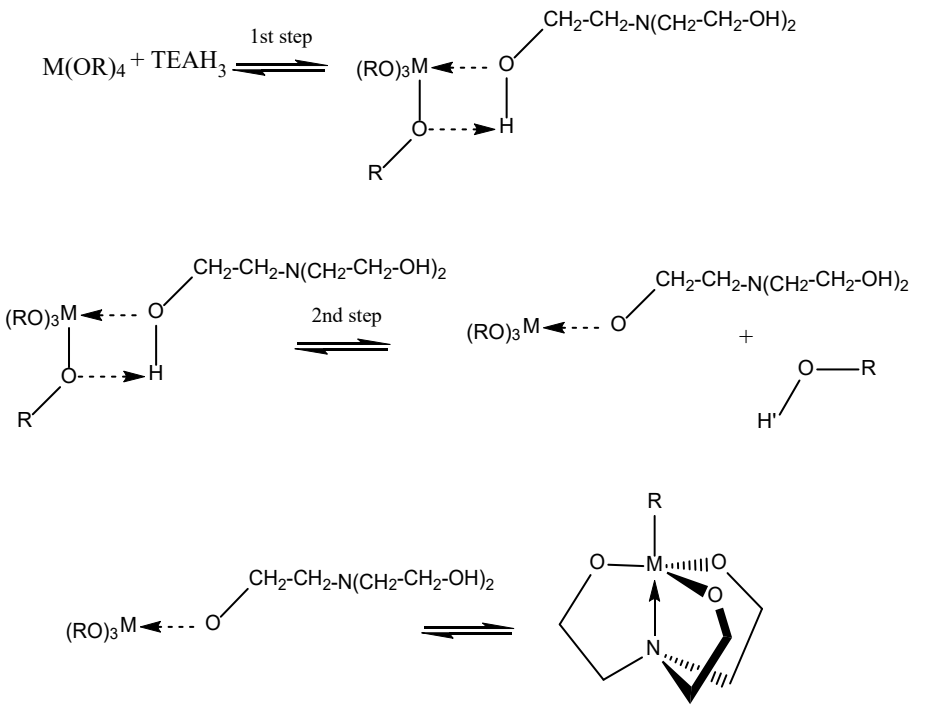

Scheme 4.1. *Mechanism for the formation of the atrane complexes.*

- **Step II:** Addition of the organic structure-directing agent (surfactant).

Several methods have been established for synthesizing mesoporous materials, with one key advancement introduced by Mobil researchers. In their study, quaternary ammonium cationic surfactants, such as cetyltrimethylammonium bromide ($C_{16}H_{33}N(CH_3)_3Br$, CTABr), were first utilized as structure-directing agents to create highly ordered M41S mesoporous silicate molecular sieves under hydrothermal and basic

conditions.[52] This method not only expanded the pore sizes from the microporous to the mesoporous scale but also marked the first use of a "template" concept in the synthesis of mesoporous silicates. Since this innovation, the use of templates has become a fundamental strategy in tailoring the pore architecture of mesoporous materials, enabling their widespread use in diverse applications.[53]

CTABr is a commonly used structure-directing agent in the synthesis of mesoporous materials via the atrane route.[50] It is a quaternary ammonium surfactant composed of a hydrophobic alkyl chain (C16) and a hydrophilic trimethylammonium headgroup, which enables it to form micelles in solution. In the synthesis process, CTABr plays a crucial role in directing the self-assembly of the inorganic precursors by forming micellar templates. These micelles guide the organization of metal precursors during hydrolysis and condensation, leading to the formation of highly ordered mesoporous structures. CTABr is widely used due to its ability to produce uniform pore sizes and well-defined mesoporous architectures, making it ideal for controlling the pore structure in mesoporous materials like those synthesized via the atrane method.

- **Step III:** Hydrolysis and condensation of the metallic precursors in the presence of surfactant micelles to form mesostructured materials.

When water is added to the system containing organometallic precursors (atranes) and the surfactant, hydrolysis reactions are initiated. During this stage, the alkoxide groups (M-OR, where M is the metal, such as silicon in the case of TEOS) in the precursors begin to react with water.

This reaction breaks the M-OR bonds, replacing the alkoxide groups with hydroxyl groups (M-OH).

$$M\text{-}OR + H_2O \rightarrow M\text{-}OH + ROH$$

Once hydroxyl groups (M-OH) have formed, they can react with each other or with partially hydrolyzed alkoxide groups (M-OR) in a condensation process. During this process, water (or alcohol) molecules are eliminated, and the hydroxyl or alkoxide groups bond together, forming metal-oxygen-metal (M-O-M) linkages. This creates an expanding inorganic network that builds the structure of the material.

$$M\text{-}OH + M\text{-}OH \rightarrow M\text{-}O\text{-}M + H_2O$$
$$M\text{-}OH + M\text{-}OR \rightarrow M\text{-}O\text{-}M + ROH$$

During this stage, the surfactant CTABr plays a crucial role as a "structure-directing agent." The surfactant molecules form micelles, which act as templates around which the inorganic framework begins to organize. The negatively charged hydrolyzed monomers of TEOS are adsorbed onto the positively charged CTAB micelles through electrostatic interactions. As the M-O-M network forms around these micelles, the characteristic mesoporous structure of the material emerges.[54]

- **Step IV:** Aging of the mesostructured solids to promote the condensation of the inorganic framework.

The aim of this stage is to promote the condensation reactions between partially hydrolyzed groups (M-OR) or hydroxyl groups (M-OH). This process is essential, as greater polymerization of the inorganic material enhances its

thermal stability, allowing for the removal of the surfactant without the collapse of the mesostructure.

- **Step V:** Calcination to remove the surfactant, exposing the pore system.

This sequence eliminates the template agent ensuring the successful formation of highly ordered mesoporous materials with well-defined pore structures.

4.3. Objectives and scope of this study

In Chapter 3, we explored the functionalization of mesoporous silica using a post-grafting method. In this Chapter, we shift our focus to a one-pot synthesis approach, which offers greater control over the incorporation of different elements during material formation. The atrane-based method, previously discussed for its simplicity and reproducibility, will serve as the foundation for this investigation, allowing us to assess its applicability in synthesizing mixed oxides with diverse heteroelements.

One of the key advantages of this approach is its ability to accommodate elements with distinct reactivities, enabling controlled competition during synthesis. To illustrate this, we will examine the formation of Ti-Si and Ce-Si mixed oxides, highlighting how the atrane route facilitates homogeneous dispersion and tailored composition. Through this study, we aim to further validate the versatility of this method and its potential for designing advanced functional materials.

Following the successful scale-up of UVM-7 synthesis, the incorporation of additional metals into the silica framework has been proposed. Specifically, we present the introduction of titanium (Ti-UVM-7), which has been previously reported, though not utilizing microwave-assisted synthesis. In this case, we incorporate both microwave synthesis and scaling-up processes. Additionally, we explore the incorporation of cerium into the structure (Ce-UVM-7), a material that has not been previously reported in UVM-7. Furthermore, we investigate a new potential application for these materials as additives in sunscreen formulations.

4.4. References

(1) Asefa, T.; Tao, Z. Mesoporous silica and organosilica materials-Review of their synthesis and organic functionalization. *Can. J. Chem.* **2012**, *90*, 1015-1031.

(2) Brühwiler, D. Postsynthetic functionalization of mesoporous silica. *Nanoscale* **2010**, *2*, 887–892.

(3) Yang, C.M.; Chao, K.J. Functionalization of molecularly templated mesoporous silica. *Journal of the Chinese Chemical Society* **2002**, *49*, 883–893.

(4) Parra, M.; Gil, S.; Gaviña, P.; Costero, A.M. Mesoporous silica nanoparticles in chemical detection: from small species to large bio-molecules. *Sens*. **2022**, *22*, 261.

(5) El Haskouri, J.; Ortiz de Zárate, D.; Guillem, C.; Latorre, J.; Caldés, M.; Beltrán, A.; Beltrán, D.; Descalzo, A.B.; Rodríguez-López, G.; Martínez-Máñez, R.; Marcos, M.D.; Amorós, P. Silica-based powders and monoliths with bimodal pore systems. *ChemComm* **2002**, *4*, 330–331.

(6) El Haskouri, J.; Ortiz de Zárate, D.; Pérez-Pla, F.; Cevilla, A.; Guillem, C.; Latorre, J.; Marcos, M.D.; Beltrán, A.; Beltrán, D.; Amorós, P. Improving epoxide production using Ti-UVM-7 porous nanosized catalysts. *New J. Chem.* **2002**, *26*, 1093–1095.

(7) Clemente-León, M.; Coronado, E.; Forment-Aliaga, A.; Amorós, P.; Ramírez-Castellanos, J.; González-Calbet, J.M. Incorporation of Mn_{12} single molecule magnets into mesoporous silica. *J. Mater. Chem.* **2003**, *13*, 3089–3095.

(8) Ortiz De Zárate, D.; Gómez-Moratalla, A.; Guillem, C.; Beltrán, A.; Latorre, J.; Beltrán, D.; Amorós, P. High-zirconium-content nano-sized bimodal mesoporous silicas. *Eur. J. Inorg. Chem*. **2006**, *2006*, 2572–2581.

(9) Huerta, L. J.; Amorós, P.; Beltrán-Porter, D; Corberán, V. C. Selective oxidative activation of isobutane on a novel vanadium-substituted bimodal mesoporous oxide V-UVM-7. *Catal. Today* **2006**, *117*, 180–186.

(10) Pardo, E.; Burguete, P.; Ruiz-García, R.; Julve, M.; Beltrán, D.; Journaux, Y.; Amorós, P. Ordered mesoporous silicas as host for the incorporation and aggregation of octanuclear nickel(II) single-molecule magnets: A bottom-up approach to new magnetic nanocomposite materials. *J. Mater. Chem.* **2006**, *16*, 2702–2714.

(11) Huerta, L.; El Haskouri, J.; Vie, D.; Comes, M.; Latorre, J.; Guillem, C.; Marcos, M.D.; Martínez-Máñez, R.; Beltrán, A.; Beltrán, D.; Amorós, P. Nanosized mesoporous silica coatings on ceramic foams: New hierarchical rigid monoliths. *Chem. Mater.* **2007**, *19*, 1082–1088.

(12) Coman, S. M.; Pop, G.; Stere, C.; Pârvulescu, V.I.; El Haskouri, J.; Beltrán, D.; Amorós, P. New heterogeneous catalysts for greener routes in the synthesis of fine chemicals. *J. Catal* **2007**, *251*, 388–399.

(13) Ros-Lis, J.V.; Casasús, R.; Comes, M.; Coll, C.; Marcos, M.D.; Martínez-Máñez, R.; Sancenón, F.; Soto, J.; Amorós, P.; El Haskouri, J.; Garró; N.; Rurack, K. A mesoporous 3D hybrid material with dual functionality for Hg^{2+} detection and adsorption. *Chem. Eur. J.* **2008**, *14*, 8267–8278.

(14) Pérez-Cabero, M.; García-García, F.R.; Vie, D.; Rodríguez-Ramos, I.; Beltrán, D.; Amorós, P. Nano-sized mesoporous carbon particles with bimodal pore system and semi-crystalline porous walls. *Mater. Lett.* **2008**, *62*, 2935–2938.

(15) Haskouri, J.; Dallali, L.; Fernández, L.; Garro, N.; Jaziri, S.; Latorre, J.; Guillem, C.; Beltrán, A.; Beltrán, D.; Amorós, P. ZnO nanoparticles embedded in UVM-7-like mesoporous silica materials: Synthesis and characterization. *Physica E Low Dimens. Syst. Nanostruct.* **2009**, *42*, 25–31.

(16) Candu, N.; Coman, S.; Parvulescu, V.I.; El Haskouri, J.; Amorós, P.; Beltrán, D. Metal triflates incorporated in mesoporous catalysts for green synthesis of fine chemicals. *Top. Catal.* **2009**, *52*, 571–578.

(17) Pârvulescu, V.I.; Coman, S.M.; Candu, N.; El Haskouri, J.; Beltrán, D.; Amorós, P. Synthesis, characterization and catalytic behavior of SnTf/MCM-41 and SnTf/UVM-7 as new green catalysts for etherification reactions. *J. Mater. Sci*. **2009**, *44*, 6693–6700.

(18) Comes, M.; Aznar, E.; Moragues, M.; Marcos, M.D.; Martínez-Máñez, R.; Sancenón, F.; Soto, J.; Villaescusa, L.A.; Gil, L.; Amorós, P. Mesoporous hybrid materials containing nanoscopic 'binding pockets' for colorimetric anion signaling in water by using displacement assays. *Chem. Eur. J.* **2009**, *15*, 9024–9033.

(19) Pérez-Cabero, M.; El Haskouri, J.; Solsona, B.; Vázquez, I.; Dejoz, A.; García, T.; Álvarez-Rodríguez, J.; Beltrán, A.; Beltrán, D.; Amorós, P. Stable anchoring of

dispersed gold nanoparticles on hierarchic porous silica-based materials. *J. Mater. Chem*. **2010**, *20*, 6780–6788.

(20) Candu, N.; Coman, S.M.; Parvulescu, V.I.; El Haskouri, J.; Amorós, P.; Beltrán, D. Synthesis, characterization and catalytic behavior of AlTf/UVM-7 as new green catalysts for the glycols etherification reactions. *Appl. Catal. A Gen* **2010**, *372*, 58–66.

(21) Candu, N.; Musteata, M.; Coman, S.M.; Parvulescu, V.I.; El Haskouri, J.; Amorós, P.; Beltrán, D. AlTf-UVM-7-Highly active catalysts for the synthesis of long chain symmetrical ethers and non-ionic surfactant structures. *Chem. Eng. J.* **2010**, *161*, 363–370.

(22) Verziu, M.; El Haskouri, J.; Beltrán, D.; Amorós, P.; Macovei, D.; Gheorghe, N.G.; Teodorescu, C.M.; Coman, S.M.; Parvulescu, V.I. Mesoporous Tin-Triflate based catalysts for transesterification of sunflower oil. *Top. Catal*. **2010**, *53*, 763–772.

(23) Solsona, B.; Pérez-Cabrero, M.; Vázquez, I.; Dejoz, A.; García, T.; Álvarez-Rodríguez, J.; El Haskouri, J.; Beltrán, D.; Amorós, P. Total oxidation of VOCs on Au nanoparticles anchored on Co doped mesoporous UVM-7 silica. *Chem. Eng. J.* **2012**, *187*, 391–400.

(24) Pérez-Cabero, M.; Hungría, A.B.; Morales, J.M.; Tortajada, M.; Ramón, D.; Moragues, A.; El Haskouri, J.; Beltrán, A.; Beltrán, D.; Amorós, P. Interconnected mesopores and high accessibility in UVM-7-like silicas. *J. Nanopart. Res.* **2012**, *14*, 1–12.

(25) Sanfeliu, C.; Martínez-Máñez, R.; Sancenón, F.; Soto, J.; Puchol, V.; Amorós, P.; Marcos, M.D. Low-cost materials for boron adsorption from water. *J. Mater. Chem*. **2012**, *22*, 25362–25372.

(26) Opriş, C.M.; Pavel, O.D.; Moragues, A.; El Haskouri, J.; Beltrán, D.; Amorós, P.; Marcos, M.D.; Stoflea, L.E.; Parvulescu, V.I. New multicomponent catalysts for the selective aerobic oxidative condensation of benzylamine to N-benzylidenebenzylamine. *Catal. Sci. Technol.* **2014**, *4*, 4340–4355.

(27) Ciobanu, M.; Tirsoaga, A.; Amorós, P.; Beltrán, D.; Coman, S.M.; Parvulescu, V.I. Comparative hydroamination of aniline and substituted anilines with styrene on different zeolites, triflate based catalysts and their physical mixtures. *Appl. Catal. A Gen.* **2014**, *474*, 230–235.

(28) Moragues, A.; Neatu, F.; Parvulescu, V.I.; Marcos, M.D.; Amorós, P.; Michelet, V. Heterogeneous gold catalyst: synthesis, characterization, and application in 1,4-addition of boronic acids to enones. *ACS Catal*. **2015**, *5*, 5060–5067.

(29) Garrido, M.D.; García-Llacer, C.; El Haskouri, J.; Marcos, M.D.; Sánchez-Royo, J.F.; Beltrán, A.; Amorós, P. Atrane complexes chemistry as a tool for obtaining trimodal UVM-7-like porous silica. *J. Coord. Chem.* **2018**, *71*, 776–785.

(30) Albiñana, P.A.; El Haskouri, J.; Marcos, M.D.; Estevan, F.; Amorós, P.; Úbeda, M.A.; Pérez-Pla, F. A new efficient, highly dispersed, Pd nanoparticulate silica supported catalyst synthesized from an organometallic precursor. Study of the homogeneous vs. heterogeneous activity in the Suzuki-Miyaura reaction. *J. Catal*. **2018**, *367*, 283–295.

(31) Pellicer-Castell, E.; Belenguer-Sapiña, C.; Amorós, P.; El Haskouri, J.; Herrero-Martínez, J.M.; Mauri-Aucejo, A. Study of silica-structured materials as sorbents for organophosphorus pesticides determination in environmental water samples. *Talanta* **2018**, *189*, 560–567.

(32) Muñoz-Pina, S.; Ros-Lis, J.V.; Argüelles, Á.; Coll, C.; Martínez-Máñez, R.; Andrés, A. Full inhibition of enzymatic browning in the presence of thiol-functionalised silica nanomaterial. *Food Chem*. **2018**, *241*, 199–205.

(33) Trandafir, M.M.; Moragues, A.; Amorós, P.; Parvulescu, V.I. Selective hydrogenation of nitroderivatives over Au/TiO_2/UVM-7 composite catalyst. *Catal. Today* **2020**, *355*, 893–902.

(34) Pellicer-Castell, E.; Belenguer-Sapiña, C.; Amorós, P.; El Haskouri, J.; Herrero-Martínez, J.M.; Mauri-Aucejo, A.R. Comparison of silica-based materials for organophosphorus pesticides sampling and occupational risk assessment. *Anal. Chim. Acta* **2020**, *1110*, 26–34.

(35) Muñoz-Pina, S.; Ros-Lis, J.V.; Argüelles, Á.; Martínez-Máñez, R.; Andrés, A. Influence of the functionalisation of mesoporous silica material UVM-7 on polyphenol oxidase enzyme capture and enzymatic browning. *Food Chem*. **2020**, *310*, 125741.

(36) Muñoz-Pina, S.; Amorós, P.; El Haskouri, J.; Andrés, A.; Ros-Lis, J. V. Use of silica based materials as modulators of the lipase catalyzed hydrolysis of fats under simulated duodenal conditions. *Nanomaterials* **2020**, *10*, 1927.

(37) Ródenas, M.; El Haskouri, J.; Ros-Lis, J.V.; Marcos, M.D.; Amorós, P.; Úbeda, M.A.; Pérez-Pla, F. Highly active hydrogenation catalysts based on Pd nanoparticles dispersed along hierarchical porous silica covered with polydopamine as interfacial glue. *Catalysts* **2020**, *10*, 449.

(38) Pellicer-Castell, E.; Belenguer-Sapiña, C.; Amorós, P.; El Haskouri, J.; Herrero-Martínez J.M.; Mauri-Aucejo, A.R. Enhancing extraction performance of organophosphorus flame retardants in water samples using titanium hierarchical porous silica materials as sorbents. *J Chromatogr. A* **2021**, *1639*, 461938.

(39) Muñoz-Pina, S.; Duch-Calabuig, A.; Ruiz de Assín David, E.; Ros-Lis, J.V.; Amorós, P.; Argüelles, Á.; Andrés, A. Bioactive compounds and enzymatic browning inhibition in cloudy apple juice by a new magnetic UVM-7-SH mesoporous material. *Food Res. Int.* **2022**, *162*, 112073.

(40) Pellicer-Castell, E.; Belenguer-Sapiña, C.; El Haskouri, J.; Amorós, P.; Herrero-Martínez, J.M.; Mauri-Aucejo, A.R. Iron-doped bimodal mesoporous silica nanomaterials as sorbents for solid-phase extraction of perfluoroalkyl substances in environmental water samples. *Nanomaterials* **2022**, *12*, 1441.

(41) Garrido, M.D.; Puchol, N.; El Haskouri, J.; Sánchez-Royo, J.F.; Folgado, J.V.; Gonzalez Marrachelli, V.; Pérez Terol, I.; Ros-Lis, J.V.; Marcos, M.D.; Ruíz, R.; Beltrán, A.; Morales, J.M.; Amorós, P. High content and dispersion of Gd in bimodal porous silica: T2 contrast agents under ultra-high magnetic fields. *Microporous Mesoporous Mat.* **2022**, *336*, 111863.

(42) Belenguer-Sapiña, C.; Pellicer-Castell, E.; El Haskouri, J.; Simó-Alfonso, E.F.; Amorós, P.; Mauri-Aucejo, A.R. A type UVM-7 mesoporous silica with γ-cyclodextrin for the isolation of three veterinary antibiotics (ofloxacin, norfloxacin, and ciprofloxacin) from different fat-rate milk samples. *J. Food Compost. Anal.* **2022**, *109*, 104463.

(43) Belenguer-Sapiña, C.; Pellicer-Castell, E.; El Haskouri, J.; Simó-Alfonso, E.F.; Amorós, P.; Mauri-Aucejo, A.R. Assessment of migrating endocrine-disrupting chemicals in bottled acidic juice using type UVM-7 mesoporous silica modified with cyclodextrin. *Food Chem*. **2022**, *380*, 132207.

(44) Pellicer-Castell, E.; Belenguer-Sapiña, C.; Amorós, P.; El Haskouri, J.; Herrero-Martínez, J.M.; Mauri-Aucejo, A.R. Mesoporous silica sorbent with gold nanoparticles for solid-phase extraction of organochlorine pesticides in water samples. *J. Chromatogr. A* **2022**, *1662*, 462729.

(45) Díaz de Greñu, B.; Muñoz-Pina, S.; De los Reyes, R.; Benítez, M.; El Haskouri, J.; Amorós, P.; Ros-Lis, J.V. Fast microwave-assisted synthesis, calcination and functionalization of a silica mesoporous nanomaterial: UVM-7. *ChemSusChem* **2023**, *16*, e202300123.

(46) Benítez, M.; Rodríguez-Carrillo, C.; Sánchez-Artero, S.; El Haskouri, J.; Amorós, P.; Ros-Lis, J.V. Scaled-up microwave-assisted batch and flow synthesis and life cycle assessment of a silica mesoporous material: UVM-7. *Green Chem*. **2023**, *26*, 785–793.

(47) Rodríguez-Carrillo, C.; Benítez, M.; De los Reyes, R.; El Haskouri, J.; Amorós, P.; Ros-Lis, J.V. Flow and batch minute-made synthesis of ce-uvm-7 using microwave-assisted reaction: scaling-up, optical and catalytic applications, and impact assessment. *ACS Sustain. Chem. Eng*. **2024**, *12*, 13208–13219.

(48) Rodríguez-Carrillo, C.; Benítez, M.; González-Fernández, M.; De los Reyes, R.; Murcia, S.; El Haskouri, J.; Amorós, P.; Ros-Lis, J.V. Solid-state microwave assisted batch and flow synthesis, and life cycle assessment, of titanium containing UVM-7 mesoporous silica. *Microporous Mesoporous Mat.* **2024**, *380*, 113314.

(49) El Haskouri, J. Materiales mesoporosos ternarios: control de la estabilidad de la pared inórganica. Doctoral Thesis, Universitat de València, España, **2000**.

(50) Garrido, M.D.; Benítez, M.; Ros-Lis, J.V.; Amorós, P. A travel though the atrane route, a versatile tool for the materials soft-synthesis: A twenty-five years perspective. *Nano Select* **2024**, *5*, 2300169.

(51) Cabrera, S.; El Haskouri, J.; Guillem, C.; Latorre, J.; Beltrán-Porter, A.; Beltrán-Porter, D.; Marcos, M.D.; Amorós, P. Generalised syntheses of ordered mesoporous oxides: the atrane route. *Solid State Sci*. **2000**, *2*, 405–420.

(52) Li, Q.; Zhou, Y. Brief history, preparation method, and biological application of mesoporous silica molecular sieves: a narrative review. *Molecules* **2023**, *28*, 2013.

(53) Wan, Y.; Zhao, D. On the controllable soft-templating approach to mesoporous silicates. *Chem. Rev*. **2007**, *107*, 2821–2860.

(54) Narayan, R.; Nayak, U.Y.; Raichur, A.M.; Garg, S. Mesoporous silica nanoparticles: a comprehensive review on synthesis and recent advances. *Pharmaceutics* **2018**, *10*, 118.

Solid-state microwave assisted batch and flow synthesis, and life cycle assessment of titanium containing UVM-7 mesoporous silica

Cristina Rodríguez-Carrillo[1], Miriam Benítez[1], Marta González-Fernández[1], Ruth de los Reyes[2], Sonia Murcia[3], Jamal El Haskouri[3], Pedro Amorós[3] and Jose V. Ros-Lis[1,*]

[1]Departamento de Química Inorgánica, Universitat de València, Doctor Moliner 50, P.O. Box 73, 46100 Butjassot, Spain

[2]Microbiotech. S.L. Villamarxant, 46191, Spain

[3]Institut de Ciència dels Materials, Universitat de València, P.O. Box 22085, 46071 Valencia, Spain

*Correspondence: j.vicente.ros@uv.es; Tel.: +34-963544856

Microporous and Mesoporous Materials **2024**, *380*, 113314

DOI: 10.1016/j.micromeso.2024.11331

Received: 9th May 2024, Accepted: 23th August 2024

Published: 26th August 2024

Abstract

UVM-7 is a bimodal mesoporous silica material that can be prepared in a short time with microwave assisted synthesis (MAS). It is prepared following the atrane route, that allows the synthesis of mixed silicas including other elements with homogeneous distribution.

We report herein the preparation of Ti-UVM-7 with using the atrane route in combination with MAS with solid-state generators. The synthesis has been optimized and scaled-up in batch. Also, the flow synthesis has been developed. These materials have not been prepared before using solid-state generators, nor microwave-assisted flow chemistry.

The materials have been characterized by XRD, N_2 adsorption-desorption, TEM, EDX, Raman, and Z potential.

The materials can be prepared in less than 10 min with a Si/Ti ratio of up to 3.8, and a homogeneous Ti distribution within the UVM-7 silica structure. Scaled-up synthesis produces 33 g of Ti-UVM-7 in 10 min and 12 g h^{-1} in batch and flow synthesis respectively. The optical properties and sun protection factor of the resulting materials were studied.

The band gap decreases as titanium concentration increases, reaching 4.1 eV for the highest concentration. Life Cycle Assessment confirms a strong reduction in the impact derived from the scale-up with similar values of approximately 10 points in the single score for the preparation of 1 kg of Ti-UVM-7.

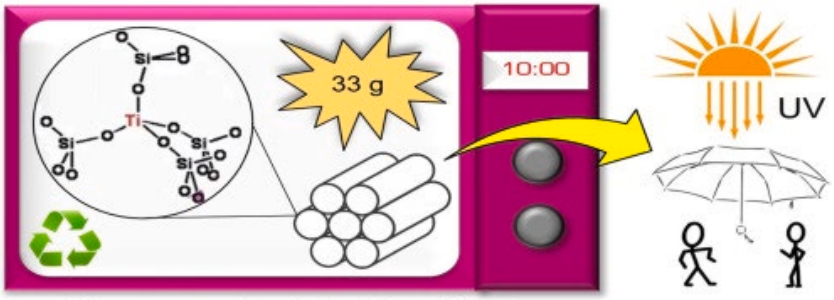

Keywords: Microwave-assisted synthesis, Titanium, Mesoporous silica, Flow synthesis, LCA.

1. INTRODUCTION

In recent years, the synthesis of advanced materials has gained significant attention in various scientific fields, owing to their unique properties and potential applications. Mesoporous silica materials such as MCM-41 (hexagonal), MCM-48 (cubic), MCM-50 (lamellar), or the SBA family, have emerged as versatile platforms for catalysis,[1] drug delivery,[2] sensing,[3] and energy storage.[4]

Within this family, UVM-7 is a material of special interest. The UVM7 material was first synthesized at the University of Valencia in 2002 via the atrane route synthesis procedure.[5] It presents a bimodal porous structure formed by intraparticle mesopores (accessible after the removal of the surfactant micelles) and an interparticle textural pore system of large-meso or macropores. It forms a connected network of covalently bonded mesoporous nanoparticles with pseudo-spherical shape, assembled to create a secondary system characterized by large, disorganized textural pores.[6] With a significantly high surface area and a remarkably pore accessibility due to the 3D interconnection of both pore systems, this material stands out as a versatile candidate for a wide range of applications as a support material in catalysis,[7] adsorption,[8] and separation processes.[9]

The main synthesis routes for mesoporous solids like UVM-7 involve the formation of intermediates, and depending on these intermediates, different routes are followed. The most commonly employed method is the hydrothermal or sol-gel process, in which a surfactant, serving as a template for the gelification process, is dissolved (either in a basic or acidic medium).

This results in the formation of a mesostructured material by self-assembly between surfactant micelles and silica oligomers under alkaline conditions, followed by template removal by calcination and consequent mesopore generation.[10] For this procedure, the atrane route is followed, which is a type of sol-gel process wherein the inorganic hydrolytic precursor is an atrane complex. Atranes can be easily prepared departing from alkoxides or salts by reaction with triethanolamine simply by heating. In the case of the alkoxides the heating removes by evaporation the alcohol formed in the reaction.[11] Atranes, akin to alkoxides, are compounds employed as oxide precursors in the synthesis of mesoporous materials, but the distinction lies in their inertness towards hydrolysis. The versatility of this method makes it suitable for the preparation of mixed or doped mesoporous oxides.[11] This procedure encounters the challenge of distinct reactivities between heteroatoms, leading to phase mixtures. However, by using atranes as precursors the rates of hydrolysis and condensation of the different heteroelements can be balanced.[12] Another method/mechanism is the liquid-crystal templating mechanism (LCT), where the inorganic phase grows within the spaces between ordered organic micelles previously auto-organized.[10] Additionally, another approach is Evaporation-Induced Self-Assembly (EISA), which involves the condensation and self-assembly of a metal-template composite via slow evaporation of non-aqueous organic solvents.[13]

The integration of titanium into mesoporous silica matrices introduces additional functionalities and expands the potential applications of these materials. Titanium exhibits excellent catalytic activity, photocatalytic properties,[1] and biocompatibility, making it a highly desirable component in

various fields including environmental remediation,[14] energy conversion,[4] and biomedicine.[15] For some time now, studies have been carried out involving the incorporation of titanium on different supports, although mainly on mesoporous materials, since these provide wide pores that allow the easy entry and exit of reagents and products.[16]

There are also numerous studies that coordinate other metals to the structure of these silicas to perform catalytic functions, such as gold.[17,18]

Microwaves have been widely applied in transmission of information and heating processes. They have been widely used in organic and inorganic synthesis.[19–21] Microwave assisted heating offers advantages such as rapid heating, improved reaction kinetics, providing a rapid and homogeneous energy transfer throughout the reaction mixture, resulting in shorter reaction times, improved product yields, and enhanced material properties.[22] Among the various microwave sources, the magnetron holds significant prominence due to its cost-effectiveness, simplicity, and high-power output. However, magnetron presents inherent limitations including challenges associated with power control, high voltage requirements, and limited operational lifespan.[23] By contrast, solid state microwave generators have emerged as an alternative to magnetrons with improved selection of parameters (potency, frequency and phase), and generate a precise and constant power. Despite these advantageous features, the relatively recent introduction of solid-state sources, their comparatively higher costs, and the absence of commercial equipment for chemistry synthesis using this technology have limited their widespread adoption and implementation.[24]

Lately, the utilization of microwave solid-state generators has emerged as a promising alternative for the synthesis of various materials, including mesoporous silica materials such as MCM-41, SBA-15, SBA-16, etc.[21] In 2023, Díaz de Greñu and coworkers reported for the first time the complete production of UVM-7 (synthesis, calcination and functionalization) using solid-state microwave generators,[25] and subsequently the adaptation to obtain large quantities in scale-up and in flow systems was described by Benitez et al. They achieved a scaling factor of 100, with the obtention of 168 g per hour in scaled-up systems, and 59 g per hour with flow methods, adding the functionalization of 59 g per hour.[26]

However, the use of solid-state microwave generators has not been validated for the preparation of mixed silica materials. Thus, we hypothesize that solid-state based microwave assisted synthesis in combination with the atrane route can be an interesting approach towards a fast, scalable, and sustainable synthesis of mixed silica mesoporous materials, in particular titanium containing ones, such as Ti-UVM-7. The resulting materials would be homogeneous, with high Ti content, and with solar shielding properties.

2. MATERIALS AND METHODS

2.1. Chemicals

All the reagents were analytically pure and were used without further purification. Tetraethyl orthosilicate, 98 % (GC) (TEOS), triethanolamine ≥99.0 % (GC) ($TEAH_3$), hexadecyltrimethylammonium bromide ≥98.0 % (CTABr), and titanium(IV)butoxide, reagent grade, 97 % were purchased from Sigma Aldrich (Madrid, Spain). Ethanol was purchased from VWR. Deionized water was

prepared in our lab. For the optical properties polymethylmethacrylate PMMA plates were used.

2.2. Microwave devices

Two different solid-state devices were employed, one designed for batch optimization and flow synthesis, and the other one for the batch scale-up, both supplied by Microbiotech. The low potency system, used for the optimization and flow synthesis, consists of a solid-state microwave source connected through coaxial cables to the irradiation cavity. The source can operate at a maximum power of 200 W, with selectable potency in 5W increments. The frequency can be adjusted to fine-tune the system and optimize absorbed power within the 2420 MHz–2480 MHz range, in 1Hz increments. The scale-up batch device comprises four microwave sources interconnected through coaxial cables to the irradiation cavity. Each source can operate at a maximum power of 200 W, with selectable potency in 1W increments, reaching a cumulative maximum power of 800W. The frequency of each source can be independently adjusted to fine-tune the system and optimize absorbed power within the 2420 MHz–2480 MHz range, in 1Hz increments, while maintaining phases within the 0-360° range.

2.3. Synthesis of the Ti-UVM-7 nanomaterials

The synthesis of Ti-UVM-7 was conducted via the atrane route employing a one-pot procedure.[27] For the batch optimization diverse Si/Ti molar ratios, potencies and reaction times were tested. They are summarized in Table 1.

Table 1. *Summary of the main synthesis parameters.*

Sample	Process type	TEOS (mL)	$Ti(OBut)_4$ (mL)	Si/Ti[a]	Power (W)	Time (min)
1	Batch	10.8	0.33	50	25	2:00
2	Batch			50	25	4:00
3	Batch			50	25	6:00
4	Batch			50	25	8:00
5	Batch	10.6	0.65	25	25	2:00
6	Batch			25	25	4:00
7	Batch			25	25	6:00
8	Batch			25	25	8:00
9	Batch	10.1	1.54	10	25	2:00
10	Batch			10	25	4:00
11	Batch			10	25	6:00
12	Batch			10	25	8:00
13	Batch	10.6	0.65	25	50	2:00
14	Batch			25	100	1:00
15	Batch			25	200	0:30
16	Batch, static	10.1	1.54	10	800	10:00
17	Batch, static	10.6	0.65	25	800	10:00
18	Batch, static	10.8	0.33	50	800	10:00
19	Batch, stirred	10.8	0.33	50	800	10:00
20	Flow	10.8	0.33	50	50	2:00
21	Flow	10.8	0.33	50	50	2:00
22	Flow	10.8	0.33	50	50	2:00
23	Flow	10.6	0.65	50	200	0:30
24	Flow	10.6	0.65	25	200	0:30

[a] Nominal molar ratio

For example, for material having a nominal Si/Ti molar ratio of 25, a mixture containing 11 mL of TEOS, 23 mL of $TEAH_3$ and 0.7 mL of the Ti precursor was heated at 140°C for 10 min to prepare the Si and Ti atrane complexes in $TEAH_3$ medium. The resulting solution was cooled to 90°C and 4.7 g of CTABr was added, resulting in an anhydrous solution containing both the atrane precursor and the template agent. 4 mL of this atrane solution was introduced in a microwave glass vial together with 10 mL of deionized water. Subsequently, the vial was placed in a solid-state microwave oven cavity and irradiated for a specified duration at the defined power. The resulting white solid was washed with water and ethanol, followed by drying in an oven at 80°C overnight to obtain the as-made material. Finally, the material is calcined at 550°C for 6 h in a conventional furnace, obtaining Ti-UVM-7 mesoporous silica.

For the scaled-up synthesis, a strategy similar to the preparation of pure silica UVM-7 was followed.[26] To obtain the samples 18 and 19 (Si/Ti 50), the solution containing atranes was prepared with a mixture of 135 mL of TEOS, 263 mL of $TEAH_3$, 4.1 mL of $Ti(OBut)_4$, and 45 g of CTABr. The detailed procedure for the preparation of the atrane can be found in the previous paragraph. Subsequently, 1 L of miliQ H_2O was added to the atrane solution, placed into the microwave oven cavity, irradiated for 10 min at 800W, washed with water and ethanol, dried in an oven at 80 °C overnight and calcined at 550°C for 6 h in a conventional furnace. This procedure was replicated both with and without stirring, to assess the influence of stirring on final product. For the samples 16 (Si/Ti = 10) and 17 (Si/Ti = 25), 125 mL of TEOS/19.3 mL of $Ti(OBut)_4$, and 132 mL of TEOS/8.2 mL of $Ti(OBut)_4$ were used, respectively.

In flow synthesis, the configuration of the system was similar has been reported elsewhere.[19] The atrane solution was prepared as in the batch synthesis, but the atrane (80°C) and water (room temperature) were mixed using two peristatic pumps before its introduction in the microwave oven. This setup enabled controlled irradiation under varying time intervals and power settings. The peristaltic pumps were calibrated to ensure the precise blending of atrane and water, configured at 5 rpm for atrane and 12 rpm for water. The resulting precipitate was washed with water and ethanol, dried at 80°C and calcined at 550°C as before.

2.4. Characterization of the materials

Nitrogen adsorption–desorption isotherms were recorded using an automated Micromeritics ASAP2010 instrument. Prior to adsorption measurements, the samples underwent in situ outgassing in vacuum conditions (10^{-6} Torr) at 110°C for 15 h to eliminate adsorbed gases. The specific surface area was determined utilizing the Brunauer–Emmett–Teller (BET model) based on adsorption data within the low-pressure range. Pore volume was calculated employing the Barrett–Joyner–Halenda model (BJH). The powder X-ray diffraction pattern (XRD) of the samples was acquired employing a D8 Advance A25 Bruker Corporation powder X-ray diffractometer. The sample underwent scanning across the requisite 2θ values range (1–80°). Transmission Electron Microscopy (TEM) was performed using a JEOL Jem 1010 instrument operating at 80 kV. HRTEM (high resolution transmission electron microscopy) images were acquired with a TECNAI microscope operated at 200 kV. Particle size analysis and Z potential for the samples were conducted using the Malvern Instruments Zetasizer Nano series particle size

analyzer. The UV/visible spectrum was obtained through a PerkinElmer Lambda 35 spectrophotometer equipped with an integrating sphere. Raman spectra were obtained using a HORIBA Jobin Yvon iHR320 Spectrometer. X-ray photoelectron spectroscopy (XPS) measurements were collected with a SPECS spectrometer equipped with a Phoibos 150 MCD 9 analyzer and a nonmonochromatic Al Kα (1486.6 eV) X-ray source. Spectra were recorded at 25 °C using an analyzer pass energy of 30 eV, an X-ray power of 50 W, and under an operating pressure of 10^{-9} mbar.

2.5. Measurement of the optical properties

The Kubelka-Munk function and the Tauc plot method (see Equation (1)) were used to measure de band gap energy (Eg), where C is a constant, h is Planck's constant, v is the frequency of vibration and α is the absorption coefficient.[28] Representing the plot of $(hvf(R))^2$ vs photon energy (hv), where (f(R)) is the absorbance, the band gap energies can be calculated.[28]

$$\propto (hv) = \frac{C(hv - E_g)^{\propto/2}}{hv} \quad (1)$$

Sun shielding properties were determined using the procedure of the European Cosmetic and Perfumery Association (COLIPA).[29] Different amounts of Ti-UVM-7 were mixed with a moisturizing cream until a consistent paste, with sunscreen-like texture, were achieved. The resulting mixture was applied into the rough surface of the PMMA plate using a gloved finger, ensuring an even distribution, followed by compressed air for 1 min to eliminate any free particles. According to the Food and Drug Administration (FDA), PMMA plates are recommended because it is transparent to ultraviolet (UV) radiation, non-

fluorescent, resistant to light degradation and inert to sunscreen ingredients.[30] The plate was then placed in a darkened environment for 15 min, allowing the sample to adapt and stabilize in a light-free setting. Finally, the transmittance was measured ten times in the range from 290 to 400 nm. Data were further analyzed to determine the UV protection calculating the Sunburn Protection Factor (SPF). SPF was calculated using equation (2), where E(λ) represents the Erythema Action Spectrum, I(λ) represents the sun's radiation power and T(λ) is the transmission for each wavelength.

$$SPF = \frac{\int_{290}^{400} E(\lambda) \cdot I(\lambda) \cdot d\lambda}{\int_{290}^{400} E(\lambda) \cdot I(\lambda) \cdot T(\lambda) d\lambda} \quad (2)$$

2.6. Data analysis and Life cycle assessment

The data analysis was performed using the IBM SPSS software version 28.0.1.1. Life Cycle Assessment (ISO 14040:2006) in a cradle to gate basis was applied to the scaled processes. The inventory was defined using the synthesis procedures and the energy consumption measured in the laboratory. The impact was calculated using the Ecoinvent 3 database and the ReCiPe 2016 Endpoint (H) V1.08/World (2010) H/A model available in the SimaPro software. If available data from Spain or Europe have been used. The method includes as impact categories global warming, stratospheric ozone depletion, ionizing radiation, ozone formation (human health), fine particulate matter formation, ozone formation (terrestrial ecosystems), terrestrial acidification, freshwater eutrophication, marine eutrophication, terrestrial ecotoxicity, freshwater ecotoxicity, marine ecotoxicity, human carcinogenic toxicity, human non-carcinogenic toxicity, land use, mineral resource scarcity, fossil

resource scarcity and water consumption. CTABr is not available in the data base, thus, esterquat (a cationic surfactant) was used for the analysis. Titanium butoxide was modelled using the molar ratio in the reaction of titanium tetrachloride with butanol, and the energy calculated with the enthalpy of reaction. For the preparation of 1 Kg of titanium butoxide, 0.5 Kg of titanium tetrachloride, 0.87 Kg of 1-butanol, and 0.03 KWh of electricity were used, and 0.43 Kg of hydrochloric acid is generated as subproduct. The sunscreen was calculated following the composition detailed by the Joint Research Centre (JRC), the European Commission's science and knowledge service.[31] The inventory can be found in the supplementary material (Table S2).

3. RESULTS AND DISCUSSION

3.1. Synthesis procedure and optimization

Considering the goal of developing sustainable processes for preparing silica-based mixed porous materials, we opted for the combination of the atrane route with microwave-assisted synthesis. Titanium is particularly suitable as a proof of concept given its compatibility with silicium in the silica, as both can give rise to tetrahedral structures with oxygen, and the numerous applications of titanium dioxide.

The synthesis of silica modified with titanium faces the obstacle of different reactivities between the two heteroatoms, resulting in the formation of phase mixtures. To address this challenge, a potential solution is the use of atranes as hydrolytic precursors to control the rates of hydrolysis and condensation. Triethanolamine ($TEAH_3$) assumes an essential role in the synthesis of UVM-7.

Its primary function is to form atrane complexes that modulate and balance the hydrolysis-condensation rate of Si and Ti. As a general rule, the synthesis of atrane complexes is carried out by transesterification reactions, starting from alkoxy derivatives in dry nonaqueous solvents. In our case, the Si and Ti atrane complexes were prepared together by heating the mixture of the corresponding commercial alkoxides in triethanolamine medium for a few minutes at 140°C.[11] Additionally, when employed in excess, $TEAH_3$ can also act as a co-solvent in the synthesis process.[32] The porosity is promoted by CTABr as structure directing agent.

The synthesis procedure has been described in Fig. 1. For the batch synthesis, an atrane mixture with molar composition (2-x):x:7:0.52:180 of Si:Ti:$TEAH_3$:CTABr:H_2O is heated by the solid-state microwave generator. In a previous study conducted by our group, the synthesis of UVM-7 was performed using 200 W for 30 s, 100 W for 1 min, and 50 W for 2 min. In this work, with the incorporation of titanium, we have reproduced these procedures and additionally conducted synthesis at 25 W for 4 min. Characterization of these four samples revealed that the optimal results were achieved by heating for 4 min at 25 W.[25] Subsequently, we conducted further experiments using different durations at the same power level to observe any potential variations. Then, the reaction time was established between 0.5 and 8 min, a time markedly low considering that, up to our knowledge, the shortest reaction time reported for the synthesis of Ti-UVM-7 is 2 h.[32] The resulting suspension is filtered, washed, dried, and calcined to remove the surfactant from the pores to obtain the mixed oxide Ti-UVM-7 materials.

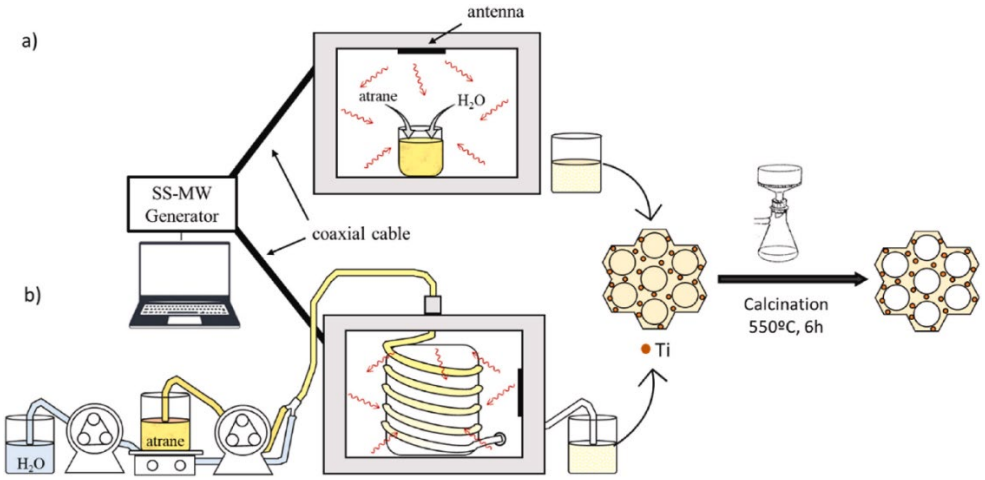

Fig. 1. *Synthesis procedure scheme in (a) batch, and (b) flow.*

Experimental conditions are summarized in Table 1. Reactions 1 to 15 were designed to evaluate the effect of the composition and operational parameters of the equipment in the properties of the materials. The rest correspond to the scaled-up reactions and will be discussed in the next section.

The main structural characteristics of the materials prepared have been collected in Table 2. The homogeneity of the materials was first studied by EDX and XRD in the range of 10 to 80° (2θ). EDX measures were used to analyze the sample composition and chemical homogeneity. As indicated in Table 2, the observed titanium content diverges significantly from the nominal values for all solid samples prepared in batch. A consistent tendency of titanium enrichment is evident. This trend can also be observed in the synthesis of Ti-UVM-7 using the conventional method,[33] indicating it is not caused by the use of the microwave, but instead it is attributed to the higher solubility of silicon oxide (SiO_2) compared to titanium oxide (TiO_2).

Table 2. *Selected synthetic and physical data for Ti-UVM-7 bimodal porous materials prepared in the batch optimization.*

Sample	Si/Ti[a]	Si/Ti[b]	S_{BET} ($m^2\ g^{-1}$)	Mesoporous diameter[c] (nm)	Textural pore diameter[c] (nm)	Mesoporous volumen[c] ($cm^3\ g^{-1}$)	Textural pore volume[c] ($cm^3\ g^{-1}$)	ζ[d] (mV)	2θ (°)	d_{100}[e] (nm)	a_0[f] (nm)	Wall thickness[g] (nm)
1	50	13.8 ± 0.7[a]	819 ± 3	2.4	20.8	0.37	0.34	-29.1 ± 0.6[a]	2.27	3.9	4.5	2.1
2	50	21.2 ± 0.5[b]	764 ± 2	2.5	20.8	0.37	0.31	-35.7 ± 0.9[b]	2.35	3.8	4.3	1.6
3	50	20.7 ± 0.8[bc]	879 ± 4	2.6	18.5	0.51	0.52	-27.3 ± 0.3[c]	2.31	3.8	4.4	1.9
4	50	24.7 ± 1.7[c]	889 ± 2	2.6	22.2	0.56	0.75	-29.6 ± 1.9[a]	2.27	3.9	4.5	1.7
5	25	3.6 ± 0.2[a]	985 ± 4	2.8	26.2	0.75	0.84	-28.7 ± 0.7[a]	2.00	4.4	5.1	2.3
6	25	4.3 ± 0.2[a]	786 ± 2	2.5	41.1	0.45	0.58	-30.0 ± 0.6[a]	2.02	4.4	5.1	2.5
7	25	11.4 ± 0.6[b]	864 ± 3	2.5	21.3	0.52	0.49	-35.1 ± 1.3[bc]	2.31	3.8	4.4	1.9
8	25	13.5 ± 0.6[c]	902 ± 2	2.9	26.1	0.71	0.65	-33.6 ± 1.7[ab]	2.27	3.9	4.5	1.6
9	10	2.0 ± 0.0[a]	454 ± 3	2.3	24.9	0.11	0.12	-33.5 ± 0.9[ab]	-	-	-	-
10	10	3.5 ± 0.3[b]	542 ± 2	2.4	26.0	0.19	0.29	-31.1 ± 0.9[bc]	-	-	-	-
11	10	3.8 ± 0.2[b]	585 ± 2	2.4	25.7	0.23	0.23	-25.3 ± 0.5[d]	2.29	3.9	4.5	2.0
12	10	3.9 ± 0.2[c]	738 ± 2	2.5	23.2	0.35	0.45	-26.6 ± 0.6[cd]	2.37	3.7	4.3	1.8
13	25	7.3 ± 0.3[d]	879 ± 3	2.5	38.2	0.49	0.35	-28.8 ± 1.3[a]	2.11	4.2	4.8	2.4
14	25	8.4 ± 0.4[e]	903 ± 4	2.5	39.2	0.52	0.38	-32.2 ± 0.4[ab]	2.12	4.2	4.8	2.4
15	25	8.7 ± 0.3[e]	788 ± 2	2.5	32.9	0.39	0.30	-39.2 ± 0.8[c]	2.15	4.1	4.7	2.3

[a]Theorical mixture. [b]Real mixture determined by EDX, letters indicate groups assigned by Tukey post hoc analysis within the materials with the same Si/Ti theoretical mixture (p = 0,05). [c]BJH pore sizes estimated from the isotherms adsorption branch. [d]Zeta potential, letters indicate groups assigned by Tukey post hoc analysis within the materials with the same Si/Ti theoretical mixture (p = 0,05). [e]Distance between planes of the hkl 100, calculated by $d_{100} = n\cdot\lambda\cdot(2\text{sen}\theta)^{-1}$ where n is the diffraction order, λ is the wavelength of the incident X-rays and θ is the diffraction angle. [f]Cell parameter calculated by $a_0 = d_{100}\cdot(\sqrt{3})^{-1}$. [g]Wall thickness was calculated by $d_w = a_0 - d_p$, where d_p is the mesopore diameter.

If we consider that the materials can be described as mixtures of SiO_2 and TiO_2 oxides, it is well known that the solubility of SiO_2 (ca. 0.12 g/mL) is much greater than that of TiO_2 (ca. 8.10–10 g/mL).[34,35] After the hydrolysis of the respective atrane complexes, condensation reactions will take place and as the oligomers interact with the surfactant molecules, the Ti-UVM-7 particles will nucleate and grow. As the Ti content (x) of the pore walls increases (1-x SiO_2: x TiO_2 or Si1-x Ti_xO_2) the titanium-rich domains will have a lower solubility than silica. Then, the Ti enrichment can be assigned to a partial silica dissolution. A similar trend was observed for other solids of the UVM-7 family containing Zr and Gd as heteroelements.[36,37]

XRD at high angles shows a typical wide signal at ca. 20–30° (2θ) which corresponds to the amorphous silica phase.[38] It should be mentioned that no peaks corresponding to TiO_2 crystalline phases were found (Fig. 2b), suggesting the incorporation of Ti atoms into the silica structure probably occurs, in a majority way, through isomorphic substitution. This was confirmed with Raman (Fig. S1), where no peaks were found for TiO_2 anatase or rutile. Only those of SiO_2 appear.[39]

Low angle XRD pattern provides information on the degree of ordering of the hexagonal porous array. Typically, the UVM-7 materials have a peak round 2° (2θ) corresponding to the plane 100 (hkl) and one weak shoulder associated with overlapped (110) and (200) planes, corresponding with an ordered hexagonal cell symmetry typical in mesoporous materials. We can observe that there are no appreciable changes in the (100) peak signal. The overall appearance of the diffractogram at low angles, including the shoulder associated with the superimposed (110) and (200) reflections, in general, does

not change significantly with the titanium content at low to medium Ti contents (Fig. 2a).

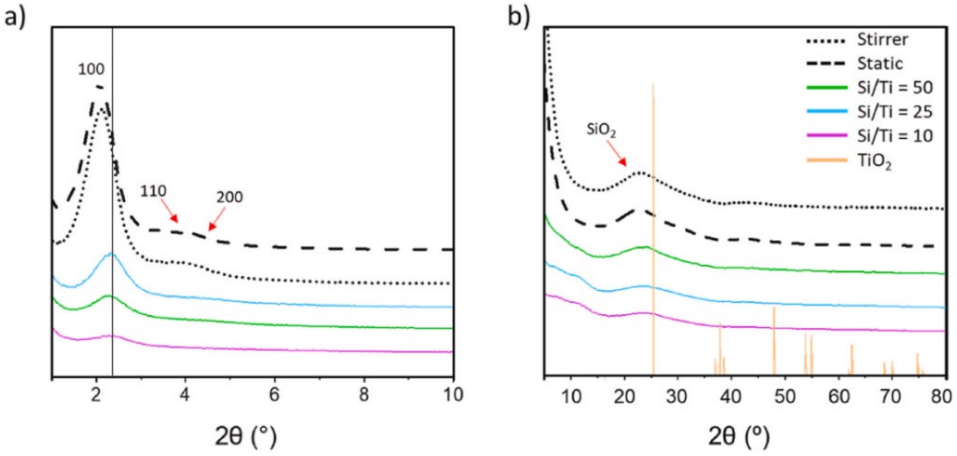

***Fig. 2**. XRD at a) low angles, and b) high angles of representative samples*

However, at large Ti content (Si/Ti = 10), although the (100) peak is observed the comparatively lower intensity suggests a loss of the large scale order of the porous system. This indicates that the variation in the Si/Ti ratio affects the particle morphology (see below) more than the XRD signal. A similar behavior has been observed for Ti-UVM-7 materials synthesized by the conventional method.[33] Probably, the ability of titanium to be largely incorporated into the silica network in environments with tetrahedral geometry implies less distortion of the mesostructure than that observed when heteroelements other than Ti are inserted. Undoubtedly, the fact that it has a formal charge identical to that of silicon (IV), together with its stabilization in tetrahedral environments, favors its isomorphic substitution (over a wide range of concentrations) and therefore less modification of the initial mesostructure of silica.

At a glance, from the information in the table, it can be deduced that an ordered pore structure can be obtained for all the concentrations tested. However, as the concentration of titanium increases, it is necessary to use longer irradiation times. In any case, 6 min is sufficient reaction time for material with a lower Si/Ti ratio. From the N_2 adsorption/desorption isotherm, we obtain type IV adsorption-desorption plots, typical of mesoporous solids (Fig. 3a).

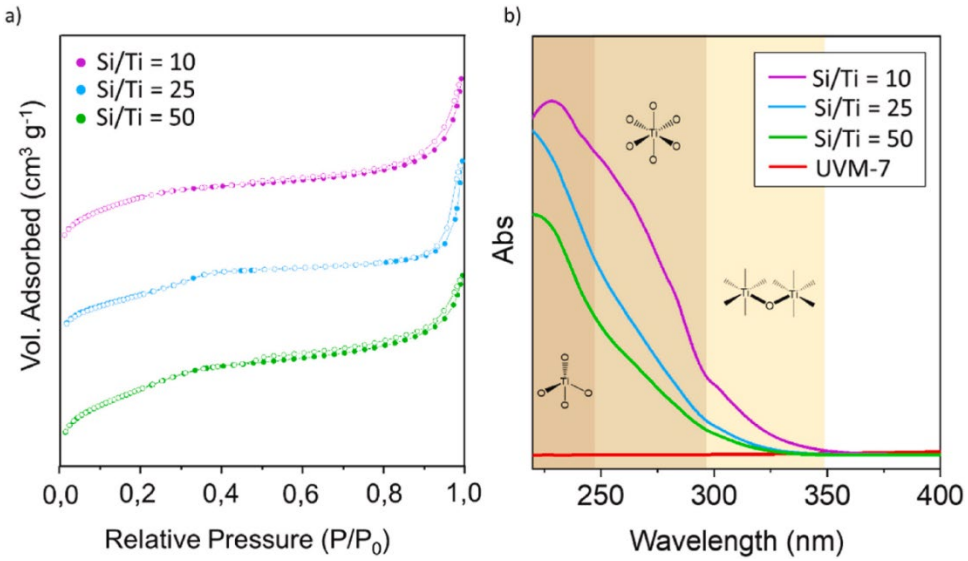

Fig. 3. *a) N_2 adsorption-desorption isotherms of samples 3, 7 and 11, and b) UV absorption, with diverse Si/Ti ratios.*

They present two adsorption steps, the first at medium relative pressures between $0.2 \leq P/P_0 \leq 0.4$ which can be associated with a mesopore system, and the second one, at high relative pressures between $0.9 \leq P/P_0 \leq 1.0$ which is due to a large-meso or macropore system. All materials, even those without peaks at low angles in XRD, show isotherms with the bimodal pore structure

typical of UVM-7, with a mesopore of 2–3 nm, and a textural large pore in the 20–40 nm range. Although a similar mesopore size is observed for all materials, in general, Ti-UVM-7 prepared with a shorter irradiation time presents differentiated structures with compared to the rest with a larger pore wall size. The area decreases due to the incorporation of titanium to values around 800 m^2 g^{-1}, which is consistent with previous results in which the UVM-7 area decreases when other elements are incorporated.[40]

In general, all materials exhibit high values of Z potential, around −30 mV. As the Z-potential is farther away from zero, the suspension is more stable, less likely to aggregate. Thus, these potentials are particularly suitable for obtaining more suspendable materials and are slightly higher than those observed for pure silica UVM-7.[40] This increase in potential can be understood if we take into account that Ti is more acidic than Si,[41] therefore in the presence of Ti, it is easier to deprotonate the OH groups, generating a greater negative charge on the surface of the material.

ANOVA with Tukey post hoc analysis applied to those materials with the same nominal Si/Ti ratio indicate that the irradiation time is able to generate materials with diverse Si/Ti ratios and Z potential, and these differences are statistically significant (Table 2, $p = 0.05$). To better understand the influence of the different variables on the textural characteristics and composition of the materials obtained, a linear adjustment was carried out, considering the Si/Ti relationship, power and time as independent variables, and the area and other characteristics of Table 2 as dependent variables. It is evident that irradiation time primarily influences the amount of titanium incorporated into the matrix. There is a clear trend indicating that increased irradiation time

leads to higher titanium enrichment in the samples. With shorter irradiation times in the microwave cavity, the material contains a higher amount of TiO_2. This occurs because SiO_2 is more soluble than TiO_2, resulting in greater dissolution of SiO_2 and less incorporation into the solid compared to TiO_2. A summary of the degree of significance for the different variables can be found in Table S1 of the Supplementary material. For a degree of significance of $p < 0.1$, in the case of the measured Si/Ti ratio, the main parameter is the nominal Si/Ti ratio, although the reaction time is also decisive. When the reaction time increases, there is a reduction in the titanium content. In the case of textural parameters determined from N_2 adsorption/desorption, the surface area depends fundamentally on the Si/Ti ratio, decreasing with increasing Ti concentration. Mesopore diameter, textural pore, and textural pore volume depend on the Si/Ti ratio and reaction time, with positive correlations. On the contrary, the textural pore diameter does not depend on the variables analyzed, corresponding to uncontrolled or random factors. Z-potential and cell size are other parameters that do not depend on the variables tested. Finally, the size of the wall, since it is related to the pore size, also depends on the Si/Ti ratio and the irradiation time.

As a complement to the above techniques, electron microscopy provides an overview of the morphology of the material. TEM images reveal the typical UVM-7 structure of this class of materials for the samples with Si/Ti nominal molar ratios of 50 or 25, consisting in small mesoporous particles that assemble, resulting in the formation of large textural pores among them (Fig. 4b).

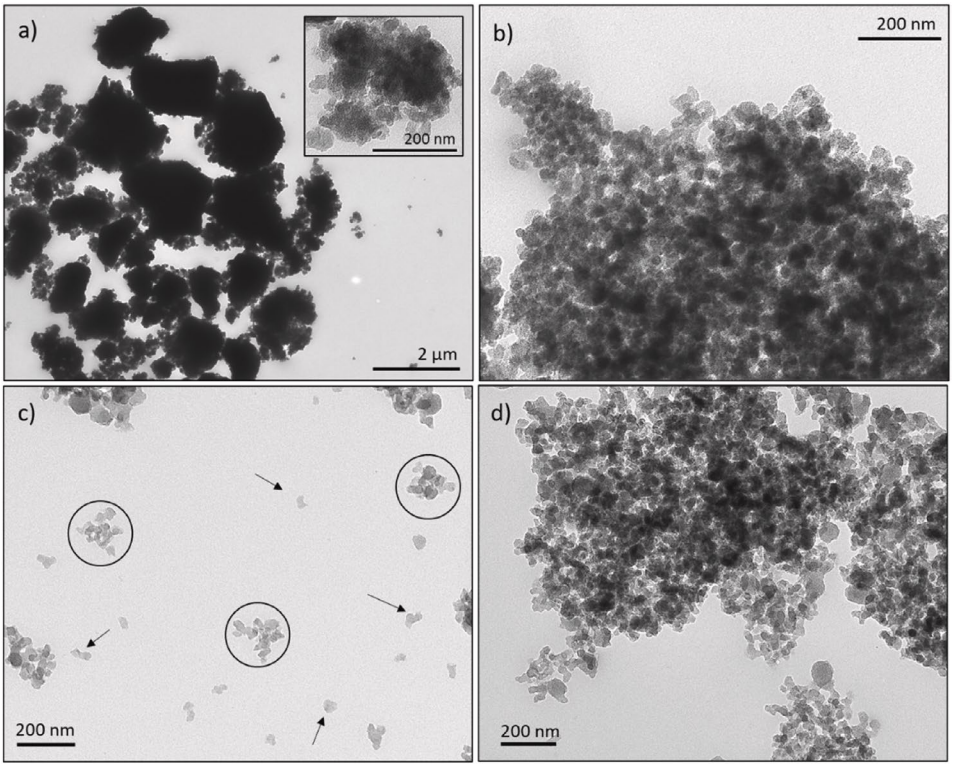

***Fig. 4**. TEM images for a) sample with a Si/Ti molar ratio of 10 (sample 11), b) sample with a Si/Ti molar ratio of 25 (sample 7), c) scale-up sample with stirring, and d) scale-up sample without stirring. The presence of aggregates of smaller nanoparticles in the case of the scale-up sample with stirring is indicated with circles and arrows.*

The study with different irradiation times and potencies (samples 6 and 13 to 15), showed similar structures, confirming that the reaction time can be significatively reduced to less than 1 min. However, when the Si/Ti ratio is 10 (samples 9 to 12), a morphological transformation occurs in the particles. Pores are less readily discernible compared with the rest of materials, particularly in sample 9. In addition, a segregation of phases is observed, finding dense phases with a crystalline appearance surrounded by a material

with the characteristic appearance of porous silica (Fig. 4a), which have a disordered structure according to the XRD data recorded at the low-angle range.

It should be borne in mind that the titanium content is very high (Si/Ti real molar ratio less than 4), which would modify the structure of the material excessively, even at long reaction times, resulting in a heterogeneous material. In the HRTEM images (Fig. 5), samples with a Si/Ti nominal molar ratio of 10 exhibit an appreciable particle size heterogeneity together with small spots attributed to Ti-rich domains of sizes around 9 ± 3 nm.

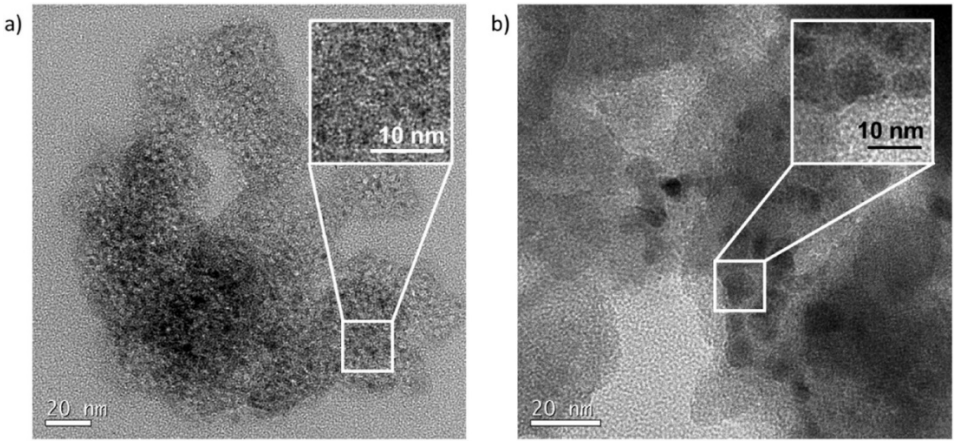

Fig. 5. *HRTEM images of a) sample 7, and b) sample 11, showing the darker domains associated with regions richer in Ti (marked with arrows). High magnification images focusing on these domains are presented in the insets.*

In contrast, samples with a lower Si/Ti nominal molar ratio show a particle size homogeneity typical of pure silica UVM-7 materials and even smaller (5 ± 3 nm) and more homogeneously distributed Ti-rich nanodomains within the porous silica matrix. This observation corroborates the XRD findings,

indicating that variations in the Si/Ti ratio significantly affect particle morphology. No order is observed in the titanium-rich domains. Their small size, even if they were TiO_2 nanoparticles, excludes their detection by X-ray diffraction. This is consistent with the absence of peaks in the high-angle XRD patterns.

Finally, the effect of titanium incorporation on the local structure can be confirmed by UV–Vis and XPS. In all cases, the UV–Vis spectra of the final mesoporous materials (Fig. 3b) show an intense adsorption in the 214–225 nm range, which is typically assigned to a ligand to metal charge transfer involving isolated and tetrahedrally coordinated Ti atoms.[42] Notwithstanding, the significant adsorption tails in the 250–350 nm range (whose intensity increases with the Ti content) further indicate the presence of octahedral environments for Ti.[43] At this point, it has to be noted that none of the samples causes appreciable absorption at $\lambda > 350$ nm, which, in principle (in good agreement with the XRD results) would be compatible with the single-phase nature of all these solids (i. e. this technique also fails to suggest the presence of extra-framework TiO_2 crystalline domains).[44] In the samples with lower Ti content, the typical Ti signal in tetrahedral environments is dominant. As the heteroelement concentration increases, the intensity of this signal increases and a certain adsorption appears at lower energy associated with Ti atoms in octahedral environments.

The Ti2p, O1s and Si2p core level XPS spectra of three representative samples with variable amounts of titanium (samples 3, 7 and 11; $3.8 \leq$ Si/Ti real molar ratio ≤ 20.7) have been recorded (Fig. 6).

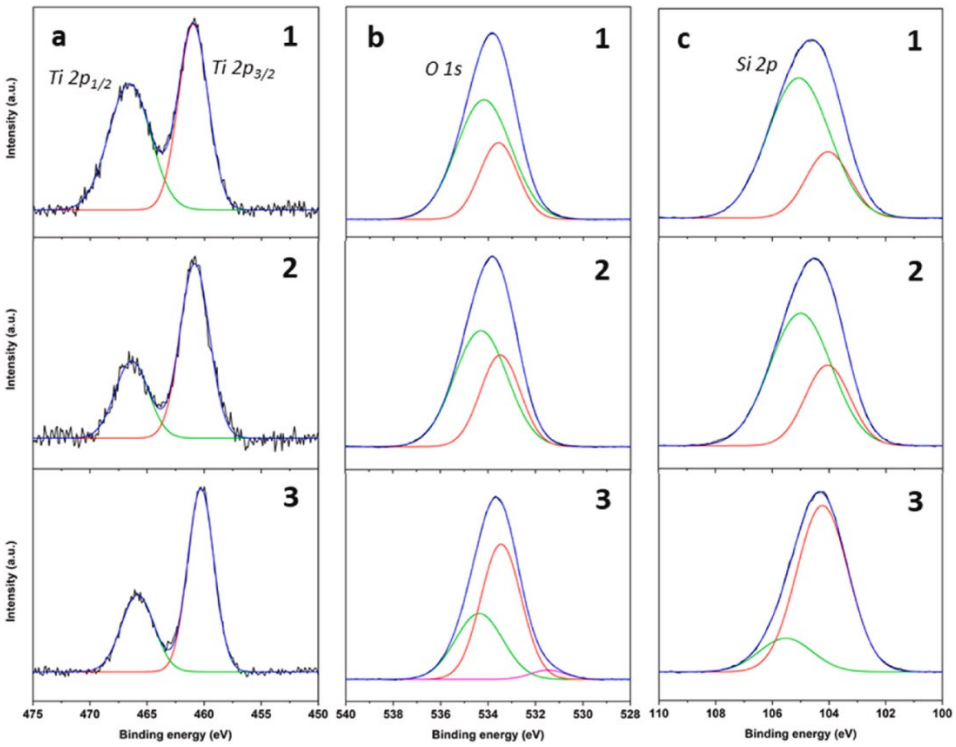

Fig. 6. *a)Ti 2p, b) O 1s and c) Si 2p XPS spectra of sample 3 (1), 7 (2) and 11 (3).*

The binding energies (BE) of the Ti2p3/2 and Ti2p1/2 bands were observed to be within the range of 460.3–460.9 eV and 465.8–466.6 eV, respectively. These values are clearly somewhat higher than those typically observed for TiO_2 particles (459.3 and 465.2 eV).[45] The Ti2p BE values observed in our materials fall within the range described for amorphous mixed oxides of Si and Ti[46] and also for solids of the Ti-MCM-41 type,[47] which is in accordance with expectations. In the case of the sample with the highest titanium content, in addition to the two aforementioned signals, an additional Gaussian centered at 531.5 eV is required in order to achieve a satisfactory fit. As evidenced in the literature,[46,48] an increase in titanium content in related systems is

associated with a shift in binding energy (BE) values towards lower energies. It was observed that the contribution of the Gaussian to higher BE exhibited a decreasing trend with increasing Ti content. The respective percentages are 70, 63 and 35 % for samples 3, 7 and 11. Concurrently, the contribution of the Gaussian centered at 533.5 eV increases in proportion to the Ti content. The respective percentages are 30, 37 and 61 % for samples 3, 7 and 11, respectively. Moreover, in the case of the material with a higher Ti content, the deconvolution of the XPS O1s spectrum indicates the presence of an additional signal, contributing 4 % to the overall result. As the binding energy (BE) decreases, the local O environments evolve from Si-O-Si to Ti-O-Ti, passing through mixed environments of the Si-O-Ti type. In no case do the BE values approach those typical for TiO_2 (ca. 530 eV). The deconvolution of the XPS Si2p spectra has been performed on a consistent basis with two Gaussian functions centered at ca. 104 and 105 eV. The contribution of both evolves inversely, from 25 % (sample 3) to 83 % (sample 11) for the function centered at 104 eV (Si environments with nearby Ti atoms) and from 75 % (sample 3) to 17 % (sample 11) for the one centered at 105 eV (Si environments preferably surrounded by Si). The data obtained from the UV–Vis and XPS analyses are in accordance with the presence of a mixed oxide of silicon and titanium, exhibiting a highly uniform distribution of both elements and the absence of TiO_2 domains. Ti is predominantly located in environments with tetrahedral geometry (isomorphic substitution of Si), and as its concentration rises, it can be stabilized in octahedral environments, resulting in the formation of Ti-rich nanodomains.

From the above data, it can be concluded that microwaves of solid-state generators are a suitable technique for the preparation, not only of pure silica UVM-7 mesoporous materials, but also mixed silicas including other elements. In this case, Ti-UVM-7 type materials with Si/Ti ratios close to 4 can be obtained without phase segregation and preserving the typical topology of these materials. Also, it is noteworthy the fact that these materials can be prepared with only 30 s of irradiation.

3.2. Batch scale-up and flow and synthesis

To evaluate the possibility of preparing large quantities of Ti-UVM-7 we followed two approaches, batch scaling and flow synthesis. The first is a priori more feasible, although the limited penetration capacity of microwaves can generate difficulties when the size of the reactor increases, and there is a risk of having cold and hot spots. To avoid these drawbacks, flow synthesis enables the maintenance of a small conduction size, achieving homogeneous irradiation, and eliminating the presence of hot and cold spots through continuous movement. Also, the flow synthesis process can be easily automated.

Considering the objective of scaling the synthesis 100 times and given that the power of the equipment is limited to 800W, it was not possible to increase it proportionally with the increase in scale and it was decided to increase the reaction time to 10 min. Batch-scaled synthesis has been executed without stirring, in agreement with the optimization process in the previous section, and with the aim of a simpler implementation. A summary of the synthesis conditions can be found in Table 3 (samples 16 to 19). In flow synthesis,

reactants are continuously introduced into the system and products are continuously removed (Table 3, samples 20 to 24). The main difference between batch and flow synthesis lies in the fact that, in the former, all reactants are combined in a single vessel and introduced into the reactor. Conversely, flow synthesis involves two solutions: one containing the atrane complexes and the template, and the other one the water. By employing two peristaltic pumps, the solutions are brought into contact just prior to entering the microwave system, with distinct flow rates selected to ensure the desired residence time within the reactor. Table 3 collects the main morphological parameters and composition of the scaled-up materials.

A first differentiating aspect in materials prepared by scaled synthesis is that there is a slight shift of the 100 (hkl) XRD peak toward lower angles, indicating an increase in cell size. However, unlike samples 13 to 15, in the scaled-up synthesis this variation can be assigned to an increase in pore size, with a lower contribution from wall size. Again, none of the materials showed the presence of the characteristic XRD peaks of TiO_2 in the high-angle domain (Fig. 2b), reinforcing the idea that Ti is effectively included in the silica network, which was also confirmed by Raman spectroscopy. The area and pore size are similar to the non-scaled-up synthesis. However, the pore volume increases, suggesting structural modifications that will be further analyzed by TEM. EDX data reveal that in the scaled synthesis nominal and measured Si/Ti ratios are similar.

***Table 3**. Selected synthetic and physical data for Ti-UVM-7 bimodal porous materials prepared in the scale-up.*

Sample	Si/Ti[a]	Si/Ti[b]	S_{BET} ($m^2\ g^{-1}$)	Mesoporous diameter[c] (nm)	Textural pore diameter[c] (nm)	Mesoporous volumen[c] ($cm^3\ g^{-1}$)	Textural pore volume[c] ($cm^3\ g^{-1}$)	ζ[d] (mV)	2θ (°)	d_{100}[e] (nm)	a_0[f] (nm)	Wall thickness[g] (nm)
16	10	8.2 ± 1.4	964 ± 4	2.7	36.5	0.74	0.94	-27.5 ± 0.6	2.15	4.1	4.7	2.0
17	25	22 ± 3	885 ± 3	2.7	50.2	0.70	1.75	-27.4 ± 0.6	2.11	4.2	4.8	2.1
18	50	49 ± 7	907 ± 2	2.8	35.0	0.77	0.77	-28.1 ± 0.4	2.07	4.3	4.9	2.1
19	50	50 ± 9	1041 ± 2	2.9	45.6	0.91	1.16	-28.6 ± 0.2	2.13	4.2	4.8	1.9
20	50	23.9 ± 0.7	1043 ± 6	2.7	20.2	0.79	0.67	-31.1 ± 0.5	2.47	3.6	4.1	1.5
21	50	25.1 ± 0.8	1070 ± 5	2.7	23.2	0.83	0.85	-31.5 ± 0.8	2.37	3.7	4.3	1.6
22	50	24.6 ± 0.6	1039 ± 7	2.7	25.0	0.77	0.88	-24.8 ± 0.4	2.37	3.7	4.3	1.6
23	50	46 ± 7	1039 ± 2	2.7	29.9	0.87	1.18	-29.4 ± 1.2	2.39	3.7	4.3	1.5
24	25	29 ± 2	1047 ± 3	2.7	42.0	0.85	1.60	-31.1 ± 0.9	2.41	3.7	4.2	1.5

[a]Theorical mixture. [b]Real mixture determined by EDX, letters indicate groups assigned by Tukey post hoc analysis within the materials with the same Si/Ti theoretical mixture (p = 0,05). [c]BJH pore sizes estimated from the isotherms adsorption branch. [d]Zeta potential, letters indicate groups assigned by Tukey post hoc analysis within the materials with the same Si/Ti theoretical mixture (p = 0,05). [e]Distance between planes of the hkl 100, calculated by $d_{100} = n\cdot\lambda\cdot(2\text{sen}\theta)^{-1}$ where n is the diffraction order, λ is the wavelength of the incident X-rays and θ is the diffraction angle. [f]Cell parameter calculated by $a_0 = d_{100}\cdot(\sqrt{3})^{-1}$. [g]Wall thickness was calculated by $d_w = a_0 - d_p$, where d_p is the mesopore diameter.

In general, all materials exhibit high values of Z potential as before. We can observe that all values approach approximately −30, but in some cases, a slightly decrease can be observed. According to a study conducted by Esin Yakin, F. in 2020, the zeta potential depends on the particle size and porosity, showing a decrease of up to 10 % in the zeta potential when decreasing the particle diameter.[48] The TEM images of samples 16 to 19 show a UVM-7 structure for all materials, even those with a higher titanium content (Si/Ti = 10). It should be noted that sample 16 has a ratio of 8.2, similar to the non-scaled Si/Ti 25 that maintain the UVM-7 structure and incorporate Ti in a homogeneous way.

Regarding the effect of stirring (samples 18 and 19), only minor variations have been found in the textural properties, lower than the natural variability of this type of synthesis.[25] However, a slightly lower tendency to aggregation is observed in the reaction with agitation, obtaining a greater number of small particles (Fig. 4c,d).

Thus, the synthesis can be scaled-up in batch conditions maintaining the main features of the materials, in only 10 min. In each batch, approximately 33 g of calcined Ti-UVM-7 are obtained, a large amount considering that the process is fast, and it is prepared in a bench equipment.

In an alternative approach, the flow synthesis departing of atrane and water mixtures was also studied. Three experiments were conducted. First, the material was collected at different intervals in order to evaluate the homogeneity of the materials obtained in different synthesis intervals (samples 20 to 22). The second studied the effect of reducing the reaction

time with equal energy (sample 23). Finally, we evaluated the possibility of using the same procedure to obtain a material with an intermediate titanium concentration (Si/Ti = 25, sample 24). From the data collected in Table 2, Table 3, compared to samples obtained in unscaled batch, flow samples show similar cell and pore sizes. However, the area is larger, exceeding 1000 $m^2 g^{-1}$. These values are common for UVM-7 materials,[33] although higher than those obtained in the batch samples. If we check the parameters measured for samples 20 to 22 collected from the reactor at different times, we can see that they all present very homogeneous values, which supports the possibility of using microwave-assisted flow reactors for the preparation of mesoporous silicas containing titanium. In the above samples, 2 min were chosen because of its similarity to the reaction conditions tested in section 2.1, however, it appears that the reduction in reaction time has a dramatic effect on the incorporation of titanium into the silica structure. When we increase the flow 4-fold and thus the dwell time in the microwave oven decreases from 2 min to 30 s, the Si/Ti ratio values measured by EDX approximate the nominal values added in the reaction mixture (samples 23 and 24). This phenomenon will require further research in the future, but it is similar to what we have found in the batch scaling process. Finally, the data from samples 23 and 24 suggest that the synthesis procedure can be applied for the preparation of samples with variable titanium contents, at least up to a Si/Ti ratio of 25. TEM photos show a typical UVM-7 structure. 0.2 g of Ti-UVM-7 min^{-1} is obtained, which is equivalent to 12 g h^{-1}. As with batch scaling, the synthesis procedure described for the preparation of mixed porous silicas can also be adapted to flow synthesis.

3.3. Optical properties of Ti-UVM-7

TiO_2 is an excellent photocatalyst, typically it shows a band at 350 nm.[49] By contrast, pure silica UVM-7 is transparent in the UV–vis zone. In general, materials of Ti-UVM-7 absorb below 300–350 nm, indicating relatively large bandgaps, in agreement with the presence of Titanium but the absence of TiO_2 nanodomains (Fig. 3b). These values are similar to titanium containing UVM-7 materials prepared by conventional procedures.[33] All the Ti-UVM-7 materials have bandgaps between 4 or 5 eV, in comparison with TiO_2 that has a value of 3.5 eV. When the Ti content increases it is observed a lower gap, with values of 4.9, 4.6 and 4.1 eV for the nominal molar ratios Si/Ti = 50, 25 and 10, respectively. However, the sample 9, with higher phase segregation, has a bandgap value of 3.80 eV, closer to the value for the TiO_2. Samples 20 to 24, synthesized under flow conditions, have a bandgap of 4.2 eV. This value is relatively low in comparison with the Ti-UVM-7 materials with similar Si/Ti ratio. As expected, Ti-UVM-7 samples with higher Ti content show stronger UV absorption, but also the textural properties can be relevant.

Considering these properties, we evaluated the properties of Sample 8 as suitable sunscreen material. Also, a commercial TiO_2 and pure silica UVM-7 were measured for comparison. The values of SPF have been collected in Table 4. We have calculated SPF values of up to 2.4 for a mixture with a 10 % of nanomaterial. This value can seem low if we consider that 5–10 % TiO_2 nanoparticles can offer SPF values between 6 and 9.[50] However, if we consider only the Ti content, Ti-UVM-7 materials would be more effective than pure TiO_2 as sun shielding materials. The effect of Ti would be complemented with the effect of the UVM-7 structure, since SiO_2 is transparent to the UV

radiation.[51] Additionally, some studies have reported that the incorporation of UV filters into mesoporous silica materials enhances the protective capacity of these compounds. A test was also conducted with 5 % UVM-7 without titanium, resulting in an SPF of 1. This result is consistent with that obtained by C.C. Li using 2 % mesoporous silica,[52] and with Y.W. Cheng, who achieved an SPF of 1.1 using 4 % of the material,[53] indicating the absence of significant photoprotection.

Table 4. *Results of the SPF measurements for different amounts of Ti-UVM-7.*

Material	% (w/w)	SPF ± SD	% TiO_2[a]
Ti-UVM-7	1	1.2 ± 0.3	0.08
Ti-UVM-7	5	1.6 ± 0.4	0.35
Ti-UVM-7	10	2.4 ± 0.9	0.68
Ti-UVM-7	30	4.0 ± 0.6	1.81
TiO_2	2	2.1 ± 0.9	2.00
UVM-7	5	1.08 ± 0.16	0.00

[a]TiO_2 equivalent calculated from the measured Si/Ti and the percentage of material used.

Although, 5 % Ti-UVM-7 has a SPF value higher than 5 % UVM-7 the differences are not statistically significant (p = 0.05). Barbosa, J.S. conducted experiments to measure SPF of commercially available TiO_2 and SiO_2-coated TiO_2, both with a concentration of 4 wt%.[54] The results indicated SPF values of 1.66 and 1.9, respectively, which closely aligns with the outcomes of our own investigation. With 1.8 % TiO_2, an SPF of 4 is achieved, which is double that obtained with 2 % TiO_2 without the mesoporous silica matrix. Using 10 % TiO_2 embedded in an SBA-15 matrix, Da Silva Marcelino achieved an SPF of

15 ± 1.[55] This value is higher than in our case, but it must be considered that a larger amount of titania is present. If we consider the SPF/%TiO_2 ratio, the data we have obtained, aligns closely with the results for the SBA-15 material.

By means of the guidelines provided by the FDA, there exist restrictions on the percentage of anatase crystalline polymorph present in titanium dioxide to minimize its photocatalytic activity. The potential occurrence of photocatalytic activity poses a risk of degrading other active ingredients present in sunscreen products containing nanoscale titanium dioxide upon exposure to light. Extensive studies on TiO_2 have been conducted, focusing on product evaluations with TiO_2 concentrations up to 10%. These concentrations have been generally acknowledged as safe and effective for use in sunscreens, with permissible concentrations reaching up to 25%.[54] However, by using Ti coated in the UVM-7, this issue can be avoided.

The integration of titanium within the mesoporous silica matrix could enhance UV blocking capabilities, but also offers additional benefits such as enhanced stability, increased photoactivity, and improved photostability. Furthermore, the unique structural properties of mesoporous materials, characterized by a well-defined pore structure and high surface area, allow for the efficient incorporation of UV filters, promoting uniform dispersion and optimal UV absorption.[56]

3.4. Life cycle assessment

The main advantage of microwaves is their efficiency in reducing reaction times. A reduced reaction time, combined with the use of low powers, enables a synthesis process with a lower energy consumption. The LCA was applied in

a cradle to gate basis. The goals are the quantification of the global impact and main impact factors associated with the preparation of Ti-UVM-7 materials, evaluate the effect of the scale-up, and identify the main processes/reagents to suggest improvements. The functional unit was defined as the preparation of 1 kg of material.

The single score offers a general mark of the impacts. The non scaled-up synthesis offers a value of 245 points. This value is high, but it should be noted that in the laboratory process the small batch size implies a use of materials and processes that are not representative of the value on a large scale. Thus, in batch-scaled synthesis this value is reduced to 10.7 points, a value similar to that obtained in flow synthesis. The single score decreases to 2.7 points for 1 kg of sunscreen cream with a 25 % of loading of the Ti-UVM-7 material.

As can be seen in Fig. 7a, for Ti-UVM-7 reactants, solvents, and energy are of similar importance. Therefore, the process could be improved by using energy with a lower environmental impact, removing or at least reducing the use of ethanol, and replacing reagents with lower-impact ones. This last point can be especially tricky since the main reagent is triethanolamine, a key reagent in the atrane route, but a reduction in the amount of triethanolamine could be studied. Also, the possibility of using novel sources of silicon, or more sustainable surfactants could be interesting topics for future works. Titanium butoxide offers an impact higher than TEOS, thus the use of inorganic titanium salts instead of titanium butoxide could be also advisable. Regarding the main impact categories, the main ones are Human carcinogenic toxicity, Freshwater ecotoxicity, Marine ecotoxicity, Freshwater eutrophication, and Ionizing radiation (see Fig. 7b), all of them related to the preparation of solvents and

chemical reagents. By contrast, other relevant factors in impact studies such as global warming potential, or water consumption offer only a minor contribution, highlighting the relevance to perform full LCA studies to evaluate the processes, not only evaluations of single impact categories.

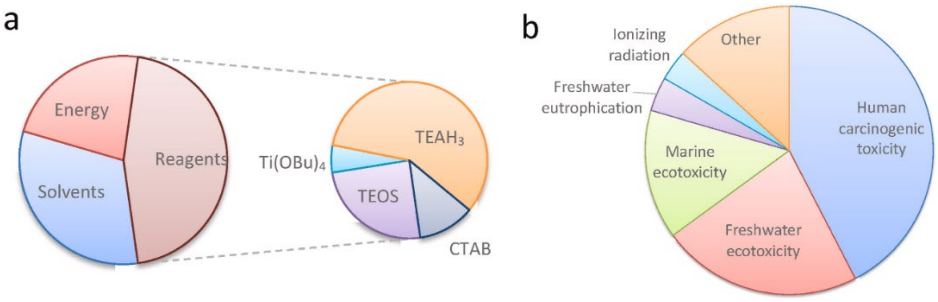

***Fig. 7**. Life Cycle Assessment. a) Contribution of the processes to the single score (Pt) of the scaled-up batch synthesis calculated following the ReCiPe 2016 Endpoint (H) V1.08/World H/A method. b) Main normalized impact category indicators of the scaled-up batch synthesis calculated following the ReCiPe 2016 Midpoint (H) V1.08/World (2010) H method.*

4. CONCLUSIONS

We have effectively demonstrated that the combination of the atrane route with the microwave assisted synthesis using solid-state generators can be an interesting approach to obtain, not only porous silica, but also mixed compound with other elements. In this study, we present for the first time the synthesis of Ti-UVM-7 successfully using a solid-state microwave generator in less than 10 min with a Ti content of up to 3.8 (Si/Ti real molar ratio). In some cases, the materials can be obtained in only 30 s. The microwave-assisted synthesis enabled efficient heating and precise control over reaction parameters, leading to the formation of Ti-UVM-7 with well-defined

mesoporous structures and uniform titanium distribution. Regarding the operative parameters, the reaction time and Si/Ti ratio are significant. The reaction can be effectively scaled-up in batch and adapted to flow synthesis maintaining the typical UVM-7 topology. This allows the preparation of hundreds of grams with a significant reduction in the impact to only 10 points in the single score of LCA per kg of Ti-UVM-7, that could be reduced in an industrial process and/or modification of the reagents. The inclusion of Ti modifies the optical properties, reducing the band gap of the material favoring the use of this type of materials as sunscreens.

CRediT authorship contribution statement

Cristina Rodríguez-Carrillo: Writing – review & editing, Writing – original draft, Methodology, Investigation, Conceptualization. Miriam Benítez: Writing – review & editing, Writing – original draft, Methodology, Investigation, Conceptualization. Marta González-Fernández: Investigation. Ruth de los Reyes: Investigation. Sonia Murcia: Visualization, Investigation. Jamal El Haskouri: Writing – review & editing, Writing – original draft, Investigation, Conceptualization. Pedro Amorós: Writing – review & editing, Writing – original draft, Supervision, Methodology, Investigation, Funding acquisition, Conceptualization. Jose V. Ros-Lis: Writing – review & editing, Writing – original draft, Supervision, Investigation, Funding acquisition, Conceptualization.

Declaration of competing interest

The authors declare the following financial interests/personal relationships which may be considered as potential competing interests: Jose V. Ros-Lis reports financial support was provided by Spain Ministry of Science and Innovation. Jose V. Ros-Lis reports financial support was provided by Government of Valencia. If there are other authors, they declare that they have no known competing financial interests or personal relationships that could have appeared to influence the work reported in this paper.

Data availability

No data was used for the research described in the article.

Acknowledgments

This research was funded by the Spanish Ministerio de Ciencia, Innovaci´on y Universidades, grant number PID2021-126304OB-C43 funded by MCIN/AEI/10.13039/501100011033 and by “ERDF A way of making Europe”; the AGROALNEXT programme supported by MCIN with funding from European Union NextGenerationEU (PRTR-C17.I1) and by Generalitat grant number EUAGROALNEXT/2022/065; and by Generalitat Valenciana grant number CIAPOT/2022/017.

References

(1) Kumari, A.; Zaman, M.; Kumar, A.; Singh, V.R.; Ghosh, A.; Sahoo, S.K.; Rahaman, A.; Mandal, S.K.; Bhunia, S.J. An alternative approach to study photocatalytic behavior of TiO_2 using synchrotron-based advanced spectroscopic techniques. *Mater. Eng. Perform*. **2023**, *32*, 10391–10401.

(2) Sábio, R.M.; Bagliotti Meneguin, A.; Martins dos Santos, A.; Monteiro, A.S.; Chorilli, M. Exploiting mesoporous silica nanoparticles as versatile drug carriers for several routes of administration. *Micropor. Mesopor. Mat.* **2021**, *312*, 110774.

(3) Ziarani, G.M.; Moradi, R.; Mohajer, F.; Badiei, A. Synthesis of SBA-Pr-NHC as a selective fluorescent sensor for the detection of Ag^+ ion in aqueous media. *Spectrochim. Acta Mol. Biomol. Spectrosc*. **2022**, *267*, 120580.

(4) Liao, L.; Wang, M.; Li, Z.; Wang, X.; Zhou, W. Recent advances in black TiO_2 nanomaterials for solar energy conversion. *Nanomaterials* **2023**, *13*, 468.

(5) El Haskouri, J.; Ortiz de Zárate, D.; Guillem, C.; Latorre, J.; Caldés, M.; Beltrán, A.; Beltrán, D.; Descalzo, A. B.; Rodríguez-López, G.; Martínez-Máñez, R.; Marcos, M. D.; Amorós, P. Silica-based powders and monoliths with bimodal pore systems. *Chem. Commun*. **2002**, *4*, 330−331.

(6) Pérez-Cabero, M.; Hungría, A.B.; Morales, J.M.; Tortajada, M.; Ramón, D.; Moragues, A.; El Haskouri, J.; Beltrán, A.; Beltrán, D.; Amorós, P. Interconnected mesopores and high accessibility in UVM-7-like silicas. *J. Nanopart. Res*. **2012**, *14*, 1045.

(7) Albiñana, P.A.; El Haskouri, J.; Marcos, M.D.; Estevan, F.; Amorós, P.; Úbeda, M.A.; Pérez-Pla, F. A new efficient, highly dispersed, Pd nanoparticulate silica supported catalyst synthesized from an organometallic precursor. Study of the homogeneous vs. heterogeneous activity in the Suzuki-Miyaura reaction. *J. Catal*. **2018**, *367*, 283–295.

(8) Pellicer-Castell, E.; Belenguer-Sapiña, C.; Amorós, P.; El Haskouri, J.; Herrero-Martínez, J.M.; Mauri-Aucejo, A.R. Comparison of silica-based materials for organophosphorus pesticides sampling and occupational risk assessment. *Anal. Chim. Acta* **2020**, *1110*, 26–34.

(9) Muñoz-Pina, S.; Duch-Calabuig, A.; Ruiz de Assín David, E.; Ros-Lis, J.V.; Amorós, P.; Argüelles, Á.; Andrés, A. Bioactive compounds and enzymatic browning inhibition in cloudy apple juice by a new magnetic UVM-7-SH mesoporous material. *Food Res. Int.* **2022**, *162*, 112073.

(10) Wan, Y.; Zhao, D. On the controllable soft-templating approach to mesoporous silicates. *Chem. Rev.* **2007**, *107*, 2821–2860.

(11) Garrido, M.D.; Benítez, M.; Ros-Lis, J.V.; Amorós, P. A travel though the atrane route, a versatile tool for the materials soft-synthesis: A twenty-five years perspective. *Nano Select* **2024**, *5*, 2300169.

(12) Pujro, R.; Crespo, P.; Amorós, P.; Blanco, M.; Cabrera, S. La ruta de los atranos en la síntesis de óxidos mixtos mesoporosos $Al_2Ti_xO_{3-2x}$. *Rev. Bol. Quim*. **2007**, *24*, 26–32.

(13) Brinker, C.J.; Lu, Y.; Sellinger, A.; Fan, H. Evaporation-induced self-assembly: nanostructures made easy. *Adv. Mater*. **1999**, *11*, 579–585.

(14) Haider, S.; Nawaz, R.; Anjum, M.; Haneef, T.; Oad, V.K.; Uddinkhan, S.; Khan, R.; Aquif, M. Property-performance relationship of core-shell structured black TiO_2 photocatalyst for environmental remediation. *Front. Environ. Sci. Eng*. **2023**, *17*, 111.

(15) Shiva Samhitha, S.; Raghavendra, G.M.; Quezada, C.; Hima Bindu, P. Green synthesized TiO_2 nanoparticles for anticancer applications: Mini review. *Mater. Today Proc.* **2022**, *54*, 765–770.

(16) Campos, R.; Primera, J.; Amorós, P.; Huerta, L. Síntesis y caracterización de materiales mesoporosos bimodales Ti-UVM7 por incorporación directa en el gel de partida. *Ciencia* **2017**, *25*, 136–142.

(17) Trandafir, M.M.; Moragues, A.; Amorós, P.; Parvulescu, V.I. Selective hydrogenation of nitroderivatives over Au/TiO_2/UVM-7 composite catalyst. *Catal. Today* **2020**, *355*, 893–902.

(18) Moragues, A.; Neatu, F.; Parvulescu, V.I.; Marcos, M.D.; Amorós, P.; Michelet, V. Heterogeneous gold catalyst: synthesis, characterization, and application in 1,4-addition of boronic acids to enones. *ACS Catal*. **2015**, *5*, 5060–5067

(19) Rodríguez-Carrillo, C.; Torres García, J.; Benítez, M.; El Haskouri, J.; Amorós, A.; Ros-Lis, J.V. Batch and flow synthesis of CeO_2 nanomaterials using solid-state microwave generators. *Molecules* **2022**, *27*, 2712.

(20) Zhang, J.; Zhao, D.; Liu, M.; Li, J. The synthesis and characterization of Ti-MCM-41 by microwave radiation. *Adv. Mater. Res*. **2012**, *557–559*, 1411–1414.

(21) Díaz de Greñu, B.; De los Reyes, R.; Costero, A.M.; Amorós, P.; Ros-Lis, J.V. Recent progress of microwave-assisted synthesis of silica materials *Nanomater* **2020**, *10*, 1092.

(22) Zhou, X.; Pedrow, P.D.; Tang, Z.; Bohnet, S.; Sablani, S.S.; Tang, J. Heating performance of microwave ovens powered by magnetron and solid-state generators. *Innov. Food Sci. Emerg. Technol*. **2023**, *83*, 103240.

(23) Dąbrowska, S.; Chudoba, T.; Wojnarowicz, J.; Łojkowski, W. Current trends in the development of microwave reactors for the synthesis of nanomaterials in laboratories and industries: a review. *Crystals* **2018**, *8,* 379.

(24) Horikoshi, S.; Watanabe, T.; Narita, A.; Suzuki, Y.; Serpone, N. The electromagnetic wave energy effect(s) in microwave-assisted organic synthesis (MAOS). *Sci. Rep*. **2018**, *8,* 5151.

(25) Díaz de Greñu, B.; Muñoz-Pina, S.; De los Reyes, R.; Benítez, M.; El Haskouri, J.; Amorós, P.; Ros-Lis, J.V. Fast microwave-assisted synthesis, calcination and functionalization of a silica mesoporous nanomaterial: UVM-7. *ChemSusChem* **2023**, *16*, e202300123.

(26) Benítez, M.; Rodríguez-Carrillo, C.; Sánchez-Artero, S.; El Haskouri, J.; Amorós, P.; Ros-Lis, J.V. Scaled-up microwave-assisted batch and flow synthesis and life cycle assessment of a silica mesoporous material: UVM-7. *Green Chem*. **2023**, *26*, 785–793.

(27) Garrido, M.D.; García-Llacer, C.; El Haskouri, J.; Marcos, M.D.; Sánchez-Royo, J.F.; Beltrán, A.; Amorós, P. Atrane complexes chemistry as a tool for obtaining trimodal UVM-7-like porous silica. *J. Coord. Chem.* **2018**, *71*, 776–785.

(28) Tauc, J.; Menth, A.; Wood, D.L. Optical and magnetic investigations of the localized states in semiconducting glasses. *Phys. Rev. Lett*. **1970**, *25*, 749–752.

(29) Matts, P.J.; Alard, V.; Brown, M.W.; Ferrero, L.; Gers-Barlag, H.; Issachar, N.; Moyal, D.; Wolber, R. The COLIPA in vitro UVA method: a standard and

reproducible measure of sunscreen UVA protection. *Int. J. Cosmet. Sci*. **2010**, *32*, 35–46.

(30) Food and Drug Administration, Labeling and effectiveness testing: sunscreen drug products for over-the-counter human use - small entity compliance guide. **2012**. (Accessed 11 April 2024).

(31) Faraca, G.; Vidal-Abarca Garrido, C.; Kaps, R.; Fernández Carretero, A.; Wolf, O.; Morera, D.; Bastos, J.; Riera, M.R.; Escamilla, M.; Escudero, R. Revision of the EU ecolabel criterio for cosmetic products and animal care products (previously rinse-off cosmetic products). **2021**. ISBN 978-92-76-41078-2.

(32) El Haskouri, J.; Morales, J.M.; Ortiz de Zárate, D.; Fernández, L.; Latorre, J.; Guillem, C.; Beltrán, A.; Beltrán, D.; Amorós, P. Nanoparticulated silicas with bimodal porosity: Chemical control of the pore sizes. *Inorg. Chem*. **2008**, *47*, 8267–8277.

(33) El Haskouri, J.; Ortiz de Zárate, D.; Pérez-Pla, F.; Cevilla, A.; Guillem, C.; Latorre, J.; Marcos, M.D.; Beltrán, A.; Beltrán, D.; Amorós, P. Improving epoxide production using Ti-UVM-7 porous nanosized catalysts. *New J. Chem.* **2002**, *26*, 1093–1095.

(34) Iller, R.K. The Chemistry of Silica: Solubility, Polymerization, Colloid and Surface Properties, and Biochemistry, John Wiley & Sons, New York, **1979**.

(35) Schmidt, J.; Vogelsberger, W. Aqueous long-term solubility of titania nanoparticles and titanium (IV) hydrolysis in a sodium chloride system studied by adsorptive stripping voltammetry. *J. Solution Chem*. **2009**, *38*, 1267–1282.

(36) Ortiz De Zárate, D.; Gómez-Moratalla, A.; Guillem, C.; Beltrán, A.; Latorre, J.; Beltrán, D.; Amorós, P. High-zirconium-content nano-sized bimodal mesoporous silicas. *Eur. J. Inorg. Chem*. **2006**, *2006*, 2572–2581.

(37) Garrido, M.D.; Puchol, N.; El Haskouri, J.; Sánchez-Royo, J.F.; Folgado, J.V.; Gonzalez Marrachelli, V.; Pérez Terol, I.; Ros-Lis, J.V.; Marcos, M.D.; Ruíz, R.; Beltrán, A.; Morales, J.M.; Amorós, P. High content and dispersion of Gd in bimodal porous silica: T2 contrast agents under ultra-high magnetic fields. *Microporous Mesoporous Mat.* **2022**, *336*, 111863.

(38) Dubey, R.S.; Rajesh, Y.B.R.D.; More, M.A. Synthesis and characterization of SiO_2 nanoparticles via sol-gel method for industrial applications. *Mater. Today: Proc*. **2015**, *2*, 3575–3579.

(39) Spallino, L.; Vaccaro, L.; Sciortino, L.; Agnello, S.; Buscarino, G.; Cannas, M.; Gelardi, F.M. Visible-ultraviolet vibronic emisión of silica nanoparticles. *Phys. Chem. Chem. Phys.* **2014**, *16*, 22028–22034.

(40) El Haskouri, J.; Cabrera, S.; Gutierrez, M.; Beltrán-Porter, A.; Beltrán-Porter, D.; Marcos, M.D..; Amorós, P. Very high titanium content mesoporous silicas. *Chem. Comm.* **2001**, *4*, 309–310.

(41) Itoh, M.; Hattori, H.; Tanabe, K. The acidic properties of TiO_2-SiO_2 and its catalytic activities for the amination of phenol, the hydration of ethylene and the isomerization of butene. *J. Catal*. **1974**, *35*, 225–231.

(42) Sayari, A. Catalysis by crystalline mesoporous molecular sieves. *Chem. Mater*. **1996**, *8*, 1840–1852.

(43) Petrini, G.; Cesana, A.; De Alberti, G.; Genoni, F.; Leofanti, G.; Padovan, M.; Paparatto, G.; Rofia, P. Deactivation phenomena on Ti-silicalite. *Stud. Surf. Sci. Catal.* **1991**, *68*, 761–766.

(44) Anpo, M.; Nakaya, H.; Kodama, S.; Kubokawa, Y. Photocatalysis over binary metal oxides. Enhancement of the photocatalytic activity of titanium dioxide in titanium-silicon oxides. *J. Phys. Chem*. **1986**, *90*, 1633–1636.

(45) Erdem, B.; Hunsicker, R.A.; Simmons, G.W.; Sudol, E.D.; Dimonie, V.L.; El-Aasser, M.S. XPS and FTIR surface characterization of TiO_2 particles used in polymer encapsulation. *Lagmuir* **2001**, *17*, 2664–2669.

(46) Gaultois, M.W.; Grosvenor, A.P. XANES and XPS investigations of (TiO_2) x (SiO_2) 1-x: the contribution of final-state relaxation to shifts in absorption and binding energies. *J. Mater. Chem*. **2011**, *21*, 1829–1836.

(47) Arellano, U.; Wang, J.A.; Chen, L.F.; Asomoza, M.; Guzmán, A.; Solís, S.; Estrella, A.; Cipagauta, S.; Noreña, L.E. Transition metal oxides disperse don Ti-MCM-41 hybrid core-shell catalysts for the photocatalytic degradation of Congo red colorant. *Catal. Today* **2020**, *349*, 128–140.

(48) Yakin, F.E.; Barisik, M.; Sen, T. Pore size and porosity dependent zeta potentials of mesoporous silica nanoparticles. *J. Phys. Chem. C* **2020**, *124*, 19579–19587.

(49) Itoh, M.; Hattori, H.; Tanabe, K. The acidic properties of TiO_2-SiO_2 and its catalytic activities for the amination of phenol, the hydration of ethylene and the isomerization of butene. *J. Catal*. **1974**, *35*, 225–231.

(50) Ghamarpoor, R.; Fallah, A.; Jamshidi, M. Investigating the use of titanium dioxide (TiO_2) nanoparticles on the amount of protection against UV irradiation. *Sci. Rep.* **2023**, *12*, 9793.

(51) Ura, S.; Nakashiba, T.; Suhara, T.; Nishihara, H.; Lambeck, P.V. Thermally-grown silicon-dioxide waveguides for use in UV light. *Jpn. J. Appl. Phys*. **2000**, *39*, 1487–1489.

(52) Li, C.C.; Chen, Y.T.; Lin, Y.T.; Sie, S.F.; Chen-Yang, Y.W. Mesoporous silica aerogel as a drug carrier for the enhancement of the sunscreen ability of benzophenone-3. *Colloids Surf. B Biointerfaces* **2014**, *115*, 191–196.

(53) Chen-Yang, Y.W.; Chen, Y.T.; Li, C.C.; Yu, H.C.; Chuang, Y.C.; Su, J.H.; Lin, Y.T. Preparation of UV-filter encapsulated mesoporous silica with high sunscreen ability. *Mater. Lett*. **2011**, *65*, 1060–1062.

(54) Barbosa, J.S.; Neto, D.M.A.; Freire, R.M.; Rocha, J.S.; Fechine, L.M.U.D.; Denardin, J.C.; Valentini, A.; De Araújo, T.G.; Mazzetto, S.E.; Fechine, P.B.A. Ultrafast sonochemistry-based approach to coat TiO_2 commercial particles for sunscreen formulation. *Ultrason. Sonochem*. **2018**, *48*, 340–348.

(55) Da Silva Marcelino, P.; Miliani Martinez, R.; Máximo Daneluti, A.L.; Morocho-Jácome, A.L.; Lima Solino Pessoa, F.V.; Rijo, P.; Rosado, C.; Robles Velasco, M.V.; Rolim Baby, A. In vitro photoprotection and functional photostability of sunscreen lipsticks containing inorganic active compounds. *Cosmetics* **2023**, *10*, 46.

(56) Department of Health and Human Services. Food and Drug Administration. 21 CFR Parts 201, 310, 347 and 352 [Docket No. 1978N-0038] (formerly Docket No. 78N- 0038) RIN 0910-AF43, **2019**, *84*, 6204-6275.

Solid-state microwave assisted batch and flow synthesis, and life cycle assessment of titanium containing UVM-7 mesoporous silica

SUPPLEMENTARY INFORMATION

Cristina Rodríguez-Carrillo[1], Miriam Benítez[1], Marta González-Fernández[1], Ruth de los Reyes[2], Sonia Murcia[3], Jamal El Haskouri[3], Pedro Amorós[3] and Jose V. Ros-Lis[1,*]

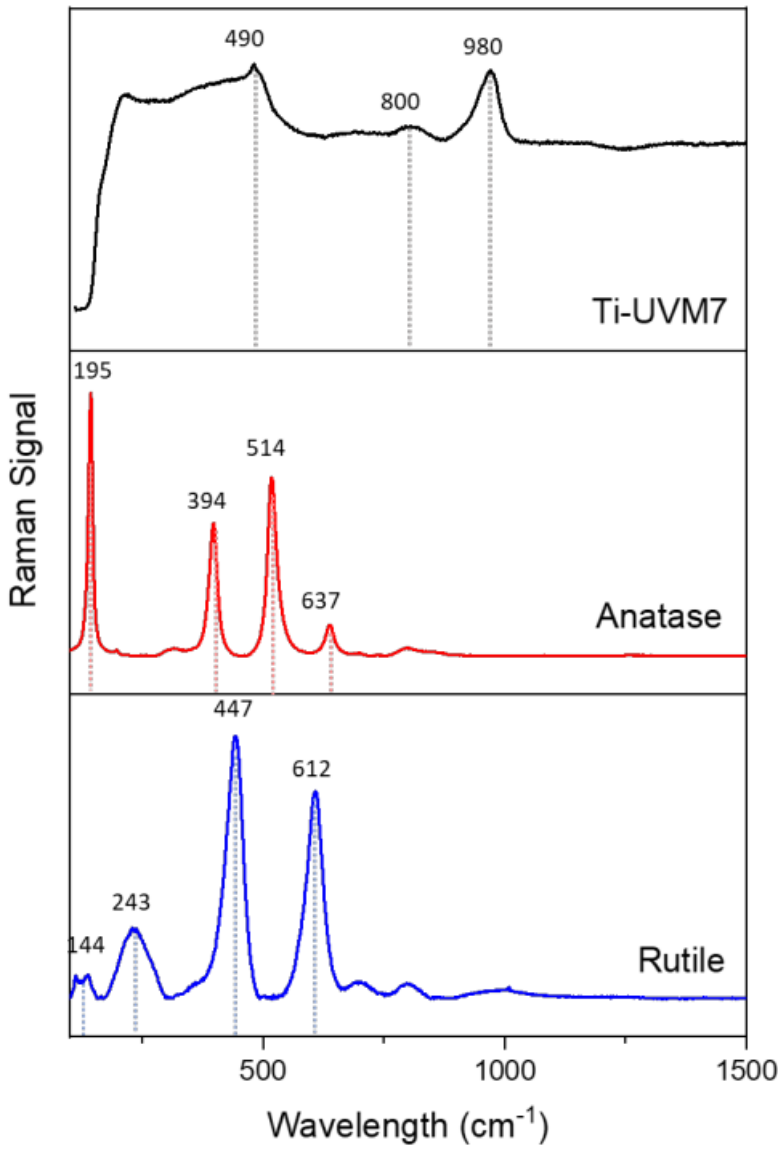

Figure S1. *Raman spectra of a representative sample (sample 1), rutile and anatase*

Table S1. *Degree of significance of the linear fitting of the physical data for Ti-UVM-7 material*

Parameter	Si/Ti theorical	Power	Time
Si/Ti measured	<0.001*	0.060*	0.001*
SBET	0.018*	0.135	0.187
Mesoporous diameter	0.023*	0.119	0.016*
Textural pore diameter	0.242	0.521	0.239
Mesoporous volume	0.070*	0.167	0.077*
Textural pore volume	0.058*	0.261	0.008*
Zeta potential	0.564	0.363	0.645
2θ	0.394	0.875	0.105
d100	0.382	0.813	0.105
a0	0.368	0.821	0.103
Wall thickness	0.057*	0.393	0.008*

***Table S2**. Life Cycle Inventory for the preparation of 1 kg of material.*

Process	*Unit*	*Non scaled*	*Scaled batch*	*Scaled flow*	*Cream*
Tetraethyl orthosilicate	kg	26.9	9.9	9.9	2.5
Triethanolamine	kg	70.3	25.9	25.9	6.5
Eterquat	kg	12.7	4.7	4.7	1.2
Water, deionized	kg	489	67	67	0.16
Ethanol, 95%	kg	322	70	70	17.5
Titanium butoxide	kg	1.8	0.65	0.65	0.17
Electricity	kWh	18068	203	216	51
Glicerine	kg	0	0	0	0.023
Fatty alcohol	kg	0	0	0	0.045
Fatty acid	kg	0	0	0	0.053
Ethylene carbonate	kg	0	0	0	0.068
Fatty alcohol sulfate	kg	0	0	0	0.011
Benzyl alcohol	kg	0	0	0	0.006
Water, decarbonised	kg	0	0	0	0.51

Flow and batch minute-made synthesis of Ce-UVM-7 using microwave-assisted reaction: scaling-up, optical and catalytic applications, and impact assessment

Cristina Rodríguez-Carrillo[1], Miriam Benítez[1], Ruth de los Reyes[2], Jamal El Haskouri[3], Pedro Amorós[3] and Jose V. Ros-Lis[1,*]

[1]Departamento de Química Inorgánica, Universitat de València, Doctor Moliner 50, P.O. Box 73, 46100 Butjassot, Spain

[2]Microbiotech. S.L. Villamarxant, 46191, Spain

[3]Institut de Ciència dels Materials, Universitat de València, P.O. Box 22085, 46071 Valencia, Spain

*Correspondence: j.vicente.ros@uv.es; Tel.: +34-963544856

ACS Sustainable Chem. Eng. **2024**, *12*, 13208–13219

DOI: 10.1021/acssuschemeng.4c03974

Received: 14th May 2024, Accepted: 12th August 2024

Published: 18th August 2024

Abstract

This study introduces the first synthesis of a cerium-containing UVM-7 material, a bimodal mesoporous silica material. It was prepared swiftly using microwave-assisted synthesis powered by solid-state generators in combination with the atrane route. This synthesis process has been meticulously optimized and scaled-up in batch form. We also developed a flow synthesis procedure for Ce-UVM-7. These materials exhibit homogeneous Ce distribution within the UVM-7 silica structure with a Si/Ce ratio of up to 15. The scaled-up synthesis process allows the preparation of 35 g of Ce-UVM-7 in just 10 min of irradiation, with batch and flow synthesis methods achieving a yield of 11 g h^{-1}. We studied the optical properties, sun protection factor (SPF), and ROS scavenging properties of the resulting materials. The results show that the band gap decreases as the cerium concentration increases, reaching only 3.15 eV for the most concentrated sample and a high SPF. The peroxidase activity of materials prepared with a Si/Ce ratio of 25 is higher than that found for pure CeOx. Life cycle assessment confirms a significant reduction in the environmental impact during the scale-up process, with values of approximately 8 points in the single score for the preparation of 1 kg of Ce-UVM-7, further highlighting the efficiency and sustainability of this novel synthesis method.

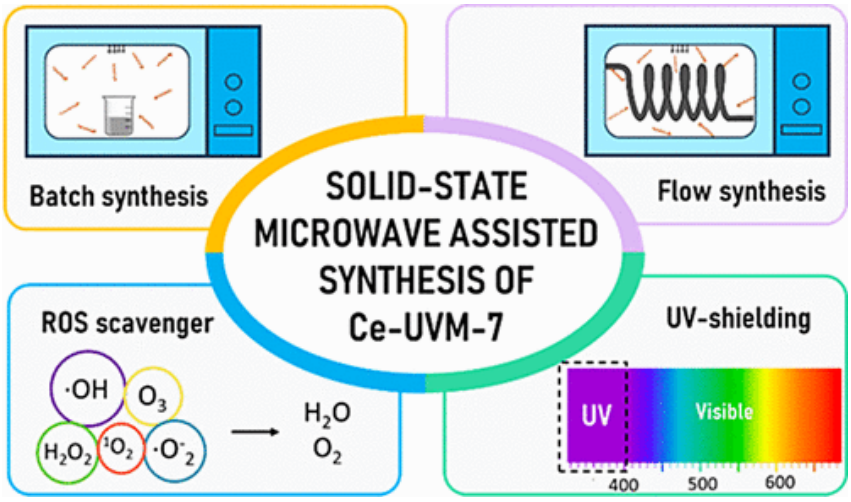

Synopsis

Microwave-assisted synthesis yields a mesoporous silica UVM-7 with UV absorption properties, while minimizing environmental impact through the process optimization.

Keywords: microwave-assisted synthesis, cerium, mesoporous silica, scale-up, flow synthesis, LCA, sunscreen.

1. INTRODUCTION

In recent years, the field of materials science has witnessed a rush in the exploration and development of advanced catalysts with superior performance and tailored functionalities.[1] Among these, mesoporous silica-based materials have emerged as versatile candidates for a wide range of applications owing to their exceptional surface area, tunable pore size, and excellent thermal stability. Incorporating additional metal or metal oxide components into mesoporous silica matrices can further enhance their catalytic properties, opening new possibilities for diverse industrial processes.[2]

The original mesoporous silica material, MCM-41, was first synthesized in 1992. It features a hexagonal two-dimensional structure, cylindrical pore geometry, and mesopore diameters ranging from 2 to 10 nm.[3] As an evolution, UVM-7 type has garnered considerable attention due to their distinctive bimodal porous structure, with mesopores and textural large pores interspersed among particles, thereby enhancing their utility and applicability.[4] One of the advantages of silica is its capacity to incorporate other elements in their structure. A relevant combination is the integration of mesoporous silica with ceria (CeO_2), a well-known rare-earth metal oxide with remarkable redox properties.[5] Cerium can exist in both Ce^{3+} and Ce^{4+} oxidation states, leading to compounds such as cerium dioxide (CeO_2) and cerium sesquioxide (Ce_2O_3).[6] These compositional and structural variations of cerium have significant implications for its properties and applications to neutralize some reactive oxygen species (ROS).[7]

The introduction of ceria into mesoporous silica matrices provides a synergistic effect, enabling enhanced catalytic performance through its oxygen storage and release capacity, high oxygen mobility, and strong oxygen activation capability.[5] Different methods for synthesizing ceria-silica mixed materials are described in the literature. The most commonly employed method is the hydrothermal or sol–gel process, followed by template removal through calcination.[8] Following this method CeO_2-silica,[9] Ce-MCM-41,[10] Ce-MCM-48,[11] Ce-SBA-15,[12] among others, have been reported. However, Ce-doped UVM-7 had not been reported previously. A suitable method for the synthesis of doped silicas is the "atrane route", wherein the inorganic precursor is an atrane complex. This complex exhibits inertness toward hydrolysis, allowing the regulation of rates of hydrolysis and condensation despite the different reactivities between heteroatoms.[13]

The conventional methods used for synthesizing mesoporous silica-based catalysts often involve time-consuming procedures, high energy consumption, and limited control over the structural parameters, which can hinder the precise tuning of their properties for specific applications.[14] Lately, the utilization of microwave solid-state generators has emerged as a promising alternative for the synthesis of various materials, including mesoporous silica-based catalysts.[15] There are different types of microwave generators, including electric vacuum devices like magnetron, commonly used in domestic microwave ovens; Klystron, used in radar and satellite communication; and Traveling-Wave Tube, capable of amplifying a wide range of frequencies with high power. Each type of microwave generator has specific characteristics and applications depending on its design and operational principles.[16] Like other

MW sources, solid-state microwave generators, also known as semiconductor generators, offer several advantages in synthesis procedures such as rapid heating rates, homogeneous energy distribution, and precise control over reaction conditions, enabling the fabrication of materials with improved characteristics, including enhanced crystallinity, reduced particle size, and better porosity.[17] This innovative approach has shown great potential for producing highly efficient catalysts with improved catalytic activity, selectivity, and stability.[18] Additionally, solid-state microwave generators show some additional advantages derived from the accurate potency control.[17]

In 2022, the synthesis of CeO_2 using solid-state microwave generators was reported, accomplished in just 30 s at 200 W, employing both batch and flow procedures.[5] Furthermore, successful synthesis of UVM-7 has been achieved using this type of generators,[19] not only in a conventional batch system but also its scaling-up and adaptation for synthesis in a continuous flow process.[20] The ability to achieve an efficient and scalable synthesis of UVM-7 under flow conditions represents a significant advancement in the production of high-quality mesoporous materials. One year later, a Ce-MCM-41 composite was successfully achieved utilizing a combination of microwave and ultrasound methods, with a microwave irradiation time of 60 min.[21] To the best of our knowledge, no other reports have been found regarding the microwave-assisted synthesis of ceria-modified mesoporous silica.

Thus, we hypothesize that solid-state-based microwave-assisted synthesis in combination with the atrane route can be an interesting approach toward a fast, scalable, and sustainable synthesis of mixed silica mesoporous materials, in particular cerium containing ones, such as Ce-UVM-7. The resulting

materials would be homogeneous, with high Ce content and solar shielding and ROS scavenging properties.

2. EXPERIMENTAL SECTION

2.1. Chemicals

All synthesis reagents employed in this study were of analytical purity and were used without additional purification steps. Tetraethyl orthosilicate 98% (GC) (TEOS), triethanolamine ≥99.0% (GC) ($TEAH_3$), hexadecyltrimethylammonium bromide ≥98.0% (CTABr), and cerium(III) chloride heptahydrate 99.9% ($CeCl_3 \cdot 7H_2O$) for synthesis were procured from Sigma-Aldrich (Madrid, Spain). To determine peroxidase activity, hydrogen peroxide (H_2O_2) 35% was procured from Panreac and 3,3',5,5'-tetramethylbenzidine (TMB) from Sigma-Aldrich (St. Louis, MO, USA). Ethanol was obtained from the VWR, and the water employed in this research was deionized. For the optical properties, poly(methyl methacrylate) PMMA plates were used.

2.2. Microwave Devices

Three different solid-state-based microwave devices were used. In all of them, the frequency of each source can be independently adjusted to fine-tune the system and optimize absorbed power within the 2420–2480 MHz range, in 1 Hz increments, while maintaining phases within the 0–360° range. The sources were connected to the irradiation cavity through coaxial cables. For initial evaluation of the synthesis conditions, an equipment with one microwave source and maximum power of 200 W, selectable in 1 W increments, equipped with a microstrip patch antenna was used. The batch

scale-up device comprises four microwave sources. Each source can operate at a maximum power of 200 W, with selectable potency in 1 W increments, reaching a cumulative maximum power of 800 W. Each source irradiates independently inside the cavity through a rod type antenna. The flow synthesis was implemented in an equipment with one microwave source and maximum power of 200 W, selectable in 5 W increments, equipped with a rod type antenna, two peristaltic pumps, and a hosepipe for the dissolution movement.

2.3. Synthesis of the Ce-UVM-7 Nanomaterials

The synthesis of Ce-UVM-7 was carried out following the atrane route.[4] The study involved tests with different Si/Ce molar ratios to evaluate the degree of cerium integration within the mesoporous material. The atrane mixture was prepared with molar ratios of 2–x TEOS/7 $TEAH_3$/x $CeCl_3{\cdot}7H_2O$/0.52 CTABr. The Si/Ce molar ratios, power, and reaction time are summarized in Table 1. As an illustrative example, for the material with a Si/Ce molar ratio of 25, 11 mL of TEOS, 23 mL of $TEAH_3$, 0.7 g of $CeCl_3{\cdot}7H_2O$, and 4.7 g of CTABr were processed following the standard procedure.[4] 4.12 mL of this solution containing the atrane mixture and the template agent was combined with 10 mL of deionized water in a microwave glass. The vial was then placed into a microwave oven cavity and subjected to microwave irradiation, with a yellow precipitate. The synthesis procedure is represented in Scheme 1. It was subsequently separated by filtration, washed with water and ethanol, and dried in an oven at 80°C overnight. The resulting material was calcined at 550°C for 6 h in a conventional furnace to obtain the Ce-UVM-7 mesoporous material.

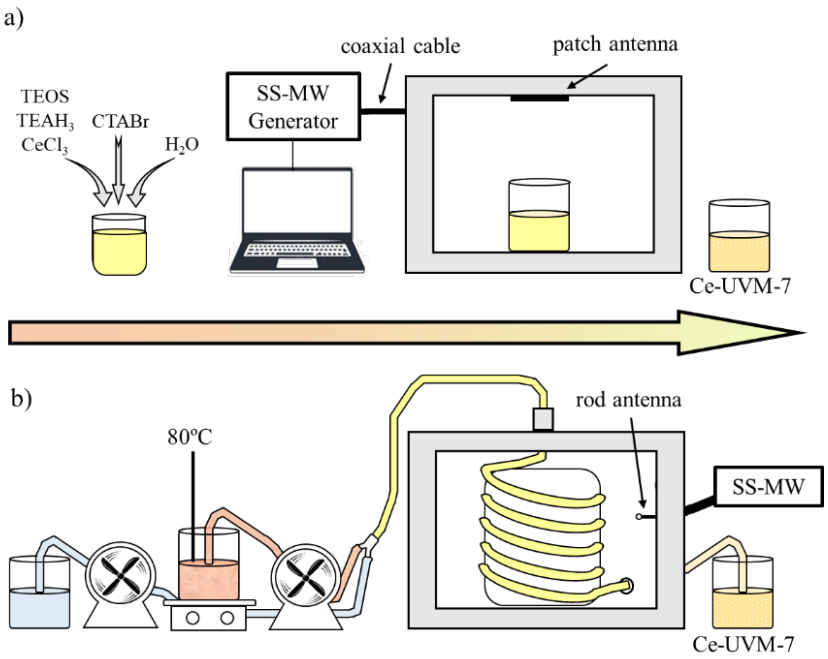

***Schema 1**: Synthesis procedures a) in batch and b) flow. In blue it is represented Milli-Q water, orange represents the atrane, and yellow represents the mixture of Milli-Q water and atrane.*

To implement the scale-up procedures of the material with a Si/Ce ratio of 25, we followed a previously reported procedure for the synthesis of pure silica UVM-7 with some modifications.[20] 1 L of Milli-Q water was added to an atrane mixture prepared with 132 mL of TEOS, 263 mL of $TEAH_3$, 8.8 g of $CeCl_3 \cdot 7H_2O$, and 45 g of CTABr. Subsequently, the mixture underwent irradiation for 10 min at 800 W until a gel was formed. The material is filtered, washed with water and ethanol, dried at 80°C overnight, and calcinated at 550°C, following the previously outlined procedure. This procedure was done with (Sample S2) and without stirring (Sample S1).

For the flow synthesis, 10.6 mL of TEOS, 22.8 mL of $TEAH_3$, 0.71 g of $CeCl_3{\cdot}7H_2O$, and 4.68 g of CTABr were used to prepare the atrane mixture. The reagents were mixed before the introduction in the microwave oven using two peristaltic pumps, as represented in Scheme 1. One pump was connected to the atrane mixture, while the other one was connected to 80 mL of H_2O. The peristaltic pumps were calibrated to ensure an appropriate mixture of atrane and water before entering the microwave cavity, with adjustments set at 5 and 12 rpm for the atrane solution and water, respectively. Subsequently, the formed precipitate was washed using water and ethanol, followed by drying at 80°C and calcination at 550°C, as previously described.

2.4. Characterization of the Materials

The powder X-ray diffraction pattern of the materials was obtained by using a powder X-ray Diffractometer D8 Advance A25 Bruker Corporation. The sample was scanned over the required range for 2θ values (1–80°). To confirm the mesoporous nature, nitrogen adsorption–desorption isotherms were recorded in an automated Micromeritics ASAP2010 instrument. Prior to the adsorption measurements, the samples were outgassed in situ in vacuum (10^{-6} Torr) at 110°C for 15 h to remove adsorbed gases. The specific surface area was determined by applying the Brunauer–Emmett–Teller (BET model) model from the adsorption data within the low-pressure range. Pore volume was calculated following the Barrett–Joyner–Halenda model (BJH). Transmission electron microscopy (TEM) microstructural characterization was carried out using a JEOL Jem 1010 instrument operating at 80 kV. A Field Emission Scanning Electron Microscope (FESEM) SCIOS 2 was utilized to conduct EDX microanalysis, which enabled the composition and purity of

samples to be investigated. The UV/visible spectrum was obtained by using a PerkinElmer Lambda 35 spectrophotometer equipped with an integrating sphere. The peroxidase activity and UV–shielding capacity were quantified by using a Jasco V-770 instrument.

2.5. Determination of the Optical Properties

The Kubelka–Munk function and the Tauc plot method (see eq 1) were used to measure the band gap energy (Eg), where C is a constant, h is Planck's constant, v is the frequency of vibration, and α is the absorption coefficient.[22] Representing the plot of $(hvf(R))^2$ vs photon energy (hv), where (f(R)) is the absorbance, the band gap energies can be calculated.

$$\propto (hv) = \frac{C(hv - E_g)^{\propto/2}}{hv} \quad (1)$$

The UV-shielding capacity was measured following the procedure defined by the European Cosmetic and Perfumery Association (COLIPA).[23] Ce-UVM-7 (Sample B9) was mixed with a non-UV absorbing cream until a homogeneous paste is obtained similar to the texture of sunscreens. Then, it was applied onto the rough surface of a poly(methyl methacrylate) (PMMA) plate using a gloved finger to ensure uniform distribution, followed by compressed air for one min to eliminate any free particles. According to the Food and Drug Administration (FDA), PMMA plates are recommended because of their transparency to ultraviolet (UV) radiation, nonfluorescence, resistance to light-induced degradation, and inertness toward sunscreen constituents.[24] Subsequently, the plate was placed in dark conditions for 15 min to ensure a proper adaptation and stabilization of the sample. Finally, 10 measures of the

UV transmittance in the 290–400 nm range were obtained. Data were further analyzed to determine the Solar Protection Factor (SPF).

The Solar Protection Factor (SPF) was calculated using eq 2, where E(λ) is the erythema action spectrum, I(λ) is the solar radiation intensity, and T(λ) is the transmission at a specific wavelength.[25,26]

$$SPF = \frac{\int_{290}^{400} E(\lambda) \cdot I(\lambda) \cdot d\lambda}{\int_{290}^{400} E(\lambda) \cdot I(\lambda) \cdot T(\lambda) d\lambda} \quad (2)$$

2.6. Determination of the Peroxidase Activity

The assessment of peroxidase activity involved the amalgamation of Ce-UVM-7 material (Sample B9), H_2O_2, and TMB, with subsequent quantification of the resultant color change in the UV/visible absorption spectrum according to Cao's established methodology.[27] In summary, 70 µL of 1.0 mg/mL Ce-UVM-7 material was introduced into 400 µL of 50.0 mM phosphate buffer (pH = 4.0) at ambient temperature. This was followed by the addition of 100 µL of 8.0 mM TMB, 100 µL of 25.0 mM H_2O_2, and 330 µL of Milli-Q water. A blank was also prepared by combining all of the reagents except for the Ce-UVM-7 sample. Then, the reaction mixtures were incubated at room temperature for 7 min. Afterward, UV–vis absorption at 652 nm was quantified using a Jasco V-770 spectrophotometer. The reaction rate was determined by subtracting the absorbance of the material from the absorbance of the blank.

2.7. Data Analysis and Life Cycle Assessment

The data analysis was performed using IBM SPSS software version 28.0.1.1. Life cycle assessment (ISO 14040:2006) on a cradle to gate basis was applied

to the scaled processes. The inventory was defined using the synthesis procedures, and the energy consumption was measured in the laboratory. The impact was calculated using the Ecoinvent 3 database and the ReCiPe 2016 End point (H) V1.08/World (2010) H/A model available in the SimaPro software. If available, data from Spain or Europe have been used. The method includes as impact categories global warming, stratospheric ozone depletion, ionizing radiation, ozone formation (human health), fine particulate matter formation, ozone formation (terrestrial ecosystems), terrestrial acidification, freshwater eutrophication, marine eutrophication, terrestrial ecotoxicity, freshwater ecotoxicity, marine ecotoxicity, human carcinogenic toxicity, human noncarcinogenic toxicity, land use, mineral resource scarcity, fossil resource scarcity, and water consumption. CTABr is not available in the database; thus, esterquat (a cationic surfactant) was used for the analysis. Cerium oxide was used instead of cerium chloride. The sunscreen was calculated following the composition detailed by the Joint Research Centre (JRC), the European Commission's science and knowledge service.[28]

3. RESULTS AND DISCUSSION

3.1. Batch Synthesis of Ce-UVM-7

The preparation of homogeneous mixed silica materials (containing an element other than oxygen in addition to silicon) is a chemically complex process. It requires that the hydrolysis and condensation rates involved in the sol–gel process are similar for both elements; otherwise, phase segregation occurs. In this sense, the atrane pathway is an excellent synthesis route for obtaining homogeneous mixed silicas with a wide variety of elements with

high heteroelement concentrations.[13] A cationic surfactant (CTABr) is used as a pore generator. The preparation of the mixture containing TEOS, $CeCl_3 \cdot 7H_2O$, and $TEAH_3$, following heating, results in the formation of a homogeneous mixture of atrane complexes of Si and Ce. In the case of Si, silatranes are formed, with $Si(TEA)_2H_2$ being the majority complex.[13] The formation of Ce atrane complexes has been described in the literature.[29] In nonaqueous solution, the presence of 1Ce:1$TEAH_3$ complexes has been detected.[30] The authors propose that as in the case of silatrane, $TEAH_3$ acts as a tridentate tripod chelate ligand. The ratio (Si + Ce):$TEAH_3$= 2:7, which was used in our synthesis, is more than sufficient to stabilize the corresponding atrane complexes and provide a moderately basic pH when incorporating water into the reaction mixture. Although the Ce source is a salt containing Ce(III), heat treatment at relatively low temperatures leads to the heteroelement to Ce(IV) by the dissolved oxygen during the synthesis.[30,31] The redox potentials of both species are $E(Ce^{4+}/Ce^{3+})$ = 1.68–0.237 pH (v) and $E(O_2/H_2O)$ = 1.23–0.059 pH (v). Consequently, Ce(III) can be oxidized to Ce(IV) at a pH of approximately neutrality, and the basic medium provided by $TEAH_3$ would facilitate this oxidation process. Furthermore, the formation of the Ce(IV)-$TEAH_3$ complex may facilitate the oxidation process, as the Ce(IV)-TEA complex exhibits greater stability than the Ce(III)-$TEAH_3$ complex. This is attributed to the higher positive charge and stronger Lewis acidity of Ce(IV) in comparison to Ce(III).[30]

The addition of water to the solution containing the mixture of atrane complexes and surfactants, followed by thermal treatment, allows the preparation of the mesostructured material. In our case, with the objective of

obtaining a fast and more sustainable procedure for the preparation of a porous silica mixed material with high concentrations of cerium, we opted for microwave-assisted synthesis as it is a much faster and more scalable approach.[20] The goal was to prepare a mesoporous silica material with a high cerium content. As a microwave source, we have used solid-state generators, as they allow continuous irradiation with precise control of power and frequency.

For the optimization in batch, the influence of different key synthesis variables was first tested: the Si/Ce ratio (25 and 8), power, and time. A list of the synthesis conditions and main characteristics of the materials obtained can be found in Table 1. As expected, the temperature is proportional (R^2 = 0.83) to the energy supplied to the system, calculated as the product of the power X irradiate ion time. There are small variations that may be due to the existence of hot and cold spots in the microwave cavity along with small displacements in the reactor position, and the loss of energy from the hot solution to the cold air of the reactor. At first glance, it can be seen that the Si/Ce ratio is a key aspect for the determination of the properties of the final material (Table 1).

Table 1. *Summary of synthesis conditions and characterization of samples. [a]Nominal molar ratio, [b]Molar ratio determined by EDX, [c]The cell parameter calculated by* $a_0 = 2d100 \cdot (\sqrt{3})^{-1}$, *being d the distance between planes of the hkl 100, [d]Wall thickness was calculated by* $d_w = a_o - d_p$, *where* d_p *is the pore diameter.*

Sample	Si/Ce		Power (W)	Time (min)	Mesopore		Large-mesopore		S BET (m^2g^{-1})	2θ (°)	a_0[c] (nm)	dw[d] (nm)
	Nom[a]	Real[b]			Size (nm)	Volume (cm^3g^{-1})	Size (nm)	Volume (cm^3g^{-1})				
B1	8	7.86	200	1	-	-	-	-	380	-	-	-
B2	8	6.87	200	0.5	-	-	-	-	389	-	-	-
B3	8	8.31	100	2	-	-	-	-	358	-	-	-
B4	8	6.93	100	1	-	-	-	-	364	-	-	-
B5	8	5.46	100	0.5	-	-	-	-	435	-	-	-
B6	8	8.04	50	2	-	-	-	-	366	-	-	-
B7	25	13.2	200	1	2.9	0.54	24.8	0.50	674	1.94	5.3	2.4
B8	25	15.3	200	0.5	2.9	0.62	28.1	0.46	771	1.92	5.3	2.4
B9	25	17.5	100	2	2.8	0.58	22.2	0.31	721	1.98	5.1	2.3
B10	25	17.6	100	1	2.9	0.60	24.7	0.35	738	2.00	5.1	2.2
B11	25	17.0	100	0.5	2.9	0.64	23.8	0.27	772	1.96	5.2	2.3
B12	25	17.2	50	2	2.8	0.64	23.2	0.25	778	1.94	5.3	2.4

In the TEM images (Figure 1, inset) corresponding to Si/Ce ratios of 25, the structure of UVM-7 is clearly observed, consistent with porous particles of approximately 40 nm that aggregate to form larger textural pores. By contrast, the images associated with the rich-Ce sample (Si/Ce = 8), and the characteristic morphology of UVM-7 is not evident. The material appears to be an aggregate of very small particles, with no typical spots visible due to the mesopores generated by the surfactant micelles. As a result, its specific surface area would be likely lower than that of a UVM-7 solid.

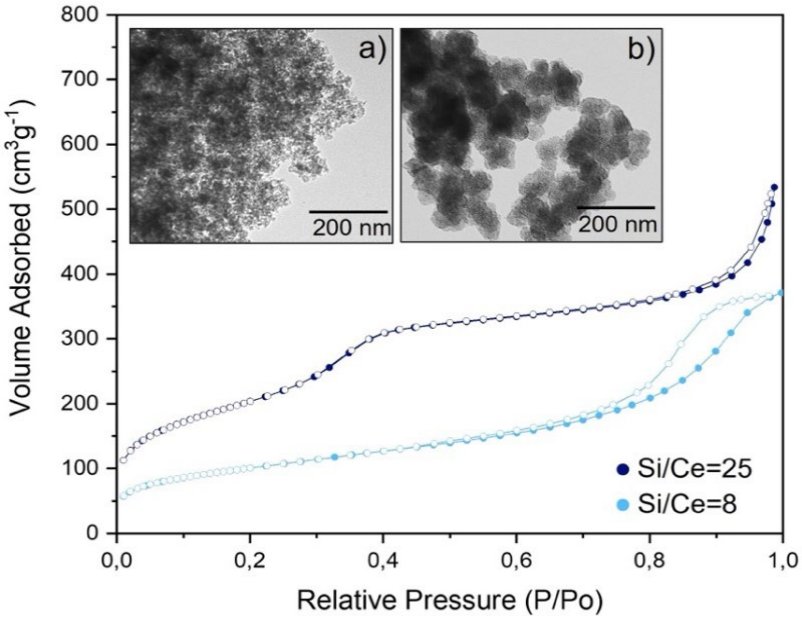

***Figure 1**. N_2 adsorption-desorption isotherm and TEM images for a) sample with molar ratio of Si/Ce of 8 and b) molar ratio of Si/Ce of 25.*

This difference in the morphology was also confirmed by N_2 gas adsorption. The N_2 adsorption/desorption isotherm can be assigned to type IV adsorption–desorption plots, typical of mesoporous solids. UVM-7 type

materials present two adsorption steps, the first at relative pressures between $0.2 \leq P/P_0 \leq 0.4$ which can be associated with a mesopore system, and the second one at relative high pressures between $0.9 \leq P/P_0 \leq 1.0$ which is due to the filling of the large meso/macropore system (Figure 1). At relatively low concentrations of Ce (Si/Ce = 25), materials with the characteristics of the UVM-7 structure are obtained: large areas, close to 1000 $m^2\ g^{-1}$, with a hierarchical bimodal pore system, and an intense peak in X-ray diffraction around 2° indicating the existence of a certain ordered array of mesopores. By contrast, in materials prepared with the nominal Si/Ce = 8 ratio, the surface area is much lower. The absence of the initial jump in the isotherm is consistent with the lack of surfactant-generated mesopores in samples B1–B6. Furthermore, the increase in the N_2 adsorption–desorption isotherm for relative pressure values between 0.7 and 1 is less abrupt and more gradual than that observed in UVM-7 type solids (Figure 1). This fact together with the hysteresis loop observed at high pressures for the B4 material could be due to the presence of cavities inside the solids, closed by narrow entrances formed by the condensation of the little Si–Ce–O nanoparticles found in these types of materials. The diffraction peak at low angles is not observed for the rich-Ce samples (Si/Ce = 8), suggesting that it would be a disordered mesoporous material with a xerogel-type amorphous architecture. Then, the mesopore size for these samples is intermediate between the small and the large mesopores observed in UVM-7 samples. On the contrary, in samples B7–F6, N_2 adsorption–desorption isotherms with two clear adsorption jumps are recorded. The first adsorption step is due to the mesoporous associated with the CTABr micelles and, consequently, their sizes range between 2.7 and 3.0

nm, and the silica wall thickness is in the range of 2.2–2.5 nm. These findings align with those obtained in a study on the size of the UVM-7 wall, where values of 2.0, 2.4, and 2.8 nm were obtained for UVM-7, UVM-12, and UVM-10, respectively.[32] Additionally, a second jump is observed at high partial pressures due to the textural porosity between the primary mesoporous particles with pore size values in the range 22–34 nm.

Potency, time, and nominal Si/Ce ratio are the main labels explored in this work. Some tendencies can be observed between the experimental conditions (power, time, and energy) and the characteristics of the resulting material (Si/Ce ratio and BET area). An increase in the irradiation time results in a higher S BET, as demonstrated by samples B1–B2, B3–B5, B7–B8, and B9–B11, which were irradiated with the same power but for increasing durations. Furthermore, when the irradiated energy is constant, the S BET values are similar across all of the cases. For instance, samples B2, B4, and B6 exhibit S BET values of 389, 364, and 366 m^2g^{-1}, respectively, which are quite comparable. Similarly, samples B8, B10, and B12 have S BET values of 771, 738, and 772 m^2g^{-1}, respectively. Therefore, the irradiated energy could play a crucial role in the formation of the mesoporous structure. A linear regression model was applied to the data. It was observed that the nominal Si/Ce ratio is highly relevant ($p < 0.001$) for the surface area. If we consider the effect of power and time as independent labels, none of them are significant ($p = 0.09$ and $p = 0.06$); however, if we consider the effect of the energy (potency x time), a significance of $p < 0.001$ is obtained. The area increases as the nominal value grows (less Ce) and decreases if the energy applied grows. If we consider separately the data for Si/Ce 8 and 25, for the former, neither power

(p = 0.38), time (p = 0.10), or energy (p = 0.20) are significant for S BET. For 25, the energy is significant (p = 0.033), Ce loading increases with energy, but there is no significant correlation with power (p = 0.22) or time (p = 0.34) independently.

EDX measurements were used to analyze the sample composition. As indicated in Table 1, the observed ceria content diverges significantly from the nominal values for all solid samples. A consistent trend of cerium enrichment is evident, attributed to the higher solubility of silicon oxide (SiO_2) compared to cerium oxide (CeO_2). Consequently, with a greater dissolution of silica, a lower amount is incorporated into the mesoporous structure, leading to an indirect enrichment in cerium. If we consider a linear regression model, there is a clear correlation between the nominal Si/Ce ratio and the measured value (p < 0.01); however, not a significant correlation can be found between the real Si/Ce ratio and the energy (p = 0.91), potency (p = 0.36), or time (p = 0.39). If we consider samples with nominal Si/Ce of 8 and 25 independently, for the Si/Ce 8, the Ce loading decreases at larger power (p = 0.015) or irradiation time (p = 0.003), but the correlation with the energy has a weaker relationship (p = 0.058). For the Si/Ce=25, neither energy (p = 0.40) nor time (p = 0.60) is relevant; only power has a certain influence, increasing the Ce content with power (p = 0.069).

The nature of the incorporation of Ce into the material can be best analyzed by using high-angle X-ray diffraction (Figure 2). In samples with a Si/Ce ratio of 8, the X-ray diffractogram reveals the presence of several peaks that can be attributed to the (111), (200), and (220) hkl planes of cerium oxide in a cubic fluorite-like structure. The presence of typical cerium oxide peaks suggests

that at these concentrations, Ce atoms cannot be included in the silica structure through isomorphic substitution, so the organization would be more similar to small CeO_2 nanodomains embedded within the silica matrix.

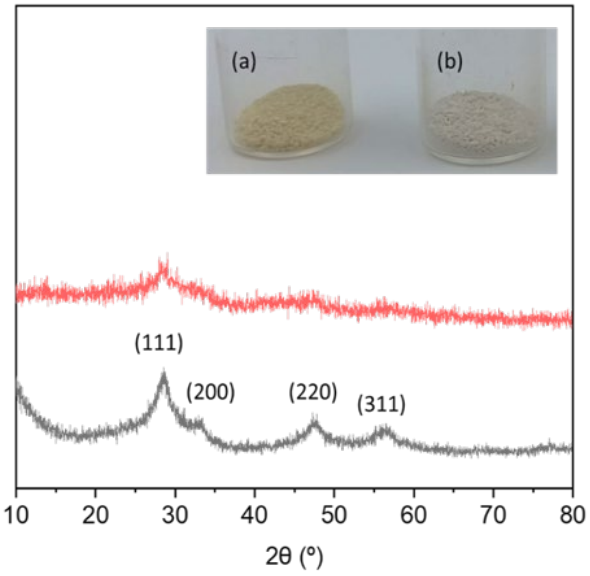

Figure 2. *X-ray diffractogram of Ce-UVM-7. In red shows the sample B10 and in black B4. Inset: Samples of Ce-UVM-7 prepared using different procedures a) batch procedure with a Si/Ce molar ratio of 8 b) batch procedure with a Si/Ce molar ratio of 25.*

Using the Scherrer equation, sizes ranging from 2.5 to 3.1 nm have been obtained. In silica-based SBA-15 materials prepared with CeO_2 confined within the pores, a similar XRD was obtained with peaks of Ce_2O_3 (220) and CeO_2 (311).[33] On the contrary, the XRD patterns of the materials with a Si/Ce ratio of 25, although the cerium oxide peaks can be envisioned, the intensity is very low, and its fwhm is extremely large, suggesting that at this concentration, Ce is probably included in the amorphous silica framework as isolated sites or small Ce-rich oligomers. This organization is confirmed by the color of the

materials (Figure 2, inset). The material with high cerium content presents the yellow color typical of the cerium oxide. Conversely, the materials B7–B12 present a white color, as expected for the UVM-7 pure silica powder. In this last case, the cerium atoms would be mainly surrounded by silicon atoms.

Adding ceria to the mesoporous silica can lead to the formation of cross-linking Ce–O–Si bonds or to the precipitation of Ce–O–Ce particles, which are very insoluble. It is known that the incorporation of heterometallic elements favors a decrease in the silica solubility, so this leads to the fastest nucleation of small nanosized mesoporous particles. That is why in samples with a higher amount of Ceria, the TEM images show a greater aggregation of small domains.The influence of the variables on the characteristics of the material was evaluated using a linear adjustment of the nominal ratio Si/Ce, time, power, and energy supplied (time × power). Only a significant influence ($p < 0.05$) is observed for the nominal ratio of Si/Ce with the real ratio Si/Ce and the surface area. For the rest of the variables, there is no clear influence being able to use any of the powers and times tested to obtain the material without significant differences in the porosity and order of the material. Thus, it is possible to obtain Ce-UVM-7 material with a Si/Ce ratio of around 17 in just 30 s.

The synthesis of Ce-UVM-7 has not been reported before as such, either through microwave-assisted or conventional methods. A silica UVM-7 with Ce and Ni was synthesized using the atrane method without microwave assistance, with a reaction time of 4 h.[34] In this study, molar ratios of Si/Ce ranging from 16 to 67 were investigated, resulting in a BET surface area of 470–566 m^2g^{-1}, respectively. Like in the present work, an increase in the

cerium content in the silica networks led to a decrease in the surface area. We employed a Si/Ce ratio of 25, achieving slightly larger surface areas (approximately 700 m^2g^{-1}) compared to their results, despite having a higher ceria content. Previous work on CeO_2–SiO_2 samples used microwave irradiation, with treatment durations of at least 30 min,[35] in contrast to the 30 s or 2 min employed in the current study.

3.2. Scale-Up Batch and Flow Synthesis

In order to evaluate the possibility of preparing large quantities of Ce-UVM-7, we followed two approaches: batch scaling-up and flow synthesis. The first is a priori more feasible, although the limited penetration capacity of microwaves can generate difficulties when the size of the reactor increases, and there is a risk of cold and hot spots. To avoid these drawbacks, flow synthesis allows a small conduction size to be maintained, achieving homogeneous irradiation, and the movement eliminates the presence of hot and cold spots. Furthermore, the flow synthesis facilitates automation. We selected the Si/Ce ratio 25 because it is the most Ce-concentrated material that maintains the UVM-7 structure. The experimental conditions for the scaled-up synthesis are summarized in Table 2, wherein sample S1 corresponds to the scale-up sample without stirring, S2 corresponds to the scale-up using stirring, and samples designated as F were synthesized using a flow procedure.

Considering our objective of scaling-up the process 100 times and the limit of potency of our equipment of 800 W, the reaction time was increased up to 10 min.

Table 2. *Summary of synthesis conditions, and characterization of samples scale-up. aNominal molar ratio, [b]Molar ratio determined by EDX, [c]The cell parameter calculated by $a_0 = 2d100 \cdot (\sqrt{3})^{-1}$, being d the distance between planes of the hkl 100, [d]Wall thickness was calculated by $d_w = a_o - d_p$, where d_p is the pore diameter.*

Sample	Si/Ce		Power (W)	Time (min)	Mesopore		Large-mesopore		S BET (m^2g^{-1})	2θ	a_o[c]	dw[d]
	Nom[a]	Real[b]			Size (nm)	Volume (cm^3g^{-1})	Size (nm)	Volume (cm^3g^{-1})		(°)	(nm)	(nm)
S1	25	15.8	800	10	2.9	0.62	26.8	0.50	747	1.80	5.7	2.7
S2	25	26.7	800	10	2.9	0.60	42.9	1.02	735	1.86	5.5	2.6
F1	25	12.6	200	0.5	2.7	0.67	28.7	0.53	833	1.90	5.4	2.7
F2	25	17.9	200	0.5	2.7	1.12	31.5	0.61	1388	2.02	5.0	2.3
F3	25	13.2	200	0.5	2.9	0.58	33.6	0.87	733	1.96	5.2	2.3
F4	25	15.4	100	1	2.8	0.62	15.3	0.52	805	1.90	5.4	2.5
F5	25	17.5	100	1	2.8	0.58	28.6	1.00	735	1.90	5.4	2.5
F6	25	17.7	100	1	2.9	0.63	32.3	1.23	793	1.88	5.4	2.6

If we observe the data gathered in Table 2, both Ce-UVM-7 batch-scaled samples, S1 and S2, have the characteristics features of UVM-7. They show surface areas over 725 $m^2 g^{-1}$, similar to the nonscaled synthesis, a XRD peak round 2° (2θ), and the bimodal pore system. The nonstirred sample S1 has a similar composition and pore size. However, there are some differences. S1 shows a shift of the XRD peak to lower angles, indicating an increase in the unit cell dimension. This difference is mainly due to a wider pore wall. These characteristics are also present in S2, with an XRD peak at 1.86° (2θ), an angle slightly larger than that for S1, with the consequent pore wall reduction. It seems that the main difference derived from stirring is the lower Ce content in the resulting material, with a Si/Ce ratio similar to the molar proportion of the reagents, which could be assigned to a better and more homogeneous mixture of the reagents during the reaction. In each batch, prepared in 10 min, enough as-made material is obtained for the preparation of round 35 g of Ce-UVM-7, which is equivalent to 210 g of material h^{-1}. In general, during the stirred scaling processes, there is a higher degree of dispersion among particles (Figure 3). However, it is noteworthy that despite this, dispersion substantial accumulations of particles are also observed. In agitation-assisted scaling, smaller clusters tend to dominate the grain distribution, while larger aggregations are more prevalent in non agitation-assisted scaling. Nevertheless, in both scenarios, the distinctive structure of UVM-7, with small mesoporous particle aggregates, remains apparent.

In the flow procedure (samples F1–F6), reagents are continuously introduced into the system, and products are continuously removed; this constant flow allows a more efficient utilization of reaction time.

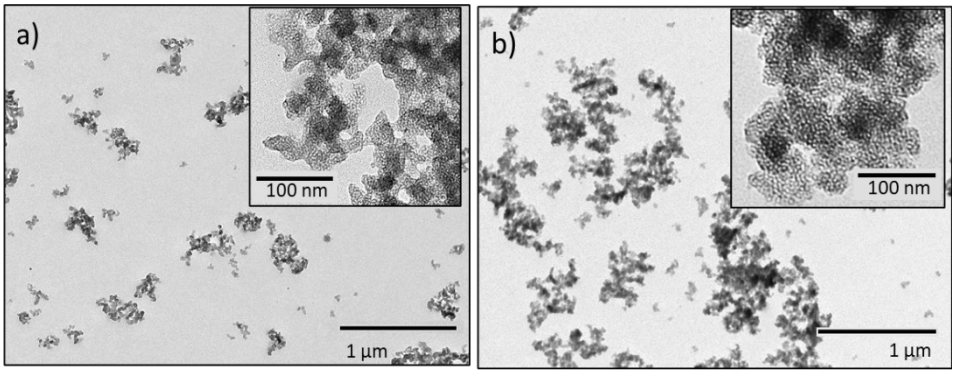

Figure 3. *Representative TEM images for UVM-7 a) sample S1, scaled-up procedure with stirring and b) sample S2, scaled-up procedure without stirring.*

As a result, the production rate can be significantly higher compared with traditional batch methods. Also, the lower volume of the reaction mixture inside the cavity reduces the necessity of microwave power. Regarding the setup, the main difference between batch and flow synthesis lies in the fact that, in the former, all reactants are combined in a single vessel and introduced into the reactor. In contrast, flow synthesis involves two solutions: one containing the atrane mixture and the other one the water. By employing two peristaltic pumps, the solutions are brought into contact just prior to entering the microwave system with distinct flow rates selected to ensure the desired residence time within the reactor. Samples F1–F3 and F4–F6 were prepared to study the effect of reducing the reaction time and maintaining the total energy. Within the series (F1–F3 or F4–F6), each sample corresponds to a different sampling time.

It must be considered that the first fractions (F1 and F4) have not reached the steady state. According to Table 2, if we consider the other four fractions

(F2/F3 and F5/F6), it seems that a reaction time of only 30 s has larger variability. It could be inadequate, even if the potency is doubled. Thus, for a practical application, it would be preferable to increase the reaction time up to 1 min. Using these conditions, 187 mg of Ce-UVM-7 min^{-1} is obtained, equivalent to 11 g of Ce-UVM-7 h^{-1}. This value is much lower than the quantity obtained by a scaled-up batch but allows the automation of the reaction.

3.3. Optical Properties

The UV–vis spectra of the Ce-UVM-7 materials display low reflectance up to 450–500 nm, but they are practically transparent at longer wavelengths in the visible region (see Figure 4). The absorption is originated by the charge transfer from the 2p states of oxygen to the 4f states of cerium.[36,37] Therefore, these ceria particles can serve as UV-blocking and -shielding materials to mitigate damage caused by ultraviolet radiation. The optical properties are dependent on the cerium content, and the absorption increases at lower Si/Ce ratios, as expected. In the samples with a molar ratio of Si/Ce = 25, the behavior is highly consistent across different samples. This consistency can be attributed to the homogeneity of the materials achievable at a low cerium content. By contrast, when the molar ratio of Si/Ce is reduced to 8, greater heterogeneity is observed among the samples, even though the same amount of irradiation energy was applied. Specifically, samples that were prepared in shorter durations exhibit a higher transparency compared to those prepared over longer periods. This suggests that the preparation time could influence the optical properties due to differences in the formation and distribution of the silica-ceria network within the material.

Although it is difficult to identify conclusively relevant parameters, in particular considering the limiter number of samples, we have found that for the materials with nominal Si/Ce 8, there is a linear relationship between the % reflectance at 450 nm and the BET area (R^2 = 0.99); conversely, there is no such correlation for the real Si/Ce ratio (R^2 = 0.15). This suggests that for the materials with higher concentration of Ce, the material structure is not innocent, and the porosity of the material can interact with the UV light. In fact, we had observed for the noncerium containing silica a certain UV absorption that can be assigned to the textural properties.

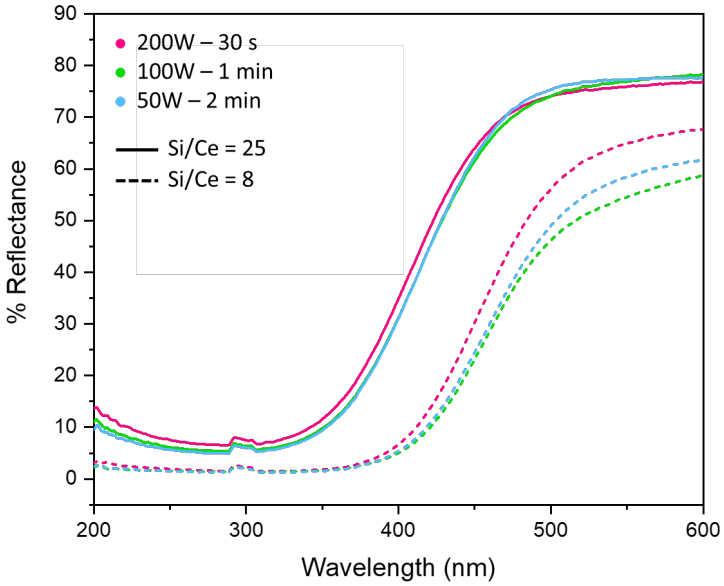

Figure 4. *Spectral reflectance curves for Ce-UVM-7 with molar ratios of 25 and 8.*

According to the results, the band gap energies have values of 3.338 ± 0.014 and 3.15 ± 0.03 eV for Si/Ce ratios of 25 and 8, respectively. These energies correspond to wavelengths of 372 and 392 nm. As expected, the material with

a lower content of cerium shows the larger bandgap. The low errors indicate that the optical properties depend mainly on the chemical composition, independently of the synthesis conditions. Commercial CeO_2 presents a bandgap of 2.79 and 2.66 eV and wavelengths of 444 and 466 nm for nanorods or nanoparticles, respectively. ANOVA analysis together with the Tukey test indicated that the three types of materials offer significant differences in their optical properties ($p = 0.05$). Although our materials have a lower absorption in the UV–vis spectrum than cerium oxide, they can filter UVA (400–320 nm) and beyond.

The nanoparticles most used in sunscreens include TiO_2 and ZnO, yet their elevated refractive index results in a pale coloration of the skin.[37] Additionally, studies have demonstrated that upon exposure to UV radiation, these compounds generate hydroxyl radicals that induce DNA damage in skin cells.[38] Cerium oxide is another material characterized by a significantly high UV absorption that possesses a lower refractive index, thereby exhibiting enhanced transparency to visible light. Furthermore, it exhibits high catalytic activity, which is why it is rarely employed in cosmetic products. Studies have been conducted demonstrating that CeO_2 nanoparticles protect cells from toxicity induced by UVA radiation.[39] Considering these optical properties, we prepared mixtures of a cream and sample B9 to study its UV-shielding properties, (Table 3). Sample B9 was selected as representative of the Ce-UVM-7 materials with a ratio of Si/Ce of 25 and UVM-7 structure. For the sake of comparison also, samples of commercial CeO_2 and pure silica UVM-7 were measured.

As can be seen in Table 3, in comparison with UVM-7, Ce-UVM-7 offers a notable increase in the SPF that can be assigned to the incorporation of cerium into the porous silica matrix. This enhancement emphasizes the efficacy of cerium as a UV-blocking agent when combined with UVM-7. The Ce-UVM-7 material is able to offer sunscreen protection, and the effect is more pronounced for the mixtures with higher loading of materials, reaching SPF values of 69 for a concentration of 20%. Nevertheless, at this concentration exists a certain material heterogeneity on the plate that could influence the measured values.

Table 3. *Solar protection factor of sample B9 in sunscreen tests.*

	% of inorganic loading (w/w)	SPF of the sunscreen	% CeO_2 in the sunscreen
Ce-UVM-7	1	1.30 ± 0.13	0.12
Ce-UVM-7	5	2.2 ± 0.24	0.62
Ce-UVM-7	10	6.4 ± 0.30	1.18
Ce-UVM-7	20	69 ± 9	2.01
CeO_2	2	4.0 ± 0.69	2.00
UVM-7	5	1.08 ± 0.16	0.00
UVM-7	20	3.2 ± 0.48	0.00

In comparison with pure CeO_2, to obtain the same SPF, it needs five times more material. However, if we consider only the cerium content, the Ce-UVM-7 would be more efficient than pure cerium oxide. A 1.2% concentration of cerium (1.2%) in the UVM-7 solid offers protection in the same range than CeO_2. Additionally, it is important to note that the values obtained for a 2% concentration of CeO_2 (4.0 ± 0.7) are markedly reduced compared to those

achieved with the same concentration of CeO_2 incorporated into UVM-7 (69 ± 9), which corresponds to a Ce-UVM-7 concentration of 20% on the plate. Intriguingly, these reduced values are comparable to those obtained when using a 20% material concentration of UVM-7 alone (3.2 ± 0.5). Thus, the support is not innocent and also has a minor contribution in the light absorption. It reaches an SPF of 1.1 and 3.1 for 5 and 20%, respectively. Boutard et al., conducted experiments to measure the sun protection factor (SPF) of the microwave-assisted synthesis of CeO_2 with a concentration of 3 wt % associated with other UVA and UVB filters, and the results indicated SPF values of 49 ± 2.[40] This slightly aligns with the outcomes of our own investigation. The SPF value of 69 ± 9 using a 20 wt % % Ce-UVM-7 (which corresponds to 2% CeO_2) implies that a higher SPF value can be achieved with a lower concentration of cerium. Additionally, Zholobak et al., conducted SPF testing on samples with 27% CeO_2 and obtained an SPF value of 30, which is still lower than our results.[38] Kozlova et al., obtained a value of 3.2 for a 10 wt %, reinforcing the superiority of our materials in terms of sun protection efficacy.[41]

Besides that, the integration of ceria within the mesoporous silica matrix not only enhances UV-blocking capabilities but also offers additional benefits such as enhanced stability, increased photoactivity, and improved photostability.[40] Furthermore, the unique structural properties of mesoporous materials, characterized by a well-defined pore structure and high surface area, allow for the efficient incorporation of UV filters, promoting uniform dispersion and optimal UV absorption.[42] This agrees with the effect of the morphology and shape of the nanostructures in the light absorption capacity. The presence of

mesopores improves light absorption because these characteristics promote the scattering of light and extend the optical pathway.[43]

Mesoporous silica is very stable under normal conditions. With time and upon exposure to acids, bases, or high temperature, the mesoporous structure can be lost, but the chemical composition is basically maintained. A primary concern when nanoscopic materials are used in sunscreen formulations is their potential absorption into the skin. An important factor in silica toxicity is its crystallinity. Mesoporous silica, with its amorphous structure, shows much reduced toxicity against in vitro cell lines as compared to crystalline materials like quartz. Even when compared to other amorphous silicas, including fumed silica, mesoporous silica has minimal levels of toxicity. Lehman and Larsen demonstrated that, compared to nonporous silicas, mesoporous silicas cause a less hazardous reaction because of their lower surface silanol densities.[44] Some studies were made with mesoporous silica SBA-15 by Lin et al. in 2021, studying the cytotoxicity of mesoporous silica against keratinocytes which are the epidermis cells.[45] After an exposure of 24h at different concentrations of SBA-15, there was no cytotoxicity even at high concentrations.

On the other hand, Mauro et al. (2019) investigated the absorption properties of cerium oxide nanoparticles (CeO_2 NPs) through human skin.[46] Their study utilized CeO_2 NPs with a diameter of 10–20 nm and demonstrated minimal skin penetration and permeation. In tests on intact skin, ceria remained largely confined to the epidermis, with negligible permeation. However, when the damaged skin was tested, a small amount of ceria penetrated the dermis, indicating low-level permeation under compromised skin conditions.

3.4. Peroxidase Activity

Cerium oxide offers ROS scavenging properties,[5] so we were interested in studying if Ce-UVM-7 materials have similar activity. In comparison to the peroxidase activity of CeO_2 prepared with microwave-assisted synthesis in a previous work,[5] which exhibits a reaction rate of 8×10^{-3} min^{-1}, an analogous result is obtained for the activity of materials prepared in batch with a molar ratio of Si/Ce = 8. However, samples prepared with a lower ceria content demonstrate higher activity, both in batch and flow conditions, with reaction rates of 23×10^{-3} and 27×10^{-3} min^{-1}, respectively (Figure 5).

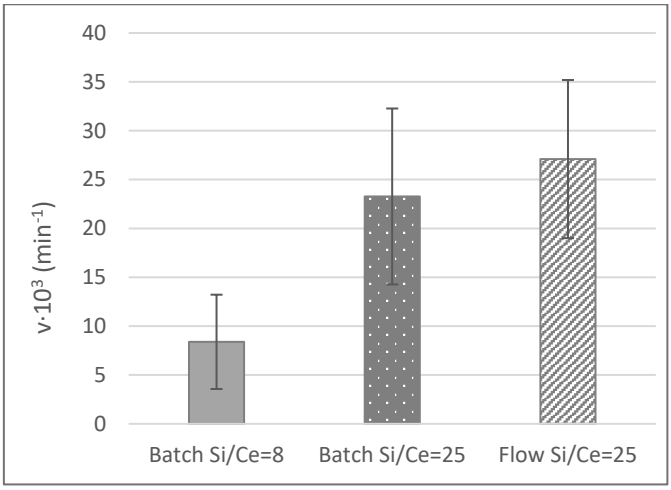

Figure 5. *Peroxidase activity reaction rate of the Ce-UVM-7 materials.*

The formation of CeO_2 clusters in the Si/Ce 8 materials could reduce the exposure of the Cerium atoms to the reagents. We cannot discard the presence of very few clusters (see XRD, Figure 2) together with single atoms incorporated into the structure, but it seems that larger clusters could show a lower activity than the little ones or single Ce atoms. It seems that the network

of mesopores promote an easy access to the active sites while inhibiting the unwanted movement and expansion of metal nanoparticles.[34] It has been previously reported that the addition of silica to nanozymes exhibiting activity against reactive oxygen species enhances their catalytic performance. In this instance, the silica coating notably enhanced the catalase activity of MnOx.[47] The comparable activity observed in materials produced under both batch and flow conditions aligns with the similarities identified in the characterization of both types of materials. This confirmation underscores that our flow synthesis approach successfully yields Ce-UVM-7 materials with properties akin to those obtained through batch synthesis.

3.5. Life Cycle Assessment

The main advantage of microwaves is their efficiency in reducing reaction times. Even considering the difficulties of microwave-assisted synthesis to achieve a linear scale-up, a reduced reaction time, combined with the use of low powers, enables a synthesis process with a lower energy consumption. The LCA was applied on a cradle to gate basis. The goals are the quantification of the global impact and main impact factors associated with the preparation of Ce-UVM-7 materials, evaluation of the effect of the scale-up, and identification of the main processes/reagents to suggest improvements. The functional unit was defined as the preparation of 1 kg of material.

The single score in the ReCiPe method offers a general reference of the impacts and allows a simple comparison between methods. The non scaled-up synthesis offers a value of 342 points, a value high for the preparation of 1 kg of Ce-UVM-7 material. However, the small size of the batches used during

optimization of the synthesis conditions is very inefficient, with large expenses in energy and solvents. It is not representative of the value on a large scale. In the batch-scaled synthesis, this value is reduced to 7.6 points; a value similar was obtained in the calculations of the flow synthesis. The single score decreases to 1.9 points for 1 kg of sunscreen cream with 25% loading of the Ce-UVM-7 material. As can be seen in Figure 6a, for Ce-UVM-7, solvents and energy account for most of the impact, followed by the reagents. Therefore, the process could be strongly improved by using energy with a lower environmental impact (i.e., from renewable origin), technologies with higher energy efficiency, and/or removing or at least reducing the use of ethanol (i.e., with recovery by distillation).

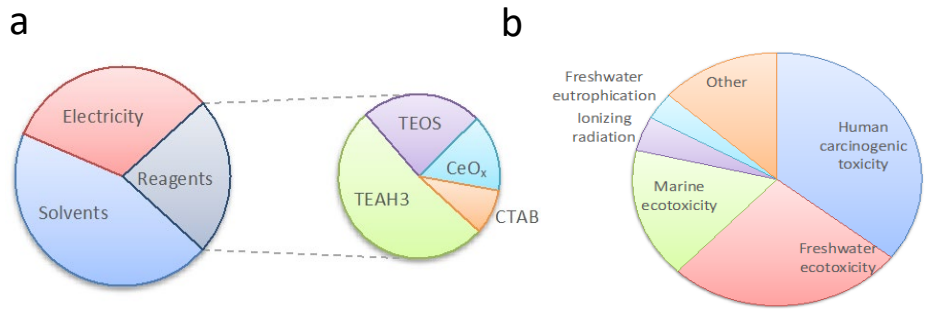

Figure 6. *Lice Cycle Assessment of the scale-up batch synthesis. a) Contribution of the processes to the single score of the scaled-up batch synthesis. b) Main normalized impact category indictors of the scaled-up batch synthesis.*

These practices are common in the step toward an industrial scale-up, thus a significant reduction in a large-scale synthesis. Regarding the reagents, they are key components difficult to exchange, and any modification requires a novel process of optimization and scale-up. The reagent with the stronger

impact is triethanolamine, which is a key reagent in the atrane route. It is required a $TEAH_3$/Si ratio ≥ 2 to ensure that all the coordination positions are covered. Typically, in the synthesis of UVM-7, a specific ratio of 3.5 (excess) is used to avoid the use of organic solvents, such as ethylene glycol. $TEAH_3$ serves both as a reagent and reaction medium. $TEAH_3$/TEOS ratio of 2, the water-atrane mixture needs thorough stirring to homogenization, in comparison with the $TEAH_3$/TEOS ratio of 3.5 that mixes immediately and has a large viscosity that could not be used in the flow synthesis. Although a slight reduction in $TEAH_3$ could be used, we cannot discard changes in the properties of the mesoporous materials if it is strongly reduced. Also, the possibility of using novel sources of silicon or more sustainable surfactants could be interesting topics for future works. Regarding the main impact categories, the main ones are Human carcinogenic toxicity, Freshwater ecotoxicity, Marine ecotoxicity, Ionizing radiation, and Freshwater eutrophication (see Figure 6b), all of them related to the preparation of solvents and chemical reagents. By contrast, other relevant factors in impact studies such as global warming potential or water consumption offer only a minor contribution, highlighting the relevance to perform full LCA studies to evaluate the processes, not only evaluations of single-impact categories.

4. CONCLUSIONS

We have effectively demonstrated that the combination of the atrane route with the microwave-assisted synthesis using solid-state generators can be an interesting approach to obtain not only porous silica but also mixed compound with other elements. It can be applied even to elements such as

cerium, with a hydrolysis–condensation rate different from that of silicon and above all with a marked difference in solubility of its species in solution. In this study, we present, for the first time, the synthesis of Ce-UVM-7. It was successfully synthesized departing from a Si/Ce molar ratio of 25. At larger Ce concentrations, cerium segregates into crystalline CeOx nanodomains, and the ordered porous structure is lost. The reaction times are short, and most of the materials can be obtained in less than 1 min of irradiation. The reaction can be effectively scaled-up in batch and adapted to the flow synthesis maintaining the typical UVM-7 topology, allowing the preparation of hundreds of grams, and with a significant reduction in the impact to only 8 points in the single score of LCA per kg of Ce-UVM-7, that could be further reduced in an industrial process and/or through modification of the reagents. Furthermore, this research highlights the potential application of Ce-UVM-7 materials in sunscreens and free radical scavengers. Ce-UVM-7 materials exhibit large absorption of ultraviolet (UV) light and improved ROS scavenging properties, probably due to the porous structure and the homogeneous distribution of Ce along the silica matrix. In summary, this study contributes to the field of advanced materials synthesis by presenting a successful methodology for the synthesis of Ce-UVM-7 using microwave solid-state generators. The demonstrated potential of these materials in catalytic applications and their potential use in sunscreens highlight their versatility and broad range of potential applications. The findings presented in this article pave the way for further research and development of mesoporous silica-based materials for various industrial and cosmetic applications.

AUTHOR INFORMATION

Corresponding Author

Jose V. Ros-Lis − REDOLí research group, Instituto Interuniversitario de Investigación de Reconocimiento Molecular y Desarrollo Tecnológico (IDM), Universitat Politènica de València, Universitat de València, Burjassot, Valencia 46100, Spain; orcid.org/0000-0001-8238-5829; Phone: +34 963544856; Email: J.Vicente.Ros@uv.es; Fax: +34 963544856

Authors

Cristina Rodríguez-Carrillo − REDOLí research group, Instituto Interuniversitario de Investigación de Reconocimiento Molecular y Desarrollo Tecnológico (IDM), Universitat Politècnica de València, Universitat de València, Burjassot, Valencia 46100, Spain

Miriam Benítez − REDOLí research group, Instituto Interuniversitario de Investigación de Reconocimiento Molecular y Desarrollo Tecnológico (IDM), Universitat Politècnica de València, Universitat de València, Burjassot, Valencia 46100, Spain

Ruth De los Reyes − Microbiotech. S.L., Villamarxant 46191, Spain

Jamal El Haskouri − Institut de Ciència dels Materials (ICMUV), Universitat de València, Paterna 46980 Valencia, Spain

Pedro Amorós − Institut de Ciència dels Materials (ICMUV), Universitat de València, Paterna 46980 Valencia, Spain; orcid.org/0000-0002-8741-3769

Notes

The authors declare no competing financial interest.

ACKNOWLEDGMENTS

This research was funded by the Spanish Ministerio de Ciencia, Innovación y Universidades, grant number PID2021-126304OB-C43 funded by MCIN/AEI/10.13039/501100011033 and by “ERDF A way of making Europe”; the AGROALNEXT program supported by MCIN with funding from European Union NextGenerationEU (PRTR-C17.I1) and by Generalitat grant number EUAGROAL- NEXT/2022/065; and by Generalitat Valenciana grant number CIAPOT/2022/017.

References

(1) Yang, R.; Bao, Z.; Sun, Y. Probing and Leveraging the structural heterogeneity of nanomaterials for enhanced catalysis. *ACS Nanosci. Au* **2023**, *3*, 140−152.

(2) Huo, Q.; MArgolese, D. I.; Ciesla, U.; Feng, P.; Hier, T. E.; Sieger, P.; Leon, R.; Petroff, P. M.; Schüth, F.; Stucky, G. D. Generalized synthesis of periodic surfactant/inorganic composite materials. *Nature* **1994**, *368*, 317−321.

(3) Kresge, C.T.; Leonowicz, M.E.; Roth, W.J.; Vartuli, J.C.; Beck, J.S. Ordered mesoporous molecular sieves synthesized by a liquid-crystal template mechanism. *Nature* **1992**, *359*, 710−712.

(4) El Haskouri, J.; Ortiz de Zárate, D.; Guillem, C.; Latorre, J.; Caldés, M.; Beltrán, A.; Beltrán, D.; Descalzo, A. B.; Rodríguez-López, G.; Martínez-Máñez, R.; Marcos, M. D.; Amorós, P. Silica-based powders and monoliths with bimodal pore systems. *Chem. Commun*. **2002**, *4*, 330−331.

(5) Rodríguez-Carrillo, C.; Torres-García, J.; Benítez, M.; El Haskouri, J.; Amorós, P.; Ros-Lis, J. V. Batch and flow synthesis of CeO_2 Nanomaterials using solid-state microwave generators. *Molecules* **2022**, 27, 2712.

(6) Da Silva Assis, M.N.; Nestal de Moraes, G.; De Souza, K. R. Cerium oxide nanoparticles: Chemical properties, biological effects and potential therapeutic opportunities (Review). *Biomed. Rep*. **2024**, *911* 20, 48.

(7) Lord, M.S.; Berret, J.F.; Singh, S.; Vinu, A.; Karakoti, A. S. Redox active cerium oxide nanoparticles: current status and burning issues. *Small* **2021**, *17*, 2102342.

(8) Wan, Y.; Zhao, D. On the controllable Soft-Templating approach to mesoporous silicates. *Chem. Rev.* **2007**, *107*, 2821−2860.

(9) Cho, E.B.; Yim, S.; Kim, D.; Jaroniec, M. Surfactant-assisted synthesis of mesoporous silica/ceria-silica composites with high cerium content under basic conditions. *J. Mater. Chem. A* **2013**, *1*, 12595−12605.

(10) Laha, S.C.; Mukherjee, P.; Sainkar, S.R.; Kumar, R. Cerium containing MCM-41-type mesoporous materials and their acidic and redox catalytic properties. *J. Catal.* **2002**, *207*, 213−223.

(11) Shao, Y.; Wang, L.; Zhang, J.; Anpo, M. Synthesis of Hydrothermally Stable and Long-Range Ordered Ce-MCM-48 and Fe-MCM-48 Materials. *J. Phys. Chem. B* **2005**, *109*, 20835−20841.

(12) Timofeeva, M.N.; Jhung, S.H.; Hwang, Y.K.; Kim, D.K.; Panchenko, V. N.; Melgunov, M.S.; Chesalov, Y.A.; Chang, J.S. Ce-silica mesoporous SBA-15-type materials for oxidative catalysis: Synthesis, characterization, and catalytic application. *Appl. Catal. A: Gen*. **2007**, *317*, 1−10.

(13) Garrido, M.D.; Benítez, M.; Ros-Lis, J. V.; Amorós, P. A travel though the atrane route, a versatile tool for the materials soft-synthesis: A twenty-five years perspective. *Nano Select* **2024**, *5*, 2300169.

(14) Tompsett, G.A.; Conner, W.C.; Yngvesson, K.S. Microwave synthesis of nanoporous materials. *ChemPhysChem* **2006**, *7*, 296−319.

(15) Díaz de Greñu, B.; de los Reyes, R.; Costero, A. M.; Amorós, P.; Ros-Lis, J. V. Recent progress of microwave-assisted synthesis of silica materials. *Nanomaterials* **2020**, *10*, 1092.

(16) Leonelli, C. Microwave generators, transmission, and interaction with different materials. In G. Cravotto & D. Carnaroglio (Ed.), *Microwave Chemistry* **2017**, 31−52. Berlin, Boston: De Gruyter.

(17) Zhou, X.; Pedrow, P.D.; Tang, Z.; Bohnet, S.; Sablani, S.S.; Tang, J. Heating performance of microwave ovens powered by magnetron and solid-state generators. *Innov. Food Sci. Emerg. Technol*. **2023**, *83*, 103240.

(18) Horikoshi, S.; Watanabe, T.; Narita, A.; Suzuki, Y.; Serpone, N. The electromagnetic wave energy effect(s) in microwave-assisted organic synthesis (MAOS). *Sci. Rep*. **2018**, *8*, 5151.

(19) Díaz de Greñu, B.; Muñoz-Pina, S.; De los Reyes, R.; Benítez, M.; El Haskouri, J.; Amorós, P.; Ros-Lis, J. V. Fast microwave-assisted synthesis, calcination and functionalization of a silica mesoporous nanomaterial: UVM-7. *ChemSusChem* **2023**, *16*, e2023001.

(20) Benítez, M.; Rodríguez-Carrillo, C.; Sánchez-Artero, S.; El Haskouri, J.; Amorós, P.; Ros-Lis, J. V. Scaled-up microwave-assisted batch and flow synthesis and life cycle assessment of a silica mesoporous material: UVM-7. *Green Chem*. **2024**, *25*, 785−793.

(21) Tovar-Rodríguez, J.; Fratini, E.; Baglioni, P.; Ferrari, C.; de los Reyes-Heredia, J.A.; Ramírez-Hernández, Y.; Galindo-Esquivel, J.R. Ultrasound and microwave-assisted synthesis of hexagonally ordered ce-promoted mesoporous silica as Ni supports for ethanol steam reforming. *Nanomaterials* **2023**, *13*, 997.

(22) Tauc, J.; Menth, A.; Wood, D. L. Optical and magnetic investigations of the localized states in semiconducting glasses. *Phys. Rev. Lett*. **1970**, *25*, 749−752.

(23) Matts, P.J.; Alard, V.; Brown, M.W.; Ferrero, L.; Gers-Barlag, H.; Issachar, N.; Moyal, D.; Wolber, R. The COLIPA in vitro UVA method: a standard and reproducible measure of sunscreen UVA protection. *Int. J. Cosmet. Sci.* **2010**, *32*, 35−46.

(24) Labeling and effectiveness testing: sunscreen drug products for over-the-counter human use - Small entity compliance guide. Published by U.S. Department of Health and Human Services, Food and Drug Administration, Center for Drug Evaluation and Research, **2012**.

(25) Webb, A. R.; Slaper, H.; Koepke, P.; Schmalwieser, A. W. Know your standard: clarifying the CIE erythema action spectrum. *Photochem. Photobiol*. **2011**, *87*, 483−486.

(26) Bilbao, J.; De Migue, A. Erythemal solar irradiance, UVER, and UV index from ground-based data in central Spain. *Appl. Sci.* **2020**, *10*, 6589.

(27) Cao, W.; Ju, P.; Wang, Z.; Zhang, Y.; Zhai, X.; Jiang, F.; Sun, C. Colorimetric detection of H_2O_2 based on the enhanced peroxidase mimetic activity of nanoparticles decorated $Ce_2(WO_4)_3$ nanosheets. *Spectrochim. Acta A Mol. Biomol. Spectrosc.* **2020**, *239*, 118499.

(28) Faraca, G.; Vidal-Abarca Garrido, C.; Kaps, R.; Fernández Carretero, A.; Wolf, O.; Morera, D.; Bastos, J.; Riera, M. R.; Escamilla, M.; Escudero, R. Revision of the EU Ecolabel criteria for Cosmetic Products and Animal Care Products (previously Rinse-off Cosmetic Products) − Preliminary Report, EUR 30809 EN; Publications Office of the European Union: Luxembourg, **2021**, ISBN 978-92-76-41078-2, DOI: 10.2760/195921, JRC126061.

(29) Wattanathana, W.; Nootsuwan, N.; Veranitisagul, C.; Koonsaeng, N.; Laosiripojana, N.; Laobuthee, A. Simple cerium- triethanolamine complex: Synthesis, characterization, thermal decomposition and its application to prepare ceria support for platinum catalysts used in methane steam reforming. *J. Mol. Struct*. **2015**, *1089*, 9999−15.

(30) Kangquiang, L.; Zhong, M. Synthesis of monodispersed nanosized CeO_2 by hydrolysis of the cerium complex precursor. *J. Rare Earths* **2010**, *28*, 680−683.

(31) Zghal, I.; Farjas, J.; Camps, J.; Dammak, M.; Roura-Grabulosa, P. Thermal decomposition of cerium triethanolamine complexes. *Thermochim. Acta* **2020**, *683*, 178430.

(32) Morales, J. M.; El Haskouri, J.; Guillem, C.; Hany, R.; Ros-Lis, J. V.; Beltrán, D.; Beltrán, A.; Amorós, P. Control of the pore wall thickness and thermal stability in low-cost bimodal porous silicas. *Polyhedron* **2019**, *170*, 544−552.

(33) Vaja, F.; Oprea, O.; Ficai, D.; Ficai, A.; Guran, C. Synthesis of CeO_2 nanoparticles on the mesoporous silica support via nanocasting. *Dig. J. Nanomater. Biostruct*. **2014**, *9*, 187−195.

(34) Opris, C. M.; Pavel, O. D.; Moragues, A.; El Haskouri, J.; Beltrán, D.; Amorós, P.; Marcos, M.D.; Stoflea, L.E.; Parvulescu, V. I. New multicomponent catalysts for the selective aerobic oxidative condensation of benzylamine to N-benzylidenebenzylamine. *Catal. Sci. Technol*. **2014**, *4*, 4340.

(35) Mohamed, R.M.; Aazam, E.S. Synthesis and characterization of CeO_2-SiO_2 nanoparticles by microwave-assisted irradiation method for photocatalytic oxidation of methylene blue dye. *Int. J. Photoenergy* **2012**, *2012*.

(36) Kim, N.W.; Lee, D.K.; Yu, H. Selective shape control of cerium oxide nanocrystals for photocatalytic and chemical sensing effect. *RSC Adv*. **2019**, *9*, 13829−13837.

(37) Minamidate, Y.; Yin, S.; Sato, T. Synthesis and characterization of plate-like ceria particles for cosmetic application. *Mater. Chem. Phys*. **2010**, *123*, 516−520.

(38) Zholobak, N.M.; Ivanov, V.K.; Schcherbakov, A.B.; Shaporev, A.S.; Polezhaeva, O.S.; Baranchikov, A. Y.; Spivak, N. Y.; Tretyakov, Y. D. UV-shielding property, photocatalytic activity and photocytotoxicity of ceria colloid solutions. *J. Photochem. Photobiol. B* **2011**, *102*, 32−38.

(39) Caputo, F.; De Nicola, M.; Sienkiewicz, A.; Giovanetti, A.; Bejarano, I.; Licoccia, S.; Traversa, E.; Ghibelli, L. Cerium oxide nanoparticles, combining antioxidant and UV shielding properties, prevent UV-induced cell damage and mutagenesis. *Nanoscale* **2015**, *7*, 15643.

(40) Boutard, F.; Rousseau, B.; Couteau, C.; Tomasoni, C.; Simonnard, C.; Jacquot, C.; Coiffard, L. J. M.; Konstantinov, K.; Devers, T.; Roussakis, C. Comparison of photoprotection efficiency and antiproliferative activity of ZnO commercial sunscreens and CeO_2. *Mater. Lett*. **2013**, *108*, 13−16.

(41) Kozlova, T.O.; Popov, A. L.; Kolesnik, I. V.; Kolmanovich, D.D.; Baranchikov, A.E.; Shcherbakov, A.B.; Ivanov, V.K. Amorphous and crystalline cerium (IV) phosphates: biocompatible ROS-scavenging sunscreens. *J. Mater. Chem. B* **2022**, *10*, 1775.

(42) Parwaiz, S.; Khan, M.M.; Pradhan, D. CeO_2-based nanocomposites: An advanced alternative to TiO_2 and ZnO in sunscreens. *Mater. Express* **2019**, *9*, 185−202.

(43) Pal, N.; Cho, E.B.; Patra, A. K.; Kim, D. Ceria-containing ordered mesoporous silica: synthesis, properties and applications. *ChemCatChem*. **2016**, *8*, 285−303.

(44) Lehman, S.E.; Larsen, S.C. Zeolite and mesoporous silica nanomaterials: greener syntheses, environmental applications and biological toxicity. *Environ. Sci.: Nano* **2014**, *1*, 200.

(45) Lin, Y.C.; Fang, Y.P.; Hung, C.F.; Yu, H.P.; Alalaiwe, A.; Wu, Z.Y.; Fang, J.Y. Multifunctional TiO_2/SBA-15 mesoporous silica hybrids loaded with organic sunscreens for skin application: The role in photoprotection and pollutant adsorption with reduced sunscreen permeation. *Colloids Surf. B Biointerfaces* **2021**, *202*, 111658.

(46) Mauro, M.; Crosera, M.; Monai, M.; Montini, T.; Fornasiero, P.; Bovenzi, M.; Adami, G.; Turco, G.; Filon, F. L. Cerium oxide nanoparticles absorption through intact and damaged human skin. *Molecules* **2019**, *24*, 3759.

(47) Garrido, M.D.; El Haskouri, J.; Marcos, M.D.; Pérez-Pla, F.; Ros-Lis, J.V.; Amorós, P. One-Pot Synthesis of MnO_x-SiO_2 porous composites as nanozymes with ROS-Scavenging Properties. *Nanomater*. **2022**, *12*, 3503.

Chapter 5:

Non-Mesoporous Oxides

5.1. Overview

In the previous Chapters, we have discussed the use of solid-state microwave technology for the synthesis of mesoporous silica materials, as well as their functionalization. In this Chapter, we will address the synthesis of non-mesoporous oxides, to demonstrate that this type of equipment has a broad range of applications and can be effectively utilized with various classes of materials.

Inorganic oxides are a common class of materials synthesized using microwave generators. This technology is particularly effective to produce inorganic oxides, as it enables the synthesis of high-purity materials with homogeneous structures and precise control over particle morphology. This is a fundamental area of materials chemistry, with significant importance due to its wide range of applications in catalysis,[1] electronics, energy storage,[2] and environmental technologies.[3] Inorganic oxides, such as silica (SiO_2), alumina (Al_2O_3), or titanium dioxide (TiO_2), play crucial roles in various industrial processes and advanced technological devices. In this Chapter, we select the cerium oxide or ceria (CeO_2).

Cerium is the most reactive element from the lanthanide series. Due to its highly electropositive nature, cerium can exist in two oxidation states: Ce^{3+} and Ce^{4+}. The Ce^{4+} state is generally more stable than Ce^{3+} because its electronic configuration, $[Xe]4f^0$, is more energetically favorable than the partially filled $[Xe]4f^1$ state of Ce^{3+}.[4]

As a result, cerium forms two primary oxides (Figure 5.1), cerium dioxide (CeO_2) and cerium sesquioxide (Ce_2O_3), with CeO_2 or ceria being the most stable oxide of this element.[5]

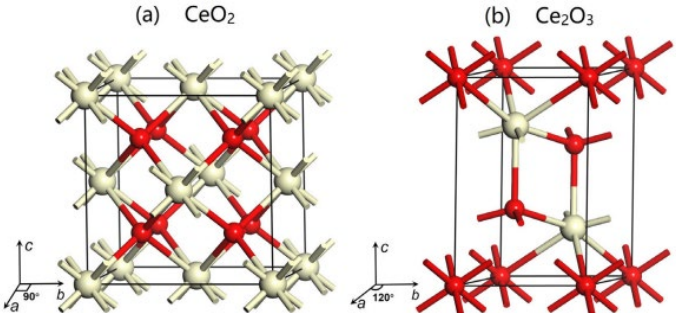

***Figure 5.1**. Unit cell of (a) CeO_2 and (b) Ce_2O_3. Reproduced with permission from Springer Nature.[6]*

In recent years, CeO_2 has gained significant attention due to its remarkable properties, making it increasingly used in different applications. These properties, which will be discussed later in this article, contribute to its growing importance over time, as evidenced with the increase of scientific papers published within the years (Figure 5.2).

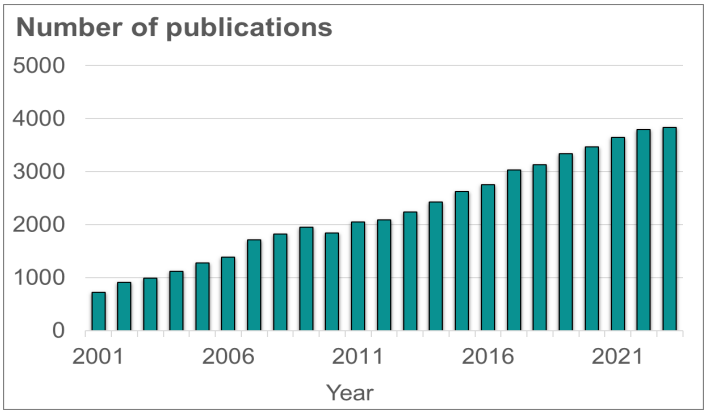

***Figure 5.2.** Number of publications on "Cerium oxide" over the years. Data from Web of Science.*

5.2. Synthetic procedures

There are different methods for synthesizing nanocrystalline CeO_2 powders, each offering distinct advantages depending on the desired properties and applications.

In comparison to conventional solid-state reaction methods, solution-based synthesis offers superior chemical homogeneity.[7] There are various synthesis methods available; however, among the most significant, we can highlight the following:

- Hydrothermal synthesis: is widely used due to its ability to produce highly crystalline materials under controlled conditions. By adjusting synthesis parameters such as pH, precursors, reaction time, etc. it is possible to obtain nanoparticles with different sizes, morphologies, and degrees of crystallinity, making this method highly versatile for various applications.[8]

- Homogeneous precipitation: in a precipitation method, metal cation precursors are formed by introducing a ligand, such as ammonia, directly into the solution.[9] In homogeneous precipitation, a key characteristic is the controlled release of reaction-participating ligands from another chemical source within the solution. This method, using agents such as urea or hexamethylenetetramine, offers a simple and effective approach to producing fine particles with controlled properties.[10]

– Flame spray pyrolysis: in this synthesis approach, a metal precursor is first dissolved in a flammable organic solution, which is then atomized into a flame (Figure 5.3). Within the high-temperature environment, metal or metal oxide nanoparticles are generated through nucleation from the gas phase. This method allows for the fast production of nanoparticles while providing precise control over their size.[11]

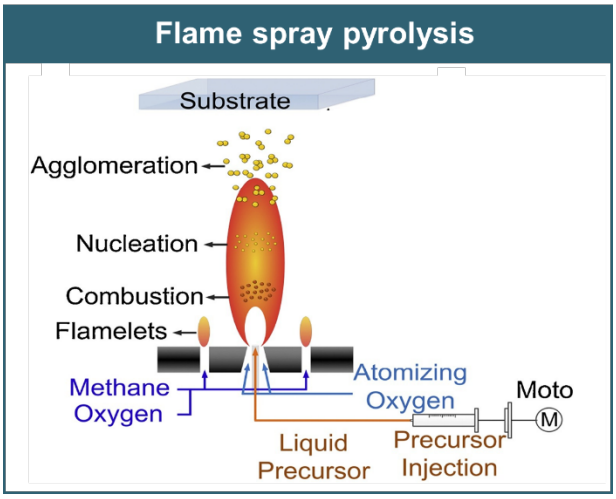

***Figure 5.3**. Schematic representation of the Flame Spray Pyrolisis procedure.*[12]

– Reverse micelle synthesis: this route is employed for precise particle size control, as the synthesis occurs within the micelle core, which constitutes the hydrophilic region (Figure 5.4). In this manner, uniform particle sizes, determined by the micelle dimensions, are achieved along with a controlled size distribution.[13,14]

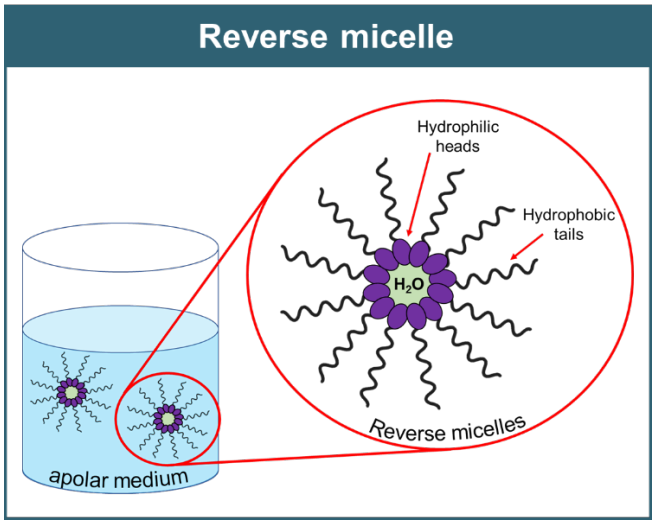

***Figure 5.4**. Schematic representation of the Reverse micelle procedure.*

– Microwave-assisted processes: they have also been explored to enhance purity, morphology, and efficiency in CeO_2 nanoparticle production. In the previous chapters, we have explored the synthesis of other materials using solid-state microwave techniques, achieving successful results in the process. The synthesis of CeO_2 via microwave irradiation has already been reported[15] and will be discussed later in this article. Therefore, we will now employ these solid-state microwave generators to assess whether this approach is also effective for CeO_2 synthesis.

5.3. Objectives and scope of this study

The objective of this study is to develop an efficient synthesis route for CeO_2 nanoparticles using solid-state microwave generators, aiming to significantly reduce synthesis time while maintaining material quality. Furthermore, in previous Chapters, we successfully optimized the continuous-flow synthesis

of other materials, demonstrating its potential for scalability and process control. Building on these results, we will also attempt to implement this approach for CeO_2 synthesis to evaluate its feasibility and effectiveness in producing high-quality nanostructured ceria.

In addition to the synthesis process, we will assess the catalytic activity of CeO_2 by comparing the batch synthesis method with the flow synthesis method. This comparison will help determine whether microwave-assisted synthesis can not only replicate the morphological characteristics of CeO_2 but also preserve or enhance its catalytic performance. By exploring both the synthesis and catalytic properties, this study aims to provide valuable insights into the potential of microwave technology for advanced ceria-based materials.

5.4. References

(1) Albertini, P.P.; Newton, M.A.; Wang, M.; Segura Lecina, O.; Green, P.B.; Stoian, D.C.; Oveisi, E.; Loiudice, A.; Buonsanti, R. Hybrid oxide coatings generate stable Cu catalysts for CO_2 electroreduction. *Nat. Mater.* **2024**, *23*, 680–687.

(2) Ozawa, M.; Matuda, K.; Miura, Y.; Hattori, M.; Okouchi, T.; Yuzuriha, H.; Sugimoto, T.; Haneda, M. Dispersion state and oxygen storage capacity properties of ceria and zirconia nanoparticles supported on alumina by the impregnation process. *J. Phys. Conf. Ser.* **2012**, *379*, 012014.

(3) Woo, T.G.; Cha, B.J.; Kim, Y.D.; Seo, H.O. Positive effects of impregnation of Fe-Oxide in mesoporous Al-Oxides on the decontamination of dimethyl methylphosphonate. *Catalysts* **2019**, *9*, 898.

(4) Younis, A.; Chu, D.; Li, S. Cerium oxide nanostructures and their applications. In "Functionalized Nanomaterials", InTech, London, **2016**.

(5) Scirè, S.; Palmisano, L. Cerium and cerium oxide: A brief introduction. *Cerium Oxide (CeO_2): Synthesis, properties and applications* **2020**, 1–12.

(6) Sun, L.; Xiao, W.; Hao, X.; Meng, Q.; Zhou, M. A first-principles study on the structural, thermal and electronic properties of cerium oxides by using different functional. *Electron. Struct.* **2019**, *1*, 015003.

(7) Supakanapitak, S.; Boonamnuayvitaya, V.; Jarudilokkul, S. Influence of the synthesis procedures on the properties of nano-sized ceria powders. *J. Chem. Eng. Jpn.* **2012**, *45*, 544–550.

(8) Tok, A.I.Y.; Boey, F.Y.C.; Dong, Z.; Sun, X.L. Hydrothermal synthesis of CeO_2 nano-particles. *J. Mater. Process Technol*. **2007**, *190*, 217–222.

(9) Chen, P.-L. & Chen, I.-W. Reactive cerium(IV) oxide powders by the homogeneous precipitation method. *J. Am. Ceram. Soc*. **1993**, *76*, 1577–1583.

(10) Souza, E. C. C. & Muccillo, E. N. S. Effect of solvent on physical properties of samaria-doped ceria prepared by homogeneous precipitation. *J. Alloys Compd.* **2009**, *473*, 560–566.

(11) Christensen, J. M.; Deiana, D.; Grunwaldt, J.-D., Jensen, A.D. Ceria prepared by flame spray pyrolysis as an efficient catalyst for oxidation of diesel soot. *Catal. Lett*. **2014**, *144*, 1661–1666.

(12) Chen, H.; Mulmudi, H.K.; Tricoli, A. Flame spray pyrolysis for the one-step fabrication of transition metal oxide films: Recent progress in electrochemical and photoelectrochemical water splitting. *Chin. Chem. Lett.* **2020**, *31*, 601–604.

(13) Wang, Y.; Li, P.; Tran, T.T.D.; Zhang, J.; Kong, L. Manufacturing techniques and surface engineering of polymer-based nanoparticles for targeted drug delivery to cancer. *Nanomaterials* **2016**, *6*, 26.

(14) Gu, F., Wang, Z., Han, D., Shi, C. & Guo, G. Reverse micelles directed synthesis of mesoporous ceria nanostructures. *Mater. Sci. Eng. B* **2007**, *139*, 62–68.

(15) Carregosa, J.D.C.; Grilo, J.P.F.; Godoi, G.S.; Macedo, D.A.; Nascimento, R.M.; Oliveira, R.M.P.B. Microwave-assisted hydrothermal synthesis of ceria (CeO_2): Microstructure, sinterability and electrical properties. *Ceram. Int*. **2020**, *46*, 23271–23275.

Batch and Flow Synthesis of CeO_2 Nanomaterials Using Solid-State Microwave Generators

Cristina Rodríguez-Carrillo[1], Juan Torres García[1], Miriam Benítez[1], Jamal El Haskouri[2], Pedro Amorós[2] and Jose V. Ros-Lis[1,*]

[1]Departamento de Química Inorgánica, Universitat de València, Doctor Moliner 50, P.O. Box 73, 46100 Butjassot, Spain

cristina.rodriguez-carrillo@uv.es (C.R.-C.); juan.torres-garcia@uv.es (J.T.G.); miriam.benitez@uv.es (M.B.)

[2]Institut de Ciència dels Materials, Universitat de València, P.O. Box 22085, 46071 Valencia, Spain

jamal.haskouri@uv.es (J.E.H.); pedro.amoros@uv.es (P.A.)

*Correspondence: j.vicente.ros@uv.es; Tel.: +34-963544856

Molecules **2022**, *27(9)*, 2712

DOI: 10.3390/molecules27092712

Received: 4 March 2022, Accepted: 20 April 2022

Published: 22 April 2022

Abstract

Microwave-assisted synthesis in combination with flow synthesis offers an interesting approach to develop faster and more sustainable procedures for the preparation of homogeneous nanomaterials. Recently, solid-state generators of microwaves appeared as a tool with improved control over power and frequency. Cerium oxide, despite its excellent catalytic activity, has not been prepared before using solid-state generators or microwave-assisted flow chemistry. We report a procedure for the preparation of nanoparticulated CeO_2 (around 4 nm) under 2.45 GHz microwaves in only 30 s. The materials are further calcined at 800 °C to increase particle size, with a better-defined particle size and crystallinity. The procedure was tested in batch at pH 11 and 12 and diverse potencies, and the products were characterized by TEM, XRD, DLS, and N_2 adsorption–desorption isotherms. The materials were similar at the diverse pH values and potencies. XRD confirms the crystallinity of the CeO_2 material with a fluorite-like structure. They are composed of particles around 40 nm that aggregate as structures of around 100 nm. The procedure was successfully adapted to flow synthesis, obtaining materials with structure and properties equivalent to batch synthesis. The batch and flow materials offer peroxidase properties, opening the door for their use as ROS scavengers.

Keywords: CeO_2; nanoparticle; microwave-assisted synthesis; solid-state generator; flow chemistry

1. INTRODUCTION

Nanomaterials have attracted broad attention in recent decades due to their high surface/volume ratio and novel properties derived from nanoscale. Among them, nanoscopic cerium oxide offers interesting catalytic properties due to the unique electronic configuration of the lanthanide atom, the reduction potentials, the reversible conversion between the oxidation states of Ce^{3+} and Ce^{4+}, and its oxygen buffering capacity. The close thermodynamic stability of CeO_2 and Ce_2O_3 favors an easy and reversible transition between these two compounds, giving rise to a range of partially reduced CeO_{2-x} phases that serve as oxygen reservoirs by creating or eliminating oxygen vacancies. The use of ceria has been explored in hydrogen production,[1] as an oxygen capacitator in automotive three-way catalysts,[2] as a chemosensor and photocatalyst,[3–5] and in ion conducting membranes.[6]

Reactive oxygen species (ROS) include compounds such as singlet oxygen, superoxide, hydrogen peroxide, and hydroxyl radical. Although these substances are naturally produced in cells as a consequence of oxidation metabolism in the mitochondria, they are highly reactive and potentially harmful to living organisms. An excess of ROS induces oxidative stress, damages biomolecules such as proteins, lipids, and nucleic acids, and finally induces apoptosis. Thus, living organisms limit the concentration of ROS at a cellular level by producing enzymes (for example, superoxide dismutase, glutathione peroxidase or catalase) or antioxidants.[7] Recently, in biological applications, CeOx was explored as a scavenger of reactive oxygen species, mimicking diverse enzymatic reactions.[8]

Microwaves (MWs) are a source of electromagnetic radiation lying between infrared and radiofrequencies that have shown interesting properties in chemical reactions. In comparison with conventional synthesis, MWs offer a higher synthesis rate and shorter reaction times (typically reduces the reaction time from hours to minutes), more homogeneous products, smaller particle size, narrower particle size distribution, higher purity, higher yields due to minimization of side products, selective heating, lower power consumption (environmentally friendly), etc.[9] Considering these advantages, it is not surprising that microwaves have been used previously for the synthesis of cerium oxide. Depending on the reagents and the synthesis conditions, the size and shape of the materials vary. They have been prepared as aggregates of particles in the nanometric to micrometric range in less than 1 h of irradiation.[10,11] They could be prepared even as 2 nm particles in the presence of PEG in only 10 min.[12] Other shapes include nanorods/nanowires[13,14] or microplates through the calcination of $Ce(OH)CO_3$.[15] Further advances in the microwave-assisted synthesis of ceria include the preparation of a mesoporous material departing from a CMK-3 carbon structure as a template[16] or the preparation of mixed oxides such as $Ce_xSm_{1-x}O_2$.[17] In all cases, the materials were prepared in batch using magnetrons as a source of microwave energy.

Despite all the advantages mentioned in the previous paragraph, conventional microwave-assisted procedures of synthesis based on the use of magnetrons as an energy source offer some restrictions. The combination of solid-state microwave generators with flow synthesis offers an interesting approach to overcome such restrictions. Solid-state generators offer greater simplicity in

the implementation and power management, with a longer duration of the power source in comparison to magnetrons.[18] On the other hand, one of the main limiting factors of microwave application is the small amount of material obtained in each batch due to the MW properties and the design of the reactors. The use of flow synthesis strategies can allow achieving large amounts of product as the materials are produced continuously.[19] So far, neither of the two strategies (the use of solid-state generators or flow synthesis) has been applied for the preparation of nanomaterials based on cerium oxide. In this work, the possibilities offered by batch and flow synthesis using solid-state microwave generators for the preparation of nanoscale cerium oxide were evaluated. Considering the possibility of using CeO_2 as a nanozyme with ROS-scavenging properties, the peroxidase activity was evaluated and verified.

2. RESULTS AND DISCUSSION

2.1. Synthesis Procedure

The synthesis was carried out using static (batch) and dynamic (flow) reactors powered by microwave solid-state generators (see Scheme 1). In batch, diverse values of pH, power, and irradiation time were tested (see Table 1). The notation used for the materials was B or F depending on whether the synthesis was in batch or flux, 11 or 12 as a function of the pH, and L, M, or H for low (50 W), medium (100 W), or high (200 W) power. NC was added before the name for the non-calcined materials.

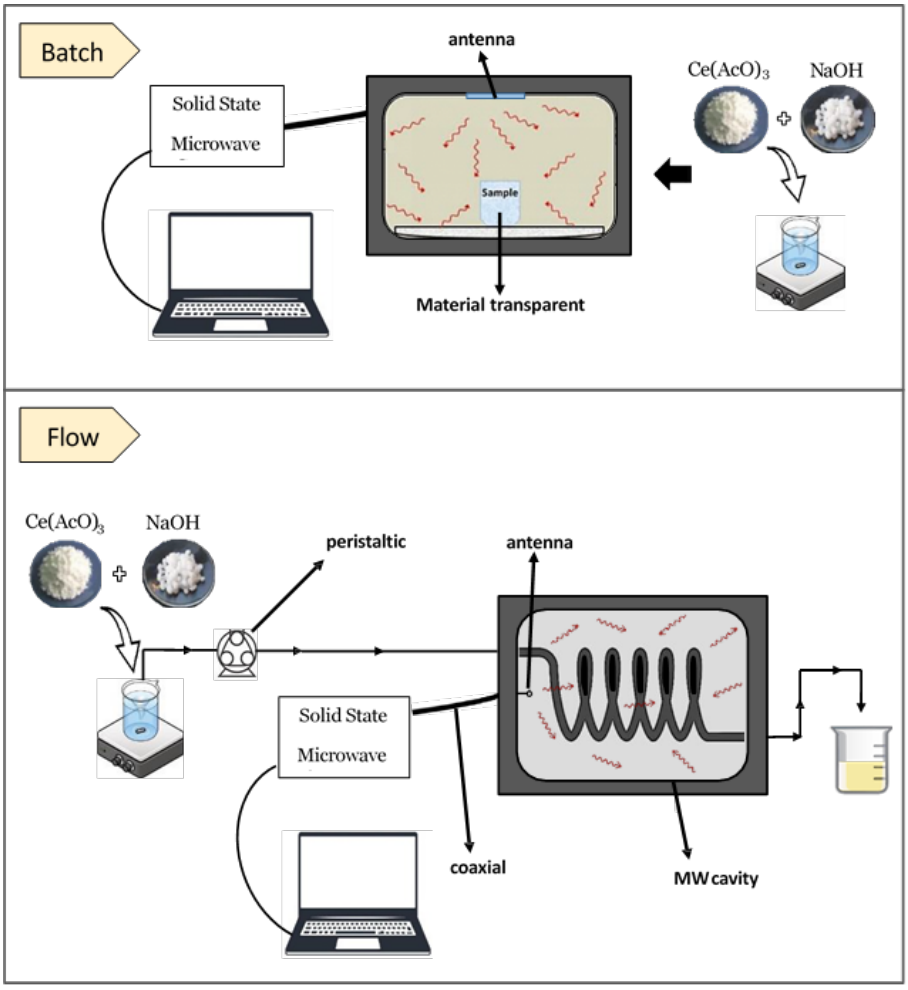

Scheme 1. *Scheme describing the setup for the synthesis in batch and flow.*

The solid-state generator allowed us to tune finely the power. In all cases, the temperature of the solution reached temperatures around 90 °C. As expected, when the power is increased, the time necessary to reach this temperature is reduced. To our knowledge, 30 s is the shortest time reported for CeO_2 synthesis in solution.[10–15] Considering the nominal power and irradiation time and the temperature reached by the solution, approximately 50% of the

energy delivered by the solid-state source is transformed into heat in the solution. Part of the energy returns to the solid-state microwave generator and is dissipated as heat in the energy source. The percentage increases when the time is reduced in agreement with a lower heat transfer to the reaction flask and the preferential heating of the water in comparison with glass under microwave irradiation.[20] In agreement with the resemblance in the composition, the dielectric properties of the solutions and, therefore, the absorption of microwaves were similar at pH 11 and 12.

***Table 1**. Summary of synthesis conditions.*

Material	Reactor	pH	Power (W)	Time (min)
B11L	Batch	11	50	2:30
B11M	Batch	11	100	1:00
B11H	Batch	11	200	0:30
B12L	Batch	12	50	2:30
B12M	Batch	12	100	1:00
B12H	Batch	12	200	0:30
NCB12H[1]	Batch	12	200	0:30
F12H	Flow	12	200	0:30
NCF12H[1]	Flow	12	200	0:30

[1] Non-calcined materials.

Furthermore, a non-calcined material prepared at pH 12 with irradiation at 200 W for 30 s was dried and collected to evaluate the effect of the calcination in the structure and morphology of the cerium oxide (NCB12H). Regarding flow synthesis, in agreement with the similarity of the materials obtained in batch at diverse synthesis conditions (see below), the fastest synthesis at pH 12 was selected. The properties of the material prepared in batch and flow

synthesis were characterized by X-ray diffraction (XRD), transmission electron microscopy (TEM), dynamic light scattering (DLS), and N_2 adsorption–desorption isotherms. Additionally, the as-made materials were characterized to evaluate the effect of calcination at 800 °C.

2.2. Crystallinity of the Materials

XRD was used to determine the chemical structure of the materials obtained during the synthesis. As can be seen in Figure 1a, the peak assignment of the B11M diffractogram corresponded to typical CeO_2 in a cubic fluorite-like structure. The most intense peaks at 2θ values of 28.7°, 47.6°, and 56.5° could be assigned to the (111), (220), and (311) hkl planes, respectively, with a cell parameter of a = 5.403 Å. No peak corresponding to Ce_2O_3 was found. The XRD of the remaining materials showed peaks in the same position and with similar full width at half maximum (FWHM) (Figure 1b), indicating that, under our experimental conditions, the phase formed and crystallinity of the materials were similar.

The yellow material obtained directly from the microwave NCB12H (dried but not treated at 800°C) was also characterized, revealing the peaks characteristic of CeO_2 (Figure 1a). This result suggests that a fast treatment in the microwave is enough to obtain Ce(IV) oxide material with a crystalline structure. However, the full width at half maximum was significantly higher than in the case of the calcined materials, suggesting a lower crystallinity or lower particle size. In the case of the material prepared under flow conditions, XRD peaks were in the same positions with the same relative intensity as the

materials prepared in batch. This result confirms that flow synthesis can be applied for the preparation of CeO_2 nanomaterials.

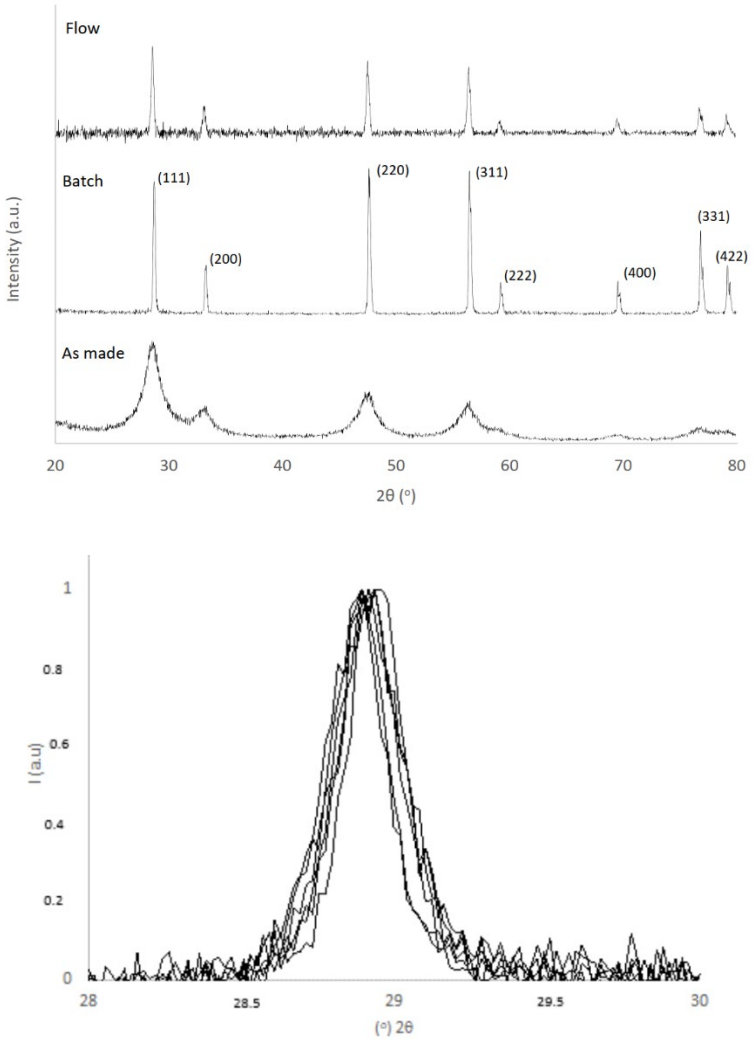

Figure 1. *XRD studies. (a) XRD of B11M, with the hkl index of each plane indicated between brackets; (b) detailed XRD 111 peak of the six batch materials (BXXX) prepared under batch conditions, with the peaks normalized for comparison purposes.*

2.3. Particle Size and Morphology

TEM analysis was used to determine the morphology and organization of the particles. As can be seen in Figure 2, in the batch (Figure 2a) and flow synthesis (Figure 2b) regimes, we obtained individual particles together with aggregates, even after applying ultrasound to disaggregate the material. It seems that the particles tended to aggregate during the synthesis in solution and filtration, and the aggregates were consolidated during calcination at high temperature (800 °C) over several hours. At higher magnification, TEM images illustrate that the materials prepared under batch conditions BXXX (Figure 2c–h) were similar. They were composed of nanometric CeO_2 particles with irregular shapes (from spherical to cubic). Measurements of particle size show that the materials were composed of particles around 40 nm, and a distribution in the range of 20 to 60 nm could be found (see Table 2).

***Table 2**. Measurement of particle size using TEM photographs.*

Material[1]	n[2]	Particle Size (x ± SD nm)	Particle Size Median (nm)
B11L[a]	146	45 ± 14	44.3
B11M[a]	158	43 ± 15	42.0
B11H[a]	78	46 ± 15	43.6
B12L[b]	117	30 ± 10	28.4
B12M[c]	107	40 ± 20	33.3
B12H[c]	159	37 ± 11	35.8
F12H[b,c]	80	34 ± 15	32.3

[1] Formation of groups using the Kruskal–Wallis test (p = 0.05), where the same letter indicates the same group.
[2] Number of particles measured.

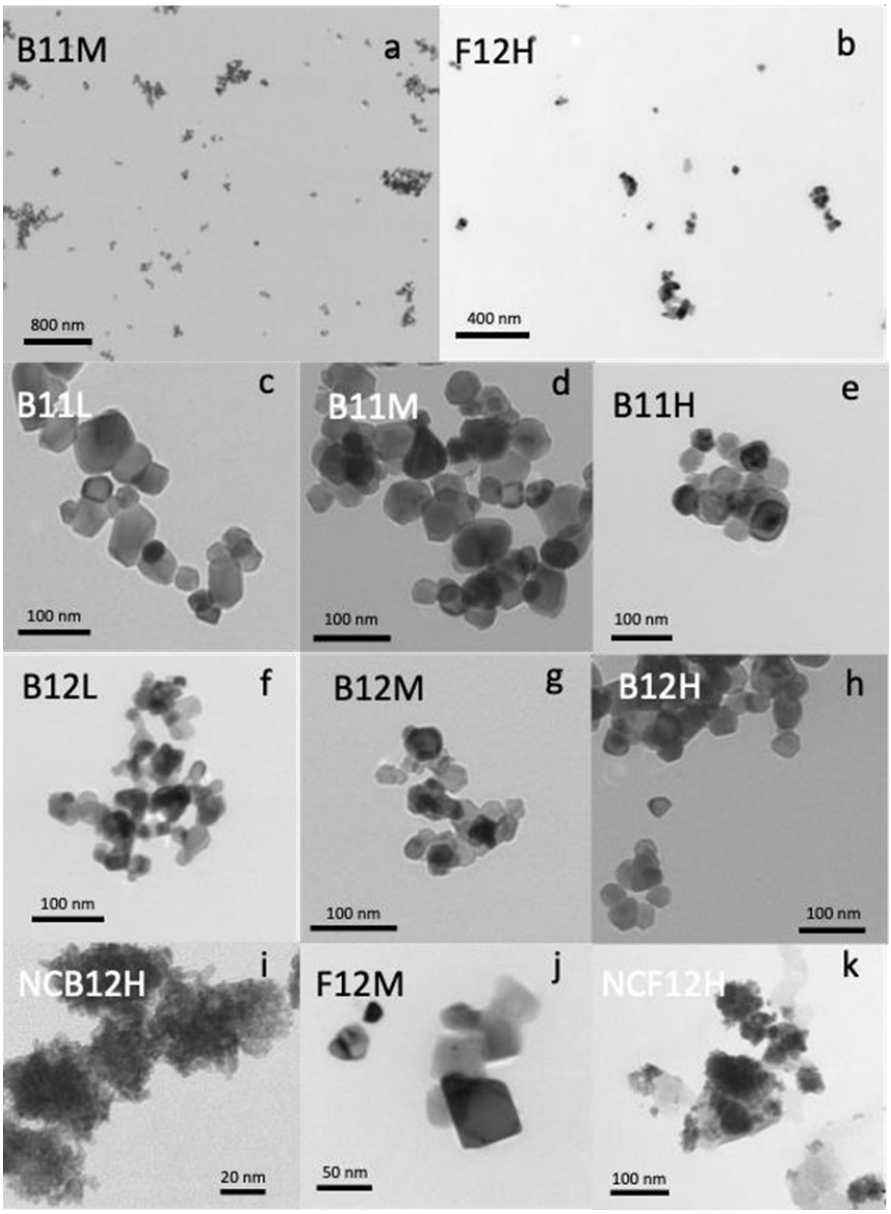

Figure 2. *TEM images of the CeO_2 materials: (a) general view of B11M, (b) F12H, (c) B11L, (d) B11M, (e) B11H, (f) B12L, (g) B12M, (h) B12H, (i) NCB12H, (j) F12H, and (k) NCF12H. B (batch); F (flow); 11 or 12 indicates the pH; L, M, or H for low (50 W), medium (100 W), or high (200 W) power. NC is added before the name for the non-calcined materials.*

The shape and size of the particles were similar to the values reported in microwave-assisted synthesis using magnetrons.[10,11] To evaluate if the variation in the synthesis conditions was able to induce significant differences in the particle size, the particle size distribution was analyzed with statistical tools. The particle distribution did not follow a normal distribution; thus, the Kruskal–Wallis test was applied. In this case, the main differences were observed upon variation of the pH. At a lower pH (11), the particles were statistically bigger than at pH 12; thus, a growth of the particles was observed. Power offered only a minor effect; however, at 50 W and pH 12, it was observed that the particles were smaller in comparison with the irradiation at higher power.

In studying the size and morphology of the material prepared under flow synthesis in comparison with batch conditions, TEM imaging showed a morphology and size similar to the materials prepared in batch (Figure 2j). Data analysis of the particle size distribution revealed that the material was assigned to the same group as the batch materials prepared at pH 12; thus, we were able to reproduce batch synthesis under flow conditions.

Regarding the effect of the calcination step on the morphology of the material, by contrast to the calcined materials that offered defined dense particles, the material obtained directly from the microwave reactor was mainly composed of smaller nanoparticles (ca. 4 nm) (Figure 2i,k). These primary nanoparticles were consolidated during the treatment at high temperature to form the final particles. In agreement with the data obtained from XRD, the non-calcined material was crystalline in nature. Since a reduced crystal size could explain the wide XRD signal observed, the Scherrer equation was applied to evaluate

the crystallite size from the full width at half maximum of the XRD peaks. A crystallite size of 4.9 was calculated. Although a particle can be formed by several crystals, in our case, the fact that the size of the crystallites determined from the XRD data and the application of the Scherrer equation was similar to the size of the nanoparticles observed by TEM suggests that, under our preparative conditions, a very fast nucleation step occurred, generating crystalline ceria from the beginning of the process. As expected, under relatively homogeneous conditions with rapid heating under microwave, the initial steps in the formation of materials from molecular sources consisted of the formation of small primary nanoparticles (ca. 4 nm and even some smaller), which grew by aggregation/coalescence and evolved to larger crystalline nanoparticles when subsequent calcination treatments were applied.

The textural porosity formed by the aggregation of the little particles was also confirmed by N_2 gas adsorption (see Supplementary Figure S1). In the case of the material NCB12H, an area of 144 m^2g^{-1} was found, in agreement with the presence of a textural porosity due to the 4 nm particles observed in TEM. The N_2 adsorption–desorption isotherm of the NCB12H sample showed a gradual nitrogen adsorption over the entire pressure range. The application of the Barrett–Joyner–Halenda model (BJH) model allowed determining a pore volume of 0.1 cm^3g^{-1}. However, there were no well-defined pores. As mentioned before, the porosity (irregular) at both the micro- and the mesoscopic scales of a textural type was related to the voids between the primary nanoparticles. The nanoparticle aggregates observed through TEM for the non-calcined sample usually generated some cage-like pores that were

responsible for the hysteresis loop observed in the isotherm. On the contrary, when the material was calcined, the specific surface was drastically reduced to 0.11 m^2g^{-1}, confirming the complete loss of textural-type porosity. Thus, in the calcined material, the low measured area was due solely to the outer surface of isolated or poorly aggregated crystalline nanoparticles.

The particle size was also determined through DLS. This technique measures a wide number of particles and informs us about the degree of aggregation and the size of the aggregates in solution. As can be seen in Figure 3, B11M exhibited a peak in the number of particles around 122 nm (other peaks could be calculated in the deconvolution at 173 nm), while B12M exhibited a peak at 91 nm (with a tail calculated by deconvolution at 137 nm).

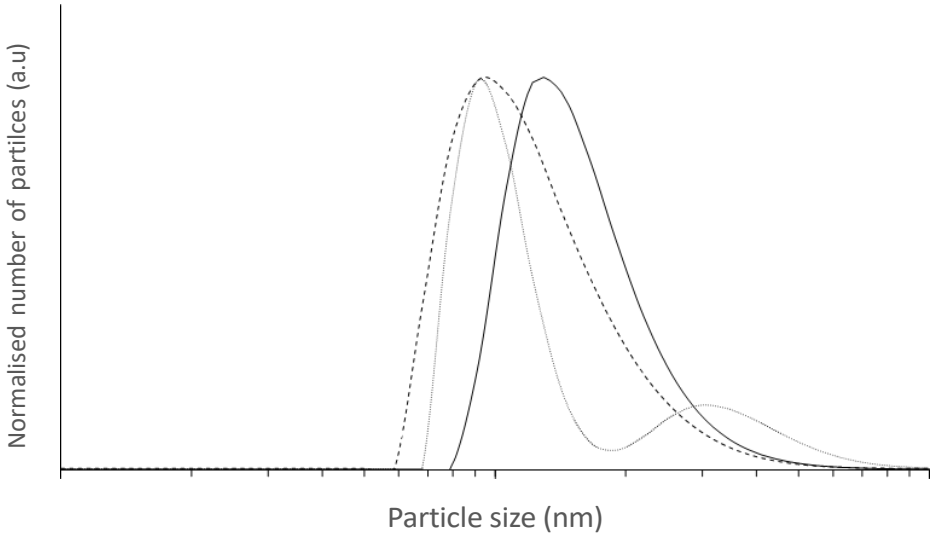

***Figure 3**. Dynamic light scattering spectra: B11M, straight line; B12M, dashed line; F12H, dotted line.*

Conversely, F12H offered two peaks at 91 nm and 314 nm. In agreement with TEM, at pH 12, the particles offered a lower size than at pH 11, and the change in the particle size at both pH values measured with DLS was proportional to the values measured with TEM. In the case of F12H, in addition to the peak at 91 nm found for the batch synthesis, a peak at larger size (314 nm) was also identified, indicating a higher aggregation possibly due to synthesis conditions in the flow reactor. DLS measured a greater hydrodynamic radius than measured with TEM; however, in this case, the wide difference suggests that the material could have been formed by a relevant number of little aggregates conformed by few particles. In any case, the resulting material remained in the nanometric range, well below 1 µm.

2.4. ROS Scavenging Properties

As noted above, cerium oxide offers interesting redox properties that have been used for catalytic application. In our case, we were interested in the ROS-scavenging properties with future biological applications in mind. We studied the peroxidase activity of the materials prepared under batch and flow conditions (Figure 4). The peroxidase-like activities of the materials were studied by the catalytic oxidation tests toward 3,3',5,5'–tetramethylbenzidine (TMB) with the assistance of H_2O_2. Upon oxidation, TMB develops a blue color; thus, higher absorbances correspond to higher peroxidase activity. In our case, we found a reaction rate of approximately 8×10^{-3} min^{-1}. The equivalent activity found for the materials prepared under batch and flow conditions was in agreement with the similarities found for both type of materials during the characterization, confirming that our flow synthesis strategy allowed us to obtain cerium oxide materials with properties similar to batch synthesis.

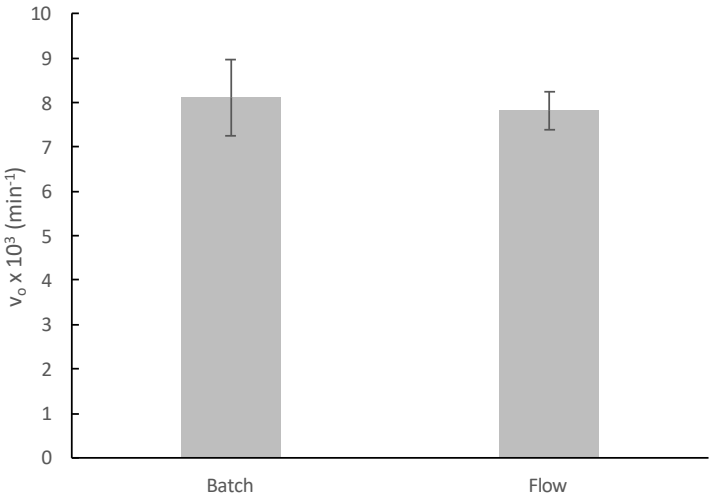

Figure 4. *Peroxidase activity of the CeO_2 materials.*

2.5. Energy Efficiency

Currently, there is a strong tendency toward the development of synthesis processes that are more sustainable and have a lower carbon footprint. One of the advantages of microwaves is the significant reduction in the reaction time. In comparison with a conventional microwave reactor, solid-state microwave generators allow the modulation of power and frequency. A low reaction time, together with the use of low potencies, affords a synthesis process with very low energy consumption. In our case, the reaction time was only 30 s. This procedure is much faster than other microwave-assisted processes previously reported in the literature and conventional methods. The energy consumed in our case was 0.010 kWh (7 g equivalent of CO_2) per synthesis and 0.14 $W{\cdot}h{\cdot}mg^{-1}$ (98 mg equivalent of CO_2 per mg of CeO_2). This amount is almost two orders of magnitude lower than the 0.55 kWh (392 g

equivalent of CO_2) used by an 800 W magnetron in 30 min, conditions found in previously reported procedures.[11]

3. MATERIALS AND METHODS

3.1. Chemicals

Cerium (III) acetate hydrate ($Ce(CH_3CO_2)_3 \cdot xH_2O$), 99% metal basis (Sigma-Aldrich, St. Louis, MO, USA), sodium hydroxide (NaOH) >98% (Sigma-Aldrich), and hydrochloric acid solution 1 N (Scharlau, Barcelona, Spain) were used to synthesize the nanoparticles of this work. Water used in this investigation was deionized. Hydrogen peroxide (H_2O_2) 35% (Panreac) and 3,3t,5,5t-tetramethylbenzidine (TMB) (Sigma-Aldrich, St. Louis, MO, USA) were used to determine peroxidase activity.

3.2. Synthesis of the CeO_2 Nanomaterials

The reaction was performed in a microwave reactor purchased from Microbiotech (Valencia, Spain). It consists of a microwave chamber equipped with a 200 W solid-state generator at 2.45 GHz. For batch synthesis, 0.95 g of cerium acetate and 0.48 g of sodium hydroxide (1:4 molar ratio) were dissolved in 50 mL of deionized water, and the pH was adjusted to 11 or 12, depending on the material. Right after, 10 mL was transferred to a microwave glass vial that was placed in the microwave oven with the power set at 50, 100, or 200 W. Irradiation times were established at 0.5, 1.5, or 2.5 min for 200, 100, or 50 W, respectively. The resulting yellow precipitate was washed with water and ethanol to neutral pH. Drying and calcination were performed in a conventional furnace. For drying, the oven was preheated at 80 °C before

its use and maintained overnight. The furnace for calcination was set with a heating ramp at 20 °C min^{-1} up to 800 °C. The temperature was maintained for 6 h and allowed to cool down until room temperature. The samples remained inside the furnace throughout the calcination process.

In flow synthesis, 4 g of $Ce(AcO)_3$ and 2 g of NaOH were dissolved in 200 mL of deionized water with a pH of 12. The mixture was pumped into the microwave oven, so that the sample was irradiated for 30 s at 200W. The resulting yellow precipitate was washed with water and ethanol to neutral pH. Lastly, the solid was dried overnight at 80°C and calcined at 800°C for 6 h.

3.3. Characterization of the Materials

The powder X-ray diffraction pattern of the nanoparticles was obtained using a powder X-ray Diffractometer (Avance A25, Bruker Cooperation, Billerica, MA, USA). The sample was scanned over the required range for 2θ values (10–80°). The size and shape of nanoparticles was obtained by transmission electron microscopy (TEM) using a HITACHI HT7800 120 KV. The particle size analysis for the sample was carried out using the particle size analyzer Zetasizer nano series of Malvern Instruments. Nitrogen adsorption–desorption isotherms were recorded in an automated Micromeritics ASAP2010 instrument. Prior to the adsorption measurements, the samples were outgassed in situ in vacuum (10^{-6} Torr) at 110°C for 15 h to remove adsorbed gases. The specific surface area was determined by applying the Brunauer–Emmett–Teller (BET model) from the adsorption data within the low-pressure range. Pore volume was calculated following the Barrett–

Joyner–Halenda model (BJH). The UV/visible spectrum for peroxidase activity was obtained using a Jasco V-770 spectrophotometer.

3.4. Determination of the Peroxidase Activity

The peroxidase activity was measured by mixing the material, H_2O_2, and TMB, and the change in color was determined in the UV/visible absorption range following Cao's protocol.[21] Briefly, 70 µL of 1.0 mg mL^{-1} CeO_2 material was added to 400 µL of 50.0 mM phosphate buffer (pH = 4.0) at room temperature, followed by the addition of 100 µL of 8.0 mM TMB, 100 µL of 25.0 mM H_2O_2, and 330 µL of Milli-Q water. Subsequently, the reaction solutions were incubated at room temperature for 7 min. Afterward, the UV/visible absorption at 652 nm was measured using a Jasco V-770 spectrophotometer.

3.5. Data Analysis

The Scherrer equation was used for the calculation of the XRD crystals. It relates the size of crystallites to the broadening of a peak in a diffraction pattern using K = 0.9.[22] Statistical analysis was performed using the SPSS software. The comparison of the particle size was performed using the independent-sample Kruskal–Wallis test at a significance level of 0.05. The significance values were adjusted by Bonferroni correction for multiple tests. The conversion of kWh to g of CO_2 was calculated using the Avoided Emissions and Generation Tool (AVERT) of the Environmental Protection Agency (EPA).[23]

4. CONCLUSIONS

We validated the viability of using a solid-state microwave generator for the synthesis of cerium oxide. This technology can be applied in batch or in flow synthesis. The flow microwave-assisted synthesis of CeO_2 has not been previously reported. The materials prepared under microwave irradiation showed a typical fluorite-like structure and were formed by 4 nm particles. After calcination at 800°C, the particles grew to the 30–45 nm range with better defined shape and improved crystallinity, which aggregated in conglomerates of 80–300 nm. Variations in the power/time did not significantly affect the size and structure of the materials. Flow synthesis was able to reproduce the particle size, morphology, crystallinity, and peroxidase activity of the materials prepared using the batch synthesis procedure. By contrast, when the pH was reduced from 12 to 11, a slight growth in the particle size was observed. The materials offered equal peroxidase activity when prepared under batch and flow conditions. These results open the door toward a wider use of solid-state generators in the synthesis of materials and confirm their potential of preparing ceria.

Supplementary Materials: The following supporting information can be downloaded at: https://www.mdpi.com/article/10.3390/molecules27092712/s1, Figure S1: N_2 adsorption-desorption isotherms of the material NCB12H.

Author Contributions: C.R.-C., J.T.G., M.B., J.E.H., P.A. and J.V.R.-L. have participated in the conceptualization, investigation and writing of the manuscript. All authors have read and agreed to the published version of the manuscript.

Funding: This research was funded by the Spanish Ministerio de Ciencia, Innovación y Universidades, grant number RTI2018-100910-B-C44, by MCIN/AEI/10.13039/501100011033, by "ERDF A way of making Europe", and by the Generalitat Valenciana (FEDEGENT/2020/006 and APOTIP/2021/017).

Institutional Review Board Statement: Not applicable.

Informed Consent Statement: Not applicable.

Data Availability Statement: Not applicable.

Conflicts of Interest: The authors declare no conflict of interest. The funders had no role in the design of the study; in the collection, analyses, or interpretation of data; in the writing of the manuscript, or in the decision to publish the results.

References

(1) Bêche, E.; Charvin, P.; Perarnau, D.; Abanades, S.; Flamant, G. Ce 3d XPS investigation of cerium oxides and mixed cerium oxide (CexTiyOz). *Surf. Interf. Anal.* **2008**, *40*, 264–267.

(2) Mullins, D.R. The surface chemistry of cerium oxide. *Surf. Sci. Rep.* **2015**, *70*, 42–85.

(3) Khan, S.B.; Faisal, M.; Rahman, M.M.; Jamal, A. Exploration of CeO_2 nanoparticles as a chemisensor and photocatalyst for environmental applications. *Sci. Total Env.* **2011**, *409*, 2987–2992.

(4) Beie, H.J.; Gnörich, A. Oxygen gas sensors based on CeO_2 thick and thin films. *Sens. Act. B Chem.* **1991**, *4*, 393–399.

(5) Jasinski, P.; Suzuki, T.; Anderson, H.U. Nanocrystalline undoped ceria oxygen sensor. *Sens. Act. B Chem.* **2003**, *95*, 73–77.

(6) Tschöpe, A. Interface defect chemistry and effective conductivity in polycrystalline cerium oxide. *J. Electroceramics* **2005**, *14*, 5–23.

(7) Wu, H.; Yin, J.-J.; Wamer, W.C.; Zeng, M.; Martin, Y. Reactive oxygen species-related activities of nano-iron metal and nano-iron oxides. *J. Food Drug Anal.* **2014**, *22*, 86–94.

(8) Song, G.; Cheng, N.; Zhang, J.; Huang, H.; Yuan, Y.; He, X.; Luo, Y.; Huang, K. Nanoscale Cerium Oxide: Synthesis, Biocatalytic Mechanism, and Applications. *Catalysts* **2021**, *11*, 1123.

(9) Díaz de Greñu, B.; Torres, J.; García-González, J.; Muñoz-Pina, S.S.; de los Reyes, R.; Costero, A.M.; Amorós, P.; Ros-Lis, J.V. Microwave-Assisted Synthesis of Covalent Organic Frameworks: A Review. *ChemSusChem* **2021**, *14*, 208–233.

(10) Prado-Gonjal, J.; Schmidt, R.; Espíndola-Canuto, J.; Ramos-Alvarez, P.; Morán, E. Increased ionic conductivity in microwave hydrothermally synthesized rare-earth doped ceria $Ce_{1-x}REx O_{2-(x/2)}$. *J. Power Sources* **2012**, *209*, 163–171.

(11) Kumar, E.; Selvarajan, P.; Muthuraj, D. Synthesis and characterization of CeO_2 nanocrystals by solvothermal route. *Mat. Res.* **2013**, *16*, 269–276.

(12) Liao, X.H.; Zhu, J.M.; Zhu, J.J.; Xu, J.Z.; Chen, H.Y. Preparation of monodispersed nanocrystalline CeO_2 powders by microwave irradiation. *Chem. Commun.* **2001**, *10*, 937–938.

(13) Phuruangrat, A.; Thongtem, S.; Thongtem, T. Microwave-assisted hydrothermal synthesis and characterization of CeO_2 nanowires for using as a photocatalytic material. *Mat. Lett.* **2017**, *196*, 61–63.

(14) Sun, C.; Li, H.; Zhang, H.; Wang, Z.; Chen, L. Controlled synthesis of CeO_2 nanorods by a solvothermal method. *Nanotechnology* **2005**, *16*, 1454.

(15) Riccardi, C.S.; Lima, R.C.; Dos Santos, M.L.; Bueno, P.R.; Varela, J.A.; Longo, E. Preparation of CeO_2 by a simple microwave– hydrothermal method. *Solid State Ion.* **2009**, *180*, 288–291.

(16) Roggenbuck, J.; Schäfer, H.; Tsoncheva, T.; Minchev, C.; Hanss, J.; Tiemann, M. Mesoporous CeO_2: Synthesis by nanocasting, characterisation and catalytic properties. *Microp. Mesop. Mat*. **2007**, *101*, 335–341.

(17) Polychronopoulou, K.; Zedan, A.F.; Katsiotis, M.S.; Baker, M.A.; AlKhoori, A.A.; AlQaradawi, S.Y.; AlHassan, S. Rapid microwave assisted sol-gel synthesis of CeO_2 and CexSm1-xO_2 nanoparticle catalysts for CO oxidation. *Molec. Catal.* **2017**, *428*, 41–55.

(18) Dinani, S.T.; Kubbutat, P.; Kulozik, U. Assessment of heating profiles in model food systems heated by different microwave generators: Solid-state (semiconductor) versus traditional magnetron technology. *Innov. Food Sci. Emer. Technol.* **2020**, *63*, 102376.

(19) Gupta, M.; Wong Wai Leong, E. "Microwave and Metals" John Willey & Sons, Hoboken, NJ, USA (**2007)**; ISBN: 978-0-470-82272-2.

(20) Britton, J.; Raston, C.L. Multi-step continuous-flow synthesis. *Chem. Soc. Rev.* **2017**, *46*, 1250–1271.

(21) Cao, W.; Ju, P.; Wang, Z.; Zhang, Y.; Zhai, X.; Jiang, F.; Sun, C. Colorimetric detection of H_2O_2 based on the enhanced peroxidase mimetic activity of nanoparticles decorated $Ce_2(WO_4)_3$ nanosheets. *Spectrochim. Acta A Mol. Biomol. Spectr.* **2020**, *239*, 118499.

(22) Scherrer, P. Estimation of the size and internal structure of colloidal particles by means of rontgen rays. *Nachr. Ges. Wiss. Gott.* **1918**, *2*, 96–100.

(23) Environmental Protection Agency. AVERT, U.S. National Weighted Average CO_2 Marginal Emission Rate, Year **2019** Data; U.S. Environmental Protection Agency: Washington, DC, USA, **2020**.

ELECTRONIC SUPPLEMENTARY MATERIAL

Batch and Flow Synthesis of CeO_2 Nanomaterials Using Solid-State Microwave Generators

Cristina Rodríguez-Carrillo[1], Juan Torres García[1], Miriam Benítez[1], Jamal El Haskouri[2], Pedro Amorós[2] and Jose V. Ros-Lis[1,*]

ELECTRONIC SUPPLEMENTARY MATERIAL

Batch and Flow Synthesis of CeO_2 Nanomaterials Using Solid-State Microwave Generators

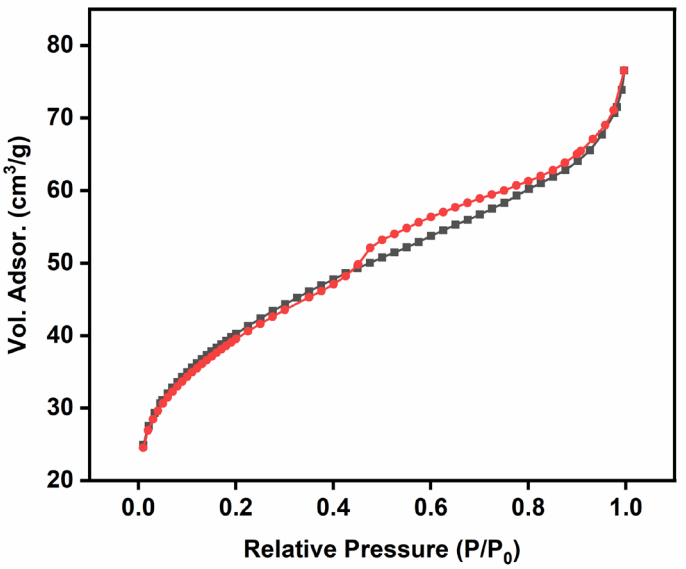

***Figure S1**: N_2 adsorption-desorption isotherms of the material NCB12H*

Final Conclusions

In conclusion, solid-state microwave generators have proven to be highly effective tools for the synthesis of mesoporous silica UVM-7. Furthermore, it has been demonstrated that these generators can also be employed in the synthesis of other mesoporous silica materials. This was evidenced by the successful and efficient synthesis of MCM-41, a material that had not previously been synthesized using this type of microwave generator. This finding broadens the applicability of solid-state microwave technology across a wider range of mesoporous materials, underscoring its versatility in materials science.

Additionally, the successful scale-up of UVM-7 synthesis under both batch and continuous flow conditions highlights the remarkable efficiency of these generators for producing large quantities of material within short timeframes. In less than one hour, it is possible to synthesize precursor material for over 150 grams of calcined UVM-7 and functionalize up to 60 grams. Moreover, approximately 35 grams of Ti-UVM-7 and Ce-UVM-7 were obtained in just 10 minutes, further demonstrating the speed and effectiveness of solid-state microwave technology for large-scale production of functionalized mesoporous materials.

Life cycle analysis of all the synthesized materials revealed a substantial reduction in environmental impact when scaled up. Specifically, there was up to a fivefold decrease in CO_2-equivalent emissions compared to small-scale synthesis and a reduction of up to 50% compared to conventional synthesis methods. These results not only validate the efficiency of microwave-assisted

synthesis and functionalization but also highlight its potential to significantly enhance the sustainability of industrial manufacturing processes.

One of the most significant contributions of this research has been the discovery of the ultraviolet (UV) absorption capabilities of the synthesized materials, revealing their potential use in cosmetic formulations such as sunscreens. To assess this, sun protection factor (SPF) measurements were conducted. The results were particularly promising: CeO_2 incorporated into UVM-7 reached an SPF of up to 69 with only 20% loading, outperforming pure CeO_2 and optimizing UV absorption without compromising transparency. This finding is especially relevant for the development of advanced, efficient sunscreen formulations. Similarly, TiO_2 incorporated into UVM-7 achieved an SPF of up to 2.4 with 10% loading, showing high efficiency relative to its titanium content. These outcomes demonstrate the potential of the synthesized materials in UV-blocking applications, significantly expanding their range of possible uses beyond catalysis and other industrial domains.

Peroxidase-like catalytic activity was also measured in Ce-UVM-7. Interestingly, samples with lower cerium content exhibited higher activity, with reaction rates of 23×10^{-3} and 27×10^{-3} min^{-1} under batch and flow conditions, respectively. This may be attributed to the reduced aggregation of CeO_2 in lower-concentration samples, which enhances the exposure of cerium atoms to reactants and thereby improves catalytic performance.

Another key milestone achieved in this work was the successful synthesis of cerium oxide (CeO_2) nanoparticles using solid-state microwave generators, including for the first time their synthesis under continuous flow conditions.

This not only demonstrates the versatility of solid-state microwave technology but also confirms, through comprehensive characterization, that the resulting materials retain both their crystalline structure and catalytic peroxidase-like activity. This validates microwave-assisted synthesis as a viable alternative to conventional methods, yielding functionally equivalent materials with potentially superior scalability and environmental profiles.

In summary, this research has made substantial progress in the development of fast, efficient, and sustainable methodologies for the production of advanced functional materials. It positions solid-state microwave heating as a powerful and scalable tool for the design and industrial-scale synthesis of high-value materials across multiple application domains.

Resumen de la tesis doctoral

Esta tesis doctoral sigue el formato de una compilación de artículos. Consta de una sección inicial, que presenta el marco general de la investigación y proporciona una introducción de la metodología que se va a utilizar. Posteriormente, se presentan una serie de capítulos relacionados con los artículos derivados de esta investigación. Cada capítulo comienza con una introducción al artículo correspondiente, explicando la motivación detrás del mismo. Luego, se incluyen los artículos en sí. En concreto, esta tesis comprende cuatro artículos de estudios empíricos que abordan los objetivos de esta investigación doctoral. Los resultados de estos estudios han sido difundidos en la comunidad académica mediante publicaciones en revistas científicas de prestigio.

OBJETIVOS

El objetivo principal de esta investigación es desarrollar y optimizar métodos de síntesis energéticamente eficientes para la producción de sílice mesoporosa UVM-7, pura o funcionalizada con cerio y titanio (UVM-7-Ce y UVM-7-Ti), utilizando tecnología de microondas en estado sólido, con un enfoque en la escalabilidad tanto en sistemas en batch como en flujo. Además, se busca extender estas metodologías a la síntesis de nanopartículas de CeO_2. A través de una investigación sistemática, la tesis explora nuevas metodologías para lograr una síntesis eficiente de materiales aprovechando las ventajas de la tecnología de microondas de estado sólido.

METODOLOGÍA

Síntesis: Antes de comenzar los experimentos, es imprescindible calibrar el microondas, con el fin de seleccionar las frecuencias más adecuadas que permitan maximizar la absorción de la radiación por la carga, evitando así pérdidas por reflexión en las paredes del reactor o el retorno de la energía hacia la antena. Para el escalado de síntesis asistida por microondas, se comienza con la selección de las condiciones óptimas para la síntesis a escala convencional utilizando microondas.

Una vez calibrado el sistema, se llevan a cabo diversos ensayos experimentales variando tanto los tiempos de irradiación como las potencias aplicadas. Tras una caracterización exhaustiva de los materiales obtenidos, se determinan las condiciones más adecuadas. A partir de estas, se inicia el proceso de escalado, comprobando que dichas condiciones se mantienen eficaces al aumentar el volumen de reacción. Es importante considerar que, a mayor volumen de carga, mayor debe ser la energía aplicada, por lo que se requiere un incremento en el tiempo y/o la potencia.

Para la síntesis en flujo, se mantiene constante la cantidad de energía aplicada, pero se incrementa considerablemente el volumen de reactivos. La mezcla se introduce mediante tubos conectados a una bomba peristáltica, que alimenta de forma continua el reactor en una configuración descendente, diseñada para evitar acumulaciones dentro del sistema. Se realizan pruebas a diferentes velocidades de bombeo, ya que esta determina el tiempo de irradiación efectivo de cada fracción. Finalmente, se recogen diversas alícuotas, que se

caracterizan verificando la homogeneidad del proceso o, en caso necesario, descartando las fracciones iniciales hasta alcanzar un régimen estacionario.

Las técnicas de caracterización utilizadas son:

- Difracción de rayos x de polvo: para determinar la estructura cristalina de los materiales.
- Microscopía de transmisión electrónica (TEM): genera imágenes de alta resolución de las partículas.
- Microanálisis de rayos X por energía dispersiva (EDX): para determinar la composición elemental del material.
- Adsorción de N_2: para determinar la porosidad y el área superficial de los materiales.
- Dispersión dinámica de luz (DLS): para determinar el tamaño hidrodinámico de los materiales.
- Potencial Z: para determinar la estabilidad mediante el estudio de la repulsión o atracción electrostática de las partículas.
- Análisis termogravimétrico: mediante el calentamiento de la muestra se determina la pérdida de masa de un material.

Capítulo 1

El primer capítulo de la tesis proporciona una introducción detallada haciendo especial hincapié en los generadores microondas, que son los equipos con los que se llevara a cabo la parte experimental del trabajo.

Nos enfocamos en las nanopartículas y nanomateriales. Su interés radica en sus propiedades únicas a escala nanométrica (1–100 nm), aunque este rango puede variar según el tipo de material. Se clasifican según su dimensionalidad (de 0D a 3D) y se pueden sintetizar mediante dos enfoques: top-down (reducción de materiales grandes) y bottom-up (construcción desde unidades pequeñas). Entre los métodos bottom-up, la síntesis asistida por microondas destaca por acelerar procesos clave y será el enfoque principal de esta tesis.

La radiación electromagnética transmite energía en forma de ondas a través del espacio y abarca un amplio espectro de frecuencias, desde ondas de radio hasta rayos gamma. Las microondas, que forman parte de este espectro, se ubican entre 300 MHz y 300 GHz. Las microondas se utilizan ampliamente en aplicaciones domésticas, industriales y científicas, especialmente en frecuencias específicas como 2.45 GHz, debido a su capacidad para interactuar eficazmente con moléculas polares como el agua, generando calor mediante fricción molecular.

La eficiencia del calentamiento por microondas depende de cómo interactúan estas con los materiales, lo cual está determinado por sus propiedades eléctricas. Materiales como metales reflejan microondas, otros como vidrio las transmiten, y los absorbentes, como el agua, las convierten en calor.

A diferencia del calentamiento convencional, las microondas calientan directamente el interior del material, acelerando los procesos y mejorando la eficiencia energética. Acelera el calentamiento de materiales, cuya síntesis convencional puede tardar días, y pueden obtenerse en minutos u horas con microondas.

Los generadores de microondas se dividen en dos tipos:

- Dispositivos electro-vacío: Usan tubos de vacío para generar o amplificar microondas, como magnetrones (domésticos) y gyrotrones (industriales).
- Dispositivos de estado sólido: Utilizan materiales semiconductores.

Los hornos de microondas domésticos usan generadores magnetrón, que producen microondas de alta potencia con frecuencia fija, pero tienen limitaciones como patrones de calefacción impredecibles. Los generadores de estado sólido permiten un control preciso de la potencia y la frecuencia, ofreciendo un calentamiento más uniforme y eficiente.

En cuanto a la escalabilidad de los procesos, la transición de laboratorio a escala industrial enfrenta desafíos como gradientes de temperatura y mezcla. Los enfoques para superar estos problemas incluyen el uso de reactores más grandes y procedimientos continuos, que permiten un control más preciso y eficiente. El uso de microondas en la síntesis industrial mejora la eficiencia energética y ofrece ventajas medioambientales y sostenibilidad.

Capítulo 2

El Capítulo 2 expone los principales objetivos de esta investigación, centrándose en el desarrollo y la optimización de métodos de síntesis escalables y energéticamente eficientes para la producción de sílice mesoporosa, ya sea pura o funcionalizada, utilizando tecnología de microondas en estado sólido. Además, se busca extender estos métodos a la síntesis de nanopartículas de CeO_2.

Capítulo 3

El Capítulo 3 explora la síntesis y producción a gran escala de la UVM-7, basándose en metodologías previamente exitosas para su preparación y funcionalización.

Los resultados obtenidos están publicados en el siguiente artículo: “Scaled-up microwave-assisted batch and flow synthesis and life cycle assessment of a silica mesoporous material: UVM-7”, con referencia: Benítez, M.; Rodríguez-Carrillo, C.; Sánchez-Artero, S.; El Haskouri, J.; Amorós, P.; Ros-Lis, J.V. *Green Chemistry* **2024**, *26*, 785-793.

UVM-7 (University of Valencia Material) es un material poroso a base de sílice que se distingue por su sistema de poros bimodal, con poros más pequeños generados por el surfactante y poros más grandes formados por la agregación de nanopartículas mesoporosas primarias pseudoesféricas. Nuestro grupo de investigación ha estado trabajando con este material desde su descubrimiento, dedicando años a profundizar en su comprensión y optimizar sus propiedades. El último avance que se había alcanzado era la síntesis de

este material utilizando calentamiento por microondas de estado-sólido para reducir el tiempo de síntesis, por lo que vamos a continuar con el desarrollo de este proceso a gran escala. Hasta donde sabemos, este es el primer ejemplo de una síntesis en flujo asistida por microondas para materiales mesoporosos de sílice.

La funcionalización de materiales mesoporosos con diferentes grupos químicos es un aspecto clave tras la calcinación, ya que dota al sólido de la funcionalidad deseada para su aplicación en distintos campos. Considerando todos los grupos químicos que pueden ser incorporados a la superficie mediante el uso de trialcoxisilanos comerciales, el grupo amina es probablemente el más utilizado para funcionalizar sólidos de sílice debido a su capacidad de interacción con proteínas, metales y ciertos gases. Por ello, se seleccionó APTES como la molécula objetivo para optimizar la funcionalización superficial asistida por microondas y compararla con la modificación obtenida mediante la metodología convencional.

En el presente trabajo, nos planteamos el objetivo de alcanzar un factor de escala de 100. El primer enfoque para obtener grandes cantidades de material consiste en continuar trabajando en batch, aumentando el tamaño del reactor.

En batch, vamos a obtener el material tras irradiar a 800W durante 12,5 minutos. El material obtenido bajo estas condiciones experimentales presenta las características típicas del UVM-7. La difracción de rayos X a bajo ángulo muestra un pico alrededor de 2° (2θ), correspondiente a la reflexión (100) de la estructura mesoporosa hexagonal. Además, se observa una señal ancha de

menor intensidad en el rango de 3.5–4.0° (2θ), atribuida a las reflexiones solapadas (110) y (200) de una red hexagonal.

Las imágenes de TEM revelan la estructura característica de esta clase de materiales, compuesta por pequeñas partículas mesoporosas que se agrupan, dando lugar a la formación de grandes poros texturales entre ellas. Esta morfología se confirma mediante el análisis de adsorción/desorción de N_2, que muestra una alta superficie específica de aproximadamente 956 $m^2 g^{-1}$ y un sistema de poros bimodal con dos etapas de adsorción bien diferenciados.

Para llevar a cabo la síntesis en flujo, se partió de dos soluciones: una que contenía el complejo atrano y otra con el agua necesaria para la hidrólisis y condensación. Ambas soluciones se mezclan justo antes de la entrada del microondas, donde son irradiadas mediante la fuente de estado sólido. Se estableció una potencia de 100 W y un tiempo de residencia de la solución dentro del horno de 1 minuto. Se recolectaron muestras del material preparado durante 20 minutos en 4 fracciones para comparar la homogeneidad a lo largo del tiempo de reacción. Existe una diferencia significativa entre el material generado en los primeros 5 minutos (FS-1) y las fracciones posteriores. En comparación con el material obtenido mediante la síntesis convencional de UVM-7, la fracción FS-1 presenta un ligero desplazamiento hacia un ángulo mayor (2,3°) en la difracción de rayos X, lo que indica un tamaño de celda ligeramente menor.

Además, las imágenes de TEM muestran que FS-1 está compuesto por grandes partículas mesoporosas rodeadas de partículas más pequeñas. Esta estructura difiere de la morfología común de UVM-7, que suele estar formada por

partículas pequeñas agregadas. Probablemente, el reactor no haya alcanzado el estado estacionario durante los primeros minutos, por lo que esta fracción debería descartarse. El resto de las fracciones presentan las características típicas del UVM-7. Las propiedades texturales de las fracciones FS-2 a FS-4 son comunes para UVM-7 y la variabilidad a lo largo de la síntesis es relativamente baja, lo que refuerza la idea de que la síntesis en flujo asistida por microondas es una estrategia adecuada para obtener materiales con propiedades homogéneas.

Los procedimientos escalados, tanto en batch como en flujo, permiten la síntesis de materiales en menos de 15 minutos, obteniendo productos con una topología similar a la obtenida mediante metodologías convencionales. El método de síntesis en batch permitiría preparar el material para obtener más de 150 g de material calcinado en solo una hora, lo que abre el camino a su aplicación industrial. La síntesis en flujo permitiría la preparación de 82 g de material tras la calcinación en una hora. Este valor es inferior al de la síntesis escalada en batch, pero, en cualquier caso, abre la puerta a una producción automatizada de UVM-7 en grandes cantidades.

Para la funcionalización con APTES, nuestro objetivo en este caso fue lograr una escala 50 veces mayor sin aumentar los tiempos de reacción. Para obtener un proceso más sostenible y reducir el volumen de reacción, se triplicaron las concentraciones de los reactivos, manteniendo constante la relación APTES:UVM-7. Se seleccionó una potencia de 200 W y se emplearon diferentes tiempos de irradiación (hasta 16 minutos). En solo 4 minutos, el análisis TGA reveló un alto grado de funcionalización, logrando la adición de 3,2 mmol de APTES por gramo de sílice en la superficie de UVM-7, un valor

similar a los 3,6 mmol de APTES por gramo de sílice obtenidos mediante síntesis convencional. La extensión del tiempo de reacción incrementó el contenido orgánico por gramo de sílice. Sin embargo, consideramos que, para la mayoría de las aplicaciones, el ligero aumento en la carga no justifica el mayor consumo de energía y tiempo en este proceso de síntesis.

La funcionalización es más compleja que la síntesis. La hidrólisis y la condensación son procesos fundamentales en un medio homogéneo, y para la funcionalización comenzamos con un sólido, lo que dio lugar a una reacción en fase heterogénea. Por este motivo la configuración del equipo fue ligeramente diferente a la de la etapa de síntesis. El APTES y el material se añadieron directamente a la solución de acetonitrilo, por lo que solo fue necesario el uso de una bomba peristáltica. Además, se realizaron algunas adaptaciones para facilitar el tránsito del material a través de la conducción. Aunque el acetonitrilo es un disolvente comúnmente utilizado para la funcionalización, se intentó aumentar la viscosidad de la solución para mejorar el arrastre cambiando el disolvente o haciendo mezclas, pero los mejores resultados se obtuvieron con el acetonitrilo, por lo que nos centramos en modificar el sistema. Entre estas adaptaciones, podemos destacar la utilización de un tubo con un diámetro interno adecuado, lo suficientemente pequeño como para conducir la solución de manera homogénea, pero lo suficientemente grande para evitar que el material bloquee la conducción. La carga orgánica se sitúa en 3,1 mmol de APTES por gramo de sílice, similar a lo obtenido en batch.

Si consideramos un tiempo de reacción de 4 minutos, en una hora se podrían funcionalizar aproximadamente 40 gramos de UVM-7 en batch, mientras que

la funcionalización continua la producción de 59 g de material funcionalizado en una hora.

En resumen, en menos de una hora, es posible sintetizar material precursor para más de 150 g de UVM-7 calcinado y funcionalizar hasta 60 g.

El Análisis de Ciclo de Vida (ACV) es una metodología que permite identificar aquellos procesos que tienen un mayor impacto ambiental. Aunque a simple vista pueda parecer que un proceso es más sostenible que otro, esta metodología nos permite cuantificarlo e identificar los reactivos o procesos con mayor impacto para intentar reducirlo. En nuestro caso, el ACV se ha aplicado a la síntesis y funcionalización escaladas y no escaladas, y la síntesis convencional. El objetivo es determinar si, mediante la aplicación de microondas y la escalabilidad, además de una reducción en el tiempo, existe una variación en el impacto ambiental de la síntesis y funcionalización de UVM-7.

La síntesis a gran escala ofrece una reducción sustancial del impacto ambiental, con una disminución de cinco veces en las emisiones de CO_2 equivalente en comparación con la síntesis no escalada y hasta la mitad en comparación con la síntesis convencional.

Capítulo 4

En este capítulo, se explora la funcionalización de la UVM-7 con titanio y cerio mediante un enfoque de síntesis en un solo paso (one-pot).

Los resultados obtenidos están publicados en dos artículos diferentes, uno referente al Ti-UVM-7 “Solid-state microwave-assisted batch and flow

synthesis, and life cycle assessment, of titanium containing UVM-7 mesoporous silica", con referencia: Rodríguez-Carrillo, C.; Benítez, M.; González-Fernández, M.; De los Reyes, R.; Murcia, S.; El Haskouri, J.; Amorós, P.; Ros-Lis, J.V. *Microporous and Mesoporous Materials* **2024**, *380*, 113314. El otro artículo que conforma este capítulo es referente al Ce-UVM-7 "Flow and Batch Minute-Made Synthesis of Ce-UVM-7 Using Microwave-Assisted Reaction: Scaling-Up, Optical and Catalytic Applications, and Impact Assessment" con referencia: Rodríguez-Carrillo, C.; Benítez, M.; De los Reyes, R.; El Haskouri, J.; Amorós, P.; Ros-Lis, J.V. *ACS Sustainable Chem. Eng.* **2024**, *12*, 13208-13219.

En el capítulo anterior hemos conseguido la síntesis y post-funcionalización de UVM-7 con APTES todo utilizando los generadores de microondas de estado-sólido. En este capítulo vamos a continuar trabajando con este material de sílice mesoporosa, pero en este caso vamos a intentar obtener una funcionalización in situ con titanio y con cerio independientemente. Para ello, en primer lugar, se realizó un estudio sistemático de las condiciones de síntesis a pequeña escala. Se evaluaron distintas combinaciones de tiempos de calentamiento y potencias de microondas, así como diferentes relaciones molares entre los heteroelementos (Si/Ti y Si/Ce). Posteriormente, se llevó a cabo la caracterización de los materiales obtenidos con el fin de identificar aquellos con las propiedades más favorables y, en consecuencia, determinar las condiciones óptimas de síntesis.

El método de atranos permite la incorporación de titanio y de cerio en la red de sílice mesoporosa. El análisis mediante EDX confirma la presencia de ambos elementos, mostrando una correlación clara entre los valores

nominales y reales: a mayor cantidad de heteroelemento añadido, mayor es la cantidad detectada mediante EDX. Además, podemos apreciar un enriquecimiento de ambos heteroelementos. Este fenómeno se explica por la diferencia en solubilidad entre los óxidos, ya que el SiO_2 es significativamente más soluble que el TiO_2 o el CeO_2. Tras la hidrólisis de los complejos atranos, tienen lugar reacciones de condensación, durante las cuales los oligómeros interactúan con las moléculas de surfactante, facilitando la nucleación y el crecimiento de las partículas de Ti-UVM-7. A medida que el contenido de heteroelementos en las paredes de los poros aumenta, las regiones enriquecidas en titanio o cerio presentan una solubilidad inferior a la de la sílice. En consecuencia, el enriquecimiento en titanio y cerio puede atribuirse a un proceso de disolución parcial de la sílice.

También se utilizó difracción de rayos X (DRX) en ángulos bajos y altos. A bajos ángulos, se identificó el pico característico de la sílice alrededor de 2° (2θ), correspondiente al plano (100), así como un hombro asociado al solapamiento de los planos (110) y (200), lo que es indicativo de la estructura hexagonal típica de los materiales mesoporosos. A altos ángulos, el análisis permitió determinar la presencia o ausencia de dominios cristalinos de TiO_2 o CeO_2 en los materiales sintetizados. En el caso de los materiales Ce-UVM-7, cuando se utilizó una relación molar Si/Ce = 8, se observaron los picos característicos del CeO_2, lo que sugiere que el cerio no se incorporó a la red de sílice. Sin embargo, con una relación Si/Ce = 25, estos picos no estuvieron presentes, indicando una posible incorporación del cerio en la estructura de la sílice. Para los materiales Ti-UVM-7, se emplearon relaciones molares Si/Ti de 10, 25 y 50, y en ninguno de los casos se detectaron picos correspondientes

a TiO_2, lo que sugiere que el titanio puede ser incorporado en la red de sílice en cantidades significativas mediante este método de síntesis.

También se llevan a cabo medidas del espectro de absorción de UV-Visible de los materiales, los cuales evidencian un mayor contenido de Ti o Ce debido a un aumento en la absorción UV a una longitud de onda de 200 nm en el caso del Ti-UVM-7 y en torno a 300 nm en el caso del Ce-UVM-7, mientras que la UVM-7 sin dopar no presenta ningún pico de absorción. Para el Ti-UVM-7 también se realizaron medidas de Raman para confirmar la ausencia de fases tanto rutilo como anatasa del titanio, lo que indica que este se encuentra predominantemente disperso dentro de la matriz.

En todos los casos, las isotermas obtenidas presentaron dos etapas de adsorción, una asociada a los mesoporos y otra a los macroporos. La única excepción se observó en la muestra Ce-UVM-7 con una relación Si/Ce = 8, en la cual no se detectaron ambas etapas de adsorción. Además, en esta muestra, las áreas superficiales obtenidas fueron aproximadamente 300 m^2/g, significativamente menores en comparación con los 700-800 m^2/g registrados en el resto de los materiales. Este comportamiento puede atribuirse a una saturación de los poros debido a la presencia de una alta concentración de nanodominios de CeO_2. Asimismo, se observó que un mayor tiempo de irradiación conduce a un incremento del área superficial, lo que sugiere que la sílice ha tenido más tiempo para organizar su estructura, favoreciendo una mayor porosidad.

Las imágenes obtenidas mediante microscopía electrónica de transmisión (TEM) confirmaron la presencia de la estructura tipo UVM-7 en todas las

muestras (tanto Ti-UVM-7 como Ce-UVM-7), con una distribución homogénea de mesoporos en todo el material y la formación de macroporos de mayor tamaño debido a la agregación de partículas.

Para evaluar la estabilidad de los materiales, se realizaron mediciones de potencial Zeta (ζ), obteniendo en todos los casos valores similares a los de la UVM-7 no funcionalizada, alrededor de -30 mV. En el caso del cerio, aunque los datos no fueron incluidos en el artículo, las mediciones mostraron valores aún más positivos que los obtenidos para el titanio. Este comportamiento se atribuye a la incorporación de titanio y cerio en la red de sílice, ya que, al ser elementos con mayor acidez de Lewis en comparación con el silicio, favorecen la desprotonación de los grupos –OH superficiales. Como consecuencia, se reduce la carga superficial negativa, lo que disminuye la repulsión electrostática entre partículas y, por lo tanto, la estabilidad coloidal de la suspensión.

Con toda esta información podemos seleccionar cuales van a ser las mejores condiciones de síntesis. En el caso del Cerio, haciendo un ajuste lineal con las diferentes variables nos sale que ninguna de las variables es significativa, únicamente la relación Si/Ce. Como hemos comentado, las muestras con relación Si/Ce=8 no se trataba de Ce-UVM-7 propiamente dicho y en el resto de casos sí, y en el caso del Ti-UVM-7 vemos que se cumple para todas las relaciones Si/Ti. Por lo tanto se pueden utilizar como válidas las diferentes relaciones de potencia y tiempo que hemos comprobado, pudiendo decir así que hemos obtenido Ce-UVM-7 y Ti-UVM-7 en tan solo 30 segundos.

Se observa que la obtención de Ti-UVM-7 con diferentes relaciones Si/Ti es más sencilla en comparación con la incorporación de cerio. Esto se debe a que el Ti^{4+} presenta una geometría tetraédrica, similar a la del Si^{4+}, mientras que el Ce^{4+} adopta una geometría octaédrica. Como consecuencia, la incorporación de titanio genera una menor distorsión en la mesoestructura en comparación con el cerio, lo que facilita su integración en la red de sílice mesoporosa.

Para hacer el escalado del material tanto en flujo como utilizando reactores más grandes se siguió el método de síntesis expuesto en el capítulo 3, utilizando las misma relaciones molares y cantidades de reactivos. Finalmente se consiguió la obtención de aproximadamente 35 g de Ti-UVM-7 y Ce-UVM-7 en tan solo 10 minutos.

Los protectores solares suelen contener nanopartículas de TiO_2 y ZnO, pero su alto índice de refracción deja un tono blanquecino en la piel y, al exponerse a la radiación UV, pueden generar radicales que dañan el ADN celular. En contraste, el CeO_2 ofrece una alta absorción UV con mayor transparencia en luz visible, aunque su elevada actividad catalítica limita su uso en cosméticos. Por ese motivo estudia la actividad de absorción de UV de los materiales preparados. Para ello se evaluó una muestra representativa de Ti-UVM-7 y de Ce-UVM-7, comparándolas con TiO_2 y CeO_2 comerciales y UVM-7 puro. En el caso del CeO_2, su incorporación en UVM-7 permitió alcanzar un SPF de hasta 69 con un 20% de material, superando al CeO_2 puro y optimizando la absorción UV sin comprometer la transparencia. Por otro lado, el TiO_2 en UVM-7 mostró un SPF de hasta 2.4 con un 10% de carga, siendo más eficiente al considerar solo su contenido de titanio. Además, la matriz mesoporosa

mejoró la estabilidad y redujo la fotocataliticidad del TiO_2. Estos resultados destacan el potencial de la sílice mesoporosa para desarrollar protectores solares más efectivos y seguros.

Con el Ce-UVM-7 se va a realizar otro estudio. El óxido de cerio posee propiedades de eliminación de especies reactivas de oxígeno (ROS), por lo que se estudió si los materiales Ce-UVM-7 presentan una actividad similar. En comparación con la actividad peroxidasa del CeO_2 sintetizado mediante un método asistido por microondas en un trabajo que presentaremos en el próximo capítulo, que mostró una velocidad de reacción de 8×10^{-3} min^{-1}, se obtuvo un resultado análogo para los materiales preparados en batch con una relación molar Si/Ce = 8. Sin embargo, las muestras con menor contenido de cerio demostraron una mayor actividad, con velocidades de reacción de 23×10^{-3} y 27×10^{-3} min^{-1} en condiciones de batch y flujo, respectivamente. La formación de agregados de CeO_2 en los materiales con Si/Ce=8 podría reducir la exposición de los átomos de cerio a los reactivos. La red de mesoporos favorece el acceso a los sitios activos e impide la expansión no deseada de las nanopartículas metálicas. La similitud en la actividad de los materiales producidos tanto en condiciones de batch como de flujo concuerda con sus características estructurales, lo que confirma que el enfoque de síntesis en flujo permite obtener materiales Ce-UVM-7 con propiedades comparables a las obtenidas mediante síntesis en batch.

Como se hizo en el capítulo anterior, se ha llevado a cabo un análisis de ciclo de vida (ACV) para evaluar el impacto ambiental del material. En este estudio, además de confirmar que la reacción puede escalarse eficazmente en batch y adaptarse a la síntesis en flujo sin alterar la topología típica de UVM-7, se logró

la producción de cientos de gramos del material. Asimismo, el análisis de ciclo de vida arrojó un impacto reducido, con un valor de 8 y 10 puntos en el ACV por kg de Ce-UVM-7 y Ti-UVM-7 respectivamente, resultado que podría optimizarse aún más a nivel industrial o mediante modificaciones en los reactivos. Estos hallazgos son consistentes con los obtenidos en estudios previos, reafirmando la viabilidad del proceso tanto desde una perspectiva sintética como ambiental.

Capítulo 5

El capítulo final amplía la investigación más allá de los materiales de sílice mesoporosa, centrándose en la síntesis de óxidos metálicos inorgánicos utilizando generadores de microondas de estado sólido. Se selecciona el CeO_2 como material modelo debido a sus amplias aplicaciones en catálisis, almacenamiento de energía y remediación ambiental.

Los resultados obtenidos están publicados en el artículo "Batch and Flow Synthesis of CeO_2 Nanomaterials Using Solid-State Microwave Generators" con referencia: Rodríguez-Carrillo, C.; Torres-García, J.; Benítez, M.; El Haskouri, J.; Amorós, P.; Ros-Lis, J. V. *Molecules* **2022**, *27*, 2712. En este trabajo presentamos la optimización de las condiciones sintéticas para la preparación de CeO_2 utilizando generadores microondas de estado-sólido.

A pesar de su excelente actividad catalítica, el óxido de cerio no había sido preparado previamente mediante generadores de estado sólido ni mediante síntesis en flujo asistida por microondas.

Para la síntesis en batch, se disolvieron acetato de cerio e hidróxido de sodio en una proporción molar de 1:4 en agua desionizada. Posteriormente, la solución se transfirió a un vial de vidrio apto para microondas, que fue colocado en el horno de microondas para su procesamiento. Para la síntesis se utilizaron diferentes relaciones de potencia y tiempo: 50W durante 2:30 minutos, 100W durante 1 minuto y 200W durante 30 segundos, y estas pruebas se hicieron a pH 11 y a pH 12. Como era de esperar, al aumentar la potencia, se reduce el tiempo necesario para obtener el producto. Posteriormente, las muestras fueron lavadas con agua y etanol hasta alcanzar un pH neutro, y luego se secaron y calcinaron a 800°C.

Para caracterizar los materiales se hizo DRX, y en todas las muestras se obtuvieron los picos característicos del CeO2 con una estructura cúbica tipo fluorita. Los picos más intensos, ubicados en los ángulos 2θ de 28.7°, 47.6° y 56.5°, corresponden a los planos cristalográficos (111), (220) y (311), respectivamente, y no se detectaron picos asociados a Ce_2O_3. El análisis de XRD de los demás materiales mostró picos en las mismas posiciones y con un ancho a media altura (FWHM) similar, lo que indica que, bajo las condiciones experimentales utilizadas, la fase cristalina formada y el grado de cristalinidad de los materiales fueron comparables. También se caracterizó el material sin calcinar, revelando picos característicos de CeO_2. Este resultado sugiere que un tratamiento rápido en el microondas es suficiente para obtener óxido de cerio (IV) con una estructura cristalina. Sin embargo, el FWHM fue significativamente mayor en comparación con los materiales calcinados, lo que indica una menor cristalinidad o un tamaño de partícula reducido.

Los materiales estaban formados por partículas individuales junto con agregados de nanopartículas de CeO_2 de formas irregulares, con un tamaño promedio de 40 nm y una distribución entre 20 y 60 nm. A un pH más bajo (11), las partículas fueron estadísticamente más grandes que a pH 12, evidenciando un mayor crecimiento, mientras que la potencia tuvo un efecto mínimo en el tamaño de las partículas.

En cuanto al efecto de la calcinación en la morfología del material, a diferencia de los materiales calcinados, que presentaban partículas densas y bien definidas, el material obtenido directamente del reactor de microondas estaba compuesto principalmente por nanopartículas más pequeñas (~4 nm). Estas nanopartículas primarias se consolidaron durante el tratamiento a alta temperatura para formar las partículas finales. Como era de esperar, en un entorno homogéneo y con un calentamiento rápido por microondas, el material comenzó a formarse a partir de pequeñas nanopartículas primarias (~4 nm o incluso menores). Estas nanopartículas se unieron y fusionaron progresivamente, dando lugar a partículas cristalinas más grandes después del tratamiento de calcinación.

Para la síntesis en flujo, se seleccionó la condición más rápida (200W durante 30 segundos) a pH 12 debido a la similitud de los materiales obtenidos en batch. Los resultados obtenidos tras la caracterización de los materiales fueron similares, lo que confirma que la síntesis en flujo es una metodología viable para la producción de nanopartículas de CeO_2.

Para evaluar las propiedades catalíticas, se determinó la actividad peroxidasa. Esta enzima descompone el peróxido de hidrógeno, utilizándolo para oxidar

otros sustratos; en este caso, el 3,3',5,5'-tetramethylbenzidine (TMB), que es incoloro, pero que adquiere un color azul en su forma oxidada. La aparición de este color indica que la reacción está ocurriendo, lo que refleja una actividad peroxidasa significativa. En nuestro estudio, todos los materiales produjeron el color azul, lo que corresponde a una alta actividad peroxidasa.

CONCLUSIONES

En conclusión, se ha logrado con éxito el escalado de la síntesis de sílice mesoporosa UVM-7 tanto en condiciones batch como en flujo, así como su funcionalización one-pot con titanio y cerio, y su postfuncionalización con grupos amina, demostrando que la tecnología de microondas no solo es eficaz para la síntesis, sino también para procesos de funcionalización avanzados. Asimismo, se ha conseguido por primera vez la síntesis y el escalado de otro óxido de cerio mediante generadores de microondas, lo que representa un avance significativo en el desarrollo de metodologías más rápidas, eficientes y sostenibles. Estos resultados posicionan al calentamiento por microondas como una herramienta clave para el diseño y la producción a escala de materiales funcionales de alto valor añadido.